STRATEGIC SYNTHESIS OF COMPLEX FUNCTIONALIZED SILANE FRAMEWORKS

by
Eric A. Marro

A dissertation submitted to Johns Hopkins University in conformity with the requirements for the degree of Doctor of Philosophy

Baltimore, Maryland
October 2019

© 2019 Eric A. Marro
All rights reserved

Abstract

Silicon nanomaterials combine earth abundance and biodegradability with compelling electronic properties. Structure-property-function relationships of inorganic silicon structures are widely studied; however, these relationships in silicon soft-matter, such as oligo- and polysilanes, are not well studied. Strategic synthesis promises access to novel architectures with well-defined surface structure, size, and shape; however, the synthetic silicon chemist possesses few tools to do so. Herein, the development of new silyl dianions (disilanides) allows for the strategic synthesis of site-selectively functionalized cyclic oligosilanes. These disilanides provide access to site-selectively functionalized cyclohexasilanes, cyclohexasilanes containing heteroatoms, and fused-ring systems. The pattern of reactive and inert functional groups derived by these strategic synthetic methods provide unique architectures upon polymerization. Extensive characterization partnered with theoretical models are used to determine the bonding architecture and electronic structure of these materials.

Advisor: Professor Rebekka S. Klausen

Reader: Professor J.D. Tovar

Reader: Professor Howard Fairbrother

Acknowledgements

"If you are not doing what you love,
you are wasting your time."
- Billy Joel

First, I would like to thank my advisor, Professor Rebekka S. Klausen for her extraordinary mentorship. She has been essential to my growth as both a scientist and a person throughout my graduate school tenure.

I want to thank my thesis committee, Professor J.D. Tovar and Professor Howard Fairbrother, for their support throughout my time as a graduate student.

I thank the Johns Hopkins community as a whole for fostering a collaborative, enjoyable, and collegial graduate school experience. My colleagues in the Klausen lab have been phenomenal to work with, and I cannot wait to see what amazing discoveries are ahead for the group. I have met many people at Johns Hopkins who I consider not just colleagues but personal friends.

My family has played a huge role in making me the person I am today. My mother and father raised me to be respectful, compassionate and stubbornly perseverant. My two brothers for whom I owe my love of video games, music, and sports. Although we would constantly get on each other's nerves as children and have heated arguments often leading to wrestling matches, it was all out of love.

Last, but not least, I would like to thank my extraordinary wife, Rebecca Gould. She is the most selfless, intelligent, incredible human being I know, and I could not have asked for a better partner to stand side-by-side with for the rest of my life. She inspires me to improve myself every day and her love and encouragement has made this achievement possible.

Table of Contents

List of Tables

List of Figures

List of Schemes

Chapter 1: Introduction to Oligosilanes

1.1 Introduction

New materials allow new technology. Modern electronic devices depend on our ability to fabricate and manipulate the structure of silicon to achieve desired properties. Silicon's appeal is derived from its low toxicity[1,2] and high availability in earth's crust.[3] Semiconductor grade silicon (99.9999999% purity) is energy intensive to produce (> 100 kWh/kg).[4] Bulk silicon's indirect band gap is not ideal for optoelectronic applications. To compensate for this, optoelectronic devices fabricated from bulk silicon are often thick, limiting its application.

Nanoscale silicon materials possess unique properties compared to bulk silicon. Canham's discovery of light emission from porous silicon[5] piqued interest in nanoscale silicon. Quantum confinement in nanoscale silicon introduces a tunable direct band gap.[6] Silicon nanowires are capable of catalyzing CO_2 fixation of ketones.[7] These properties inspire investigation of molecular and polymeric materials with silicon frameworks.[8,9]

1.2 Synthesis of Silicon Based Small Molecules

Two factors limit the synthesis of silicon based compounds: limitations in commercial starting materials and limitations in Si-Si bond forming reactions. Organosilanes are not found in nature, thus, they must be made from inorganic sources. First, silica (SiO_2) is reduced to form elemental silicon,[10] followed by passing methyl chloride gas over solid elemental silicon at elevated temperatures in the presence of a copper catalyst.[11] Variations in catalyst loading, temperature, and the nature of the gas passed over elemental silicon in this process provide access to organosilanes with different permutations of halides and simple alkyl chains.[12] Most commercially available

organosilanes are made by this process and contain one or two silicon atoms. Further organic side-chain diversity is obtainable by nucleophilic substitution of halosilanes with Grignard reagents.

The most common method for Si-Si bond formation is the salt metathesis of a silyl anion (silanide) and a halosilane. Silanides containing one silicon atom are generally prepared by the reduction of chlorosilanes with lithium metal. This method of preparation involves reduction of the silicon-chlorine bond which couples with a second chlorosilane molecule to produce a disilane. Lithium metal then reduces the silicon-silicon bond to form the desired silanide. This method of action makes it unattractive for the preparation of silanides bearing silicon based substituents.

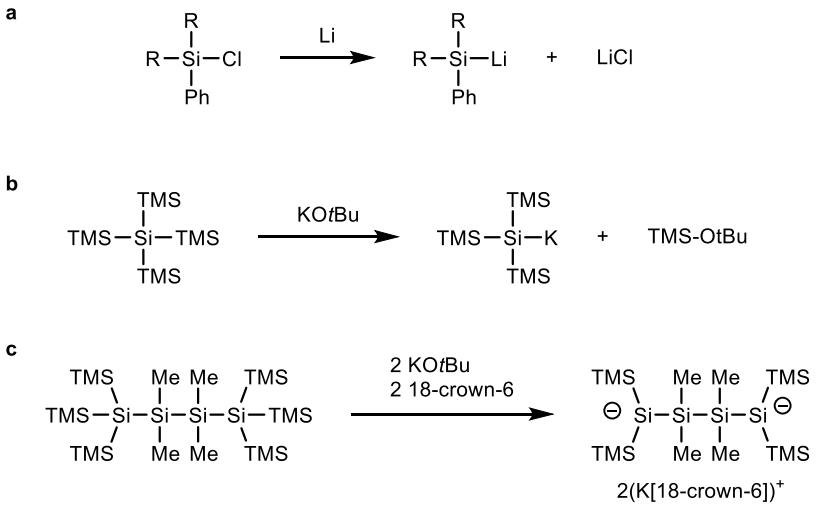

Scheme 1.1. Methods of generating silanides. (a) Reduction of a silicon-halide bond with an alkali earth metal. (b, c) Removal of terminal trimethylsilyl (TMS) groups with potassium *tert*-butoxide (KO*t*Bu) can make silanides bearing silicon substituents and silyl dianions.

Since the above methods can generally break unintended silicon-silicon bonds, milder methods are needed to prepare silanides containing multiple silicon atoms. Sakurai first described the use of potassium *tert*-butoxide (KO*t*Bu) to cleave trimethylsilyl (TMS)

groups to produce silanides.[13] Marschner used these methods to develop the synthesis of disilanides.[14] These disilanides have allowed the synthesis of site-selectively functionalized cyclosilanes and incorporation of heteroatoms into cyclosilanes.[15]

Phenyl groups are an orthogonal functionality to the TMS group. The air stable phenyl groups can be easily replaced with a leaving group upon treatment with strong acid or Freidel Crafts conditions.[16,17] Silyl phenyl groups impart a crystallinity to oligosilanes which makes purification by non-chromatographic methods easier.

1.3 Polysilane Synthesis

Three methods are commonly used to make polysilanes: Wurtz-type reductive coupling, dehydrocoupling, and anionic ring-opening polymerization, each with strengths and limitations.

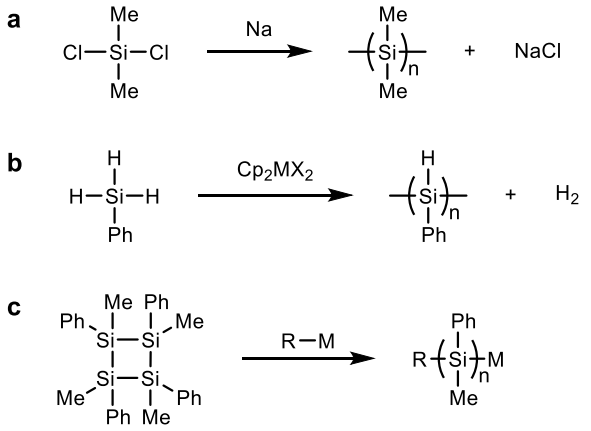

Scheme 1.2. Common synthetic methods of polysilanes. (a) Wurtz-type polymerization. (b) Dehydrocoupling polymerization. (c) Anionic ring-opening polymerization.

Wurtz-type reductive coupling of dihalosilanes is the oldest and most common method of synthesizing polysilanes.[18] Typical reaction conditions are harsh (refluxing sodium in toluene) which limits compatible monomers to dihalosilanes with simple alkyl or aryl side chains. Of the three polymerization methods, it does produce high molecular weight polymers; however, that comes with a high dispersity. Post-polymerization

functionalization of polyphenylsilanes facilitated by triflic acid[19–21] or aluminum chloride/acyl chloride[22] provides access to side chains not compatible with Wurtz conditions; however, these methods are not quantitative and often lead to polymer scission.

Temperature, solvent, the use of additives, the sidechains of the chlorosilane, and the nature of the reductant employed effect the yield and size of the resulting polymers. Sodium is the reductant of choice to obtain high molecular weight polysilanes. Lithium favors cyclic oligomers instead of linear polymers. Potassium and sodium-potassium alloys degrade high molecular weight polymers.[8] Yittrium and lead react at very slow rates resulting in low molecular weight polymers.[23] Polysilanes of moderately high dispersity and length were made using Sm/SmI_2, however the yields were fairly low.[24]

Anionic ring opening polymerization (AROP) offers access to polymer architectures not accessible by the other two. Ring opening of strained cyclotetrasilanes[25] and masked disilenes[26] by organometallic or silanide initiators provide polymers with narrower dispersities than reductive coupling and moderate molecular weights. These polymerizations can be quick, sometimes taking as little as 15 minutes to fully consume monomer. AROP has many handles for control of polymer properties. Relative stereochemistry of the monomer can impart a desired tacticity.[27] End group functionality can be controlled by using the appropriate initiator or quench. Often, AROP has "living" character. Block copolymers of styrene, isoprene, or methyl methacrylate[26] with polysilane blocks have been made.[22,26] However, AROP is handicapped by the difficulty of monomer synthesis.

Dehydrocoupling polymerization is a type of condensation polymerization; each bond formation is accompanied by release of a H_2 molecule.[28] Group four metallocenes

(Cp_2MX_2) have been very well studied as dehydrocoupling catalysts.[29] They are known to be sensitive to the substitution of the silane monomer. Primary silanes, such as $PhSiH_3$ are capable of producing moderately sized polymers under dehydrocoupling conditions.[30,31] However, most secondary silanes such as Ph_2SiH_2 will only form dimers under the similar conditions.[32] Dehydrocoupling polymerization is appealing because the residual Si-H bonds after polymerization can be transformed into a wide array of functional groups.

1.4 σ-Conjugation in Oligosilanes

Unlike alkane chains, permethylated oligosilanes absorb in the near ultra-violet region.[33] This phenomenon is due to delocalization across Si-Si bonds, termed σ-conjugation. Similar to π-conjugated materials, as the length of the silane chain increases, the absorbance red-shifts. However, σ-conjugation is conformation dependent.

Conformational analysis of a tetrasilane is complicated (Figure 1.1a). Conformational analysis of *n*-butane describes a series of energetic maxima and minima spaced 60° apart in dihedral angle. Prelog-Klyne nomenclature is often used to describe these systems, however, analysis of the tetrasilane equivalent, Si_4Me_{10}, reveals a more complex energy profile for which this nomenclature is insufficient. For this reason, Michl devised a nomenclature to describe the additional conformations found in oligosilanes based on their dihedral angle (Figure 1.1c).[34] The conformations are labeled *syn* (S, ω ~ 0°), *cisoid* (C, ω ~ ±40°), *gauche* (G, ω ~ ±55°), *ortho* (O, ω ~ ±90°), *eclipsed* (E, ω ~ ±120°), *deviant* (D, ω ~ ±150°), *transoid* (T, ω ~ ±165°), and *anti* (A, ω = 180°).

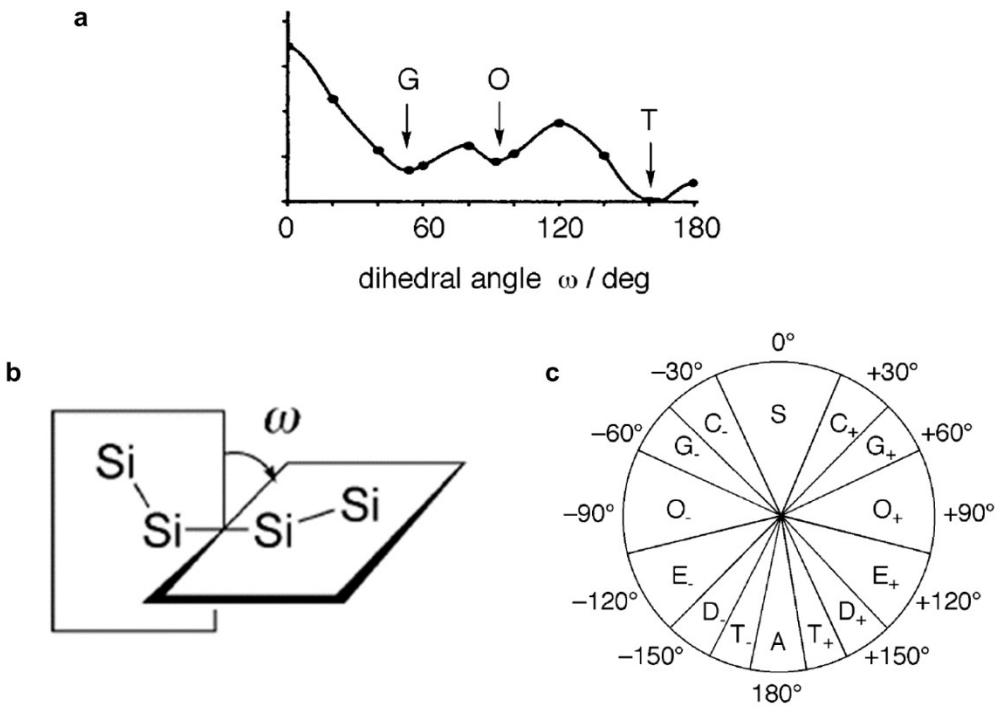

Figure 1.1. (a) Conformational analysis of a tetrasilane reveals multiple energetic minima. Nomenclature for hydrocarbons is not sufficient to describe the stable conformations. (b) Definition of dihedral angle ω (c) Michl's devised nomenclature: S = *syn*, C = *cisoid*, G = *gauche*, O = *ortho*, E = *eclipsed*, D = *deviant*, T = *transoid*, and A = *anti*. Image adapted from Tamao.[35]

Conformational freedom of molecular silanes can be constrained by hydrocarbon tethers to adopt otherwise unstable conformers. [35–39] Michl tethered the ends of a tetrasilane unit with alkyl chains of 1-4 carbon atoms long. Dihedral angles range from 0° - 70°, as determined by geometry optimization (DFT B3LYP/6-311G(d)).[40] As dihedral angle increases, the 1B transition, assigned to a σσ* transition, grows in magnitude (Figure 1.2). A similar trend is observed for tethered silanes synthesized by Tamao. Tamao also used these building blocks to synthesize oligosilanes with alternating *anti* and *cisoid* conformations, ideal geometry for breaking σ-conjugation. As expected, these oligosilanes

all observe absorption maxima at ~240 nm. Unconstrained oligosilanes observe an increasing trend of absorption maxima as the silane chain increases (Figure 1.3).

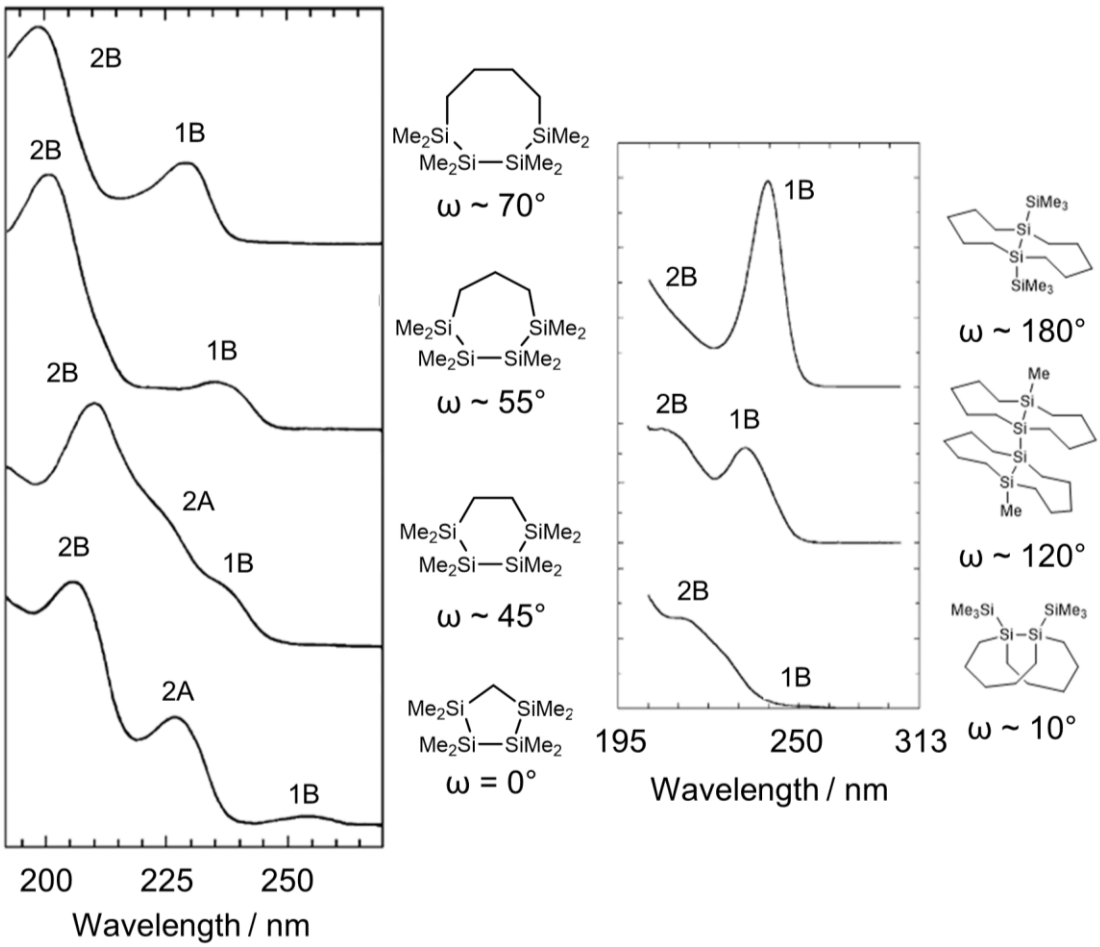

Figure 1.2. Experimental evidence for conformational dependence of σ-conjugation. A series of constrained oligosilanes shows an absorbance feature (1B) ascribed to σσ* grow in intensity as the dihedral angle (ω) goes from 0° to 180°. Image adapted from Tamao.[35]

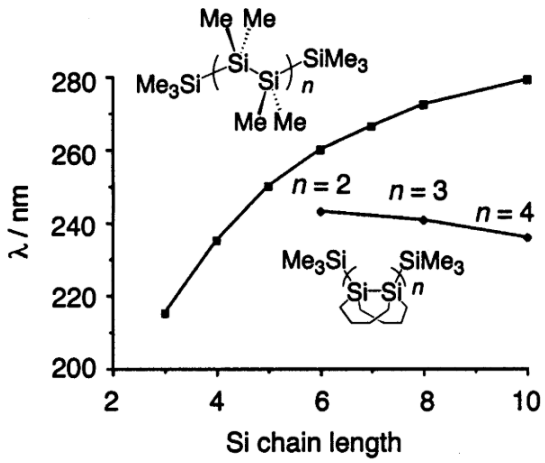

Figure 1.3. Maximum absorption wavelength for a series of alternating *anti*/*cisoid* silanes, and unconstrained oligosilanes. Image adapted from Tamao.[37]

The ladder H and ladder C models are two models devised to explain σ-conjugation. The ladder C model is the simpler of the two; it only considers the sp^3 hybrid orbitals of the silicon chain, which is sufficient for describing the conformation dependence of σ-conjugation. Three orbital interactions are considered; β_{prim} (primary), β_{gem} (geminal), and β_{vic} (vicinal). (Figure 1.4) The magnitude of the β_{vic} interaction is the only one dependent on the dihedral angle of the oligosilane chain. As the dihedral angle of oligosilanes goes from 180° (*anti*) to 0° (*cisoid)*, the magnitude of β_{vic} decreases. As the strength of this interaction decreases, the HOMO-LUMO gap increases, indicative of a decrease in conjugation. The ladder C model is sufficient to explain conformational dependence of σ-conjugation, but falls short explaining excited states of oligosilanes. The ladder H model makes up for the ladder C model's deficiency by also considering orbitals contributed by the organic side chains.

This discussion of σ-conjugation mainly considers linear oligosilanes. Cyclic silanes are not well studied, and the conclusions drawn from linear systems may not extrapolate to cyclic systems.

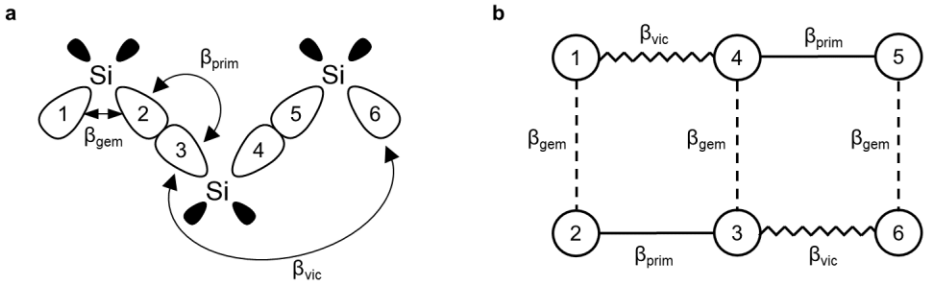

Figure 1.4. (a) Orbitals and resonance integrals included in the ladder C model. (b) Graphical representation of resonance integrals between orbitals (β_{prim} = solid, β_{gem} = dotted, β_{vic} = zig-zag). Adapted from Michl.[41]

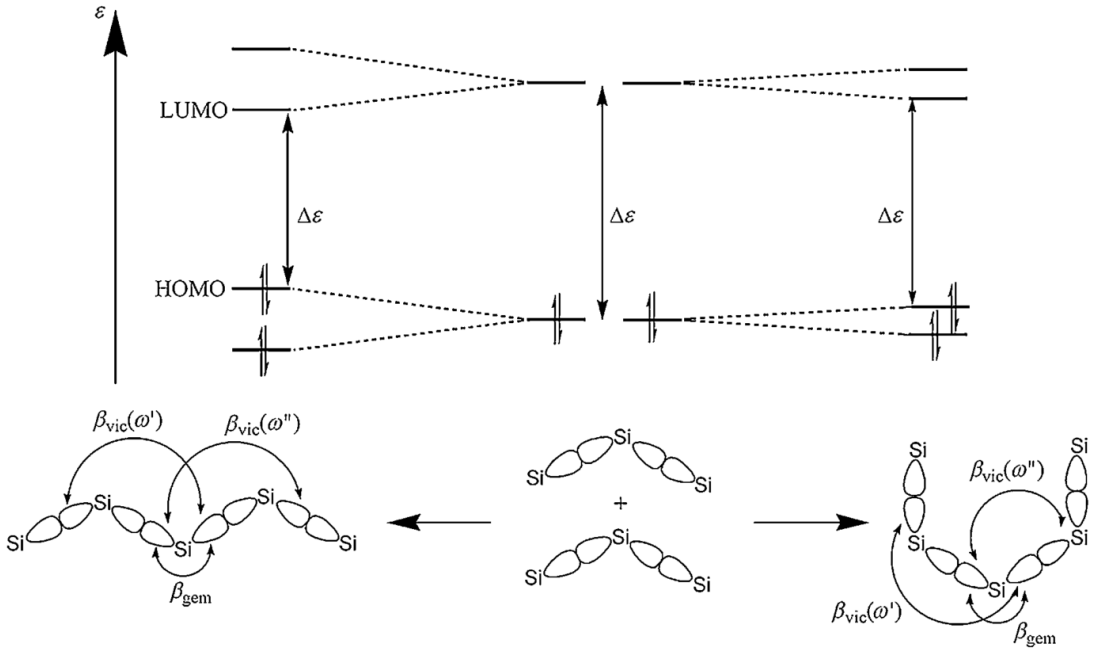

Figure 1.5. Conformational effect on the HOMO – LUMO gap of an oligosilane. *anti*-Configuration (left) displays a smaller HOMO – LUMO gap compared to the *cis*-configuration (right). Adapted from Michl.[41]

1.5 Conclusion

The following chapters will highlight efforts to use strategic synthesis to make novel site selective cyclic silanes. The development and investigation of a new class of disilanides led to the discovery of a unique structure in the solid state. A rigorous study

about the cause of this unique structure helped inform reaction conditions for the synthesis of cyclic silanes. These cyclic silanes are further elaborated to polymers which possess unique functionalities imparted on them by their structure.

1.6 References

(1) Low, S. P.; Voelcker, N. H.; Canham, L. T.; Williams, K. A. *Biomaterials* **2009**, *30* (15), 2873–2880.
(2) Liu, J.; Erogbogbo, F.; Yong, K.-T.; Ye, L.; Liu, J.; Hu, R.; Chen, H.; Hu, Y.; Yang, Y.; Yang, J.; Roy, I.; Karker, N. A.; Swihart, M. T.; Prasad, P. N. *ACS Nano* **2013**, *7* (8), 7303–7310.
(3) Emsley, J. *The Elements*, 3rd ed.; Oxford: Clarendron Press, 1998.
(4) Pizzini, S. *Sol. Energy Mater. Sol. Cells* **2010**, *94* (9), 1528–1533.
(5) Canham, L. T. *Appl. Phys. Lett.* **1990**, *57* (10), 1046–1048.
(6) Sailor, M. J.; Lee, E. J. *Adv. Mater.* **1997**, *9* (10), 783–793.
(7) Liu, R.; Yuan, G.; Joe, C. L.; Lightburn, T. E.; Tan, K. L.; Wang, D. *Angew. Chemie Int. Ed.* **2012**, *51* (27), 6709–6712.
(8) Miller, R. D.; Michl, J. *Chem. Rev.* **1989**, *89* (6), 1359–1410.
(9) Marschner, C. 2013; pp 163–228.
(10) Filsinger, D. H.; Bourrie, D. B. *J. Am. Ceram. Soc.* **1990**, *73* (6), 1726–1732.
(11) Clarke, M. P. *J. Organomet. Chem.* **1989**, *376* (2–3), 165–222.
(12) Herzog, U. In *The Chemistry of Organic Silicon Compounds Volume 3*; Rappoport, Z., Apeloig, Y., Eds.; John Wiley & Sons, Ltd: Chichester, UK, 2001; pp 469–489.
(13) Sakurai, H.; Kondo, F. *J. Organomet. Chem.* **1975**, *92* (3), C46–C48.
(14) Kayser, C.; Kickelbick, G.; Marschner, C. *Angew. Chemie Int. Ed.* **2002**, *41* (6), 989–992.
(15) Fischer, R.; Konopa, T.; Ully, S.; Baumgartner, J.; Marschner, C. *J. Organomet. Chem.* **2003**, *685* (1–2), 79–92.
(16) Uhlig, W. *Chem. Ber.* **1996**, *129* (7), 733–739.
(17) Deller, K.; Rieger, B. *J. Organomet. Chem.* **2015**, *794*, 188–196.
(18) Koe, J.; Fujiki, M. *Organosilicon Compd.* **2017**, 219–300.
(19) Fischer, R.; Baumgartner, J.; Kickelbick, G.; Hassler, K.; Marschner, C. *Monatshefte fur Chemie* **2006**, *137* (5), 613–625.
(20) Tretner, C.; Zobel, B.; Hummeltenberg, R.; Uhlig, W. *J. Organomet. Chem.* **1994**, *468* (1–2), 63–68.
(21) Uhlig, W. *J. Organomet. Chem.* **1991**, *402* (3), C45–C49.
(22) Fossum, E.; Love, J. A.; Matyjaszewski, K. *J. Organomet. Chem.* **1995**, *499* (1–2), 253–260.
(23) Benfield, R. E.; Cragg, R. H.; Jones, R. G.; Swain, A. C. In *Proceedings of the 3rd Euro-American Conference on Functional Polymers and Biopolymers,*; 1992; pp 1271–1278.
(24) Li, Z.; Iida, K.; Tomisaka, Y.; Yoshimura, A.; Hirao, T.; Nomoto, A.; Ogawa, A. *Organometallics* **2007**, *26* (5), 1212–1216.
(25) Cypryk, M.; Gupta, Y.; Matyjaszewski, K. *J. Am. Chem. Soc.* **1991**, *113* (3), 1046–

1047.
(26) Sakamoto, K.; Obata, K.; Hirata, H.; Nakajima, M.; Sakurai, H. *J. Am. Chem. Soc.* **1989**, *111* (19), 7641–7643.
(27) Cypryk, M.; Chrusciel, J.; Fossum, E.; Matyjaszewski, K. *Makromol. Chemie. Macromol. Symp.* **1993**, *73* (1), 167–176.
(28) Waterman, R. *Chem. Soc. Rev.* **2013**, *42*, 5621–5980.
(29) Tilley, T. D. *Acc. Chem. Res.* **1993**, *26* (1), 22–29.
(30) Corey, J. Y.; Xiao-Hong, Z. *J. Organomet. Chem.* **1992**, *439* (1), 1–17.
(31) Chang, L. S.; Corey, J. Y. *Organometallics* **1989**, *8* (8), 1885–1893.
(32) Corey, J. Y.; Zhu, X. H.; Bedard, T. C.; Lange, L. D. *Organometallics* **1991**, *10* (4), 924–930.
(33) Gilman, H.; Atwell, W. H.; Schwebke, G. L. *J. Organomet. Chem.* **1964**, *2* (4), 369–371.
(34) Michl, J.; West, R. *Acc. Chem. Res.* **2000**, *33* (12), 821–823.
(35) Tsuji, H.; Michl, J.; Tamao, K. *J. Organomet. Chem.* **2003**, *685* (1–2), 9–14.
(36) Tamao, K.; Tsuji, H.; Terada, M.; Asahara, M.; Yamaguchi, S.; Toshimitsu, A. *Angew. Chemie* **2000**, *39* (18), 3287–3290.
(37) Tsuji, H.; Terada, M.; Toshimitsu, A.; Tamao, K. *J. Am. Chem. Soc.* **2003**, *125* (25), 7486–7487.
(38) Fukazawa, A.; Tsuji, H.; Tamao, K. *J. Am. Chem. Soc.* **2006**, *128* (21), 6800–6801.
(39) Imhof, R.; Teramae, H.; Michl, J. *Chem. Phys. Lett.* **1997**, *270* (5–6), 500–505.
(40) Tsuji, H.; Fogarty, H. A.; Ehara, M.; Fukuda, R.; Casher, D. L.; Tamao, K.; Nakatsuji, H.; Michl, J. *Chem. - A Eur. J.* **2014**, *20* (30), 9431–9441.
(41) Bande, A.; Michl, J. *Chem. - A Eur. J.* **2009**, *15* (34), 8504–8517.

Chapter 2: Cooperative Noncovalent Interactions Induce Ion Pair Separation in Diphenylsilanides

The work presented in this chapter has been published as:

Marro, E. A.; Press, E. M.; Purkait, T. K.; Jimenez, D.; Siegler, M. A.; Klausen, R. S. *Chem. - A Eur. J.* **2017**, *23*, 15633.

Mr. Eric Marro performed the bulk of the experimental work.

Dr. Eric Press performed all computational work.

Dr. Tapas Purkait did some experimental work.

Mr. Daniel Jimenez prepared some of the starting materials used with methods previously established by Mr. Eric Marro.

Dr. Maxime Siegler obtained single crystal x-ray data and solved crystal structures.

2.1 Introduction

Silyl anions (silanides) are an important synthetic tool, but not as well studied as their carbon counterparts. They are an important reagent in organic[1] and main group[2–4] synthesis. Gilman's first report of tris(trimethylsilyl)silyl anion[5], from tetrakis(trimethylsilyl)silane and methyllithium (MeLi), was a landmark discovery for the synthesis of oligosilanes (Scheme 2.1a). It has become a highly used reagent in main-group and organometallic chemistry,[6] opening the door for the synthesis of structurally complex oligosilanes. Marschner developed the simple synthesis of α,ω-disilanides using KO*t*Bu(Scheme 2.1b, c).[7] These disilanides were used to synthesisze TMS-functionalized cyclosilanes in high yields.

While the structural diversity achieved with these silanides and disilanides is impressive, there is still room for more. Marschner's dianions can only add anionic

functionality to silanes. The Klausen group was interested in synthesizing site-selective hydro cyclohexasilanes. TMS-functionalized cyclohexasilanes derived from Marschner's dianions were incapable of producing these desired products.

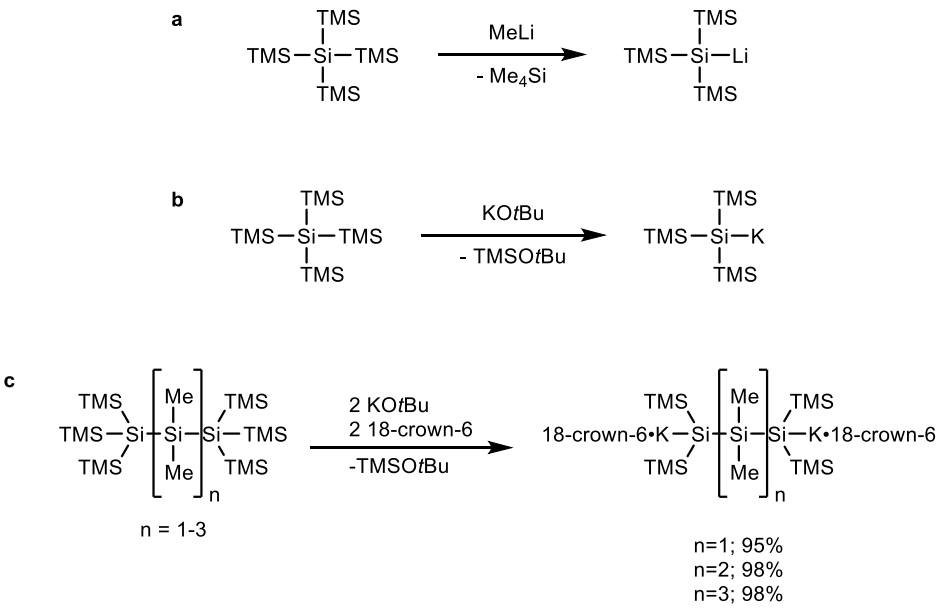

Scheme 2.1. (a) Gilman's landmark synthesis of tris(trimethylsilyl)lithium. (b) Marschner's improved method of tris(trimethylsilyl) anion. (c) α,ω-disilanides which allow for rational synthesis of cyclosilanes.

The terminal TMS groups are important for disilanide synthesis. The bulky trimethylsilyl substituents impart kinetic stability and promote exclusively terminal desilylation. Additionally, they impart thermodynamic stability by stabilizing the negative charge through hyperconjugative mixing of the 3p Si_α anionic orbitals with Si_β-C σ^* orbitals.

Inspired by this disilanide chemistry, replacing the terminal TMS groups with a "masked electrophile" could allow the synthesis of functionalized oligosilanes with orthogonal functionalities. The functional group of choice was the phenyl group. Phenyl groups can be transformed into electrophiles with strong acid. A relatively large functional group, it can also block the internal silicon chain from nucleophilic attack by KO*t*Bu.

Lastly, the conjugated π system could potentially stabilize the negatively charged silicon atom through resonance.

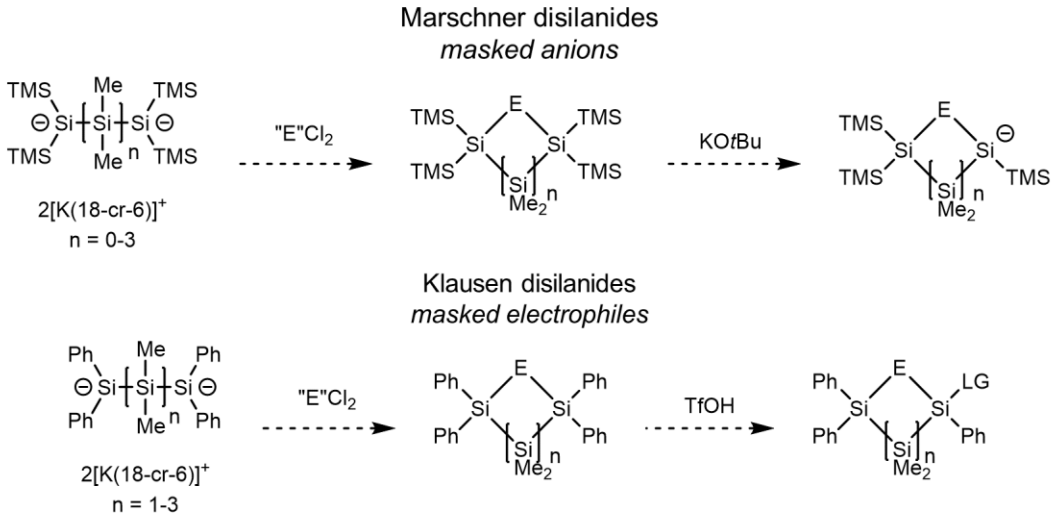

Scheme 2.2. Synthetic strategy using orthogonal functionalities. TMS groups in Marschner dianions can be considered masked anions, while Ph groups can be considered masked electrophiles.

Understanding the reactivity of these new disilanides can unlock the potential for a multitude of new silicon frameworks. A comprehensive understanding of the structure-reactivity relationships of known silanides can help guide a study of this new class of disilanide.

Silanides in the solid state adopt three structural motifs: tetrahedral, silylenoid and inverted (Figure 2.1a).[8] Kinetic stability of silanides is imparted by bulky substituents such as phenyl, branched alkanes, and silyl. Electronegativity and π-donating capabilities of silanide substituents dictate conformational stability.[9] Examples of planar silanides with π-accepting substituents such as -BH_2 exist, [9] but planar silanides have not been observed experimentally. Solvent separated anions, silylenes, and sila-ylides exist in solution.[10] As seen in carbanions, the structure of a silanide can be indicative of its reactivity.

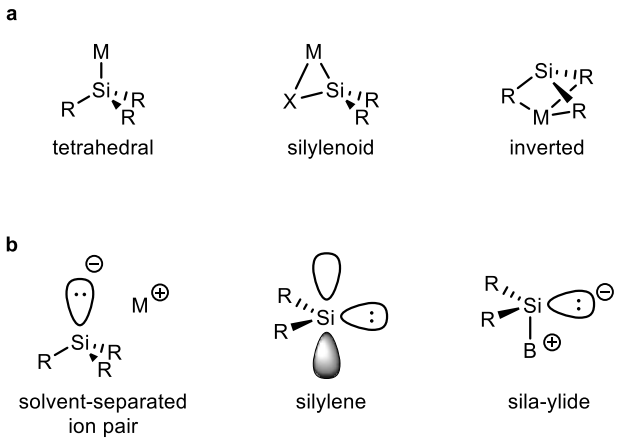

Figure 2.1. (a) Structural motifs which silanides adopt in the solid state. (b) Structural motifs possible in solution. M = metal, X = heteroatom, R = alkyl, aryl, or silyl, B = base.

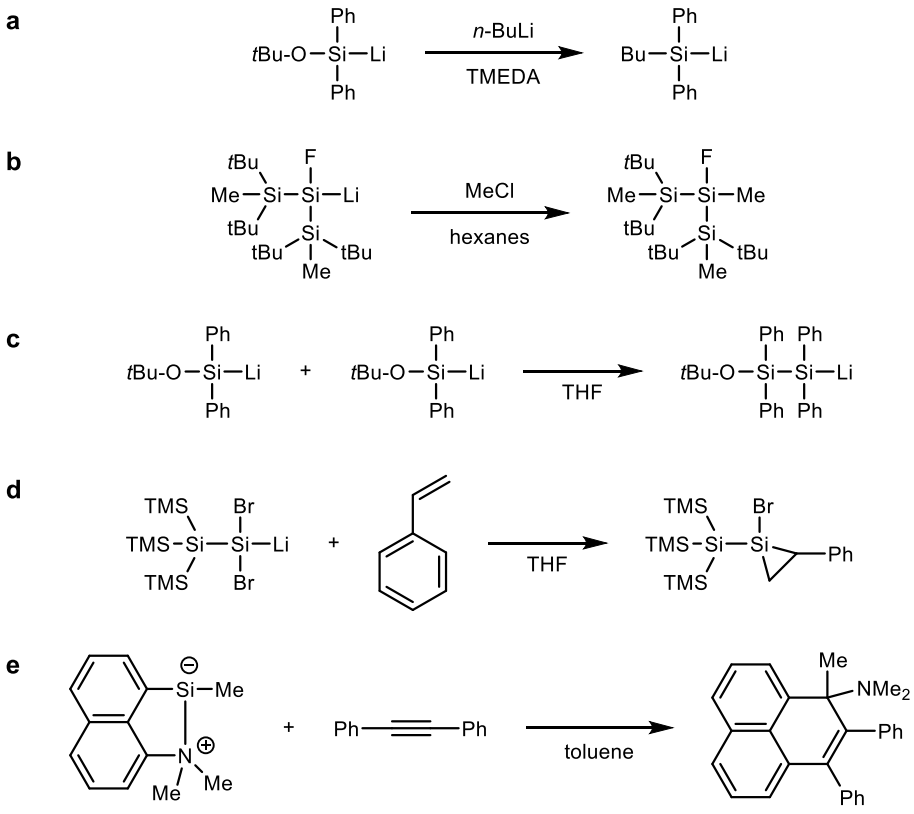

Scheme 2.3. Multiple modes of reactivity for silylenes (a) electrophile (b) nucleophile (c) self-condensation (d) silylene (e) sila-ylide.

Of the motifs listed above, silylenoids are the most interesting. In solution, silylenoids can adopt a silylene structure. Similar to carbenes, silylenes display multiple

modes of reactivity due to the presence of a lone pair and an empty p-orbital. Silylenes have exhibited electrophilic character when exposed to *n*-butyllithium (*n*-BuLi)[11] (Scheme 2.3a) and nucleophilic character when exposed to chloromethane (Scheme 2.3b).[12] They can also undergo self-condensation due to this ambiphilic character.[10] (Scheme 2.3c) A tethered Lewis base can give make a silylene exhibit ylide behavior[13] (Scheme 2.3e).

The most common solid state structure for silanides is tetrahedral. When crystallized from a tetrahydrofuran (THF)/hexane mixture, TMS_3SiLi is isolated with a tetrahedral geometry with three THF molecules coordinated to the lithium atom.[14] The formally negative silicon atom has a distorted tetrahedral structure; Si-Si-Si angles range from 101.6°-103.1° and Si-Si-Li angles range from 112.8°-117.1°. Bond lengths are not distorted. The average Si-Si bond length is 2.331(3) Å and the Si-Li length is 2.669(13). When TMS_3SiLi is prepared in and crystallizes out of heptane, dimeric crystals form.[15] One of the two TMS_3Si silanide units has disorder. Both formally negative silicon atoms are pyramidal; Si-Si-Si bond angles are between 100.5°-107.1°, the average Si-Si bond length is 2.332 Å and the average Si-Li distance is 2.664 Å.

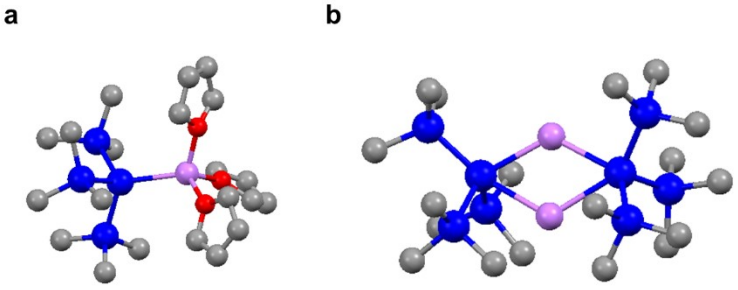

Figure 2.2 Crystal structures of (a) monomeric[14] and (b) dimeric[15] TMS_3SiLi. Hydrogens and disorder in (b) are omitted for clarity. Blue = silicon, grey = carbon, red = oxygen, purple = lithium.

Carbanions are well known to form aggregates in solid state and solution which can temper their reactivity.[16] Few examples of silanide aggregates exist. Bulkier substituents and preparation with coordinating solvents and/or additives hinder aggregation. Tetrahedral silanides become solvent separated ion pairs when dissolved in coordinating solvents. Coupling reactions of TMS_3SiLi•3THF in pentane are generally much cleaner and higher in yield.[17] Dimer formation in pentane may tune the reactivity of TMS_3SiLi relative to the solvent separated ions in coordinating solvents.

Phenyl silanides are commonly tetrahedral, but possess some unexpected qualities. Benzyllithium compounds possess a planar geometry. The lone pair of electrons of the anionic carbon are located in a p-orbital, and are delocalized into the conjugated aromatic system. This delocalization is observed in ^{13}C NMR, the signal for carbon atoms *ortho* and *para* to the anionic carbon are shifted -5.1 and -14.3 ppm respectively relative to Ph_3CH. The trend observed for phenylsilanides is consistent with π polarization instead of delocalization (Figure 2.3).

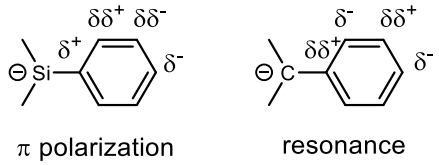

Figure 2.3. ^{13}C Chemical shift changes of an aromatic ring bonded to an anion compared to the neutral species. + refers to an increase in chemical shift consistant with deshielding of that nucleus.

Another interesting phenomenon was realized by Strohman.[18] In a study of tetrahedral lithium silanides with amine coordinating groups, he observed phenyl ring bending. Defined as a deviation from a 180 ° ∠ Si-C_i-C_m-C_o torsion angle (Figure 2.4a), this phenomenon is present in every lithium silanide he found in the literature. Calculations reveal that by adopting a bent phenyl ring, lithium phenylsilanides relieve electron

repulsion between the lone pair of the silicon atom and the π system of the phenyl ring (Figure 2.4b).

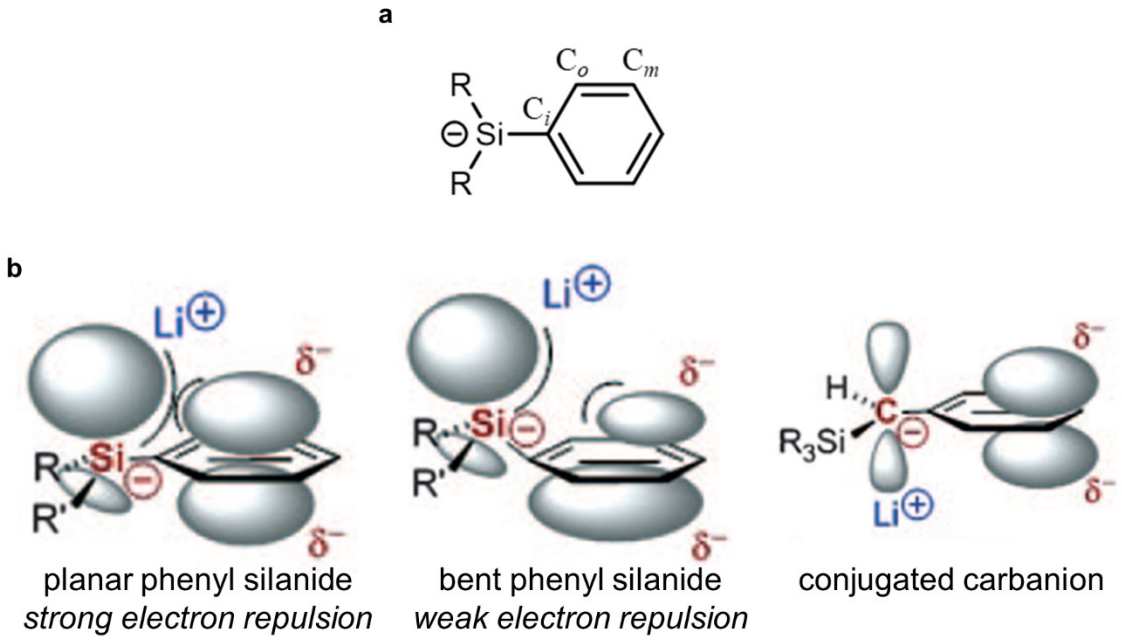

Figure 2.4. Explaining the origins of phenyl ring bending. (a) Torsion angle (∠ Si-C_i-C_m-C_o) used to measure the extent of phenyl ring bending. (b) Illustration of results of calculations. Images adapted from Strohmann.[19]

2.2 Synthesis of Diphenylsilanides

Trisilane **2.1** is a common precursor to all silyl dianions synthesized in this study. Desylation of **2.1** with KO*t*Bu in THF produces a silanide *in situ*. Salt metathesis with a dichlorosilane of desired length produces a linear silane chain with terminal TMS groups. Treatment with two equivalents of KO*t*Bu and 18-crown-6 in diethyl ether produces the respective disilanide. Subjecting **2.1** to similar conditions provides monoanion **2.8**. Lastly, substituting NaO*t*Bu and 15-crown-5 for KO*t*Bu and 18-crown-6 in benzene gives access to disilanide **2.9**, the sodium analog of **2.6**. Attempts at making the lithium analog of **2.6** were unsuccessful.

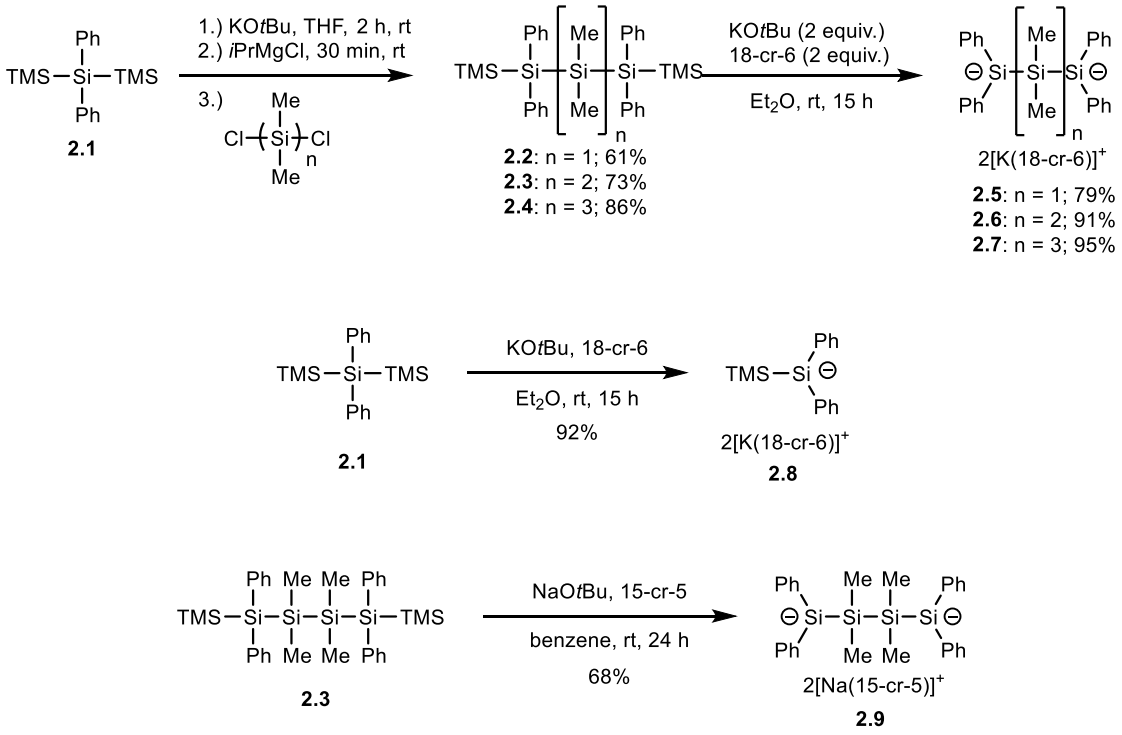

Scheme 2.4: Synthesis of the studied diphenylsilanides.

2.3 An Unexpected cation-π Interaction

Diphenylsilanide **2.6** has an unexpected crystal structure (Figure 3.5); the Si1-K distance (4.6897(7) Å) is much longer than expected for a Si-K contact ion pair. Crown ethers suppress ion pairing in solution; however, the approximately two dozen crown ether ligated silanides in the Cambridge Structural Database are contact ion pairs.[7,20–28] For example, tetrahedral triphenylsilyl potassium has a Si-K distance of 3.456(3) Å.[29] Separated ion pair silanides in the solid state are limited to silanides bearing functionalities with lone pairs[30,31] and crystals which contain coordinating solvent molecules.[32]

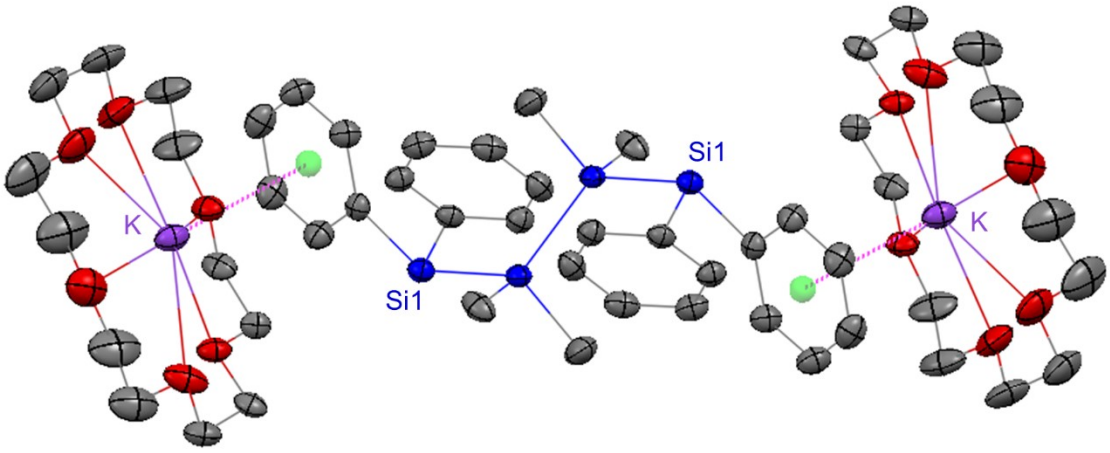

Figure 2.5. Crystal structure of **2.6**. K-Centroid distance: 3.190(2) Å (pink line). K-Si1 distance: 4.6897(7) Å. Displacement ellipsoids shown at 50% probability level. Hydrogens and minor component of 18-crown-6 disorder omitted for clarity. Grey = carbon, blue = silicon, red = oxygen, purple = potassium, Green = centroid of Ph ring.

Instead of a contact-ion pair, each potassium cation is engaged in a cation-π interaction with a phenyl ring bonded to a terminal silicon atom (Si1). The K-centroid distance is 3.190(2) Å and is slightly off-center from the aromatic ring (θ = 14.7°**),** consistent with theoretical benzene-K^+ interactions.[33] The silanide is not a free anion; Si1 forms close contacts (<3.30 Å, the sum of the van der Waals radii of silicon and hydrogen) with hydrogen atoms of two adjacent 18-crown-6 molecules (Figure 2.6).

The unique structure of **2.6** prompted further investigation. Hydrogen atoms can be difficult to locate by x-ray crystallography and inadvertent protonation of **2.6** could result in this unexpected crystal structure. Advantageous water may have protonated the crystal during data collection. Lewis bases used to increase the reactivity of alkyllithiates can be deprotonated by the alkyllithiate.[34]

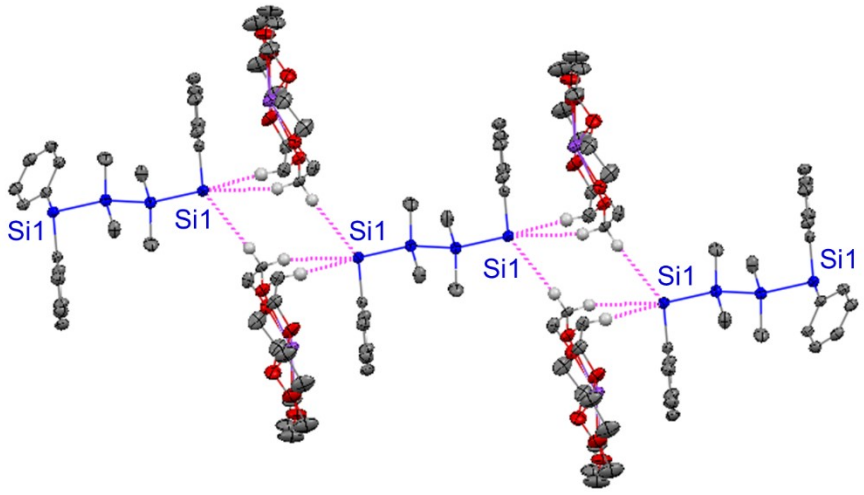

Figure 2.6. Crystal Packing of **2.9**. One phenyl ring, most hydrogens, and disorder in 18-crown-6 omitted for clarity. Grey = carbon, blue = silicon, red = oxygen, purple = potassium, white = hydrogen. Dashed pink lines indicate Si1-H short contacts.

Inadvertant protonation is not the cause of this unique structure. While hydrogens can be difficult to locate accurately by means of single crystal X-ray diffraction, the oligosilanes chain itself is well ordered and hydrogen atoms at other positions have been readily identified. Difference Fourier maps show that all carbon atoms in the aromatic rings are protonated. The structure refinement of **2.6** shows no residual electron density peaks larger than $0.45e^{-3}$ (the highest peak being found at 0.87 Å from K1). Residual electron density peaks found near Si1 are always found along the Si-Si and Si-C bonds, and there are no peaks pointing outward, which strongly indicate that Si1 is not protonated. The ^{1}H NMR spectrum of the crystals are inconsistent with an authentic sample of $HSiPh_2(SiMe_2)_2Ph_2SiH$, the product of protonating **2.6** (Figure 2.7). Crystals of **2.6** are a deep red color, while $HSiPh_2(SiMe_2)_2Ph_2SiH$ is white. Data collection was conducted under a cold stream of $N_{2(g)}$ and no change in the color of the crystal was observed during data collection.

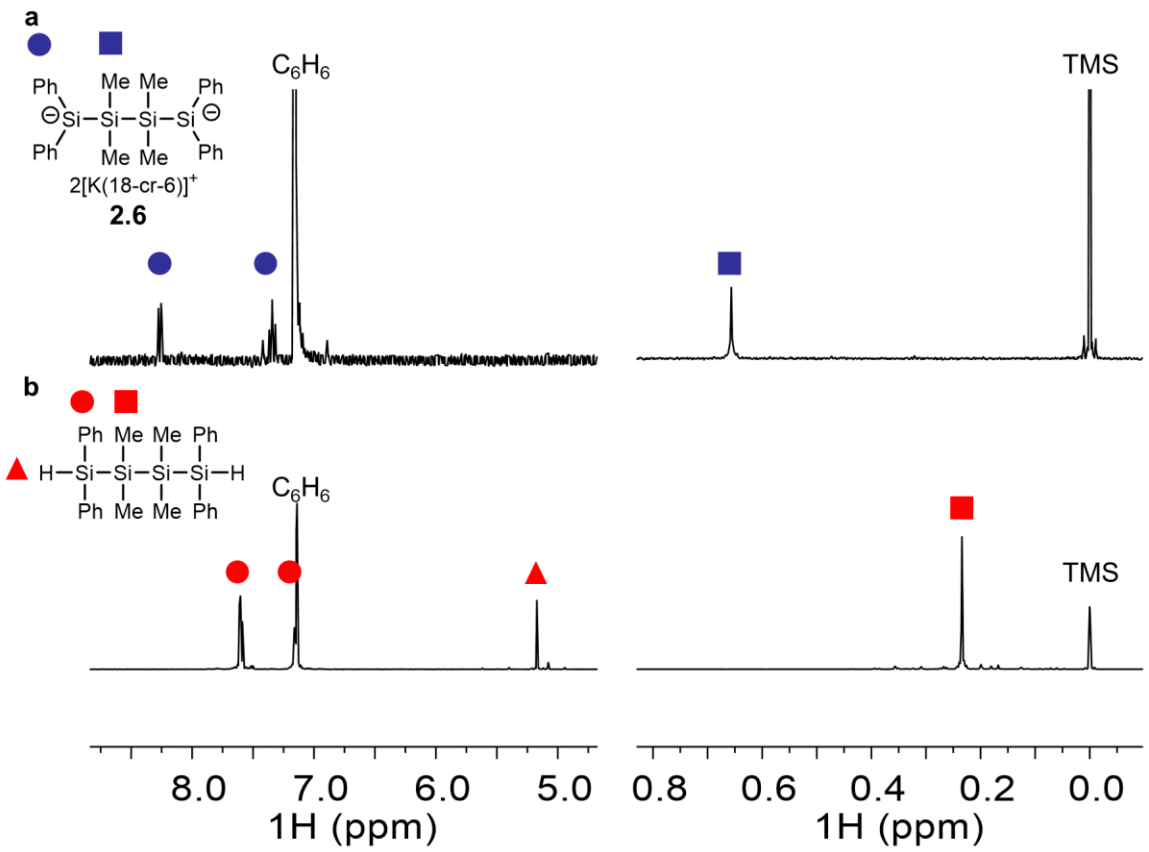

Figure 2.7. ^{1}H NMR spectrum of (a) **2.6** and (b) $HSiPh_2(SiMe_2)_2Ph_2SiH$. Evidence that inadvertent protonation is not the cause of the cation-π interaction seen in the crystal structure of **2.6**.

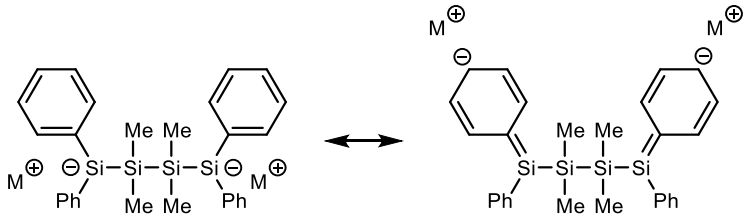

Figure 2.8. Resonance structures of diphenyldisilanide, a possible explanation for cation-π interaction in solid state.

Cation-π binding observed in **2.6** may arise due to charge delocalization from the anionic silicon to the aromatic ring (Figure 2.8). Prior work done on lithiated phenylsilandes[19,35] and quantum mechanical calculations do not support this hypothesis. HOMOs calculated for the oligosilyl anion ($[SiPh_2(SiMe_2)_2SiPh_2]^{-2}$) suggest delocalization

across the silicon framework, but no delocalization into the aryl groups (Figure 2.9a). In addition, the electrostatic potential (ESP) map of the same oligosilyl anion shows anionic character concentrated on the terminal silicon atoms, not the aryl groups (Figure 2.9b).

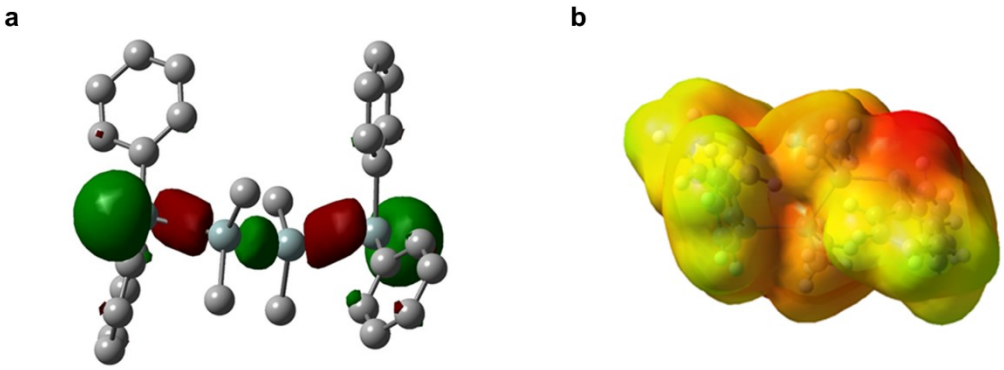

Figure 2.9. (a) HOMO of silanide core optimized in vacuum. (b) ESP map of the gas phase optimized silanide core. Values for electrostatic potential range from -149 kcal mol^{-1} (red) to 63 kcal mol^{-1} (blue). DFT CAM-B3LYP/6-31+G(d). Hydrogens omitted for clarity.

2.4 Crystallographic Analysis of Additional Disilanides

The soft silanide may prefer diffuse interactions in contrast to hard anions that prefer charge-controlled interactions. Recent progress in the molecular recognition of large multinuclear anions suggests significant differences between hard and soft species. While hosts for hard anions like fluoride typically feature classical hydrogen bond donors (e.g. NH•••F^-), high binding constants are measured between large anions and CH donors. The binding cavities of Flood's polyaryl macrocyclic hosts are lined only with CH bonds and show exceptional affinity for large nonspherical anions like perchlorates.[36–38] Johnson reports that the thiolate anion (HS^-) is more tightly bound by a benzenoid than pyridinyl host.[39] Sindelar has shown strong binding of large anions in water by aliphatic CH donors.[40]

If hard-soft theory rationalizes the binding modes observed in **2.6**, then crown ether-driven ion pair separation might be observed in other potassium silanides.

Table 2.1. Selected Parameters of Silanide Crystal Structures

Silanide	**Si-M Distance (Å)**		**Si-C_i Distance (Å)**		**Torsion Angle ∠ Si-C_i-C_m-C_o**	
2.6	Si1-K1	4.6897(7)	Si1-C1	1.915(2)	Si1-C1	-173.3° / +173.7°
			Si1-C2	1.919(2)	Si1-C2	-179.8° / -178.9°
2.7	Si1-K2	4.820(1)	Si1-C1	1.924(3)	Si1-C1	+175.0°/ -175.7°
			Si1-C2	1.923(3)	Si1-C2	+176.8°/ -176.1°
	Si5-K1	4.088(1)	Si5-C1	1.917(3)	Si5-C1	+174.3°/ -175.0°
			Si5-C2	1.927(3)	Si5-C2	+175.9°/ -175.8°
2.8	Si1-K1	3.6142(7)	Si1-C1	1.922(2)	Si1-C1	+172.9°/ -172.3°
			Si1-C2	1.936(2)	Si1-C2	+177.2°/ -178.6°
2.9	Si1-Na2	3.0491(7)	Si1-C1	1.925(2)	Si1-C1	-177.8° / +176.5°
			Si1-C2	1.925(2)	Si1-C2	-176.2° / +176.8°
	Si4-Na1	2.9691(7)	Si4-C1	1.992(2)	Si4-C1	-178.2°/ +178.2°
			Si4-C2	1.917(2)	Si4-C2	-171.8° / +171.5°

In an effort to explore the ubiquity of this interaction in the solid state, silanides **2.5**, **2.7**, **2.8**, and **2.9** were synthesized. X-ray quality single crystals of **2.5** could not be grown. Analysis of silanide crystal structures is summarized in table 2.1. Crystal structures of dianions **2.7**, **2.9** and monoanion **2.8** show that contact ion pairs and separated ion pairs are both possible structures in diphenylsilanides, but that they can also coexist within a single structure. Monoanion **2.8** is a typical contact ion pair: it adopts a tetrahedral geometry and a Si-K distance 3.6142(7) Å, well within the range of typical distances.

In the crystal structure of pentasilane **2.7** each terminal silicon participates in a different interaction with potassium (Figure 2.10). At Si1, a cation-π separated ion pair is observed. The K2-centroid distance is short (3.114(3) Å) and the cation is centered over the aromatic ring (θ = 8.5°). At Si5, a contact ion pair is observed. The Si5-K1 distance of 4.0882(13)Å is longer than usual for Si-K contact ion pair, attributed to the influence of

THF and crown ether binding. The differences between tetrasilane **2.6** and pentasilane **2.7** may reflect odd-even effects in oligosilane packing.[41] Solution phase NMR of **2.7** has only two signals for Si-Me groups, which suggests that both ends of **2.7** form a solvent separated ion pair in solution.

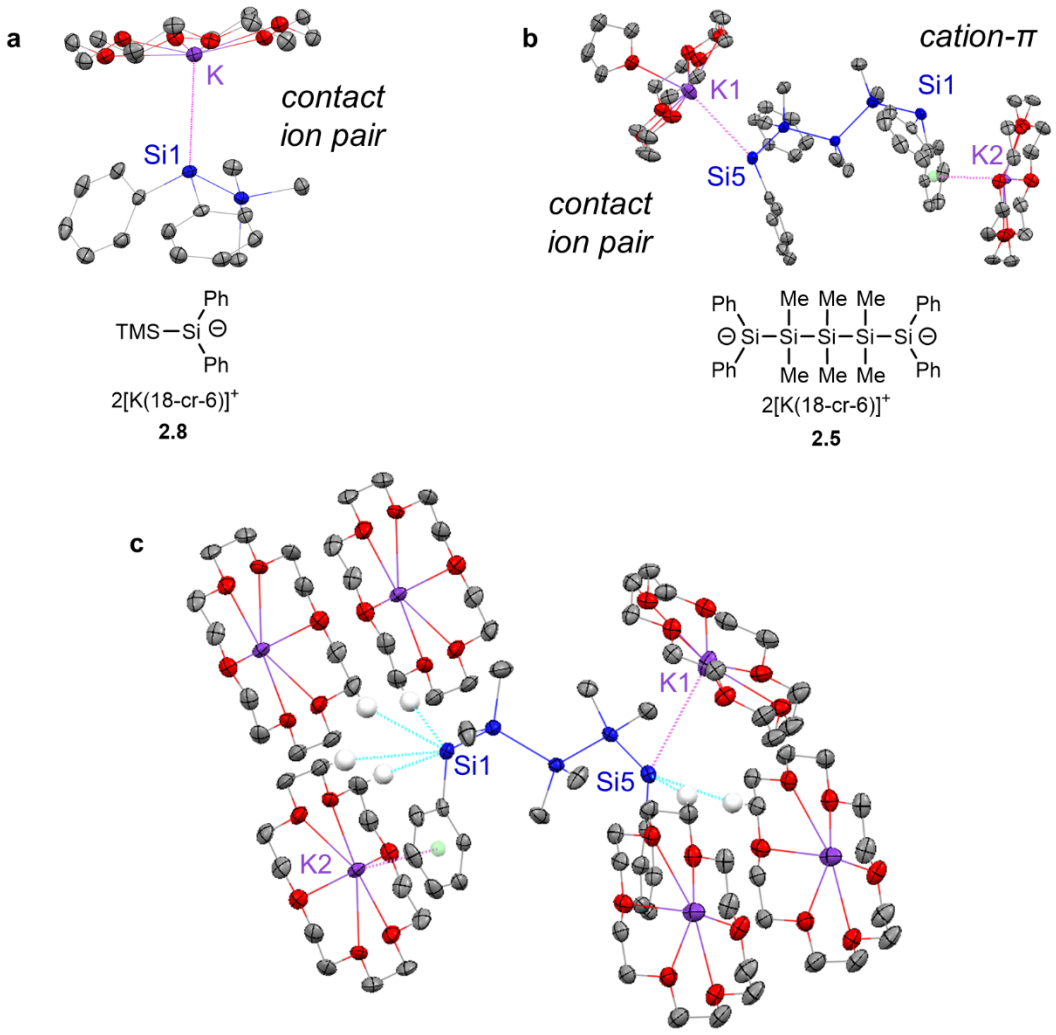

Figure 2.10. Crystal structures of (a) **2.8** and (b) **2.5**•THF. Pink lines denote cation interactions. Hydrogens and minor component of the disorder are omitted for clarity. (c) Crystal structure of **2.5** expanded to show all neighboring 18-crown-6 molecules with anion-CH contacts.

Anion-CH contacts are observed in **2.7** (Figure 2.10c). At the cation-π terminus, the anionic silicon Si1 contacts four different hydrogens atoms from three crown ether

molecules (3.159-3.414 Å). Two of the Si1-CH contacts arise from the [K(18-cr-6)]+ complex bound to a phenyl ring. Close contacts between Si5 and ethereal CHs are also observed (3.259-3.266 Å) at the other chain terminus.

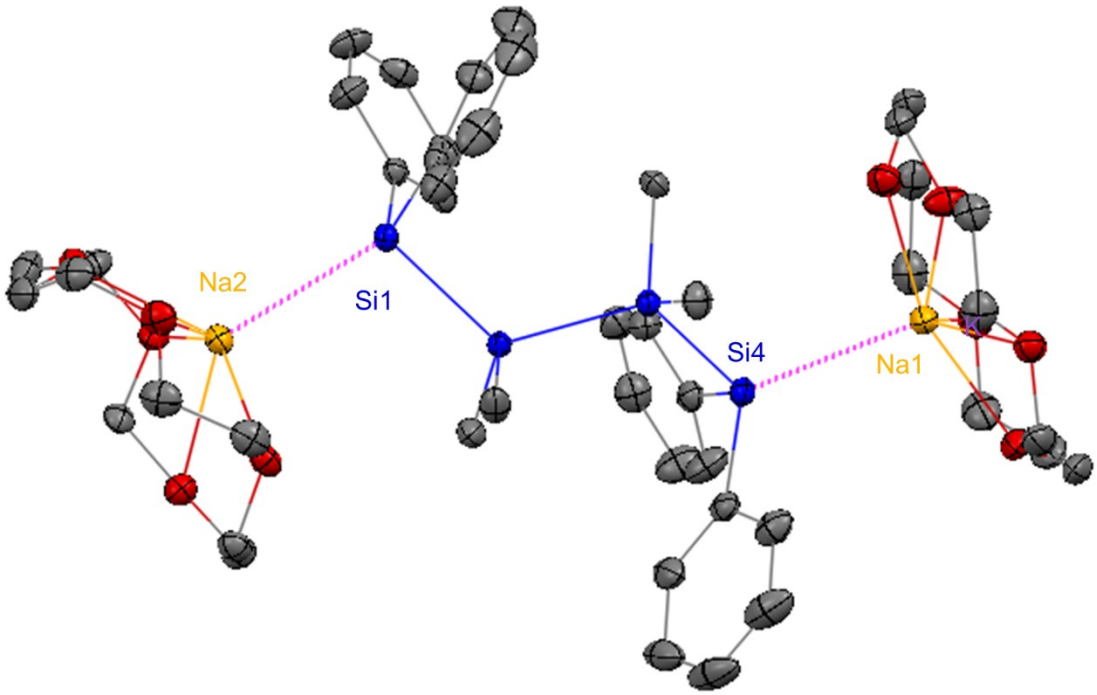

Figure 2.11. Crystal structure of **2.9**. Si1-Na2 distance: 3.0491(7) Å. Si4-Na1: 2.9691(7). Displacement ellipsoids shown at 50% probability level. Hydrogens and THF molecule omitted for clarity. Grey = carbon, blue = silicon, red = oxygen, gold = sodium.

The size of the countercation can also effect solid state structure of silanides. Disilanide **2.9**, the sodium analog of **2.6**, possesses contact-ion pairs in the solid state (Figure 2.11). Unlike **2.9**, **2.6** is not symmetrical. Si1-Na2 measures 3.0491(7) Å and Si4-Na1 measures 2.9691(7) Å, consistent with triphenylsilyl sodium (2.983(4) Å), also a contact-ion pair.[29] This suggests that steric considerations may also account for the observed cation-π interactions. Solution phase NMR of **2.6** and **2.9** taken in benzene are very similar, which suggests that both form solvent separated ion pairs (Figure 2.12).

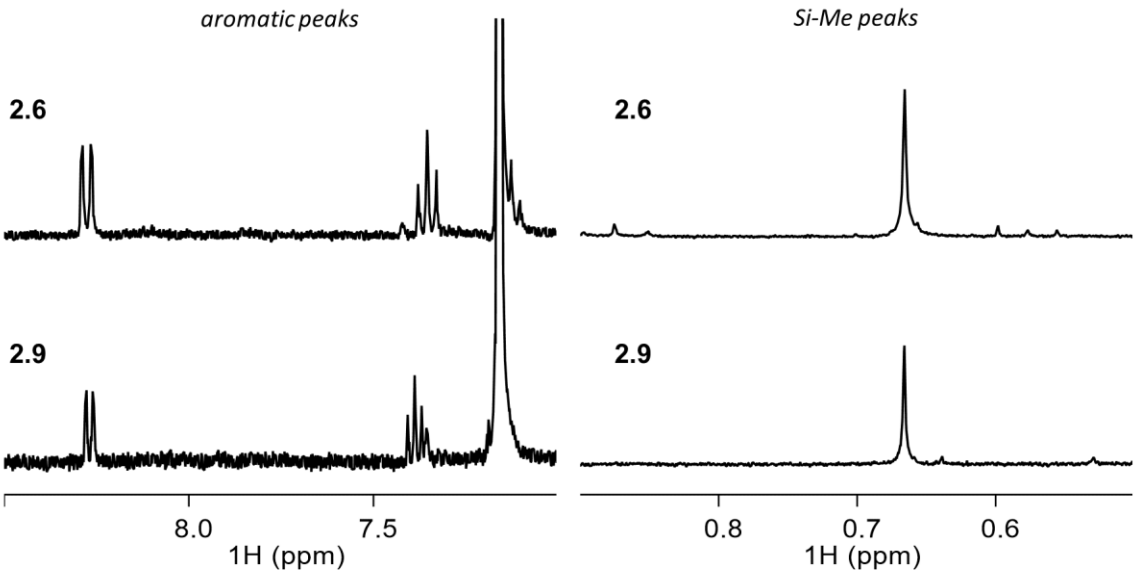

Figure 2.12. Stacked NMR spectra of **2.6** and **2.9** (C_6D_6, 400 MHz). Signals derived from the silanide core are very close in chemical shift, suggesting similar structures in solution.

The results obtained across three related $[K(18\text{-crown-6})]^+$ diphenylsilanides suggest that the Si-K bond is weak. Cooperative noncovalent interactions can outcompete the contact ion pair with the help of steric interractions. The crown ether is an integral contributor. Cation-binding delocalizes the positive charge across the $[K(18\text{-crown-6})]^+$ complex. The electrostatic potential map of the $[K(18\text{-crown-6})]^+$ complex shows positive charge character of both the central potassium and the CH bonds (Figure 2.13). This is consistant with Glendening's findings that cation binding polarizes the crown ether and

uniformly distributes greater positive charge on the methylene groups.[42]

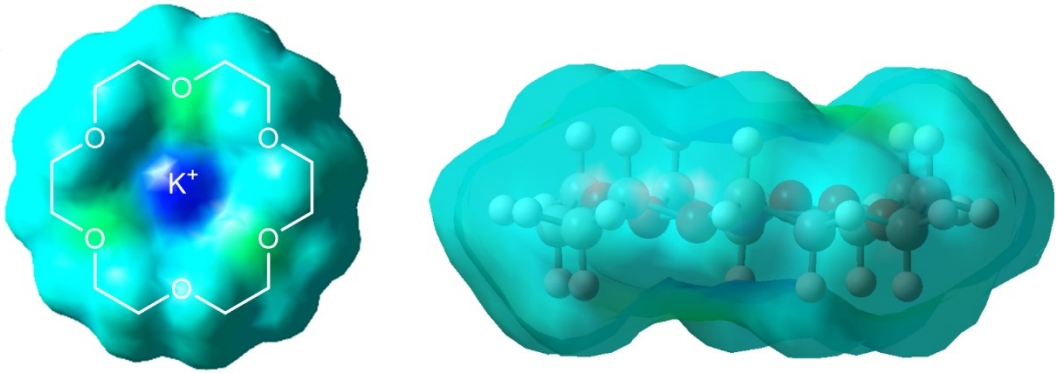

Figure 2.13. Electrostatic potential map of the $[K(18\text{-crown-6})]^+$ complex. DFT CAM-B3LYP/6-31+G(d). Values for electrostatic potential range from -63 kcal mol^{-1} (red) to 119 kcal mol^{-1} (blue).

2.5 Conclusion

A new class of diphenyl disilanides were synthesized which have orthogonal functionality to Marschner's TMS functionalized disilanides. The crystal structures of these disilanides challenge intuition of electrostatic attraction. The discussion of this chapter can help the understanding of large and complex soft cations and anions. These results have implications for understanding and predicting ion recognition events with structurally complex soft cations and anions. The findings in this chapter will educate choices in reaction conditions toward the synthesis of site-selectively functionalized cyclosilanes.

2.6. Experimental Section

All experimental procedures and data (except those listed below) can be found in *Chem. - A Eur. J.* **2017**, *23*, 15633.

General Experimental Procedures: All experiments were performed under an atmosphere of dry nitrogen or argon with the rigid exclusion of air and moisture using

standard Schlenk techniques or in a nitrogen glovebox. All glassware was oven-dried overnight in a 175 °C oven.

Instrumentation: ^{1}H NMR, ^{13}C {^{1}H} NMR, ^{29}Si {^{1}H} DEPT NMR, and ^{1}H-^{29}Si HSQC NMR spectra were recorded on either a Bruker Avance 300, 400 or III HD 400 MHz Spectrometer and chemical shifts are reported in parts per million (ppm). Spectra were recorded in benzene-d_6, chloroform-d, or tetrahydrofuran-d_8 with tetramethylsilane or the residual solvent peak as the internal standard (^{1}H NMR: C_6HD_5 δ = 7.16 ppm; $CHCl_3$, δ = 7.26 ppm, THF δ = 1.72). Multiplicities are as indicated: s (singlet), d (doublet), t (triplet), dd (doublet of doublets), m (multiplet), and br (broad). Coupling constants, *J*, are reported in Hertz and integration is provided, along with assignments, as indicated. In ^{29}Si {^{1}H} DEPT NMR and ^{1}H-^{29}Si HSQC NMR experiments evolution times are correlated to *J* coupling values reported in figure captions. Mass Spectrometry (MS) and High Resolution Mass Spectrometry (HRMS) were either performed in the Department of Chemistry at Johns Hopkins University using a VG Instruments VG70S/E magnetic sector mass spectrometer with EI (70 eV) or in the Department of Chemistry mass spectrometry facility at Columbia University using a Waters XEVO G2XS QToF mass spectrometer equipped with a UPC2 SFC inlet, electrospray ionization (ESI) probe, atmospheric pressure chemical ionization (APCI) probe, and atmospheric solids analysis probe (ASAP). The UNIlab Plus Glove Box by MBRAUN was maintained under nitrogen atmosphere. All column chromatography was performed on a Teledyne ISCO Combiflash Rf using Redisep Rf silica columns.

Computational Methods

All DFT calculations were performed using the Gaussian 09 package.[43] Geometries were optimized using the CAM-B3LYP functional with the 6-31+G(d) basis set. The Polarizable Continuum Model (PCM) was used for optimization in implicit solvent. No symmetry restrictions were applied to geometry optimizations. All optimized structures possess 0 imaginary frequencies. Coordinates used for single point calculations were adopted from the respective X-ray crystal structures. Single point calculations were performed using the CAM-B3LYP functional with the 6-31+G(d) basis set. Natural Bond Orbital (NBO) analysis was performed using NBO version 3.1.[44]

Preparation of 2.2

In a glove box, an oven dried 250 mL Schlenk flask was charged with KO*t*-Bu (2.00 equiv., 45.60 mmol, 5.13 g) and sealed with a rubber septum. The Schlenk flask was removed from the glove box and attached to a Schlenk line under argon. THF (90.0 mL) was added by syringe to the Schlenk flask. **2.1** (2.00 equiv., 45.60 mmol, 15.01 g) was added dropwise over 5 minutes by syringe to the Schlenk flask. The reaction mixture changed color from colorless to yellow to red. The reaction mixture was stirred for 2 hours.

After 2 hours, *i*PrMgCl (2M in THF, 2.00 equiv., 45.60 mmol, 22.8 mL) was added to the Schlenk flask by syringe over 10 minutes, and the solution changed color from red to a light brown/yellow color. The reaction mixture was stirred at room temperature for 30 minutes. Dichlorodimethylsilane (1.00 equiv., 22.80 mmol, 2.75 mL) was added dropwise by syringe over 5 minutes, and the reaction mixture was stirred overnight.

The reaction mixture was cooled to 0 °C in an ice-water bath. The rubber septum was removed and the reaction mixture was quenched with deionized water (100 mL) added dropwise at first, then poured after the quench is no longer vigorous. The mixture was

transferred to a separatory funnel, and the organic and aqueous layers were separated. The aqueous layer was extracted with diethyl ether (3 x 100 mL). The combined organics were dried over $MgSO_4$, filtered and concentrated to a white solid. Recrystallization of the crude solid by liquid-liquid diffusion using dichloromethane as the solvent and methanol as the anti-solvent yielded **2.2** as colorless crystals. (7.94 g, 61%).

Tabulated Characterization Data for **2.2**

^{1}H NMR	(400 MHz, $CDCl_3$) δ = 7.30 – 7.20 (m, 12H), 7.19 – 7.09 (m, 8H), 0.43 (s, 6H), 0.08 (s, 18H).
^{13}C {^{1}H} NMR	(101 MHz, $CDCl_3$) δ 136.34, 135.48, 128.24, 127.82, -0.08, -1.53.
^{29}Si {^{1}H} NMR	(79 MHz, $CDCl_3$) δ -14.45, -34.26, -41.02.
HRMS	Calcd. for $C_{32}H_{44}Si_5$: 568.2289. Found $[M]^+$: 568.2281.

Preparation of 2.5

In a glove box, an oven dry 200 mL round bottom flask with stir bar was charged with KO*t*Bu (2.00 equiv., 10.54 mmol, 1.18 g), 18-crown-6 (2.00 equiv., 10.54 mmol, 2.79 g), and diethyl ether (20.0 mL). A white suspension formed. In a separate 100 mL round bottom flask, a solution of **2.2** (1.00 equiv., 5.27 mmol, 3.00 g) in diethyl ether (20.0 mL) is prepared. The solution of **2.2** was added to the white suspension dropwise by pipette. The round bottom flask with residual **2.2** was rinsed with diethyl ether (2 x 5 mL), and added to the reaction mixture, and the round bottom flask was sealed with a rubber septum. After addition, the white suspension became a dark red suspension. The reaction was stirred overnight (15 hours).

The red precipitate was filtered, washed with diethyl ether (~40 mL), and dried under vacuum to yield **2.5** as a red powder (4.28 g, 79%).

Tabulated Characterization Data for **2.5**

^{1}H NMR (300 MHz, C_6D_6) δ = 8.39 – 8.13 (m, 8H), 7.27 (t, *J*=7.4, 8H), 7.12 – 7.04 (m, 4H), 3.13 (s, 52H), 0.67 (s, 6H).

^{13}C {^{1}H} NMR (101 MHz, C_6D_6) δ 163.07, 137.10, 126.22, 121.04, 70.22, 2.50.

^{29}Si {^{1}H} NMR (79 MHz, C_6D_6) δ -25.54, -35.18.

Preparation of 2.9

In a glove box, an oven dry 2 dram vial with stir bar was charged with NaO*t*Bu (2.00 equiv., 0.638 mmol, 0.061 g), 15-crown-5 (2.00 equiv., 0.638 mmol, 0.13 mL), and benzene (1.0 mL). In a separate 2 dram vial, a solution of **2.3** (2.00 equiv., 0.319 mmol, 0.201 g) in benzene (1.0 mL) was prepared. The solution of **2.3** was added by pipette to the other vial, and the colorless solution became red. Residual **2.3** was washed out of the vial with benzene (0.5 mL) and added to the reaction mixture. The reaction mixture was stirred for 24 hours.

After stirring overnight (~15 hours), an orange precipitate formed. The orange precipitate was filtered with a glass fritted funnel, washed with pentane, and dried under vacuum to yield **2.9** as an orange solid (0.209 g, 68%). X-ray quality crystals were grown by vapor diffusion using THF as the solvent and pentane as the anti-solvent.

Tabulated Characterization Data for **2.9**

^{1}H NMR (400 MHz, C_6D_6) δ = 8.31 – 8.23 (m, 8H), 7.43 – 7.35 (m, 8H), 3.63-2.94 (s, 115H), 0.67 (s, 12H). *A third aromatic peak overlaps with

the NMR solvent and can not be accurately integrated. Also, the broad peak from 3.63-2.94 ppm assigned to 15-crown-5 protons is extremely broad.

Single Crystal X-Ray Crystallography

2.9

All reflection intensities were measured at 110(2) K using a SuperNova diffractometer (equipped with Atlas detector) with Mo *K*α radiation (λ = 0.71073 Å) under the program CrysAlisPro (Version 1.171.36.32 Agilent Technologies, 2013). The same program was used to refine the cell dimensions and for data reduction. The structure was solved with the program SHELXS-2014/7 (Sheldrick, 2015) and was refined on F^2 with SHELXL-2014/7 (Sheldrick, 2015). Numerical absorption correction based on gaussian integration over a multifaceted crystal model was applied using CrysAlisPro. The temperature of the data collection was controlled using the system Cryojet (manufactured by Oxford Instruments). The H atoms were placed at calculated positions using the instructions AFIX 23, AFIX 43 or AFIX 137 with isotropic displacement parameters having values 1.2 or 1.5 *U*eq of the attached C atoms. The structure is partly disordered.

The asymmetric unit contains one disordered THF lattice solvent molecule. The solvent molecule is found at sites of inversion symmetry, and thus is disordered over two orientations with a constrained occupancy factor of 0.5.

Table 2.2. Experimental details for x-ray crystal structure of **2.9**.

	2.9
Crystal data	
Chemical formula	$2(C_{48}H_{72}Na_2O_{10}Si_4)\cdot C_4H_8O$
M_r	2006.89
Crystal system,	Triclinic, *P*-1

space group	
Temperature (K)	110
a, *b*, *c* (Å)	11.5920 (3), 14.2609 (3), 18.1691 (4)
α, β, γ (°)	90.2886 (18), 96.8516 (18), 110.630 (2)
V (Å^3)	2787.31 (12)
Z	1
Radiation type	Mo *K*α
μ (mm^{-1})	0.18
Crystal size (mm)	0.23 × 0.18 × 0.10
Data collection	
Diffractometer	SuperNova, Dual, Cu at zero, Atlas
Absorption correction	Gaussian *CrysAlis PRO*, Agilent Technologies, Version 1.171.36.32 (release 02-08-2013 CrysAlis171 .NET) (compiled Aug 2 2013,16:46:58) Numerical absorption correction based on gaussian integration over a multifaceted crystal model
T_{min}, T_{max}	0.762, 1.000
No. of measured, independent and observed [$I > 2\sigma(I)$] reflections	42778, 12796, 10623
R_{int}	0.029
$(\sin\theta/\lambda)_{max}$ (Å^{-1})	0.650
Refinement	
$R[F^2 > 2\sigma(F^2)]$, $wR(F^2)$, S	0.039, 0.096, 1.04
No. of reflections	12796
No. of parameters	626
No. of restraints	36
H-atom treatment	H-atom parameters constrained
$\Delta\rho_{max}$, $\Delta\rho_{min}$ (e Å^{-3})	0.49, -0.27

Computer programs: *CrysAlis PRO*, Agilent Technologies, Version 1.171.36.32 (release

02-08-2013 CrysAlis171 .NET) (compiled Aug 2 2013, 16:46:58), *SHELXS2014*/7 (Sheldrick, 2015), *SHELXL2014*/7 (Sheldrick, 2015), *SHELXTL* v6.10 (Sheldrick, 2008).

2.7 References

(1) Colvin, E. W. *Silicon Reagents in Organic Synthesis*; Academic Press: London, 1988.
(2) Nöth, H.; Höllerer, G. *Angew. Chemie Int. Ed. English* **1962**, *1* (10), 551–552.
(3) Wiberg, N.; Lerner, H.-W.; Vasisht, S.-K.; Wagner, S.; Karaghiosoff, K.; Nöth, H.; Ponikwar, W. *Eur. J. Inorg. Chem.* **1999**, *1999* (8), 1211–1218.
(4) Marschner, C. **2006**.
(5) Gilman, H.; Smith, C. L. *J. Organomet. Chem.* **1968**, *14* (1), 91–101.
(6) Kornev, A. N. *Russ. Chem. Rev.* **2004**, *73* (11), 1065–1089.
(7) Fischer, R.; Konopa, T.; Ully, S.; Baumgartner, J.; Marschner, C. *J. Organomet. Chem.* **2003**, *685* (1–2), 79–92.
(8) Flock, M.; Marschner, C. *Chem. - A Eur. J.* **2005**, *11* (16), 4635–4642.
(9) Hopkinson, A. C.; Lien, M. H. *Tetrahedron* **1981**, *37* (6), 1105–1112.
(10) Tamao, K.; Kawachi, A.; Asahara, M.; Toshimitsu, A. *Pure Appl. Chem.* **1999**, *71* (3), 393–400.
(11) Tamao, K.; Kawachi, A. *Angew. Chemie Int. Ed. English* **1995**, *34* (7), 818–820.
(12) Molev, G.; Bravo-Zhivotovskii, D.; Karni, M.; Tumanskii, B.; Botoshansky, M.; Apeloig, Y. *J. Am. Chem. Soc.* **2006**, *128* (9), 2784–2785.
(13) Tamao, K.; Nagata, K.; Asahara, M.; Kawachi, A.; Ito, Y.; Shiro, M. *J. Am. Chem. Soc.* **1995**, *117* (46), 11592–11593.
(14) Dias, H. V. R.; Olmstead, M. M.; Ruhlandt-Senge, K.; Power, P. P. *J. Organomet. Chem.* **1993**, *462* (1–2), 1–6.
(15) Klinkhammer, K. W.; Becker, G.; Schwarz, W. *Organosilicon Chemistry II*; Auner, N., Weis, J., Eds.; Wiley, 1995.
(16) Reich, H. J. *Chem. Rev.* **2013**, *113* (9), 7130–7178.
(17) Gutekunst, G.; G. Brook, A. *J. Organomet. Chem.* **1982**, *225* (1), 1–3.
(18) Strohmann, C.; Däschlein, C. *Chem. Commun.* **2008**, No. 24, 2791.
(19) Gessner, V. H.; Däschlein, C.; Strohmann, C. *Chem. - A Eur. J.* **2009**, *15* (14), 3320–3334.
(20) Kleeberg, C.; Borner, C. *Eur. J. Inorg. Chem.* **2013**, *2013* (15), 2799–2806.
(21) Klink, R.; Schrenk, C.; Schnepf, A. *Dalt. Trans.* **2014**, *43* (42), 16097–16104.
(22) Fischer, R.; Frank, D.; Gaderbauer, W.; Kayser, C.; Mechtler, C.; Baumgartner, J.; Marschner, C. *Organometallics* **2003**, *22* (18), 3723–3731.
(23) Wallner, A.; Hlina, J.; Konopa, T.; Wagner, H.; Baumgartner, J.; Marschner, C.; Flörke, U. *Organometallics* **2010**, *29* (12), 2660–2675.
(24) Fischer, R.; Konopa, T.; Baumgartner, J.; Marschner, C. *Organometallics* **2004**, *23* (8), 1899–1907.
(25) Kayser, C.; Kickelbick, G.; Marschner, C. *Angew. Chemie Int. Ed.* **2002**, *41* (6), 989–992.
(26) Blanton, J. R.; Diminnie, J. B.; Chen, T.; Wiltz, A. M.; Xue, Z. *Organometallics*

2001, *20* (26), 5542–5546.
(27) Jenkins, D. M.; Teng, W.; Englich, U.; Stone, D.; Ruhlandt-Senge, K. *Organometallics* **2001**, *20* (22), 4600–4606.
(28) Kayser, C.; Fischer, R.; Baumgartner, J.; Marschner, C. *Organometallics* **2002**, *21* (6), 1023–1030.
(29) Leich, V.; Lamberts, K.; Spaniol, T. P.; Okuda, J. *Dalt. Trans.* **2014**, *43* (38), 14315–14321.
(30) Krempner, C.; Chisholm, M. H.; Gallucci, J. *Angew. Chemie Int. Ed.* **2008**, *47* (2), 410–413.
(31) Li, H.; Hope-Weeks, L. J.; Krempner, C. *Chem. Commun.* **2011**, *47* (14), 4117.
(32) Teng, W.; Englich, U.; Ruhlandt-Senge, K. *Angew. Chemie - Int. Ed.* **2003**, *42* (31), 3661–3664.
(33) Marshall, M. S.; Steele, R. P.; Thanthiriwatte, K. S.; Sherrill, C. D. *J. Phys. Chem. A* **2009**, *113* (48), 13628–13632.
(34) Gessner, V. H.; Strohmann, C. *J. Am. Chem. Soc.* **2008**, *130* (44), 14412–14413.
(35) Olah, G. A.; Hunadi, R. J. *J. Am. Chem. Soc.* **1980**, *102* (23), 6989–6992.
(36) Qiao, B.; Anderson, J. R.; Pink, M.; Flood, A. H.; Moruzzi, M. S.; Vacca, A.; Raghavachari, K.; Flood, A. H. *Chem. Commun.* **2016**, *52* (56), 8683–8686.
(37) Flood, A. H. *Beilstein J. Org. Chem.* **2016**, *12* (1), 611–627.
(38) Li, Y.; Flood, A. H. *Angew. Chemie Int. Ed.* **2008**, *47* (14), 2649–2652.
(39) Hartle, M. D.; Hansen, R. J.; Tresca, B. W.; Prakel, S. S.; Zakharov, L. N.; Haley, M. M.; Pluth, M. D.; Johnson, D. W. *Angew. Chemie Int. Ed.* **2016**, *55* (38), 11480–11484.
(40) Yawer, M. A.; Havel, V.; Sindelar, V. *Angew. Chemie - Int. Ed.* **2015**, *54* (1), 276–279.
(41) Okumoto, H.; Yatabe, T.; Richter, A.; Peng, J.; Shimomura, M.; Kaito, A.; Minami, N. *Adv. Mater.* **2003**, *15* (9), 716–720.
(42) Glendening, E. D.; Feller, D.; Thompson, M. A. *J. Am. Chem. Soc.* **1994**, *116* (23), 10657–10669.
(43) Gaussian 09, Revision D.01, M. J. Frisch, G. W. Trucks, H. B. Schlegel, G. E. S.; M. A. Robb, J. R. Cheeseman, G. Scalmani, V. Barone, B. Mennucci, G. A. Petersson, H.; Nakatsuji, M. Caricato, X. Li, H. P. Hratchian, A. F. Izmaylov, J. Bloino, G. Zheng, J. L.; Sonnenberg, M. Hada, M. Ehara, K. Toyota, R. Fukuda, J. Hasegawa, M. Ishida, T.; Nakajima, Y. Honda, O. Kitao, H. Nakai, T. Vreven, J. A. Montgomery, Jr., J. E. P.; F. Ogliaro, M. Bearpark, J. J. Heyd, E. Brothers, K. N. Kudin, V. N. Staroverov, T. K.; R. Kobayashi, J. Normand, K. Raghavachari, A. Rendell, J. C. Burant, S. S. Iyengar, J.; Tomasi, M. Cossi, N. Rega, J. M. Millam, M. Klene, J. E. Knox, J. B. Cross, V. Bakken, C.; Adamo, J. Jaramillo, R. Gomperts, R. E. Stratmann, O. Yazyev, A. J. Austin, R. C.; C. Pomelli, J. W. Ochterski, R. L. Martin, K. Morokuma, V. G. Zakrzewski, G. A. Voth, P.; Salvador, J. J. Dannenberg, S. Dapprich, A. D. Daniels, O. Farkas, J. B. Foresman, J. V.; Ortiz, J. Cioslowski, and D. J. Fox, Gaussian, Inc., Wallingford CT, 2013. .
(44) NBO Version 3.1, Glendening, E. D.; Reed, A. E.; Carpenter, J. E.; Weinhold, F. .

Chapter 3: Synthesis of a Fragment of Crystalline Silicon: Poly(Cyclosilane)

The work presented in this chapter has been published as:

Press, E. M.; Marro, E. A.; Surampudi, S. K.; Siegler, M. A.; Tang, J. A.; Klausen, R. S. *Angew. Chem., Int. Ed*. **2017**, *56*, 568.

Mr. Eric Marro optimized the synthesis of **3.3** from commercially available starting materials. Additionally, Eric Marro aided in the NMR characterization and grew X-ray quality crystals of **1,4Si$_6$**.

Dr. Eric Press optimized the synthesis of **1,4Si$_6$** from compound **3.3**, polymerized **1,4Si$_6$** to yield poly(**1,4Si$_6$**), and further functionalized poly(**1,4Si$_6$**) by hydrosilylation. He also characterized the monomer, polymer, and functionalized polymer by IR, NMR, and UV-Vis spectroscopy and GPC.

Dr. Sravan Surampudi performed initial synthesis of **1,4Si$_6$** from commercially available starting materials as well as initial polymerization of **1,4Si$_6$**.

Dr. Maxime Siegler obtained single crystal x-ray data and solved crystal structures.

Dr. Joel Tang suggested NMR techniques for characterization of poly(**1,4Si$_6$**) and helped interpret spectra.

3.1 Introduction

Preparation of complex silicon-based polymers is limited by the complexity of available monomers and scope of synthetic methods. Even with the limitations outlined in chapter one, polymers derived from Wurtz polymerization show some diversity through varying the organic side chain. Polysilanes with large alkyl side introduce steric repulsions that induce a distorted *transoid* conformation (ω = 165°). This results in the linear

polysilane to adopt a helical global conformation instead of a rigid rod. Theoretical studies on small model systems, circular dichroism, and x-ray diffraction all provide evidence for this.[1–4] Fujiki observed a spectrum of global structures by changing the position of a stereogenic methyl group located on the side chain.[5,6] Changes in global structure were accompanied by changes in the sharpness, intensity, and energy of absorbance spectra.

Few examples of polymers with complex polysilane backbones derived from Wurtz polymerization exist.[7] Reductive coupling of alkyltrichlorosilanes ((*n*-hexyl)$SiCl_3$) produced a random network polymer of fused silicon rings.[8] The network polymer had a redshifted onset of absorption of ca. 50 nm compared to a linear polysilane.

The Klausen group takes inspiration from substructures found in crystalline silicon to design site-selective cyclohexasilane building blocks. One such subunit is a linear chain of cyclohexasilane units (Figure 3.1a). Designing a building block for this substructure, one could imagine a six-membered ring with reactive groups in the 1 and 4 positions (Figure 3.1b).

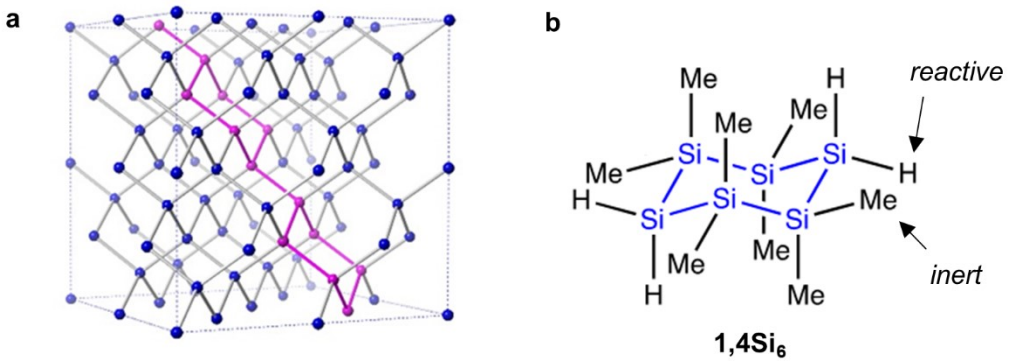

Figure 3.1. (a) Crystalline silicon lattice with cyclohexasilane subunits highlighted in pink. (b) **1,4Si$_6$**, the directional building block designed from the pink substructure in the silicon lattice.

Synthesis of site-selective cyclohexasilanes is not trivial. Reductive coupling of diphenyldichlorosilane and dichlorotetramethyldisilane with lithium produces a 1,4

functionalized cyclic silane in 2% yield (Scheme 3.1a).[9] Unselective chlorination of a permethylated cyclohexasilane produces a difficult to separate mixture of 1,3 and 1,4 functionalized isomers (Scheme 3.1b).[10] Salt metathesis of disilanides and dihalosilanes was a promising synthetic route, but conversion of all four TMS groups to hydrogen atoms did not work (Scheme 3.1c).[11]

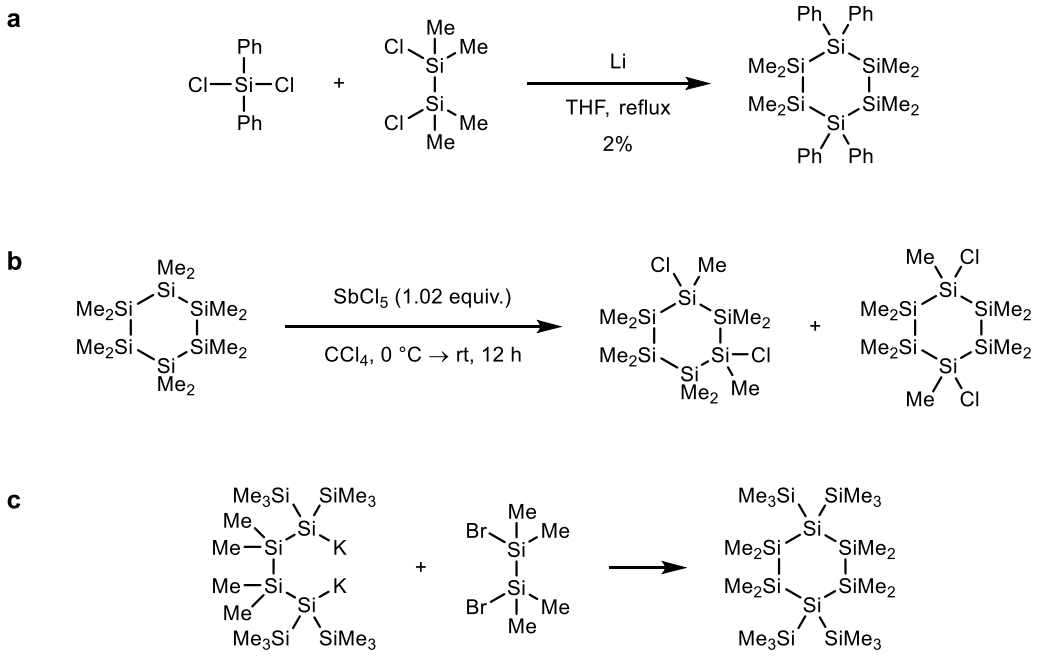

Scheme 3.1. Synthetic methods for site-selective cyclohexasilanes. (a) Reductive coupling. (b) Unselective chlorination. (c) Salt metathesis.

3.2 Scale-up and Improvements to Synthesis of 1,4Si$_6$

The first synthesis of **1,4Si$_6$** was developed by Dr. Sravan Surapundi (Scheme 3.2) was an impressive four step synthesis. When he left the group, he left the synthesis of **1,4Si$_6$** at a 100 milligram scale. Scale-up and optimization of this synthesis led to higher yields. Improvements included the use of less hazardous reagents and reducing waste by eliminating purification by column chromatography, two green chemistry principles[12]. These improvements allowed an easy, comprehensive study of polymerization conditions and polymer characterization.

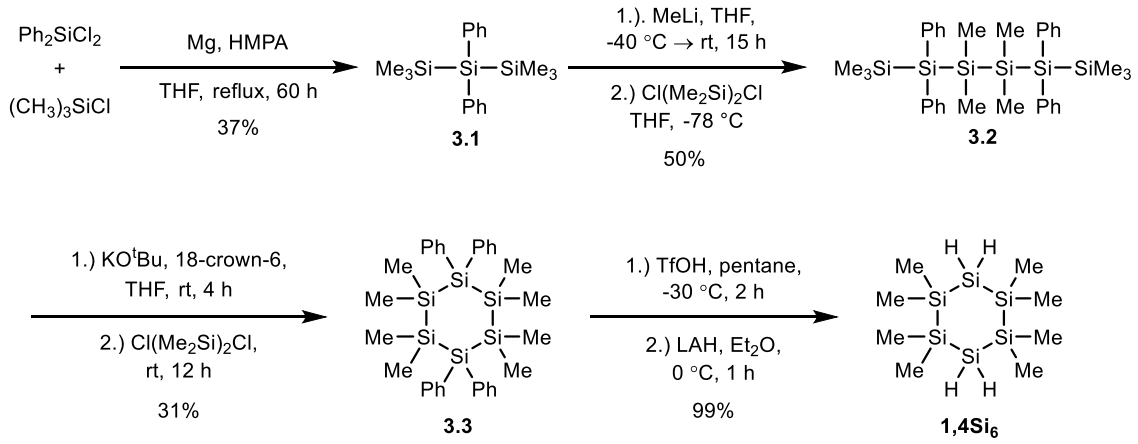

Scheme 3.2. Dr. Surampudi synthesis of **1,4Si$_6$**, with an overall yield of 5.7%.

The synthesis of **3.1** saw many improvements. Stir rate can have a strong effect on heterogeneous chemistry.[13] Consistent use of a high stir rate increased the yield of **3.1** from 37% to 41%. Isolation of **3.1** by distillation instead of column chromatography reduced solvent waste for this multi-decagram scale reaction. Controlled, slow addition of the chlorosilane reagents to the stirred magnesium suspension later improved the yield to 61% yield.

A better understanding of the silanide formation in the synthesis of **3.2** was important. Formation of the silanide initially proceeded by the removal of a TMS group from **3.1** with methyllithium to produce a known lithium silanide.[14] The starting material is completely consumed after only adding 0.8 equivalents of methyllithium, instead of the expected 1.0 equivalent. Excess methyllithium, upon addition of the chlorosilane, could cause multiple side reactions; salt metathesis with the chlorosilane and silicon-silicon bond breakage (Scheme 3.3). When only 0.8 equivalents of methyllithium was used, yields increased from 50% to 70% yield.

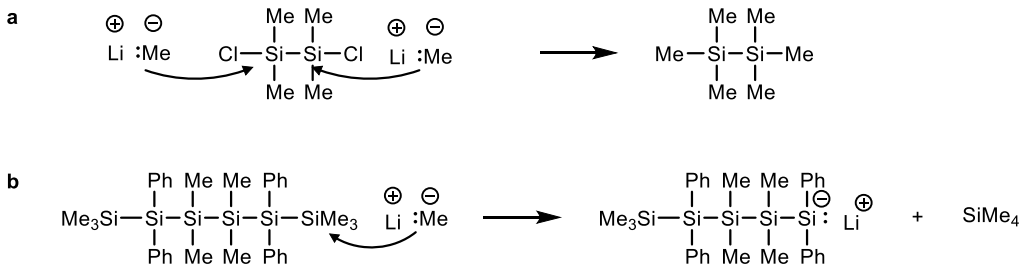

Scheme 3.3. Possible side reactions from excess methyllithium. (a) Salt metathesis with a chlorosilane (b) Silicon-silicon bond breaking.

Further improvements to the synthesis of **3.2** provided a greener procedure. KO*t*Bu replaced the pyrophoric methyllithium in the silanide formation step, which made the reaction safe enough for undergraduates to perform. To achieve a comparable yield, the potassium had to be added to the chlorosilane. When the potassium cation is exchanged with *i*PrMgCl, the method of combining the silanide and chlorosilane was no longer relevant, and it provided the highest yield. Lastly, **3.2** purification by column chromatography was replaced by liquid diffusion recrystallization using dichloromethane as the solvent and methanol as the anti-solvent.

Isolation of disilanide **3.4** led to the studies outlined in chapter 2. Findings of these studies doubled of the yield of **3.3** from **3.2**. Exchange of the potassium disilanide to magnesium did not have a significant effect on the yield of **3.3**, a stark contrast from other reactions. Dearylation of **3.3** with five equivalents of triflic acid forms a tetrasilyltriflate *in situ*.[15] Reduction of this silyl triflate with 2.4 equivalents of lithium aluminum hydride[16] and isolation by sublimation provided **1,4Si$_6$** in a 79% yield. The overall yield of **1,4Si$_6$** has seen almost a fourfold increase to 20.8%.

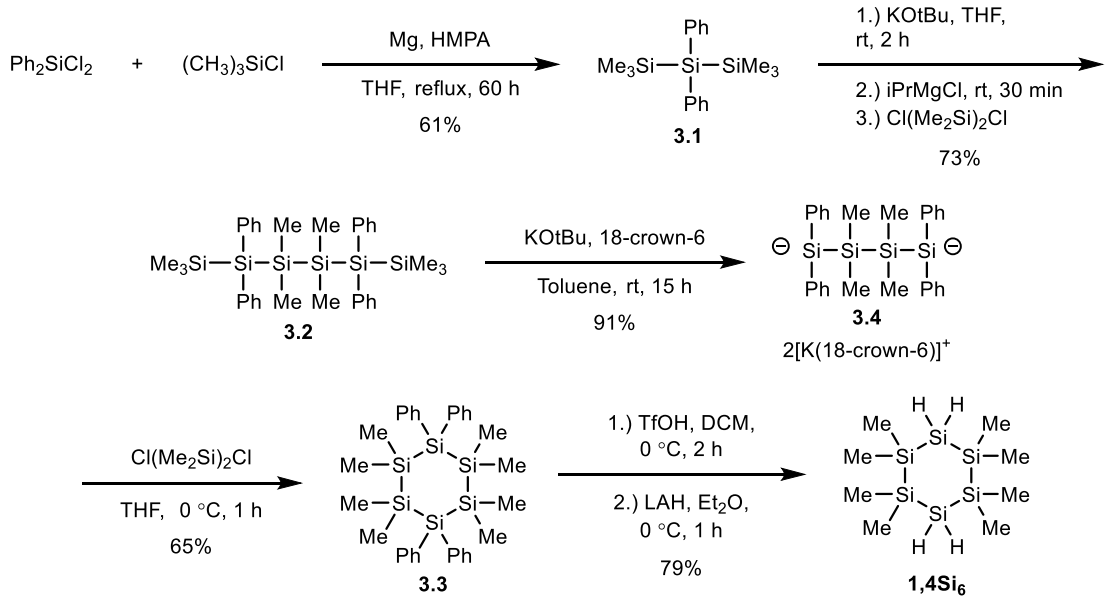

Scheme 3.4. Improved synthesis of **1,4Si$_6$**.

3.3 Characterization of 1,4Si$_6$

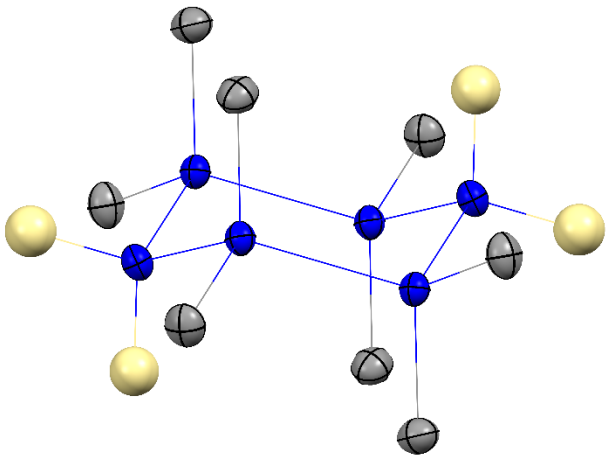

Figure 3.2. Crystal structure of **1,4Si$_6$**. Blue = silicon, grey = carbon, gold = hydrogen. Some hydrogen atoms are omitted for clarity. Thermal ellipsoids for non-hydrogen atoms are set at the 50% probability.

Single-crystal x-ray crystallography provides evidence that **1,4Si$_6$** favors the chair conformation in the solid state. Sublimation of **1,4Si$_6$** provided single crystals suitable for x-ray crystallography (Figure 3.2). The molecule is found at sites of inversion symmetry

and only one-half of **1,4Si$_6$** is crystallographically independent. The Si-Si-Si bond angle at SiH_2 is wider (115.591(16)°) than the $SiMe_2$ positions (108.351(16)° and 09.329(16)°).

1,4Si$_6$ possess C_{2h} symmetry in the chair conformation, predicting unique ^{1}H NMR for axial and equatorial protons and methyl groups. However, only two ^{1}H NMR signals are seen, one for the Si-H protons (3.27 ppm) and another for the methyl group protons (0.31 ppm). This observation is consistent with rapid chair flipping.[17] Two signals are observed in the ^{29}Si {^{1}H} NMR DEPT (Distortionless Enhancement by Polarization Transfer) spectrum of **1,4Si$_6$**. Assignment of the $SiMe_2$ (-39.35 ppm) and SiH_2 (-101.28 ppm) silicon atoms are typical for silicon atoms with those substituents.[18] These assignments are supported by 2D NMR spectroscopy. In the ^{1}H-^{29}Si HSQC (Heteronuclear Single Quantum Coherence) NMR spectrum, a correlation is seen between the 0.31 ppm ^{1}H signal and -39.35 ^{29}Si NMR signal. A second correlation is seen between the 3.27 ppm ^{1}H signal and -101.28 ppm ^{29}Si NMR signal (Figure 3.3).

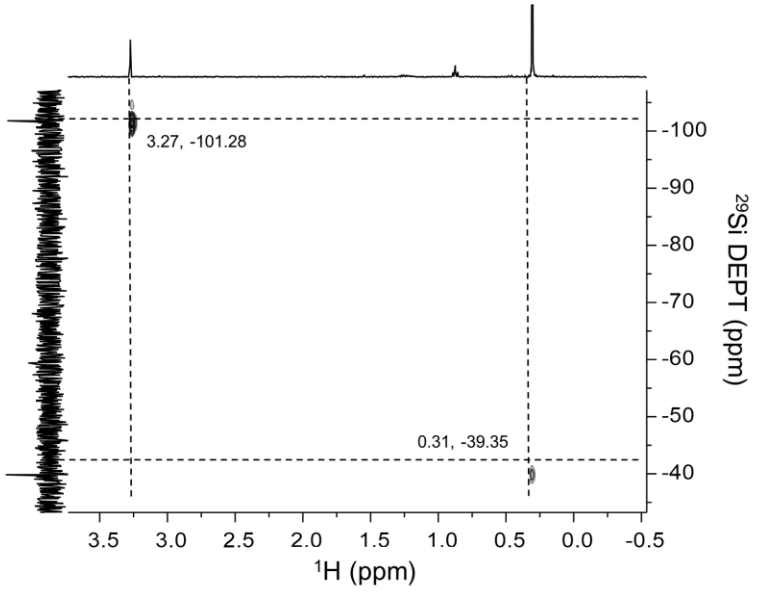

Figure 3.3. ^{1}H-^{29}Si HSQC NMR spectrum (C_6D_6, 400 MHz) of **1,4Si$_6$**. J coupling value for evolution time $^1J_{SiH}$ = 120 Hz. Cross peaks show correlation between ^{1}H and ^{29}Si nuclei.

The ATR-IR spectrum of **1,4Si6** is interesting (Figure 3.4). Two peaks are seen in the Si-H stretching region (2074, 2100 cm^{-1}), and a shoulder can be seen in the Si-Me stretching peak (1241 cm^{-1}). One possible explanation could be distinct stretching frequencies for axial and equatorial bond stretches. A second explanation is multiple ring conformations contribute to the collected spectrum. Flock concurrently observes chair and twist-boat conformations of dodecamethylcyclohexasilane at room temperature by raman spectroscopy.[19] Lastly, an Si-O-Si stretch (1021 cm^{-1}) is observed due to the autooxidation of **1,4Si6**, a known phenomenon of protonated oligosilanes.[20]

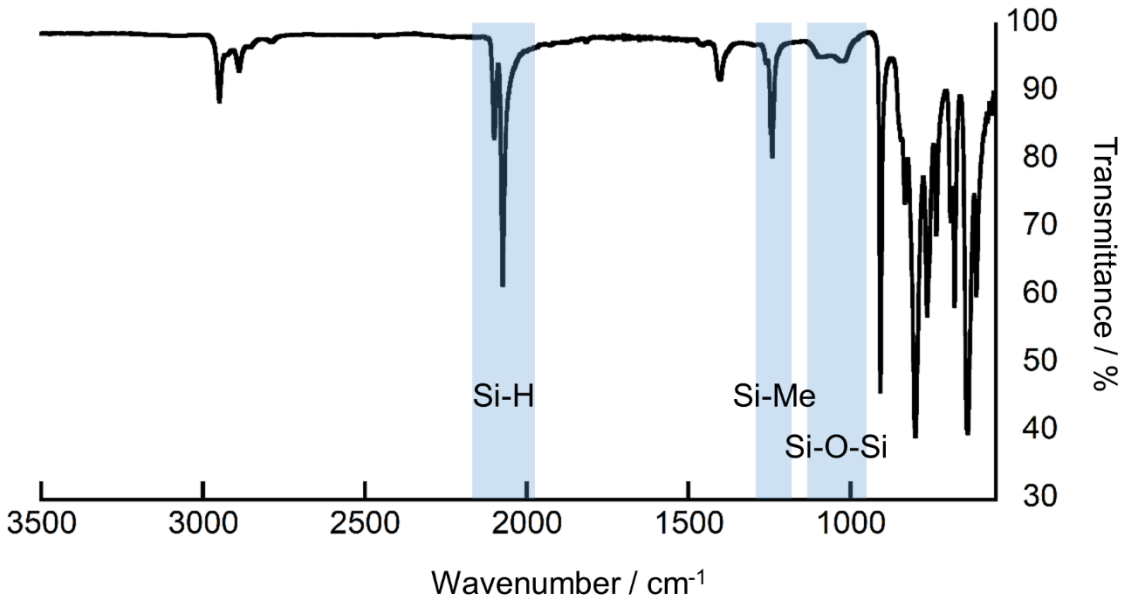

Figure 3.4. ATR-IR spectrum of **1,4Si6**. Peaks for Si-H, Si-Me and Si-O-Si stretches are labeled.

3.4 Polymerization and Structural Determination

Transition-metal metallocenes are known to promote dehydrocoupling of silanes.[21] Dehydrocoupling polymerization is sensitive to the degree of silane substitution. Primary silanes react faster than secondary silanes under mild conditions while tertiary silanes do

not react.[22–24] Dehydrocoupling polymerization is a step-growth polymerization. The first Si-Si bond formation in the polymerization of a primary silane produces a secondary silane which couple further to form polymer (Scheme 3.5a). **1,4Si$_6$** is a secondary silane; however, upon the first Si-Si bond formation, the chain termini are still secondary silanes (Scheme 3.5b). Dehydrocoupling of **1,4Si$_6$** using mild conditions typical of primary silanes and more forcing conditions typical of secondary silanes yield polymers of similar structure (Table 3.1), with nearly identical ^{1}H NMR spectra.

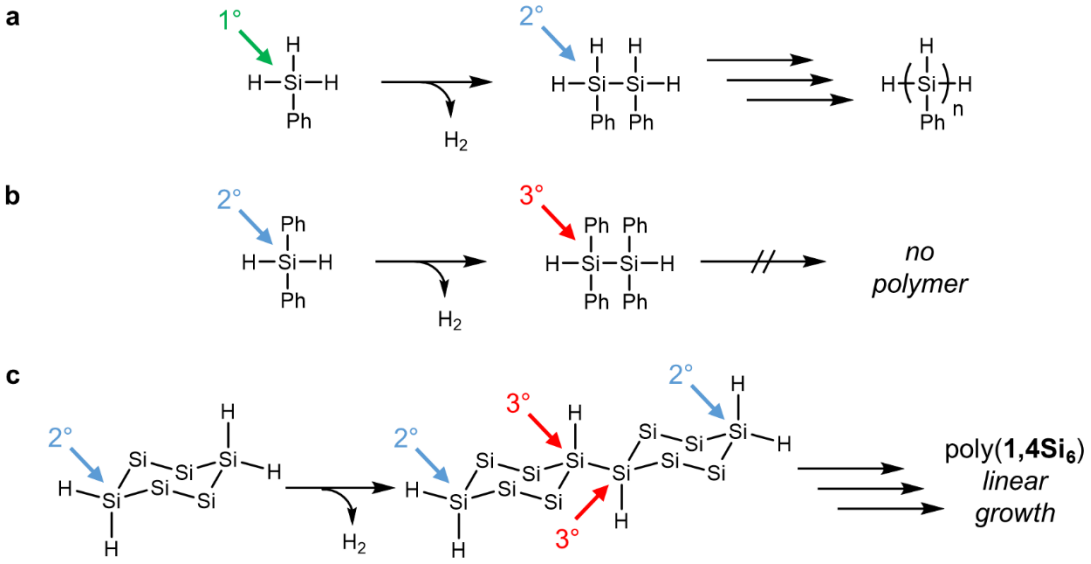

Scheme 3.5. Dehydrocoupling polymerization favors linear growth over branching. (a) Dimerization of a primary silane yields a secondary silane, which is still reactive. (b) Dimerization of a secondary silane yields a tertiary silane, which is not reactive (c) Dimers of **1,4Si$_6$** possess secondary silane termini which are reactive and tertiary silanes which are not reactive.

^{1}H NMR spectroscopy supports polymerization; the sharp Si-H signal of **1,4Si$_6$** is replaced by a family of broad and poorly defined Si-H signals between 3.10 and 3.40 ppm. In addition, a broad set of peaks is observed for the Si-Me groups (0.35 – 0.55 ppm). (Figure 3.5) Both sets of peaks diffuse at the same rate in ^{1}H DOSY NMR spectroscopy,

and at a different rate than molecular species such as residual solvent and catalyst (Figure 3.6)

Table 3.1. Polymerization Conditions

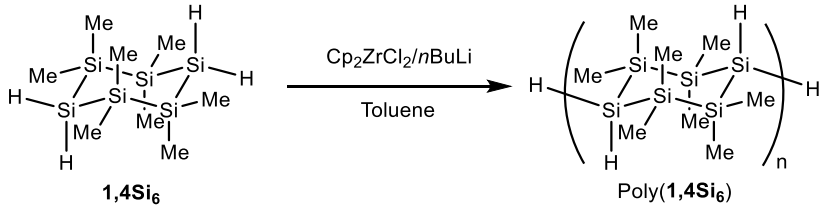

Entry	Catalyst	Temp (°C)	Time (h)	M_n (Da)	M_w/M_n
Primary	Cp_2ZrCl_2/*n*BuLi	25 °C	24	2771	1.31
Secondary	Cp_2ZrCl_2/*n*BuLi	90 °C	90	2299	1.51

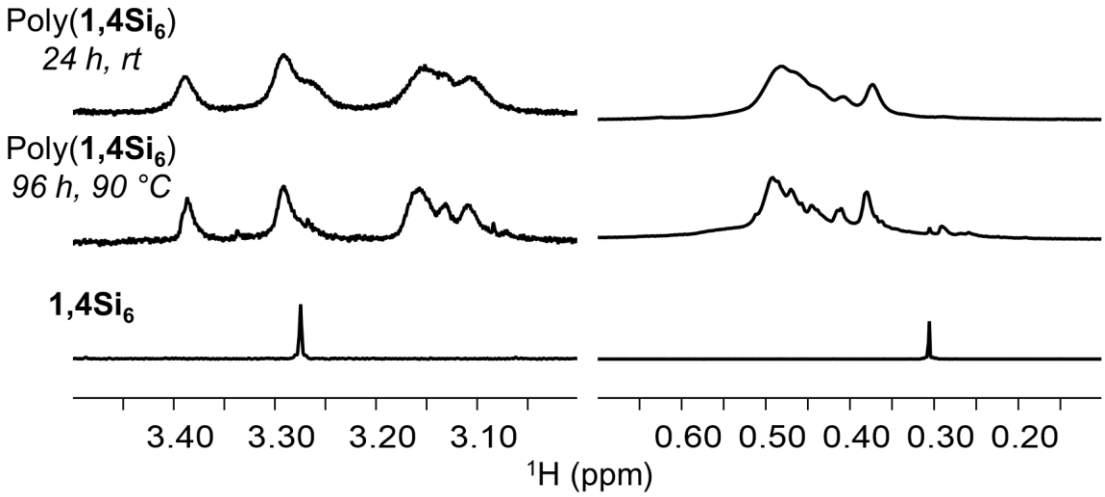

Figure 3.5. Comparing ^{1}H NMR spectra of poly(**1,4Si$_6$**) derived from both polymerization conditions and **1,4Si$_6$**.

^{29}Si NMR spectroscopy provides much structural information about poly(**1,4Si$_6$**) (Figure 3.7). In the ^{29}Si {^{1}H} DEPT NMR spectrum, three sets of peaks are observed around -35, -102, and -120 ppm. The -35 ppm set of peaks is assigned to dimethylated silanes. The peaks at -102 and -120 ppm are consistent with protonated silanes with differing number of silane substituents. Increased silane branching results in a large

difference in chemical shift between secondary, tertiary, and quaternary silanes which could result from end groups, linear polymer growth and branched polymer growth. The ^{29}Si NMR spectra of an authentic sample of **3.4** was used to assign the peak at -102 ppm of poly(**1,4Si$_6$**) to the secondary silane end groups and the set of signals at -120 ppm to internal tertiary silanes. No signals consistent with quaternary silanes that would arise from a branched polymer were observed (Si(SiMe$_3$)$_4$ = -135.5 ppm).

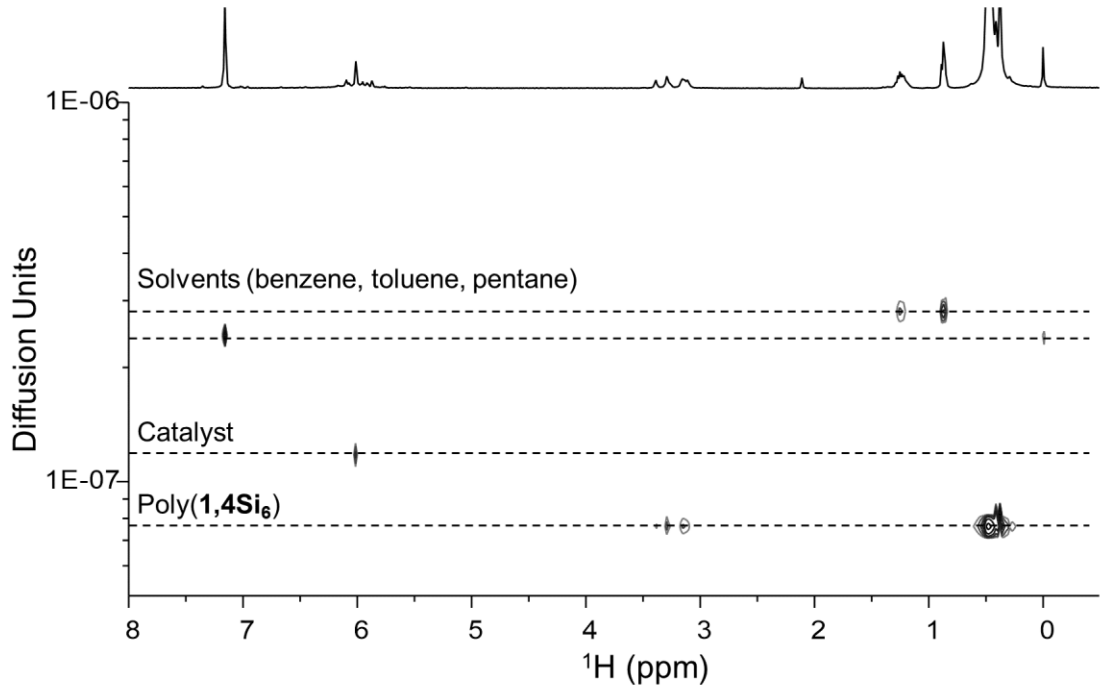

Figure 3.6. ^{1}H NMR DOSY spectrum of poly(**1,4Si$_6$**). Different diffusion rates help differentiate signals assigned to poly(**1,4Si$_6$**) from signals assigned to molecular species (solvent and residual catalyst).

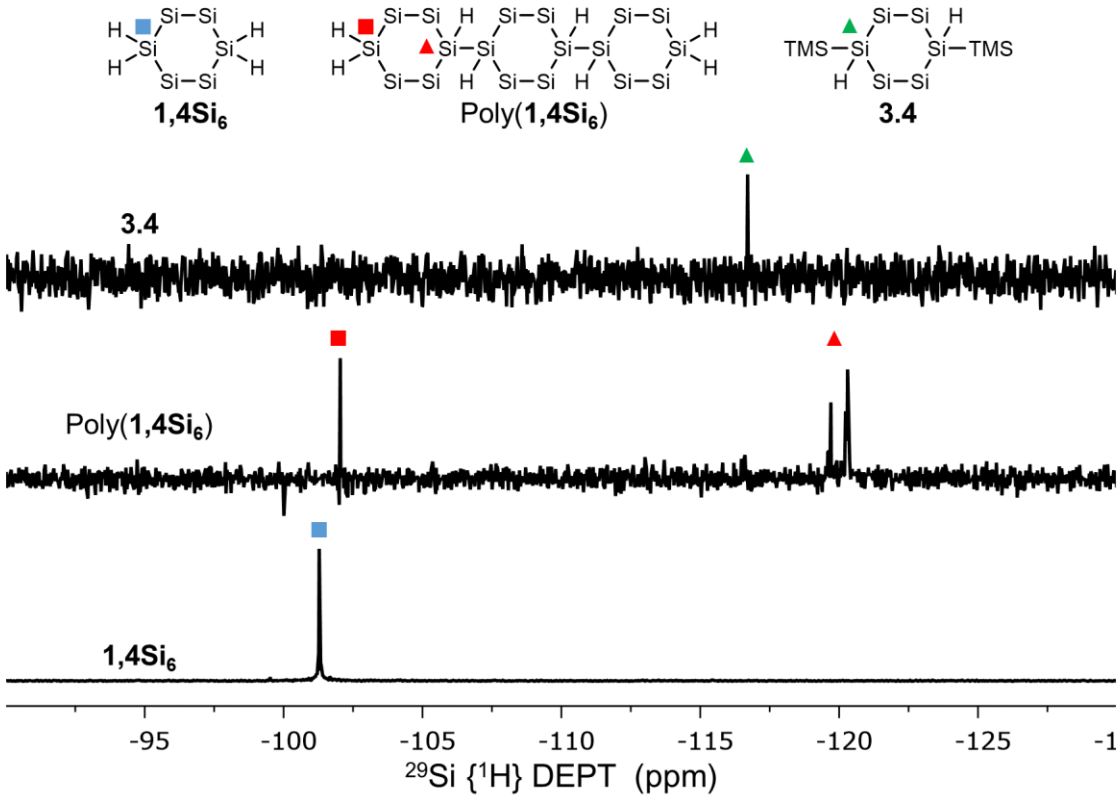

Figure 3.7. Structures of **1,4Si$_6$**, poly (**1,4Si$_6$**), and **3.4** (implicit methyl groups) with their respective assignments in ^{29}Si{^{1}H} DEPT NMR (C_6D_6). Squares (■) indicate secondary silanes and triangles (▲) indicate tertiary silanes.

These assignments are further supported by the ^{1}H-^{29}Si coupling patterns in the ^{29}Si INEPT+ NMR spectrum (Figure 3.8). Dimethylated silicon peaks at -35 ppm appear as weak singlets. Signals assigned to internal tertiary silanes at -120 ppm appear as a set of doublets ($^1J_{SiH}$ = 158.2-157.9 Hz). The peak assigned to secondary silane end groups at -102 ppm is a triplet ($^1J_{SiH}$ = 170.5 Hz). Finally, ^{1}H-^{29}Si HSQC NMR spectroscopy assigned ^{1}H NMR signals for protons attached to secondary and tertiary silanes. (Figure 3.8). Protons attached to secondary silanes are assigned to two broad signals at 3.39 ppm and

3.29 ppm, while protons attached to tertiary silanes are assigned to a signal at 3.26 ppm and a family of signals centered at 3.13 ppm.

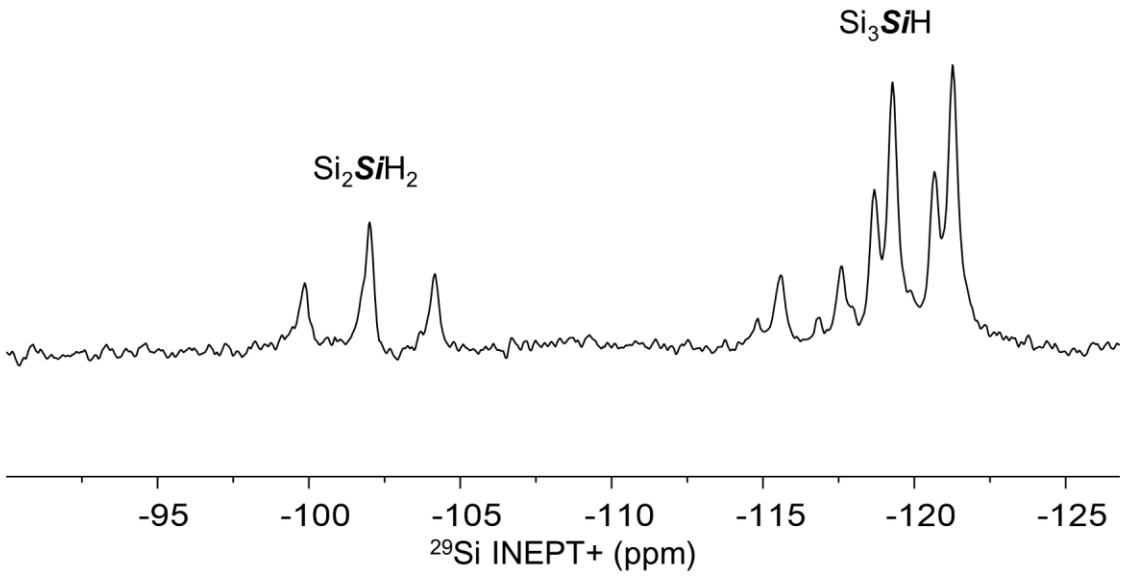

Figure 3.8. ^{29}Si INEPT+ specrum of poly(**1,4Si$_6$**). Assignments based on splitting patterns: -102 ppm is the secondary silane end groups (triplet) and the family of doublets at -120 ppm is assigned to tertiary silanes found at repeat unit linkages.

3.5 Post-Polymerization Functionalization and Optical Properties

Poly(**1,4Si$_6$**) represents a new structural motif for σ-conjugated polysilanes. Internal Si-H groups allow the opportunity for further functionalization. Borane-catalyzed hydrosilylation of poly(**1,4Si$_6$**) with an electron-poor phenylacetylene produces poly(**1,4Si$_6$**)DCV, a yellow σ-π conjugated donor-acceptor polymer. Poly(**1,4Si$_6$**)DCV is sparingly soluble in organic solvents so an NMR spectrum of it could not be attained. The ATR-IR spectrum of poly(**1,4Si$_6$**)DCV contains a peak consistent with a nitrile group (2147 cm^{-1}) and Si-H group (2041 cm^{-1}), suggesting that functionalization did not proceed to completion.

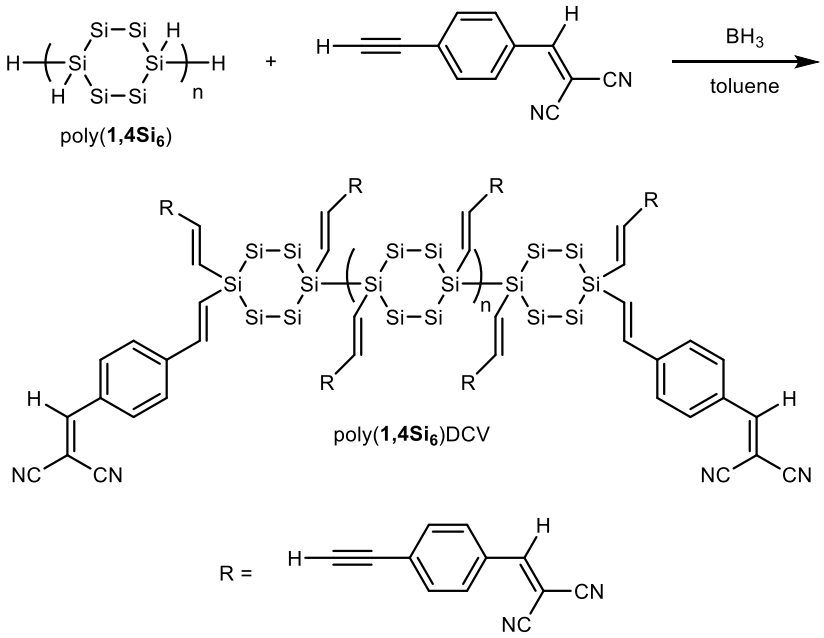

Scheme 3.6. Postpolymerization functionalization of poly(**1,4Si$_6$**) to form the donor-acceptor polymer poly(**1,4Si$_6$**)DCV.

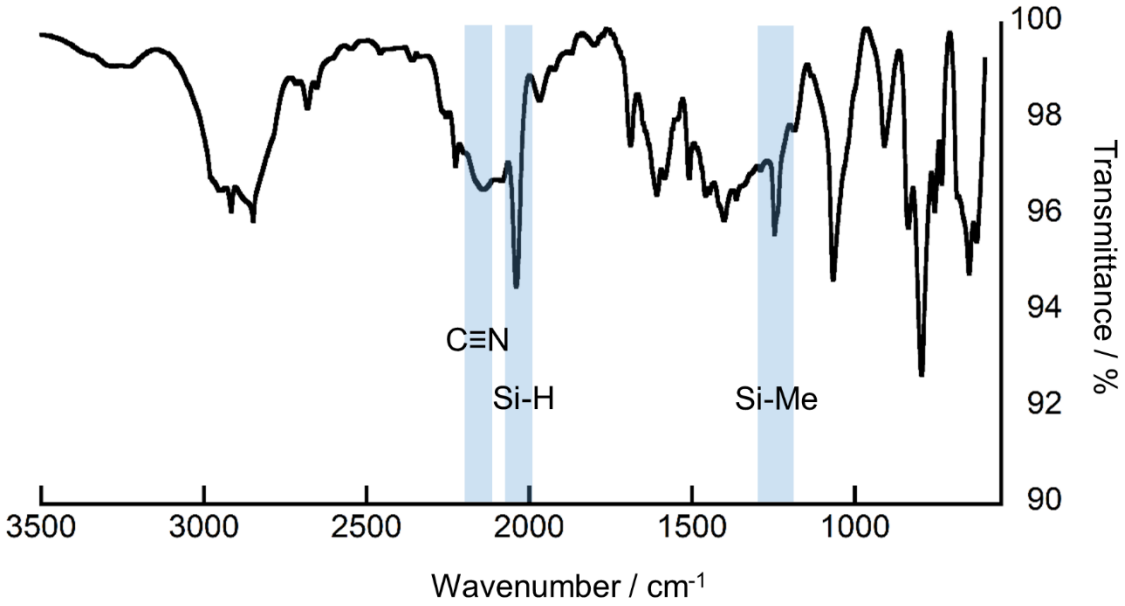

Figure 3.9. ATR-FTIR spectrum of poly(**1,4Si$_6$**)DCV. Diagnostic stretches are labeled.

Poly(**1,4Si$_6$**) strongly absorbs UV light, and has an onset of absorbance red-shifted 50 nm from **1,4Si$_6$**. This suggests extended σ-conjugation along the polysilane framework. The UV vis absorbance spectrum of poly(**1,4Si$_6$**) has an additional broad transition at 340

nm, consistent with σ-π* transitions in linear molecular silanes capped with electron poor cyanovinyl groups.[25]

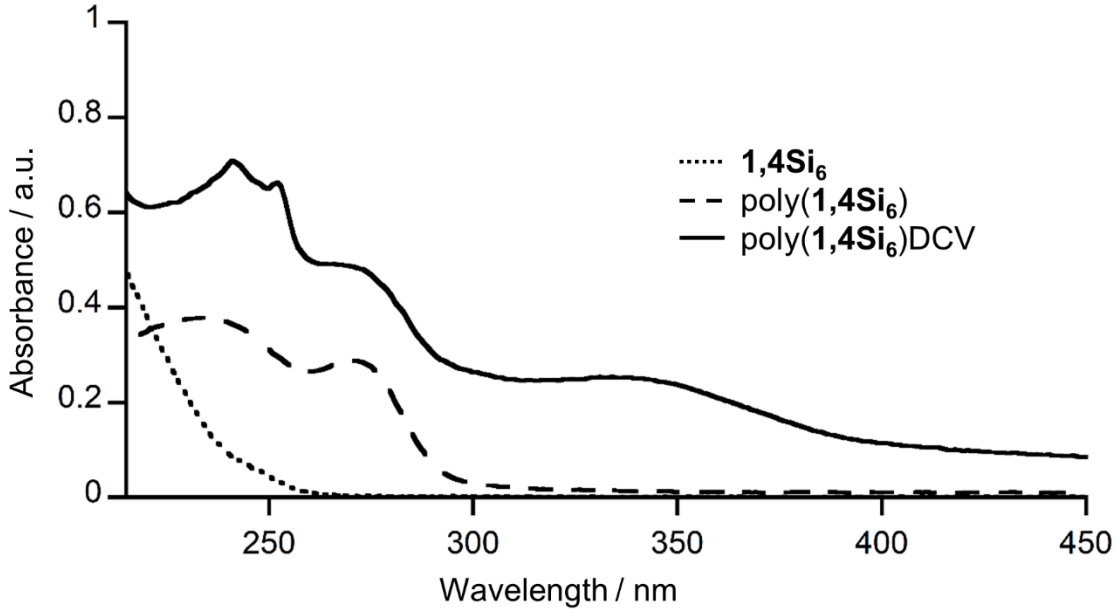

Figure 3.10. UV-Vis spectra of **1,4Si$_6$**, poly(**1,4Si$_6$**), and poly(**1,4Si$_6$**)DCV.

3.6 Conclusion

1,4Si$_6$ is the first cyclohexasilane directional building block synthesized and studied by the Klausen lab. Improvements made to the synthesis of **1,4Si$_6$** guided future syntheses of site-selectively functionalized cyclic silanes. Functional groups in the 1 and 4 positions produce a linear backbone of cyclosilanes. Residual Si-H functional groups of poly(**1,4Si$_6$**) have proven their utility in structural characterization of this class of polymers and through the potential of post-polymerization functionalization. Solid-state NMR provides conformational information about poly(**1,4Si$_6$**).

3.7 Experimental Details

Experimental details can be found in *Angew. Chem., Int. Ed*. **2017**, *56*, 568.

3.8 References

(1) Albinsson, B.; Teramae, H.; Downing, J. W.; Michl, J. *Chem. - A Eur. J.* **1996**, *2* (5), 529–538.
(2) Albinsson, B.; Antic, D.; Neumann, F.; Michl, J. *J. Phys. Chem. A* **1999**, *103* (14), 2184–2196.
(3) Koe, J. R.; Fujiki, M.; Motonaga, M.; Nakashima, H. *Macromolecules* **2001**, *34* (4), 1082–1089.
(4) Schilling, F. C.; Lovinger, A. J.; Zeigler, J. M.; Davis, D. D.; Bovey, F. A. *Macromolecules* **1989**, *22* (7), 3055–3063.
(5) Fujiki, M. *J. Am. Chem. Soc.* **1996**, *118* (31), 7424–7425.
(6) Fujiki, M. *Macromol. Rapid Commun.* **2001**, *22* (8), 539–563.
(7) Krempner, C.; Krempner; Clemens. *Polymers (Basel).* **2012**, *4* (1), 408–447.
(8) Bianconi, P. A.; Weidman, T. W. *J. Am. Chem. Soc.* **1988**, *110* (7), 2342–2344.
(9) Hengge, E. F.; Hassler, K.; Schrank, F. *Heteroat. Chem.* **1990**, *1* (6), 455–459.
(10) Hengge, E.; Eibl, M. *J. Organomet. Chem.* **1992**, *428* (3), 335–343.
(11) Fischer, R.; Konopa, T.; Ully, S.; Baumgartner, J.; Marschner, C. *J. Organomet. Chem.* **2003**, *685* (1–2), 79–92.
(12) Poliakoff, M.; Fitzpatrick, J. M.; Farren, T. R.; Anastas, P. T. *Science* **2002**, *297* (5582), 807–810.
(13) Smith, G. V.; Notheisz, F.; Smith, G. V.; Notheisz, F. *Heterog. Catal. Org. Chem.* **1999**, 1–28.
(14) El-Sayed, I.; Hatanaka, Y.; Onozawa, S. Y.; Tanaka, M. *Journal of the American Chemical Society*. American Chemical Society 2001, pp 3597–3598.
(15) Uhlig, W.; Tzschach, A. *J. Organomet. Chem.* **1989**, *378* (1), C1–C5.
(16) Gudnason, P. I.; Arnason, I. *Org. Lett.* **2009**, *11* (9), 2015–2017.
(17) Casarini, D.; Lunazzi, L.; Mazzanti, A. *J. Org. Chem.* **1998**, *63* (24), 9125–9127.
(18) Uhlig, F.; Marsmann, H. C. *29Si NMR Some Practical Aspects - Gelest Inc.*; 2008.
(19) Tekautz, G.; Binter, A.; Hassler, K.; Flock, M. *ChemPhysChem* **2006**, *7* (2), 421–429.
(20) Chatgilialoglu, C.; Guerrini, A.; Lucarini, M.; Pedulli, G. F.; Carrozza, P.; Da Roit, G.; Borzatta, V.; Lucchini, V. *Organometallics* **1998**, *17* (11), 2169–2176.
(21) Tilley, T. D. *Acc. Chem. Res.* **1993**, *26* (1), 22–29.
(22) Corey, J. Y.; Xiao-Hong, Z. *J. Organomet. Chem.* **1992**, *439* (1), 1–17.
(23) Chang, L. S.; Corey, J. Y. *Organometallics* **1989**, *8* (8), 1885–1893.
(24) Corey, J. Y.; Zhu, X. H.; Bedard, T. C.; Lange, L. D. *Organometallics* **1991**, *10* (4), 924–930.
(25) Zhou, J.; Surampudi, S. K.; Bragg, A. E.; Klausen, R. S. *Chem. - A Eur. J.* **2016**, *22* (18), 6204–6207.

Chapter 4: Directional Building Blocks Determine Linear and Cyclic Architectures

The work presented in this chapter has been published as Marro, E. A.; Press, E. M.; Siegler, M. A.; Klausen, R. S. *J. Am. Chem. Soc.* **2018**, *140*, 5976.

Mr. Eric Press performed the majority of the computational work.

Mr. Eric Marro performed all experimental work and some computational work.

Dr. Maxime Siegler obtained single crystal x-ray data and solved crystal structures.

4.1 Introduction

Nanoscale silicon possesses unusual properties with great promise in energy, optoelectronic, and biomedical applications.[1] Silicon's high theoretical charge capacity has motivated extensive studies in lithium-ion batteries.[2–4] Quantum confinement introduces a tunable band gap[5,6] and porous silicon (p-Si) has been intensely investigated for optoelectronic applications since Canham's discovery of light emission.[7,8] Silicon nanomaterials appeal in biological applications due to their biodegradability and low toxicity.[9–12] Free-standing silicon nanoparticles and nanocrystals exhibit similar promise and their properties are tunable by particle size and surface modification.[13–19] While bottom-up synthetic approaches have led to great advances,[20,21] control of shape, size, and interface and surface structure is a topic of significant current interest.[15,22–25]

Strategic synthesis is an established tool for the construction of complex organic nanomaterials[26,27] that has more recently found application in the preparation of inorganic nanostructures.[28,29] Notable examples include superatoms,[30–32] hierarchical nanoparticle assemblies,[33] and magic number precursors to indium phosphide quantum dots.[34,35]

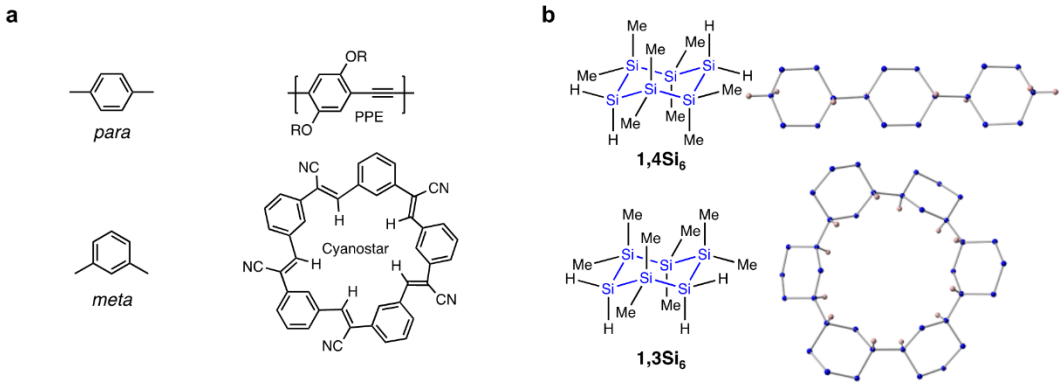

Figure 4.1. Comparing directionality in (a) carbon-based π-conjugated and (b) silicon-based σ-conjugated building blocks. Optimized structures of a linear trimer of **1,4Si$_6$** and a cyclic hexamer of **1,3Si$_6$**. DFT B3LYP/6-31G(d). Blue = silicon; pink = hydrogen. Methyl groups omitted for clarity.

Directionality of organic building blocks give rise to unique and predictable nanomaterial shapes (Figure 4.1a). A *para*-functionalized aromatic ring templates the growth of linear materials like the poly(phenylene ethynylene) (PPE) derivatives used in organic light-emitting diodes.[36,37] *meta*-Functionalized arenes template macrocycles, like the anion-binding cyanostar.[38,39] Building block directionality is an essential design concept in coordination polymers, supramolecular assemblies, and framework materials.[40–45]

This chapter describes how chair-like cyclohexasilane rings can act as directional precursors to distinct nanomaterial structures. In contrast to cyclohexane rings, cyclohexasilanes are optically active in the UV region.[46,47] "*meta*"-Like cyclohexasilane can act as a precursor to macrocyclic oligomers of cyclohexasilane. Macrocycles have wide-ranging applications in supramolecular chemistry and represent enduring challenges

for chemical synthesis.[48] Porosity in silicon, especially with nanoscale dimensions, introduces unique functionality to a powerful and ubiquitous semiconductor.[8,9,49]

4.2 Synthesis of Poly(1,3Si$_6$)

The synthesis of site-selectively functionalized cyclohexasilanes is nontrivial. Reductive coupling of dichlorodimethylsilane yields dodecamethylcyclohexasilane (Si_6Me_{12}).[50] Chlorination of Si_6Me_{12}, while yielding a mixture of structural isomers and diastereomers, is a popular route to substituted cyclohexasilanes via substitution and chromatographic separation.[51,52] Reductive heterocouplings are unselective and yield complex mixtures.[53]

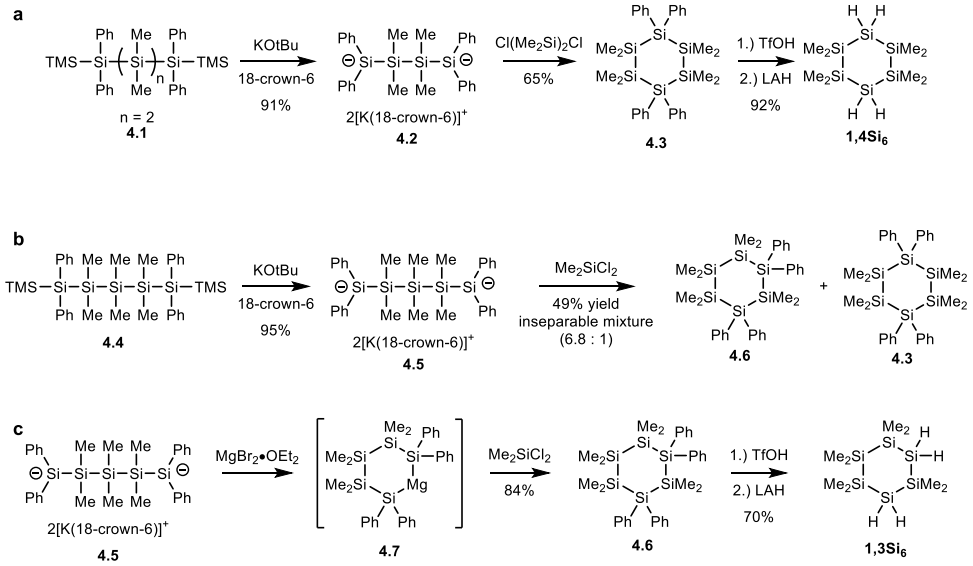

Scheme 4.1. Cyclosilane synthesis. (a) Synthesis of **1,4Si$_6$** via salt metathesis of **4.2** and Cl(Me$_2$)$_2$Cl. (b) Rearrangment occurs when coupling **4.5** and dichlorodimethylsilane (c) Magnesium silanide **4.7** provides higher yield and suppresses rearrangement.

Salt metathesis of dianions is more promising for the synthesis of isomerically pure functionalized cyclosilanes. Marschner reported that crown ether-activation of potassium *tert*-butoxide (KO*t*-Bu/18-cr-6) is an excellent method for the preparation of

terminal disilanides.[54–56] In chapter 3, potassium silanide **4.2** was a useful intermediate in the synthesis of **1,4Si$_6$** (Scheme 4.1a).[57,58]

Much like the synthesis of **1,4Si$_6$**, the ring forming coupling of potassium diphenylsilanide **4.5** and dichlorodimethylsilane (Me_2SiCl_2) was a key step in the synthesis of 1,3-functionalized cyclohexasilane **4.6**. Salt metathesis with potassium disilanide promoted skeletal rearrangement and provided an inseparable mixture of the structural isomers **4.3** and **4.6** with more unidentified byproducts (Scheme 4.1b) in 49% yield. The ratio of **4.6** to **4.3** was 6.8:1. The crystallographic analysis of disilanides from chapter 2 provided insight into the nature of silanide reactivity and offered a solution to this synthetic problem.[57] Potassium silanides are very strong nucleophiles due to weak ion-pairing between silicon and potassium in both solution and the solid state. The weak ion pairing is attributed to silicon's "soft anion" character, which contributes to weak charge-controlled interactions.

The reactivity of **4.6** can be tuned by exchanging the countercation. Magnesium forms a more covalent interaction with silanides and suppresses skeletal rearrangement. Magnesium diphenylsilanide **4.7**, arising from the addition of magnesium bromide to **4.5**,[59] couples cleanly with Cl_2SiMe_2 to yield **4.6** in 84-93% yield (Scheme 4.1c). The crystal structure of **4.6** obtained from x-ray data analysis is shown in Figure 4.2a. A chair conformation is observed in the solid state. Subsequent dearylation with TfOH[60,61] and LAH reduction yielded the desired building block in 70% yield over two steps. **1,3Si$_6$** is a clear, colorless liquid at room temperature (Figure 4.2b). The synthesis of **1,3Si$_6$** can be done on the gram scale.

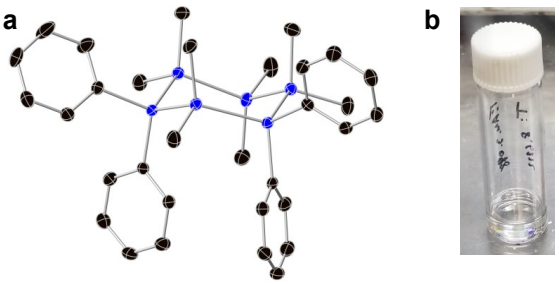

Figure 4.2. (a) X-ray crystal structure of cyclosilane **4.6**. Displacement ellipsoids shown at 50% probability. Hydrogens omitted for clarity. Blue = silicon, black = carbon. (b) Image of clear, colorless liquid **1,3Si$_6$** monomer synthesized on the gram scale.

4.3 Polymerization Studies

Primary and secondary monosilanes (e.g. phenylsilane and diphenylsilane) are polymerized by transition metal-catalyzed dehydrocoupling, yielding polysilanes with the general formula $[SiR_2]_n$ (R = H, alkyl, or aryl) and hydrogen gas.[62,63] Group 4 metallocenes are among the best-studied dehydrocoupling polymerization catalysts.[64–68] These complexes are known to be sensitive to the degree of monomer substitution, with primary silanes ($RSiH_3$) producing the highest molecular weight polymers.[67–69] Secondary silanes (R_2SiH_2) typically yield a mixture of dimers and trimers.[67] This is due to the step-growth polymerization mechanism, in which dimerization of the secondary silane provides a molecule with unreactive tertiary silane end groups. Bifunctional monomers like **1,3Si$_6$** and **1,4Si$_6$** retain reactive secondary end groups after dimerization. This combination of monomer properties and the steric sensitivity of the promoter predicts that the greater reactivity of the chain ends of the growing poly(**1,3Si$_6$**) compared to internal tertiary sites facilitates propagation and suppresses chain branching.

Dehydrocoupling polymerization of **1,3Si$_6$** was initiated by a series of early transition metal metallocenes (Table 4.1).[62] The highest molecular weight polymer was obtained with zirconocene dichloride in combination with *n*-butyllithium (Cp_2ZrCl_2/n-

BuLi, entry 1), a catalytic system first reported by Corey.[67–69] Variation of the group 4 metal center did not lead to higher degrees of polymerization (entries 2-3), as observed in **1,4Si6** polymerization.[70] A several day induction period was observed with dimethylzirconocene (Cp_2ZrMe_2),[64] however, performing the reaction neat resulted in a reasonable degree of polymerization (entry 4). High polymer molecular weights are only observed at high reaction extents in step growth polymerization and several factors including catalyst deactivation and competitive depolymerization under forcing conditions contribute to modest degrees of polymerization in silane dehydrocoupling.[62,70]

Table 4.1. Metallocene-initiated dehydrocoupling polymerization of **1,3Si6**.

Catalyst	M_n (kDa)[c]	M_w (kDa)[c]	$Đ$	$\overline{DP}$[d]
Cp_2ZrCl_2/*n*-BuLi[a]	3.26	4.78	1.47	10
Cp_2TiCl_2/*n*-BuLi[a]	1.04	1.35	1.30	3
Cp_2HfCl_2/*n*-BuLi[a]	1.32	1.46	1.11	4
Cp_2ZrMe_2[b]	2.69	3.43	1.28	8

[a] Typical polymerization conditions: [metallocene]:[monomer]$_0$ = 1:18, toluene, rt, 24 h. [b] Reaction conditions: [metallocene]:[monomer]$_0$ = 1:18, neat, 24 h. [c] Determined by GPC at 254 nm relative to a polystyrene standard. [d] The ratio of poly(**1,3Si6**) M_n and **1,3Si6** M_n, as determined by GPC.

A unimodal distribution of molecular weights is shown by gel permeation chromatography (GPC) (Figure 4.3). The number average molecular weight (M_n) of poly(**1,3Si6**) corresponds to an average degree of polymerization of 10, comparable to the average degree of polymerization of 8 observed with poly(**1,4Si6**) under similar polymerization conditions.[58,70] The similar molecular weight distributions rule out the possibility that spectroscopic differences in poly(**1,3Si6**) and poly(**1,4Si6**) arise from differences in chain length.

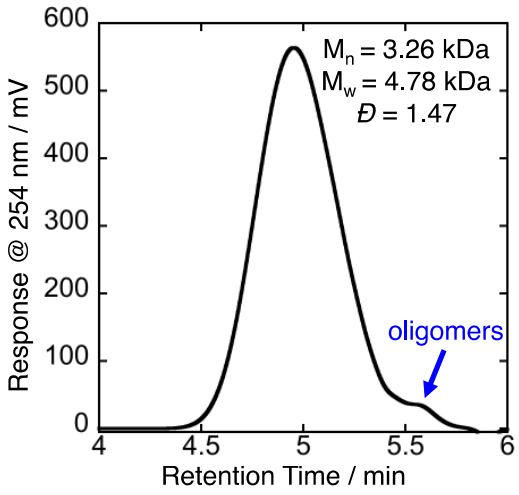

Figure 4.3. Gel permeation chromatography (GPC) analysis of poly(**1,3Si$_6$**). Determined relative to a polystyrene standard at 254 nm (THF, [poly(**1,3Si$_6$**)] = 1 mg mL^{-1}, 40 °C, 0.35 mL min^{-1}, 10 µL injection). The blue arrow indicates a low molecular weight shoulder attributed to linear oligomers.

Poly(**1,3Si$_6$**) is stored in a nitrogen atmosphere glove box to minimize autoxidation of the reactive Si−H bonds.[71] Under these conditions, poly(**1,3Si$_6$**) is stable and no decomposition is observed over several weeks. Poly(**1,3Si$_6$**) is highly soluble in dichloromethane, chloroform, tetrahydrofuran, and toluene, as well as in simple hydrocarbons like pentane, whereas poly(**1,4Si$_6$**) is sparingly soluble in chlorinated and ethereal solvents.

Extensive characterization supports the assignment of poly(**1,3Si$_6$**) to an ensemble of macrocycles with between 5 to 15 repeat units, as well as linear oligomers that are too short to cyclize (a shoulder in the size exclusion chromatogram assigned to short oligomers is labeled with a blue arrow in Figure 4.3). These conclusions are made on the basis of analysis of molecular weight distribution, comparison of experimental and calculated spectroscopic data, vibrational and absorbance spectroscopy, and polymer end group characterization.

4.4 DFT – Structure

DFT calculations provide insight into the structure and expected characteristics of linear and cyclic forms of poly(**1,3Si$_6$**). The cyclic hexamer *c*-(**1,3Si$_6$**)$_6$ and linear hexamer *n*-(**1,3Si$_6$**)$_6$ were chosen for these studies as the best compromise between computational tractability and experimental relevance. Geometry optimization was performed at the B3LYP/6-31g(d) level of theory. The linear structure adopts a helical conformation due to an approximately 95° torsion angle between rings (Figure 4.4 and Table 4.2). Depending on the starting structure before geometry optimization, two different conformations of *c*-(**1,3Si$_6$**)$_6$ are identified as energetic minima, a low symmetry conformer assigned to the C_1 point group and a butterfly-like high-symmetry conformer assigned to the D_{3d} point group (Figure 4.5). The low symmetry conformer is higher in energy by 7.65 kcal mol^{-1} relative to the butterfly conformer.

Both optimized *c*-(**1,3Si$_6$**)$_6$ conformers are approximately 2 nm across, with a central pore between 5 and 7 Å wide. Both structures exhibit twisting between adjacent cyclohexasilane rings. In the butterfly conformer, rings alternate up and down and torsion angles are relatively small (between 1.4° and 14°). The same up-down alternation exists in the C_1 conformer, but with a wider range of torsion angles (7.8° - 125°) (Table 4.2). This results in modest curvature. The *exo* and *endo* faces are labeled in Figure 4.5c-d.

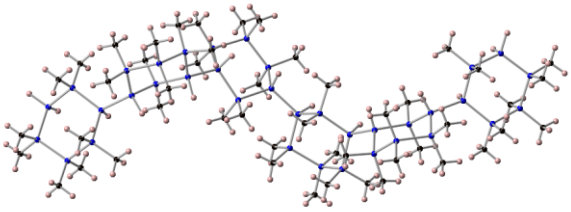

n-(**1,3Si$_6$**)$_6$

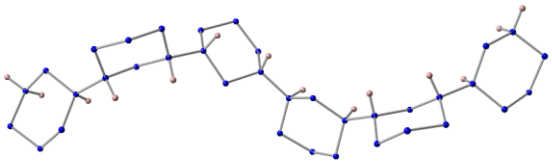

n-(**1,3Si$_6$**)$_6$
Methyl groups omitted

Figure 4.4. DFT optimized structures of *n*-(**1,3Si$_6$**)$_6$ with and without methyl groups. Blue = silicon, black = carbon, pink = hydrogen. DFT B3LYP/6-31G(d).

Table 4.2. Selected structural parameters for *c*-(**1,3Si$_6$**)$_6$ and *n*-(**1,3Si$_6$**)$_6$.

	Linear		
	Minimum	Maximum	Mean
Si-Si Bond Length (Å)	2.37	2.39	2.38
Torsion Angle (deg)	93.6	96.1	94.7
Ring Angle (deg)	107	119	112
	Butterflyy		
	Minimum	Maximum	Mean
Si-Si Bond Length (Å)	2.37	2.40	2.38
Torsion Angle (deg)	1.35	14.2	6.65
Ring Angle (deg)	106	115	110
	Nonsymmetric		
	Minimum	Maximum	Mean
Si-Si Bond Length (Å)	2.37	2.41	2.38
Torsion Angle (deg)	7.84	125	58.9
Ring Angle (deg)	106	117	111

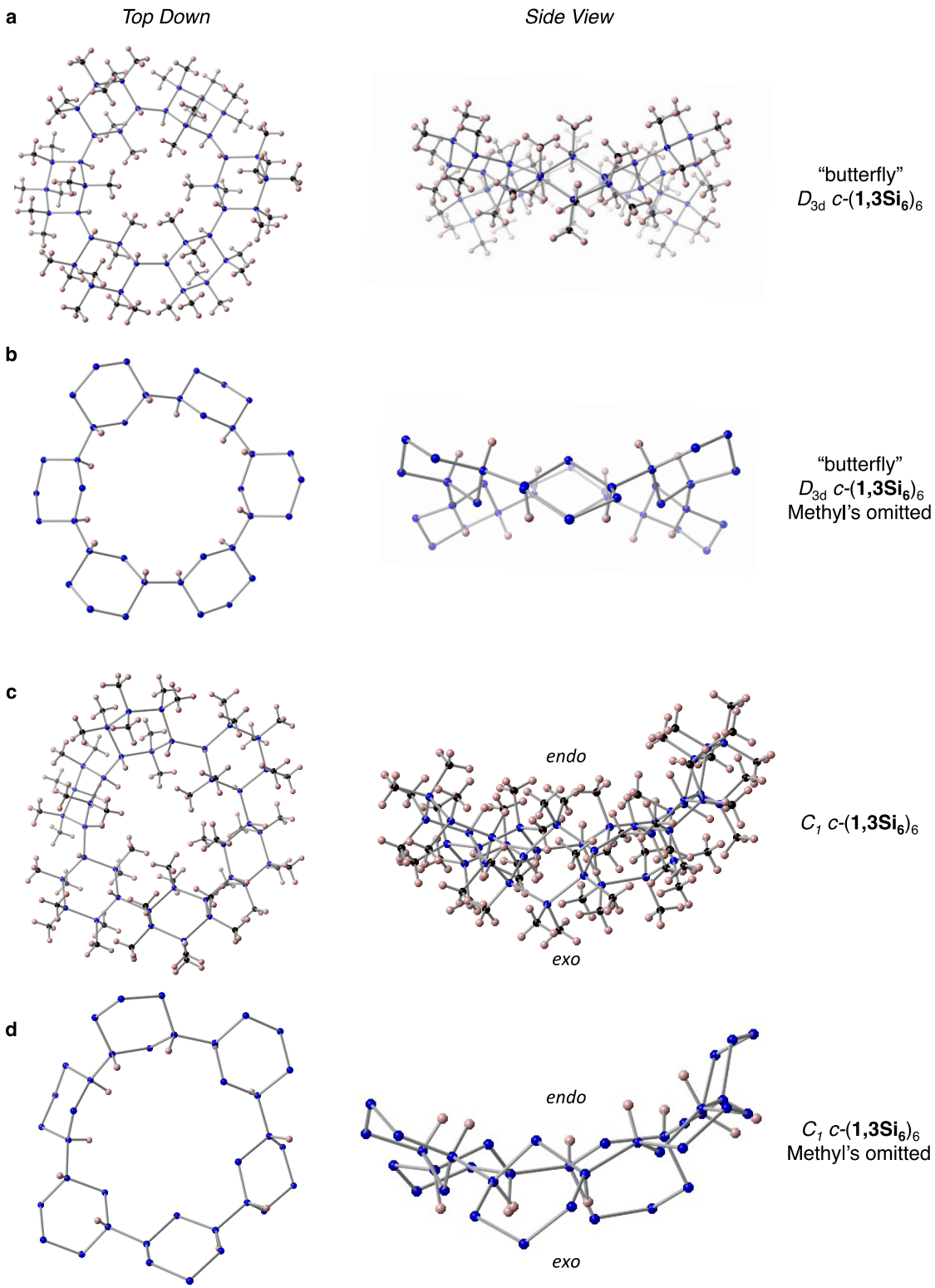

Figure 4.5. Geometry optimized structures of *c*-(**1,3Si$_6$**)$_6$. (B3LYP/6-31G(d). (a,b) "butterfly" geometry possesses D_{3d} symmetry. (c,d) Contorted structure with C_1 symmetry. Methyl groups omitted for clarity where indicated. Blue = silicon, black = carbon, pink = hydrogen.

Every cyclohexasilane ring in the linear and cyclic structures adopts a chair conformation. Evidence of significant ring strain is not apparent (Table 4.2). Within each ring, bond angles are close to the expected value for a tetrahedral center (109.5°). The average calculated Si-Si bond length (2.38 Å) is typical of oligosilanes and corresponds well with the Si-Si bond lengths observed in the crystal structure of **1,4Si$_6$** (2.34± 0.001 Å).[58] In both conformers of *c*-(**1,3Si$_6$**)$_6$, all hydrides are in the axial position, while the larger neighboring **1,3Si$_6$** rings are in the equatorial positions. This is most easily seen in a simplified representation of the *c*-(**1,3Si$_6$**)$_6$ skeleton in which methyl groups are omitted for clarity (Figure 4.5b and 4.5d). The central pore is lined with Si−H bonds. Pairs of diaxial Si−Hs alternate orientation between the two faces of the macrocycle. In the C_1 conformer, the curvature results in the *endo* face having the directional Si−H pairs oriented towards the interior of the pore, while the *exo* face is somewhat less organized.

4.5 NMR Characterization

The calculations described above point to two features that distinguish the macrocyclic from the linear structure: high symmetry and the absence of SiH_2 end groups. ^{1}H and ^{29}Si NMR spectroscopies provide compelling evidence that poly(**1,3Si$_6$**) is both highly symmetric and lacking resonances consistent with SiH_2 functional groups. Comparison of experimental NMR spectra of the "*para*" and "*meta*"-like structural isomers **1,4Si$_6$** and **1,3Si$_6$** supports the ability of these building blocks to template unique product architectures.

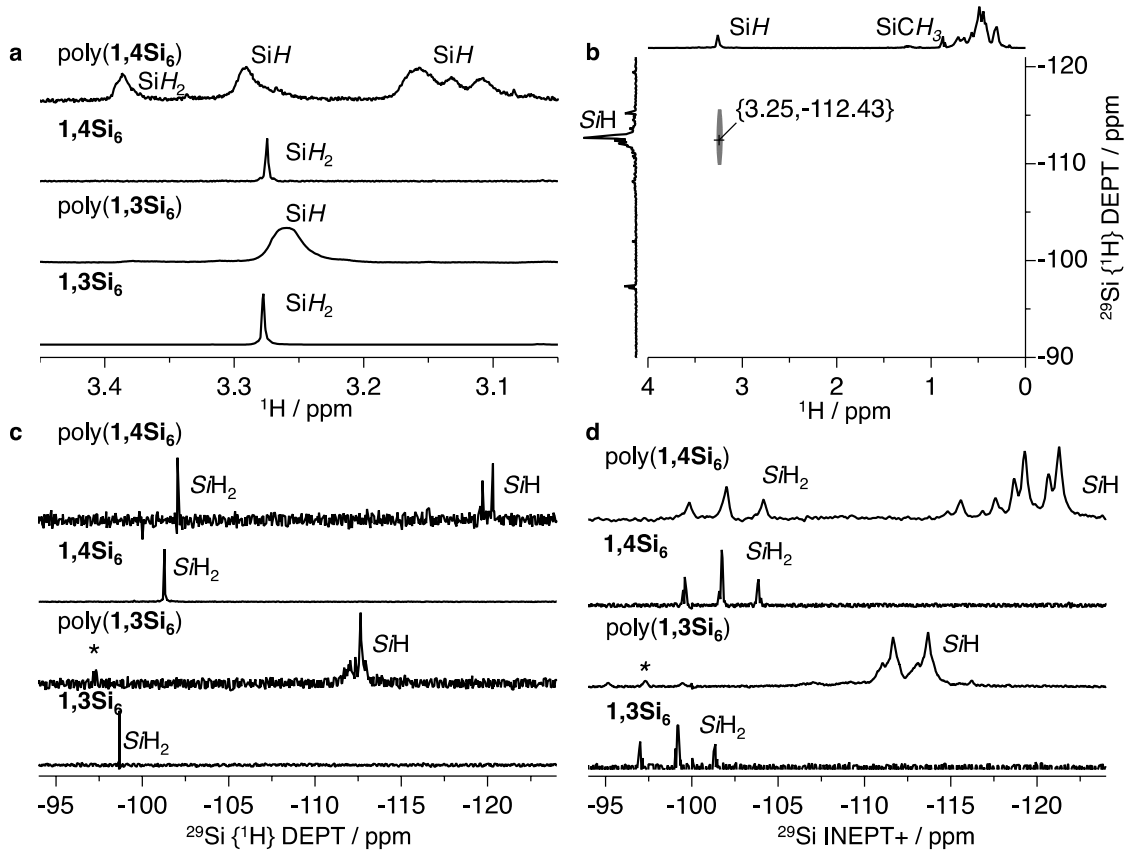

Figure 4.6. Structural characterization of poly(cyclosilane)s by NMR spectroscopy (C_6D_6). (a) Cropped ^{1}H NMR spectra of (top to bottom) poly(**1,4Si$_6$**), **1,4Si$_6$**, poly(**1,3Si$_6$**), and **1,3Si$_6$**. Only the SiH region is shown. (b) ^{1}H–^{29}Si HSQC spectrum of poly(**1,3Si$_6$**). (c) Cropped ^{29}Si{^{1}H} DEPT NMR spectra of (top to bottom) poly(**1,4Si$_6$**),**1,4Si$_6$**, poly(**1,3Si$_6$**), and**1,3Si$_6$**. Only the SiH region is shown. (d) ^{29}Si INEPT+ NMR of (top to bottom) poly(**1,4Si$_6$**),**1,4Si$_6$**, poly(**1,3Si$_6$**), and **1,3Si$_6$**. Only the SiH region is shown.

The ^{1}H NMR spectra of monomers and polymers are shown in Figure 4.6a. A sharp singlet at δ 3.28 is assigned to the SiH_2 groups of **1,3Si$_6$**. Rapid ring inversion on the NMR time scale causes the inequivalent axial and equatorial protons to coalesce.[72] The SiH_2 groups of **1,4Si$_6$** have a similar chemical shift (δ 3.27) as observed in **1,3Si$_6$**. Upon polymerization, however, poly(**1,3Si$_6$**) and poly(**1,4Si$_6$**) exhibit very different ^{1}H NMR spectra. Linear poly(**1,4Si$_6$**) has several broad resonances of roughly equal intensity in the typical Si–H region (3.5 to 3.0 ppm). These resonances are assigned to internal

tertiary silanes (SiH) and secondary (SiH_2) end group silanes arising from a linear polymer structure on the basis of ^{1}H-^{29}Si HSQC NMR spectroscopy.[58] In poly(**1,3Si$_6$**), the SiH region of the ^{1}H NMR spectrum is dominated by one broad singlet at δ 3.25. The ^{1}H NMR spectrum of poly(**1,3Si$_6$**) is more consistent with the high symmetry macrocyclic structure than a linear polymer structure. Initial assignment of the poly(**1,3Si$_6$**) δ 3.26 resonance to a silane proton is supported by ^{1}H-^{29}Si HSQC NMR spectroscopy, which shows a cross-peak between this resonance and a family of ^{29}Si NMR resonances centered around an intense peak at δ –112 (Figure 4.6b).

Further support for the assignment of the correlated resonances to tertiary silanes arises from ^{29}Si NMR spectroscopy.[73,74] The degree of H-substitution strongly influences the chemical shift of the ^{29}Si nuclide. ^{29}Si $\{^{1}H\}$ DEPT NMR spectra for **1,3Si$_6$**, poly(**1,3Si$_6$**), **1,4Si$_6$**, and poly(**1,4Si$_6$**) are shown in Figure 4.6c. Poly(**1,3Si$_6$**)'s δ –112 resonances are observed at lower frequency than the δ –98.7 resonance assigned to the secondary silane (SiH_2) group of the monomer. A less intense resonance (labeled with an asterisk) is assigned to the secondary silane end groups of short linear oligomers that have not macrocyclized.

Coupling constants are consistent with the proposed assignments. In the ^{29}Si INEPT+ NMR spectrum, the δ –112 resonances appear as a family of overlapping doublets. The coupling constant (J = 160.9 Hz) is consistent with typical one-bond coupling constants between proton and silicon ($^{1}J_{Si\text{-}H}$ = 420 – 75 Hz). The resonance assigned to the end group of uncyclized short oligomers (labeled with an asterisk, Figure 4.6d) has the expected triplet splitting pattern (J = 169.9 Hz).

4.6 Vibrational Spectroscopy

Experimental attenuated total reflectance-Fourier transform infrared (ATR-FTIR) spectroscopy and calculated vibrational spectra for the linear and cyclic hexamers provide additional evidence for a high-symmetry structure featuring Si_3SiH functional groups. Figure 4.7 compares the experimental ATR-FTIR spectra of monomer and polymer. Both materials show resonances consistent with a Si−H stretch and with a Si−Me stretch. While the Si−Me stretching frequency changes minimally on polymerization, the Si−H stretching frequency shifts to lower frequency by appx. 30 cm^{-1} (Table 4.3).

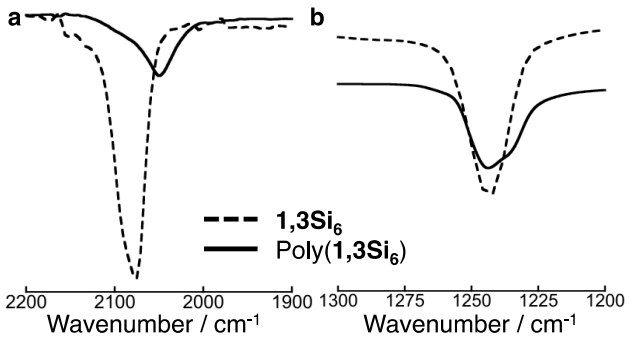

Figure 4.7. Cropped ATR-FTIR spectra of **1,3Si$_6$** (dashed) and poly(**1,3Si$_6$**) (solid) Only (a) Si-H and (b) Si-Me stretching peaks are shown.

Table 4.3. Selected functional group stretching frequencies of **1,3Si$_6$**, poly(**1,3Si$_6$**) and TMS_3SiH.

	1,3Si$_6$ (cm^{-1})	**Poly(1,3Si$_6$) (cm^{-1})**	**TMS_3SiH (cm^{-1})**
ν(Si−H)	2077	2046	2049
ν(Si−Me)	1243	1243	1243

The lower frequency of the Si-H stretch in poly(**1,3Si$_6$**) compared to **1,3Si$_6$** is consistent with a change from a secondary to tertiary silyl-substituted silane. Tris(trimethylsilyl)silane (TMS_3SiH) is a representative silyl-substituted tertiary silane. The Si−H bond in TMS_3SiH is significantly weaker than in triethylsilane (79.0 versus

90.1 kcal mol^{-1}) due to the weakening effect of silyl-substitution compared to alkyl-substitution.[75,76] Weaker bonds of the same atoms resonate at lower frequencies and the Si−H stretching frequency in TMS_3SiH (2049 cm^{-1}) is observed at a lower frequency than in **1,3Si$_6$** (2077 cm^{-1}) or triethylsilane (2107 cm^{-1}). The observed close agreement of the poly(**1,3Si$_6$**) and TMS_3SiH Si–H stretching frequencies (2046 versus 2049 cm^{-1}, Table 4.3) support assignment to a tertiary silyl-substituted silane.

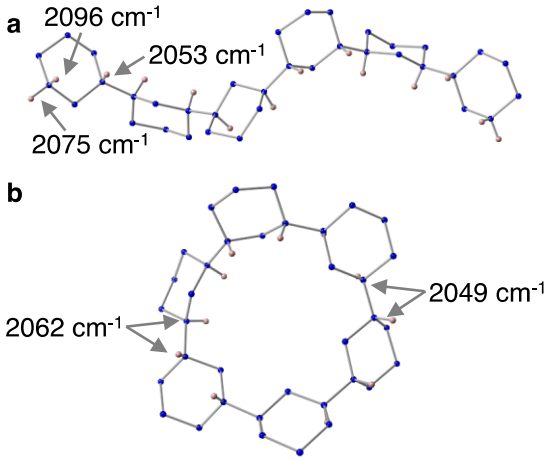

Figure 4.8. Geometry optimized structures of (a) *n*-(**1,3Si$_6$**)$_6$ and (b) C_1 *c*-(**1,3Si$_6$**)$_6$. Si-H stretching frequencies of selected Si-H bonds are labeled.

Selected Si–H stretching frequencies from simulated IR spectra of the linear and cyclic hexamers are shown in Figure 4.8. The experimental observation of a single broad Si–H stretching frequency centered at 2049 cm^{-1} is in better agreement with the simulated spectrum of the cyclic hexamer than the linear hexamer. The Si–H region of the *n*-(**1,3Si$_6$**)$_6$ simulated spectrum is complex, as multiple factors (axial or equatorial, degree of substitution, and symmetry) influence the frequency. Higher frequency resonances correspond to vibrations of the secondary silane end groups, such as the symmetric stretch of the equatorial Si–H end group at 2075 cm^{-1}, while internal Si–H stretching frequencies are found at lower frequency (Figure 4.8a).

The higher symmetry of the cyclic conformers leads to simulated spectra that are simpler than observed for the linear hexamer. Both conformers have similar simulated IR spectra, with features at appx. 2050 and 2060 cm^{-1} (Figures 4.8b). Comparison of the calculated spectra of **1,3Si$_6$** and *c*-(**1,3Si$_6$**)$_6$ reproduces the experimentally observed 30 cm^{-1} shift to lower frequency of the Si–H stretching frequency upon macrocyclization. After bench top handling, both TMS_3SiH and poly(**1,3Si$_6$**) show resonances consistent with Si-O-Si features, suggesting that the weak Si_3SiH bond accelerates autoxidation.[71]

4.7 Absorbance Spectroscopy

The optical properties of extended silanes are very different from the structurally analogous long-chain alkanes.[46] Oligo- and polysilanes strongly absorb ultraviolet light, while alkanes have higher energy excitations (<200 nm). The HOMO-LUMO gap and ionization potential of an oligosilane narrows as the number of silicon atoms in a chain increases, consistent with σ-conjugation.[77,78] However, the effective conjugation length of polysilanes is short, attributed to the strong conformational dependence of σ-conjugation, and polysilane absorbance typically only extends to 300-350 nm.[79] Consistent with conformational effects, polysilanes exhibit thermochromism in solution and in the solid state attributed to increased population of the all-*anti* conformation.[80,81] Conformationally constrained model systems show narrower and red-shifted absorption profiles compared to simple oligosilanes.[82,83]

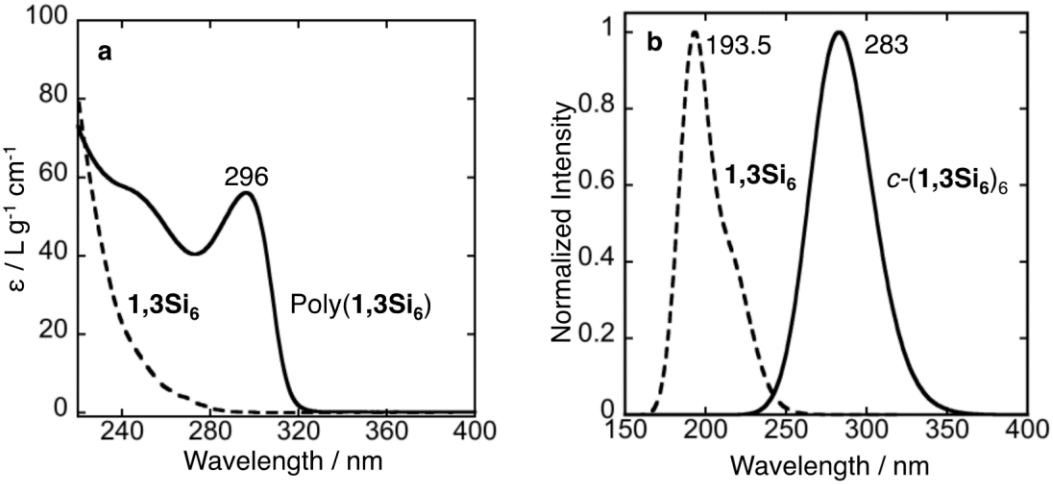

Figure 4.9. (a) Experimental absorbance spectra of **1,3Si$_6$** (dashed) and poly(**1,3Si$_6$**) (solid) in THF. [**1,3Si$_6$**] = 3.0 x 10^{-5} M, [poly(**1,3Si$_6$**)] = 1.0 x 10^{-2} mg mL^{-1}. (b) Calculated absorbance spectra of **1,3Si$_6$** (dashed) and "butterfly" *c*-(**1,3Si$_6$**)$_6$ (solid). TD−PBE0/6-311G(d)//B3YLP/6-31G(d).

Both **1,3Si$_6$** and poly(**1,3Si$_6$**) absorb strongly in the deep- to mid-ultraviolet (UV) region. A modest 50-nm redshift in absorbance observed upon polymerization is observed (Figure 4.9a). The shift in onset of absorbance to lower energy is consistent with increased σ-conjugation. However, based on the number of silicon atoms present in the polymer a larger redshift was expected. The presence of multiple *gauche*-like linkages, which are not optimal for σ-conjugation, may be attributable for a modest redshift.[84] Molecular orbital calculations on *c*-(**1,3Si$_6$**)$_6$ in the butterfly conformation confirm that electron density is not delocalized over the entire silicon framework and is instead concentrated on the silicon atoms lining the macrocycle pore (Figure 4.10). Similar results are obtained for the conformer with C_1 symmetry.

Calculated UV-Vis spectra reproduce the red-shift in absorbance on polymerization (Figure 4.9b). The HOMO–1 to LUMO transition is the dominant contribution to λ_{max}. Reasonable agreement is observed between theory and experiment in

predicting the λ_{max} of absorbance (283 vs. 296 nm), but theory does not predict the high-energy shoulder at approximately 250 nm observed in the experimental poly(**1,3Si$_6$**) spectrum. Calculations are performed on an isomerically pure and conformationally constrained hexamer, while the experimental sample is an ensemble of different ring sizes that is expected to be conformationally dynamic in solution. This may explain the lack of a higher energy shoulder in the calculated spectrum.

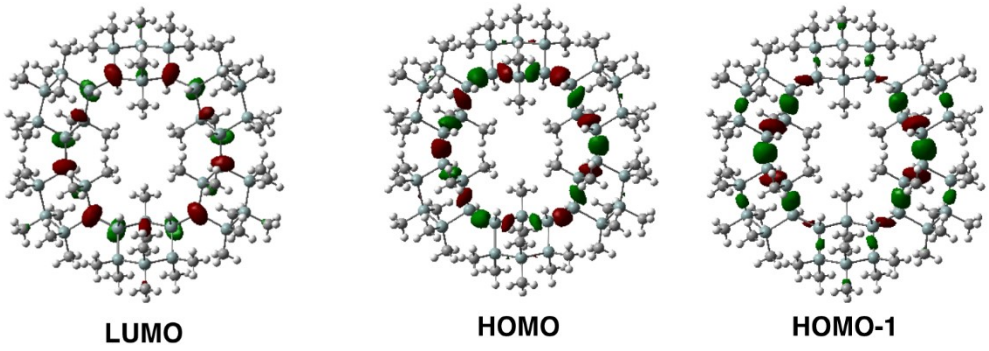

Figure 4.10. Calcluated LUMO, HOMO and HOMO-1 of D_{3h} *c*-(**1,3Si$_6$**)$_6$. Orbital density lines the pore of the macrocycle. TD−PBE0/6-311G(d)//B3YLP/6-31G(d).

4.8 Macrocycle Polarization

DFT calculations predict that the residual Si−H bonds lining the pore of poly(**1,3Si$_6$**) polarize the macrocycle. The electronegativity difference between silicon and hydrogen lends the Si−H bond hydridic character.[85] This can be seen in the electrostatic surface potential (ESP) maps of the butterfly *c*-(**1,3Si$_6$**)$_6$, in which orange patches representing greater electron density are centered over axial Si−H bonds (Figure 11). The most significant charge density (red) is between two diaxial Si−H groups, suggesting a through space interaction. More electron deficiency is found on the methyl groups on the edges of the macrocycle.

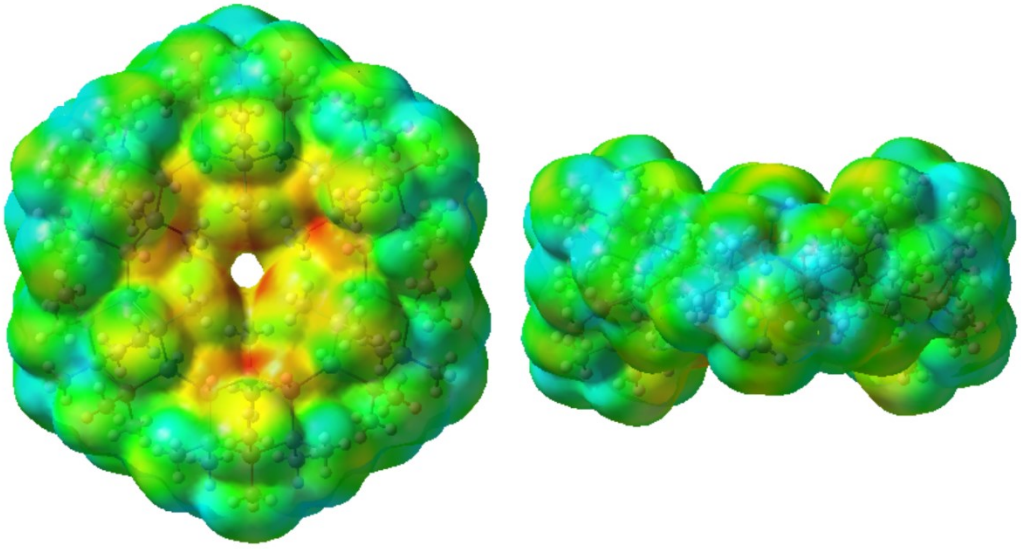

Figure 4.11. Electrostatic potential map of D_{3h} *c*-(**1,3Si$_6$**)$_6$. DFT B3LYP/6-31G(d). Values for electrostatic potential range from −9.97 kcal mol^{-1}(red) to 9.97 kcal mol^{-1}(blue).

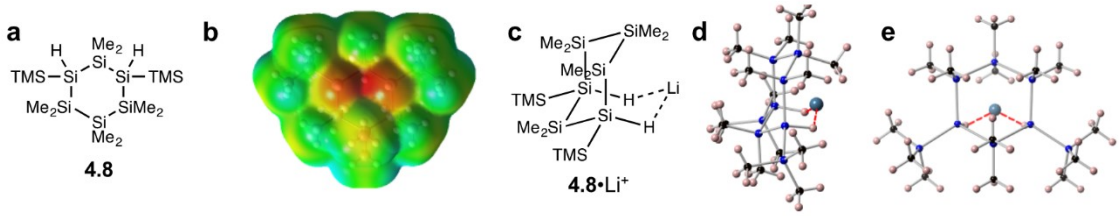

Figure 4.12. Calculated SiH−Li$^+$ interactions. (a) Chemical structure of model compound **4.8**. (b) ESP map of **4.8**. Values for electrostatic potential range from -9.97 kcal mol-1 (red) to 9.97 kcal mol-1 (blue). (c) Chemical structure of **4.8•**Li$^+$ complex. Calculated structure of **4.8•**Li$^+$ complex in d) side and e) top views. DFT B3LYP/6-31G(d). Blue = silicon, black = carbon, pink = hydrogen, teal = lithium. SiH−Li$^+$ interactions shown with dashed red lines.

Quantum chemical calculations support the proposed cation-binding abilities of the H-functionalized polymer. A simplified model system **4.8** was employed for all calculations (Figure 4.12a). Like *c*-(**1,3Si$_6$**)$_6$, **4.8** contains a pair of diaxial Si−H bonds with hydridic character. In the ESP map, electron density is concentrated between the diaxial hydrides (Figure 4.12b), suggesting that a bridging interaction with a Li$^+$ cation is

feasible (Figure 4.12c). Gas phase calculations were performed on the formation of a complex between **4.8** and Li^+. The binding enthalpy between **4.8** and Li^+ is significant, calculated at −53.5 kcal mol^{-1} ((B3LYP/6-31G(d)). For comparison, the binding enthalpy between benzene (C_6H_6) and Li^+ at this level of theory is −39.6 kcal mol^{-1}. High level coupled cluster theory calculations place the C_6H_6•Li^+ binding enthalpy at -36.8±0.2.[86] In the calculated **4.8**•Li^+ complex, bridging SiH−Li^+ interactions form a chair cyclohexane-like ring (∠Si−H−Li = 108.1°, Figure 12d-e). The SiH−Li^+ contacts in the **4.8**•Li^+ complex are 1.85 Å long. A search of the Cambridge Structural Database (CSD) identified a very limited number of SiH−Li contacts, but the calculated distance is comparable to reports by Apeloig (1.90 Å) and Kira (1.95 Å) on hydridosilyllithiums.[87,88]

4.9 Conclusions

This chapter highlights the vast potential for strategic synthesis to provide access to complex and functional silicon-based materials. Macrocyclic poly(cyclosilane)s are synthesized from dehydrocoupling of the "*meta*" like building block **1,3Si$_6$**. Countercation choice in the key cyclization salt metathesis step is essential for pure product. Extensive characterization with IR, ^{1}H and ^{29}Si NMR, and UV-vis spectroscopy partnered with calculated spectra allow for proof of structure. The poly(cyclosilane)s have well-defined structures patterned with Si−Me and Si−H groups. An electron rich pore arises from polarized Si-H groups lining the pore of the macrocycle. Calculations suggest the polarized Si-H bond can bind cations. Poly (**1,3Si$_6$**) a prime candidate for electrodes in lithium-ion batteries and other reversible cation binding applications.[2–4,89]

4.10 Experimental Details

Experimental details can be found in *J. Am. Chem. Soc.* **2018**, *140*, 5976.

4.11 References

(1) Priolo, F.; Gregorkiewicz, T.; Galli, M.; Krauss, T. F. *Nat. Nanotechnol.* **2014**, *9* (1), 19–32.
(2) Chan, C. K.; Peng, H.; Liu, G.; McIlwrath, K.; Zhang, X. F.; Huggins, R. A.; Cui, Y. *Nat. Nanotechnol.* **2008**, *3* (1), 31–35.
(3) Chan, C. K.; Patel, R. N.; O'Connell, M. J.; Korgel, B. A.; Cui, Y. *ACS Nano* **2010**, *4* (3), 1443–1450.
(4) Li, X.; Gu, M.; Hu, S.; Kennard, R.; Yan, P.; Chen, X.; Wang, C.; Sailor, M. J.; Zhang, J. G.; Liu, J. *Nat. Commun.* **2014**, *5*, 4105.
(5) Canham, L. T. *Appl. Phys. Lett.* **1990**, *57* (10), 1046–1048.
(6) Sailor, M. J.; Lee, E. J. *Adv. Mater.* **1997**, *9* (10), 783–793.
(7) Cullis, A. G.; Canham, L. T. *Nature* **1991**, *353* (6342), 335–338.
(8) Sailor, M. J.; Wu, E. C. *Adv. Funct. Mater.* **2009**, *19* (20), 3195–3208.
(9) Anglin, E. J.; Cheng, L.; Freeman, W. R.; Sailor, M. J. *Adv. Drug Deliv. Rev.* **2008**, *60* (11), 1266–1277.
(10) Park, J.-H.; Gu, L.; von Maltzahn, G.; Ruoslahti, E.; Bhatia, S. N.; Sailor, M. J. *Nat. Mater.* **2009**, *8* (4), 331–336.
(11) Alsharif, N. H.; Berger, C. E. M.; Varanasi, S. S.; Chao, Y.; Horrocks, B. R.; Datta, H. K. *Small* **2008**, *5* (2), 221–228.
(12) Liu, J.; Erogbogbo, F.; Yong, K.-T.; Ye, L.; Liu, J.; Hu, R.; Chen, H.; Hu, Y.; Yang, Y.; Yang, J.; Roy, I.; Karker, N. A.; Swihart, M. T.; Prasad, P. N. *ACS Nano* **2013**, *7* (8), 7303–7310.
(13) Dasog, M.; Kehrle, J.; Rieger, B.; Veinot, J. G. C. *Angew. Chemie Int. Ed.* **2016**, *55* (7), 2322–2339.
(14) Mastronardi, M. L.; Henderson, E. J.; Puzzo, D. P.; Ozin, G. A. *Adv. Mater.* **2012**, *24* (43), 5890–5898.
(15) Mastronardi, M. L.; Maier-Flaig, F.; Faulkner, D.; Henderson, E. J.; Kübel, C.; Lemmer, U.; Ozin, G. A. *Nano Lett.* **2012**, *12* (1), 337–342.
(16) Purkait, T. K.; Iqbal, M.; Wahl, M. H.; Gottschling, K.; Gonzalez, C. M.; Islam, M. A.; Veinot, J. G. C. *J. Am. Chem. Soc.* **2014**, *136* (52), 17914–17917.
(17) Purkait, T. K.; Iqbal, M.; Islam, M. A.; Mobarok, M. H.; Gonzalez, C. M.; Hadidi, L.; Veinot, J. G. C. *J. Am. Chem. Soc.* **2016**, *138* (22), 7114–7120.
(18) Dasog, M.; De Los Reyes, G. B.; Titova, L. V.; Hegmann, F. A.; Veinot, J. G. C. *ACS Nano* **2014**, *8* (9), 9636–9648.
(19) Qian, C.; Sun, W.; Wang, L.; Chen, C.; Liao, K.; Wang, W.; Jia, J.; Hatton, B. D.; Casillas, G.; Kurylowicz, M.; Yip, C. M.; Mastronardi, M. L.; Ozin, G. A. *J. Am. Chem. Soc.* **2014**, *136* (45), 15849–15852.
(20) Yang, C. S.; Bley, R. A.; Kauzlarich, S. M.; Lee, H. W. H.; Delgado, G. R. *J. Am. Chem. Soc.* **1999**, *121* (22), 5191–5195.
(21) Baldwin, R. K.; Pettigrew, K. A.; Garno, J. C.; Power, P. P.; Liu, G. Y.; Kauzlarich, S. M. *J. Am. Chem. Soc.* **2002**, *124* (7), 1150–1151.
(22) Dasog, M.; Yang, Z.; Regli, S.; Atkins, T. M.; Faramus, A.; Singh, M. P.; Muthuswamy, E.; Kauzlarich, S. M.; Tilley, R. D.; Veinot, J. G. C. *ACS Nano* **2013**,

7 (3), 2676–2685.
(23) Yu, Y.; Fan, G.; Fermi, A.; Mazzaro, R.; Morandi, V.; Ceroni, P.; Smilgies, D.-M.; Korgel, B. A. *J. Phys. Chem. C* **2017**, *121* (41), 23240–23248.
(24) Yu, Y.; Lu, X.; Guillaussier, A.; Voggu, V. R.; Pineros, W.; de la Mata, M.; Arbiol, J.; Smilgies, D.-M.; Truskett, T. M.; Korgel, B. A. *Nano Lett.* **2016**, *16* (12), 7814–7821.
(25) Lu, X.; de la Mata, M.; Arbiol, J.; Korgel, B. A. *Chem. Mater.* **2017**, *29* (22), 9786–9792.
(26) Segawa, Y.; Ito, H.; Itami, K. *Nat. Rev. Mater.* **2016**, *1* (1), 15002.
(27) Segawa, Y.; Yagi, A.; Matsui, K.; Itami, K. *Angew. Chemie Int. Ed.* **2016**, *55* (17), 5136–5158.
(28) Buck, M. R.; Schaak, R. E. *Angew. Chemie Int. Ed.* **2013**, *52* (24), 6154–6178.
(29) Tan, G.; Zhao, L.-D.; Kanatzidis, M. G. *Chem. Rev.* **2016**, *116* (19), 12123–12149.
(30) Redl, F. X.; Cho, K.-S.; Murray, C. B.; O'Brien, S. *Nature* **2003**, *423* (6943), 968–971.
(31) Roy, X.; Lee, C.; Crowther, A. C.; Schenck, C. L.; Besara, T.; Lalancette, R. A.; Siegrist, T.; Stephens, P. W.; Brus, L. E.; Kim, P.; Steigerwald, M. L.; Nuckolls, C. *Science* **2013**, *341* (6142), 157–160.
(32) Tomalia, D. A.; Khanna, S. N. *Chem. Rev.* **2016**, *116* (4), 2705–2774.
(33) Hodges, J. M.; Schaak, R. E. *Acc. Chem. Res.* **2017**, *50* (6), 1433–1440.
(34) Gary, D. C.; Flowers, S. E.; Kaminsky, W.; Petrone, A.; Li, X.; Cossairt, B. M. *J. Am. Chem. Soc.* **2016**, *138* (5), 1510–1513.
(35) Friedfeld, M. R.; Stein, J. L.; Cossairt, B. M. *Inorg. Chem.* **2017**, *56* (15), 8689–8697.
(36) Swager, T. M.; Gil, C. J.; Wrighton, M. S. *J. Phys. Chem.* **1995**, *99* (14), 4886–4893.
(37) Weder, C.; Wrighton, M. S. *Macromolecules* **1996**, *29* (15), 5157–5165.
(38) Li, Y.; Flood, A. H. *Angew. Chemie Int. Ed.* **2008**, *47* (14), 2649–2652.
(39) Flood, A. H. *Beilstein J. Org. Chem.* **2016**, *12* (1), 611–627.
(40) Feng, X.; Ding, X.; Jiang, D. *Chem. Soc. Rev.* **2012**, *41* (18), 6010.
(41) Boott, C. E.; Nazemi, A.; Manners, I. *Angew. Chemie Int. Ed.* **2015**, *54* (47), 13876–13894.
(42) Mo, Y.-P.; Liu, X.-H.; Wang, D. *ACS Nano* **2017**, *11* (11), 11694–11700.
(43) Liu, W.; Ulaganathan, M.; Abdelwahab, I.; Luo, X.; Chen, Z.; Rong Tan, S. J.; Wang, X.; Liu, Y.; Geng, D.; Bao, Y.; Chen, J.; Loh, K. P. *ACS Nano* **2018**, *12* (1), 852–860.
(44) Holliday, B. J.; Mirkin, C. A. *Angew. Chemie Int. Ed.* **2001**, *40* (11), 2022–2043.
(45) Leininger, S.; Olenyuk, B.; Stang, P. J. *Chem. Rev.* **2000**, *100* (3), 853–908.
(46) Miller, R. D.; Michl, J. *Chem. Rev.* **1989**, *89* (6), 1359–1410.
(47) West, R.; Carberry, E. *Science (80-.).* **1975**, *189* (4198), 179–186.
(48) Liu, Z.; Nalluri, S. K. M.; Stoddart, J. F. *Chem. Soc. Rev.* **2017**, *46* (9), 2459–2478.
(49) Ikonen, T.; Nissinen, T.; Pohjalainen, E.; Sorsa, O.; Kallio, T.; Lehto, V.-P. *Sci. Rep.* **2017**, *7* (1), 7880.
(50) Chen, S.-M.; Katti, A.; Blinka, T. A.; West, R. *Synthesis (Stuttg).* **1985**, 684–686.
(51) Kaats-Richters, V. E. M.; Cleij, T. J.; Jenneskens, L. W.; Lutz, M.; Spek, A. L.; van Walree, C. A. *Organometallics* **2003**, *22* (11), 2249–2258.
(52) Chernyavskii, A. I.; Larkin, D. Y.; Buzin, M. I.; Chernyavskaya, N. A. *Russ. Chem.*

Bull. **2011**, *60* (2), 304–309.
(53) Hengge, E. F.; Hassler, K.; Schrank, F. *Heteroat. Chem.* **1990**, *1* (6), 455–459.
(54) Fischer, R.; Frank, D.; Gaderbauer, W.; Kayser, C.; Mechtler, C.; Baumgartner, J.; Marschner, C. *Organometallics* **2003**, *22* (18), 3723–3731.
(55) Fischer, R.; Konopa, T.; Baumgartner, J.; Marschner, C. *Organometallics* **2004**, *23* (8), 1899–1907.
(56) Kayser, C.; Kickelbick, G.; Marschner, C. *Angew. Chemie Int. Ed.* **2002**, *41* (6), 989–992.
(57) Marro, E. A.; Press, E. M.; Purkait, T. K.; Jimenez, D.; Siegler, M. A.; Klausen, R. S. *Chem. - A Eur. J.* **2017**, *23* (62), 15633–15637.
(58) Press, E. M.; Marro, E. A.; Surampudi, S. K.; Siegler, M. A.; Tang, J. A.; Klausen, R. S. *Angew. Chemie - Int. Ed.* **2017**, *56* (2), 568–572.
(59) Gaderbauer, W.; Zirngast, M.; Baumgartner, J.; Marschner, C.; Tilley, T. D. *Organometallics* **2006**, *25* (10), 2599–2606.
(60) Uhlig, W.; Tzschach, A. *J. Organomet. Chem.* **1989**, *378* (1), C1–C5.
(61) Gudnason, P. I.; Arnason, I. *Org. Lett.* **2009**, *11* (9), 2015–2017.
(62) Tilley, T. D. *Acc. Chem. Res.* **1993**, *26* (1), 22–29.
(63) Waterman, R. *Chem. Soc. Rev.* **2013**, *42*, 5621–5980.
(64) Aitken, C.; Harrod, J. F.; Samuel, E. *Can. J. Chem.* **1986**, *64* (8), 1677–1679.
(65) Woo, H. G.; Walzer, J. F.; Tilley, T. D. *J. Am. Chem. Soc.* **1992**, *114* (18), 7047–7055.
(66) Tilley, T. D.; Woo, H. *Polym. Prepr.* **1990**, *31*, 228–229.
(67) Corey, J. Y.; Zhu, X. H.; Bedard, T. C.; Lange, L. D. *Organometallics* **1991**, *10* (4), 924–930.
(68) Corey, J. Y.; Xiao-Hong, Z. *J. Organomet. Chem.* **1992**, *439* (1), 1–17.
(69) Chang, L. S.; Corey, J. Y. *Organometallics* **1989**, *8* (8), 1885–1893.
(70) Folster, C. P.; Klausen, R. S. *Polym. Chem.* **2018**, *9*, 1938–1941.
(71) Chatgilialoglu, C.; Guerrini, A.; Lucarini, M.; Pedulli, G. F.; Carrozza, P.; Da Roit, G.; Borzatta, V.; Lucchini, V. *Organometallics* **1998**, *17* (11), 2169–2176.
(72) Casarini, D.; Lunazzi, L.; Mazzanti, A. *J. Org. Chem.* **1998**, *63* (24), 9125–9127.
(73) Blinka, T. A.; Helmer, B. J.; West, R. *Adv. Organomet. Chem.* **1984**, *23*, 193–218.
(74) Sørensen, O. .; Ernst, R. . *J. Magn. Reson.* **1983**, *51* (3), 477–489.
(75) Kanabus-Kaminska, J. M.; Hawari, J. A.; Griller, D.; Chatgilialoglu, C. *J. Am. Chem. Soc.* **1987**, *109* (17), 5267–5268.
(76) Chatgilialoglu, C. *Chem. Rev.* **1995**, *95* (5), 1229–1251.
(77) Gilman, H.; Atwell, W. H.; Schwebke, G. L. *J. Organomet. Chem.* **1964**, *2* (4), 369–371.
(78) Ortiz, J. V. *J. Chem. Phys.* **1991**, *94* (9), 6064–6072.
(79) Bande, A.; Michl, J. *Chem. - A Eur. J.* **2009**, *15* (34), 8504–8517.
(80) Trefonas, P.; Damewood, J. R.; West, R.; Miller, R. D. *Organometallics* **1985**, *4* (7), 1318–1319.
(81) Yuan, C. H.; West, R. *Macromolecules* **1994**, *27* (2), 629–630.
(82) Tsuji, H.; Terada, M.; Toshimitsu, A.; Tamao, K. *J. Am. Chem. Soc.* **2003**, *125* (25), 7486–7487.
(83) Fukazawa, A.; Tsuji, H.; Tamao, K. *J. Am. Chem. Soc.* **2006**, *128* (21), 6800–6801.
(84) Michl, J.; West, R. *Acc. Chem. Res.* **2000**, *33* (12), 821–823.

(85) Allen, L. C. *J. Am. Chem. Soc.* **1989**, *111* (25), 9003–9014.
(86) Feller, D.; Dixon, D. A.; Nicholas, J. B. *J. Phys. Chem. A* **2000**, *104* (48), 11414–11419.
(87) Bravo-Zhivotovskii, D.; Ruderfer, I.; Melamed, S.; Botoshansky, M.; Tumanskii, B.; Apeloig, Y. *Angew. Chemie Int. Ed.* **2005**, *44* (5), 739–743.
(88) Iwamoto, T.; Okita, J.; Kabuto, C.; Kira, M. *J. Am. Chem. Soc.* **2002**, *124* (39), 11604–11605.
(89) Gao, Y.; Zhao, Y.; Li, Y. C.; Huang, Q.; Mallouk, T. E.; Wang, D. *J. Am. Chem. Soc.* **2017**, *139* (43), 15288–15291.

Chapter 5: Stereocontrolled Syntheses of Functionalized *cis*- and *trans*-Siladecalins

The work in this chapter has been published as Marro, E. A.; Folster, C. P.; Press, E. M.; Im, H.; Ferguson, J. T.; Siegler, M. A.; Klausen, R. S. *J. Am. Chem. Soc.*, ASAPs. (DOI: 10.1021/jacs.9b09902)

Dr. Eric Press and Mr. Carlton Folster synthesized and fully characterized **5.13**.

Mr. Carlton Folster performed the first successful synthesis of **5.8**.

Mr. Hoyeon Im synthesized some early stage reagents using procedures optimized by Mr. Eric Marro.

Mr. Jack Ferguson introduced the concept of W-coupling to the group.

Dr. Maxime Siegler obtained single crystal x-ray data and solved crystal structures.

5.1 Introduction

Polycyclic silanes are a significant challenge for target-oriented synthesis.[1–5] Silicon clusters (e.g. octasilacubane[6,7]) are typically more oxidatively sensitive than the corresponding hydrocarbons.[8] Octasilacubanes are prepared by reductive coupling of halosilane precursors, limiting their molecular diversity. Reductive coupling conditions are not compatible with many functional groups, unselective and low yielding.

Polycyclic silanes exhibit unusual properties which are less-well understood than linear silanes.[9,10] The aforementioned octasilacubanes have absorbance spectra with features up to 500 nm. Kyushin synthesized bowl-shaped tricyclic silane **5.1** in 5% yield by reduction of a hexabrominated decasilane.[11] The molecule's bowl shape induces overlap of the Si-C σ* orbitals such that the LUMO has "pseudo-π*" symmetry, resulting in a

bathochromically shifted absorption spectrum relative to linear oligosilanes of a similar size.

Silanides are important intermediates for selective synthesis of cyclosilanes. Marschner synthesized bridged cyclosilane **5.2** and silanorbornane **5.3**,[12,13] by coupling potassium silanides[14] with halosilanes. Lewis acid-mediated skeletal rearrangement of a derivative of **5.3** led to the landmark synthesis of siladamantane **5.4**.[15] Silanide chemistry[16] has allowed the rare preparation of functionalized polycyclic silanes. Nuckolls et al. converted **5.2** into thiomethyl-functionalized **5.6**, as part of a study demonstrating conformational control of σ-conjugation and molecular conductance.[17,18]

Siladecalin is a long-standing challenge for chemical synthesis. In 1972, West isolated and characterized the multiple products of dimethyldichlorosilane and trimethylchlorosilane reductive coupling.[19] The major products were a polysilane (78%) and dodecamethylcyclohexasilane (Si_6Me_{12}, 10%). Six other silanes were isolated including one with a molecular weight of $Si_{10}Me_{18}$ (4% yield). West suggested it was permethylsiladecalin; however, definitive assignment was not possible until Hengge identified this product as the *trans*-siladecalin by X-ray crystallography.[20]

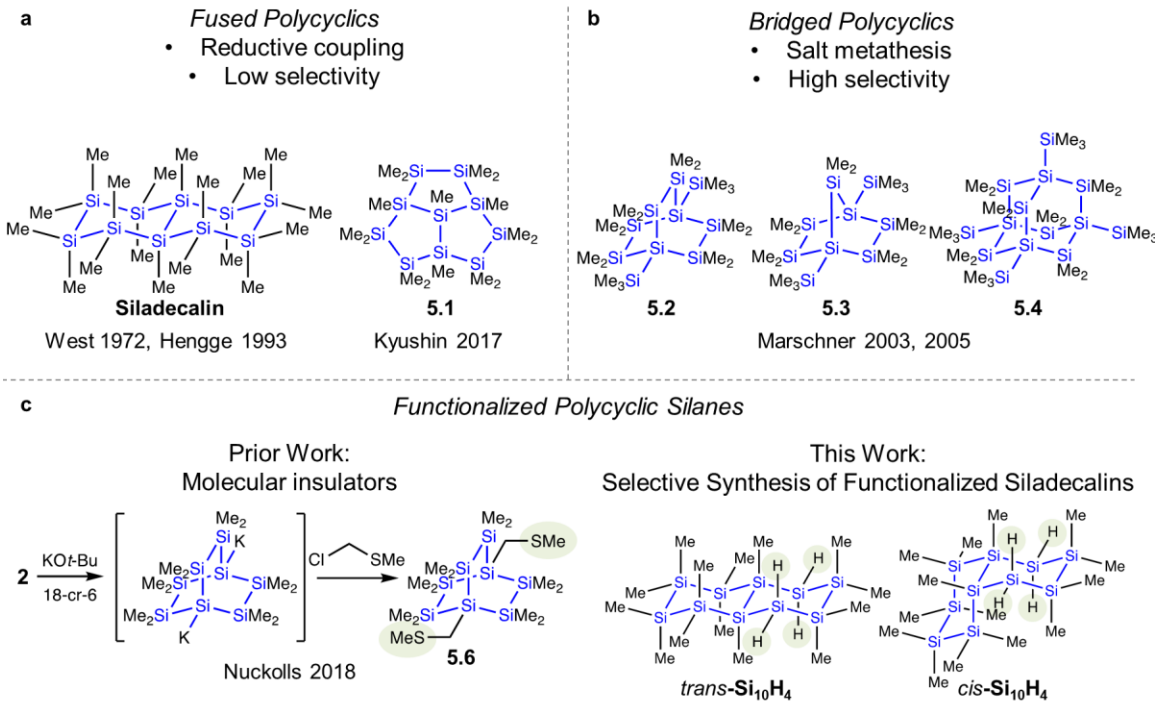

Figure 5.1. Polycyclic silanes. (a) Examples of fused polycyclic methylsilanes synthesized by reductive coupling. (b) Examples of bridged polycyclic methylsilanes synthesized by salt metathesis. (c) Functionalized polycyclic silanes.

The siladecalins in this chapter possess *cis*- and *trans*- isomers. The preparation of silicon-stereogenic silanes has focused on monosilanes as reagents and intermediates in asymmetric organic synthesis,[21–26] with isolated examples of cyclohexa- or cyclopentasilanes exhibiting *cis*-*trans* stereoisomerism.[27,28] Strategies to control relative stereochemistry at the siladecalin ring fusion are discussed in this chapter.

The selective synthesis of both diastereomers enables the determination of isomer-dependent properties. Diastereomers of carbocyclic decalin have markedly different properties.[29] The *trans*-decalin structure does not allow for ring inversion (chair flipping) and the room temperature ^{1}H NMR spectrum shows a broad, partially resolved band composed of overlapping axial and equatorial protons.[30,31] In contrast, chair interconversion in *cis*-decalin is rapid, resulting in coalescence of axial and equatorial

protons and shaper peaks even at –121 ºC.[30] Similar conformational dynamics in siladecalin scaffolds underlie differences in optical properties described herein.

5.2 Synthesis of Siladecalin Framework

Siladecalin **$Si_{10}Ph_4$** was synthesized by coupling of disilanide **5.7** and dichlorocyclohexasilane **5.8**. Disilanide $[(18\text{-cr-6})K]^+_2$**5.7** is a versatile intermediate in the preparation of site-selectively functionalized silicon rings.[32–35] **$Si_{10}Ph_4$** can serve as a common intermediate for a family of siladecalin frameworks, such as **$Si_{10}H_4$**, via acid-mediated dearylation and derivitization.[36]

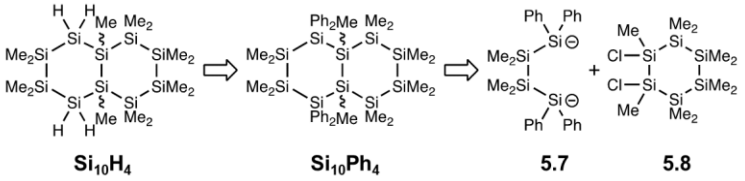

Scheme 5.1. Retrosynthesis of functionalized siladecalin.

This synthetic approach provides at least two avenues for control of the relative stereochemistry at the siladecalin ring fusion. Cyclohexasilane **5.8** is itself chiral – could the building block dictate the outcome of the coupling reaction? The stereochemical course of nucleophilic substitution at tetrahedral silicon atoms has long been recognized to be more complex than for alkanes and examples of both retention and inversion of configuration are known.[37–39] Substitution at a silicon-stereogenic chlorosilane with a structurally similar achiral lithium silanide was reported to proceed with inversion of stereochemistry.[40] Another avenue for stereochemical control is the possibility of thermodynamic equilibration of the *cis*- and *trans*-siladecalins.

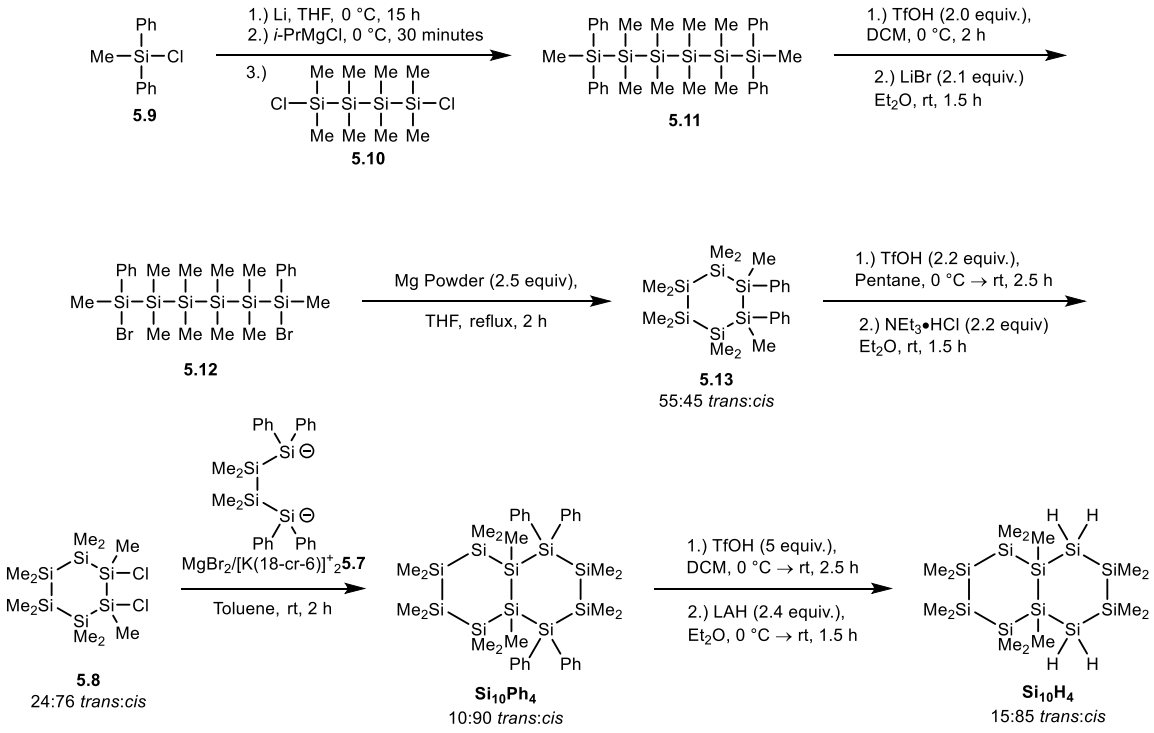

Scheme 5.2. Synthesis of *cis*-enriched siladecalin framework.

Chlorosilane **5.9** was reduced by lithium metal to form a lithium silanide. The corresponding magnesium silanide formed upon addition of *i*-PrMgCl. Salt metathesis with **5.10** produced hexasilane **5.11** in 73% yield. Two equivalents of triflic acid in dichloromethane selectively dearylated one phenyl group from each terminal silicon to form the ditriflate. Solvent exchange to diethyl ether and addition of lithium bromide produces **5.12** in 98% yield. Slow addition of a solution of **5.12** in tetrahydrofuran to a refluxing suspension of powdered magnesium in tetrahydrofuran produces **5.13** in a 54% yield (55:45 *trans:cis*). Treatment of **5.13** with triflic acid in pentane, solvent exchange to diethyl ether and addition of trimethylamine hydrochloride provides **5.8** in a 90% yield with a *dr* of 24:76 *trans:cis*. Under optimized conditions (*vide infra*), 24:76 *trans:cis* **5.8**

coupled to $MgBr_2$•[(18-cr-6)K]$^+_2$**5.7** in THF to produce **$Si_{10}Ph_4$** in 68% yield. **$Si_{10}Ph_4$** was isolated as a 10:90 mixture of diastereomers, favoring the *cis* isomer.

Table 5.1. Investigation of Salt Metathesis Synthesis of $Si_{10}Ph_4$.

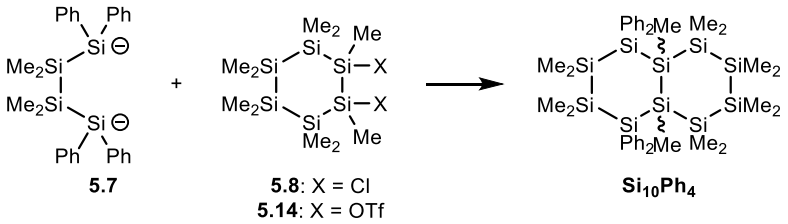

Entry	SM[a]	Countercation	Solvent	Yield	dr[b] (trans:cis)
1	5.14	K	Toluene	10%	19:81
2[b]	5.14	K	Toluene	5%	67:33
3	5.14	Mg	Toluene	0 %	-
4	5.8	K	THF	0 %	-
5	5.8	Cu	THF	0 %	-
6	5.8	Mg	THF	68%	10:90
7	5.8	K	Toluene	50%	23:77

[a] SM = starting material. [b] *dr* = diastereomeric ratio. [c] Reaction performed at 60 °C.

Leaving group, silanide countercation, and solvent have a large effect on the reactivity of silanides.[34,41,42] Table 5.1 summarizes screening these conditions. Coupling [(18-cr-6)K]$^+_2$**5.7** and **5.14** in toluene provided **$Si_{10}Ph_4$** in 10% yield with a 19:81 *trans:cis* ratio (entry 1). The assignment of diastereomers was based on X-ray crystallography (*vide infra*). Heating the reaction to 60 °C did not increase the yield; however, *trans*-siladecalin was the major isomer (entry 2). Magnesium bromide ($MgBr_2$) was added to [(18-cr-6)K]$^+_2$**5.7** to modify the countercation. The composition of this reagent has not been determined, but Marschner has shown the formation of Si_2Mg species from potassium silanides and $MgBr_2$ (2 SiK + $MgBr_2$ → Si_2Mg + 2KBr).[43] No reaction was observed between **5.14** and $MgBr_2$•[(18-cr-6)K]$^+_2$**5.7**, presumably due to the

magnesium silanide's low solubility in toluene (entry 3). Attempts to investigate other solvents were thwarted by **5.14**'s poor compatibility with other solvents: upon addition of **5.14** to THF, an insoluble gel formed, presumably due to ring-opening polymerization of THF.

While coupling **5.8** with either $[(18\text{-cr-6})K]^+_2$**5.7** or $CuCl_2$•$[(18\text{-cr-6})K]^+_2$**5.7** in THF did not yield the desired product (entries 4-5), $MgBr_2$•$[(18\text{-cr-6})K]^+_2$**5.7** in THF provided $\mathbf{Si_{10}Ph_4}$ in 68% yield (entry 6). Coupling of $[(18\text{-cr-6})K]^+_2$**5.7** and **5.8** in toluene provided $\mathbf{Si_{10}Ph_4}$ in 50% yield (entry 7). Polymeric material was the major byproduct in all cases.

With the exception of the heated reaction (entry 2), all reactions yielded predominantly the *cis* diastereomer. Many details of this reaction remain to be elucidated, a combination of the *cis* enrichment in **8** and **14** and an intramolecular tethering effect after formation of the first Si-Si bond may contribute to the diastereoselectivity.

The ability to isolate samples enriched in the *cis*-siladecalin framework encouraged efforts to isolate a high purity sample of *trans*-$\mathbf{Si_{10}Ph_4}$. Separation techniques were able to separate both isomers of **5.13**; however, no separation was observed by silica gel chromatography. Chiral HPLC separation was also unsuccessful. Recrystallization of 67:33 *trans:cis* $\mathbf{Si_{10}Ph_4}$ in cold hexanes provided 88:12 *trans:cis* $\mathbf{Si_{10}Ph_4}$, but further recrystallizations did not improve the *trans:cis* ratio.

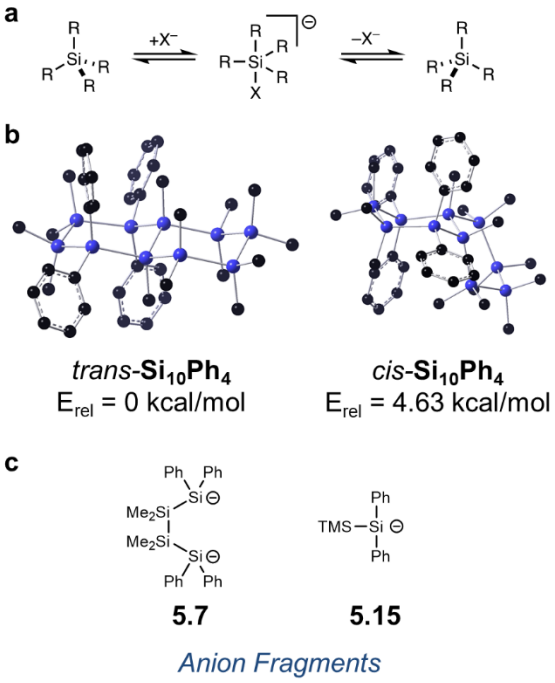

Figure 5.2. Epimerization studies. (a) "Weak-anion" induced inversion of a stereogenic silane via pentavalent intermediate or transition state. (b) Calculated energy difference between *trans*-**Si$_{10}$Ph$_4$** and *cis*-**Si$_{10}$Ph$_4$** (B3LYP/6-31G(d)). (c) Disilanide **5.7** and silanide **5.15** used in epimerization studies.

Thermodynamic equilibration ultimately allowed the isolation of 97:3 *trans:cis* **Si$_{10}$Ph$_4$**. Silanes are known to form pentavalent structures in the presence of anions that could serve as a pathway for inversion of a tetrahedral center (Figure 5.2a).[38,44] Density functional theory (DFT) calculations suggested that *trans*-**Si$_{10}$Ph$_4$** is the lower energy isomer by 4.63 kcal mol^{-1} (Figure 5.2b). Further evidence that thermodynamic equilibration might be possible included the observation of a change in isomer ratio upon heating during exploratory studies towards **Si$_{10}$Ph$_4$** (Table 5.1, entry 1 vs 2). Since organometallic reagents such as methyllithium (MeLi) and potassium tert-butoxide (KO*t*-Bu) are known to cleave Si-Si bonds, silanide reagents structurally related to **Si$_{10}$Ph$_4$** were explored to equilibrate *cis*-**Si$_{10}$Ph$_4$** to *trans*-**Si$_{10}$Ph$_4$** (Figure 5.2c).

Table 5.2. Anion-Induced Epimerization.

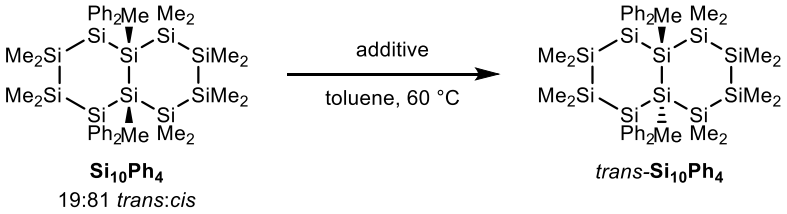

$Si_{10}Ph_4$
19:81 *trans*:*cis*

trans-**$Si_{10}Ph_4$**

Entry	Additive	Time	Equiv.	*dr* (*trans:cis*)
1	None	1 h	-	19:81
2	KCl	1 h	2.0	19:81
3	18-crown-6	1 h	2.0	19:81
4	KCl, 18-crown-6	1 h	2.0	19:81
5	$[(18\text{-cr-6})K]^+_2$**7**	3 h	0.25	97:3
6	$[(18\text{-cr-6})K]^+_2$**7**	1 h	0.10	45:55
7	$[(18\text{-cr-6})K]^+_2$**7**	3 h	0.10	53:47
8	$[(18\text{-cr-6})K]^+_2$**7**	24 h	0.10	69:31
9	$[(18\text{-cr-6})K]^+_2$**7**	48 h	0.10	85:15
10	$[(18\text{-cr-6})K]^+_2$**7**	72 h	0.10	92:8
11	$[(18\text{-cr-6})K]^+$**15**	4.33 h	0.50	89:11
12	$[(18\text{-cr-6})K]^+$**15**	72 h	0.25	92:8

Heating a 19:81 *trans*:*cis* sample of **$Si_{10}Ph_4$** in toluene alone or with benign species such as KCl or 18-cr-6 did not change the *dr* (Table 5.2, Entries 1-4). However, heating a solution of $[(18\text{-cr-6})K]^+_2$**7** and **$Si_{10}Ph_4$** to 60 °C for three hours had a dramatic effect on *dr* (Table 5.2, entry 5). With 0.25 equivalents of $[(18\text{-cr-6})K]^+_2$**5.7**, a 97:3 *trans:cis* ratio was reached in ca. 3 hours. A lower anion loading (0.1 equivalents of $[(18\text{-cr-6})K]^+_2$**7**) required 72 hours to obtain a 92:8 mixture of *trans*-**$Si_{10}Ph_4$**. In both cases, a small amount of an unidentified byproduct was seen by ^{1}H NMR spectroscopy, which does not correspond to $[(18\text{-cr-6})K]^+_2$**7**. Isolated yield with 0.1 loading of $[(18\text{-cr-6})K]^+_2$**5.7** is slightly lower than 0.25 equivalents. $[(18\text{-cr-6})K]^+$**5.15** also epimerized

Si$_{10}$Ph$_4$; however, longer reaction times (4.33 h) and lower isolated yields (56%) were observed compared to [(18-cr-6)K]$^+_2$**5.7**.

A combination of selective synthesis and postsynthetic equilibration provided synthetic routes to the functionalized siladecalin **Si$_{10}$Ph$_4$** framework enriched in either the *cis* or the *trans* isomer. Each of these isomers could be further derivatized without significant erosion of the ring fusion relative stereochemistry (Scheme 5.3). Dearylation of 10:90 *trans*:*cis* **Si$_{10}$Ph$_4$** with TfOH and reduction with LAH provided 15:85 *trans*:*cis* **Si$_{10}$H$_4$** in 65% yield. Similar reaction conditions with 97:3 *trans:cis* **Si$_{10}$Ph$_4$** provided 95:5 *trans*:*cis* **Si$_{10}$H$_4$** in 68% yield.

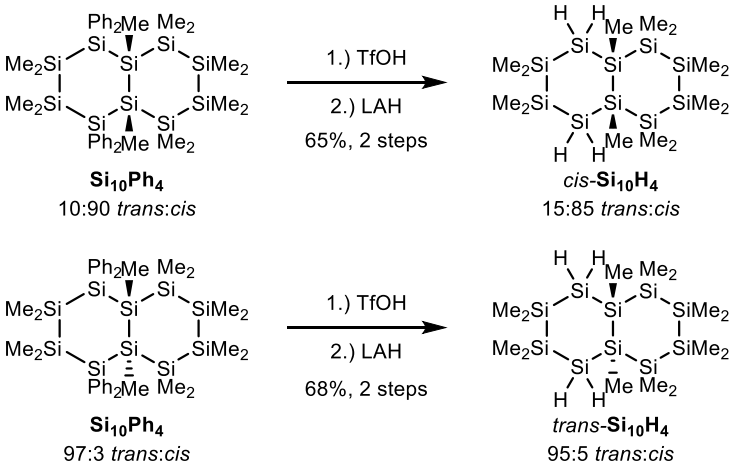

Scheme 5.3. Synthesis of *cis*- and *trans*-**Si$_{10}$H$_4$**.

5.3 Single-crystal X-Ray Crystallography

Single crystal X-ray crystallography facilitated assignment of the *cis* and *trans* isomers of **Si$_{10}$Ph$_4$** and **Si$_{10}$H$_4$**. Recrystallization of 67:33 *trans*:*cis* **Si$_{10}$Ph$_4$** in cold hexanes provided crystals enriched to 88:12 *trans:cis* **Si$_{10}$Ph$_4$**. Both diastereomers were found in the crystal structure. The occupancy factor matched the isomer ratio determined

by ^{1}H NMR spectroscopy: the occupancy factor of the *trans*-**Si$_{10}$Ph$_4$** isomer (major component) refines to 0.8867(13).

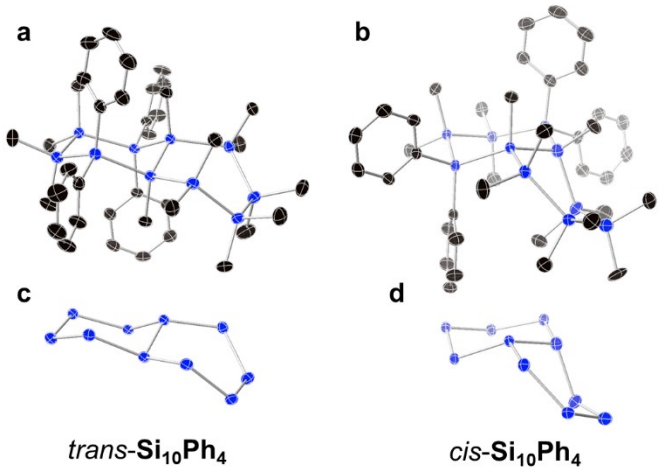

Figure 5.3. Displacement ellipsoid plots (50% probability level)of a) *trans*- and b) *cis*-**Si$_{10}$Ph$_4$**. Silicon frameworks of c) *trans*- and d) *cis*-**Si$_{10}$Ph$_4$** at 110(2) K. Black = carbon, blue = silicon. Hydrogens are omitted for clarity.

While DFT calculations predicted a chair-chair conformation for *trans*-**Si$_{10}$Ph$_4$** in the gas phase (Figure 5.2b), in the solid state the $SiPh_2$ ring adopted a chair conformation, while the permethylated ring adopted a twist-boat conformation (Figure 5.3a,c). DFT calculations suggested that both the chair-chair and chair-twist conformers are energetic minima, in which the chair-chair conformer is lower in energy by 1.19 kcal mol^{-1}. *cis*-**Si$_{10}$Ph$_4$** also adopted a contorted geometry in the solid state (Figure 5.3b,d). The $SiPh_2$ ring adopted a chair conformation, but the permethylated ring adopted a half-chair conformation. Hengge's crystal structure of permethyl trans-siladecalin adopted a chair-chair conformation,[20] so these distortions presumably alleviate steric interactions with the phenyl substituents.

Crystals of *trans*-**Si$_{10}$H$_4$** were grown by slowly cooling a hot acetonitrile solution of a 95:5 *trans:cis* **Si$_{10}$H$_4$**. In the solid state, *trans*-**Si$_{10}$H$_4$** adopts a chair-chair

conformation (Figure 5.4). X-ray diffraction quality crystals of *cis*-**$Si_{10}H_4$** could not be grown.

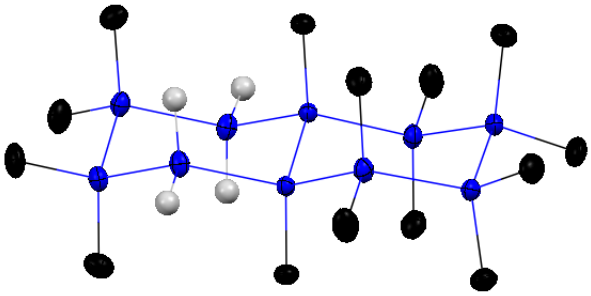

Figure 5.4. Displacement ellipsoid plot (50% probability level) of *trans*-**$Si_{10}H_4$** at 110(2) K. Black = carbon, blue = silicon, grey = hydrogen. Except for Si-H bonds, hydrogens are omitted for clarity. Disorder is omitted for clarity.

5.4 Siladecalin Conformational Analysis

Like carbocyclic decalin, a key difference between *cis*- and *trans*-siladecalin skeletons is that *cis* isomers can fully invert both rings simultaneously, while *trans* isomers are conformationally locked. Although the *trans*-siladecalins are not able to invert both rings simultaneously, individual rings may still contort and sample twist-boat conformers even at room temperature. This is supported by the X-ray crystallographic structures above which show both chair and twist-boat conformations in the solid state.

Cyclohexasilanes are more conformationally flexible than cyclohexanes. NMR studies of dodecamethylcyclohexasilane (Si_6Me_{12}) showed that axial and equatorial methyl resonances do not resolve until –165 °C, whereas much higher temperatures are typical for cyclohexanes (ca. –20 °C).[45] *Ab initio* calculations predict that the energy difference between chair and twist conformers of Si_6Me_{12}, and the barrier to twisting is smaller, than for cyclohexane.[46] Flock et al. provided evidence that twist-boat conformers contribute to the room temperature solid state Raman spectrum of Si_6Me_{12}.[46]

5.5 Vibrational Spectroscopy

Experimental ATR-FTIR spectra of neat 15:85 *trans:cis* **$Si_{10}H_4$** and 95:5 *trans:cis* **$Si_{10}H_4$** showed intriguing differences between isomers in the ν(SiH) region (Figure 5.5). The 15:85 *trans:cis* **$Si_{10}H_4$** spectrum displayed two broad stretches at 2069 cm^{-1} and 2085 cm^{-1}. The 95:5 *trans:cis* **$Si_{10}H_4$** spectrum displayed three sharper stretches at 2089 cm^{-1}, 2080 cm^{-1}, and 2070 cm^{-1}.

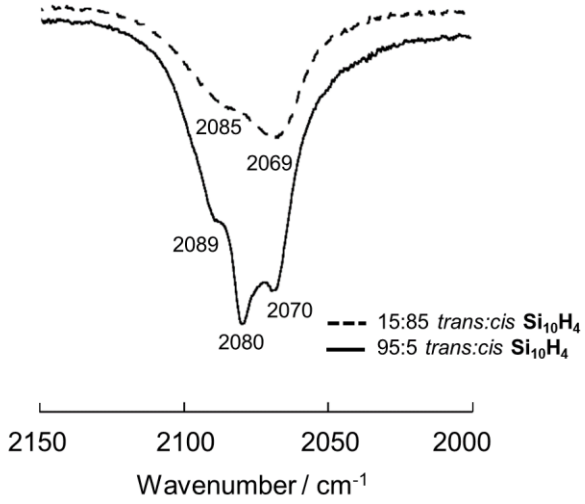

Figure 5.5. Experimental ATR-FTIR spectra of 15:85 *trans*:*cis* **$Si_{10}H_4$** (dashed) and 95:5 *trans*:*cis* **$Si_{10}H_4$** (solid).

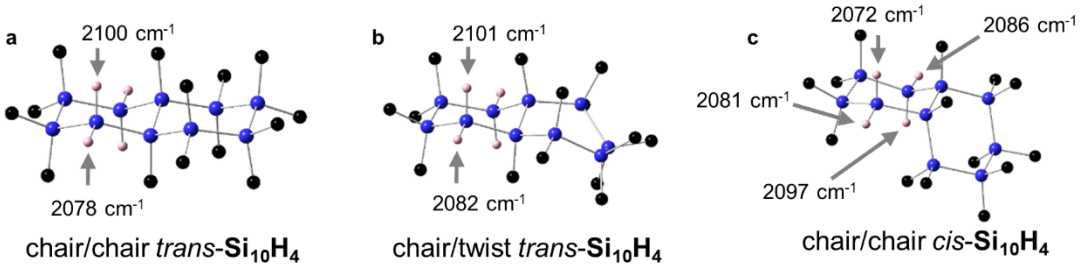

Figure 5.6. Calculated **$Si_{10}H_4$** structures and predicted ν(SiH) frequencies. a) *trans*-**$Si_{10}H_4$** (chair-chair conformer), b) *trans*-**$Si_{10}H_4$** (chair-twist conformer), and c) *cis*-**$Si_{10}H_4$** (chair-chair conformer). B3LYP/6-31G(d).

Simulated FTIR spectra (B3LYP/6-31G(d)) were calculated to understand how configuration affects the vibrational spectra. For *trans*-**$Si_{10}H_4$**, two conformations were

considered: the chair-chair conformer seen in the crystal structure and a chair-twist conformer consistent with the crystal structure of **$Si_{10}Ph_4$** (Figure 5.6). Good overall agreement between theory and experiment was observed, with ν(SiH) resonances predicted to fall between 2100 and 2050 cm^{-1}. For *trans*-**$Si_{10}H_4$** in either conformer, the axial and equatorial Si–H bonds resonated at significantly different frequencies, with the equatorial ν(SiH) approximately 20 cm^{-1} lower. These calculations suggest subtle but real differences in bond strength between axial and equatorial Si–H bonds in *trans*-$Si_{10}H_4$. Due to symmetry, both axial SiH groups have identical stretching frequencies and the same for equatorial SiH groups. Since *trans*-**$Si_{10}H_4$** cannot chair flip, the experimental FTIR spectrum likely reflects a mixture of chair and twist isomers in which axial and equatorial SiH bonds have unique resonances. Theory predicts four unique resonances for the Si–H bonds in *cis*-**$Si_{10}H_4$** due to the lower symmetry of the *cis* isomer. The overall greater conformational heterogeneity expected in the *cis*-**$Si_{10}H_4$** could explain the broad and featureless experimental FTIR spectrum.

5.6 UV Vis Spectroscopy

Oligosilane optical properties are strongly conformation dependent.[47] The HOMO-LUMO gap of linear silanes decreases as chain length increases, indicative of σ-conjugation.[48] σ-Conjugation is strongest in an all-*anti* conformation.[49,50] Deviations from the *anti* geometry contribute to short effective conjugation lengths and typical polysilanes absorb ultraviolet light ≤350 nm[51] and silane dendrimers ≤290 nm.[52]

Different conformational profiles of the *cis* and *trans* diastereomers suggested the possibility of stereoisomer-dependent optical properties. The absorbance spectra of aryl-

substituted oligosilanes are generally bathochromically shifted compared to methylated oligosilanes due to σ,π-mixing and other effects.[48,53,54]

Table 5.3. Tabulated UV-vis spectral data.[a]

Compound	λ (nm)	ϵ (L mol^{-1} cm^{-1})
***trans*-Si$_{10}$Ph$_4$**	192	235000
	257	45600
***cis*-Si$_{10}$Ph$_4$**	193	194000
***trans*-Si$_{10}$H$_4$**	207	74300
	240	21100
	270	9230
***cis*-Si$_{10}$H$_4$**	293	*Onset of Absorption

[a] Recorded in *n*-pentane at room temperature.

Absorbance spectra of all four siladecalins were obtained in *n*-pentane at room temperature (Table 5.3). There was a ca. 20 nm bathochromic shift in *cis*-**Si$_{10}$Ph$_4$**'s onset of absorbance compared to *cis*-**Si$_{10}$H$_4$** (315 vs 293 nm) (Figure 5.7a). Time-dependent DFT calculations reproduced this trend (TD-PBE0/6-311G(d)//B3LYP/6-31G(d)) (Figure 5.7b). The calculated highest occupied molecular orbital of **Si$_{10}$Ph$_4$** showed minimal electron density on the aromatic rings. Indeed, the HOMO's of **Si$_{10}$Ph$_4$** and **Si$_{10}$H$_4$** were markedly similar and concentrated on the σ-framework (Figure 5.8). The change in onset of absorption is attributed to low-lying π* orbitals centered on the aromatic rings.

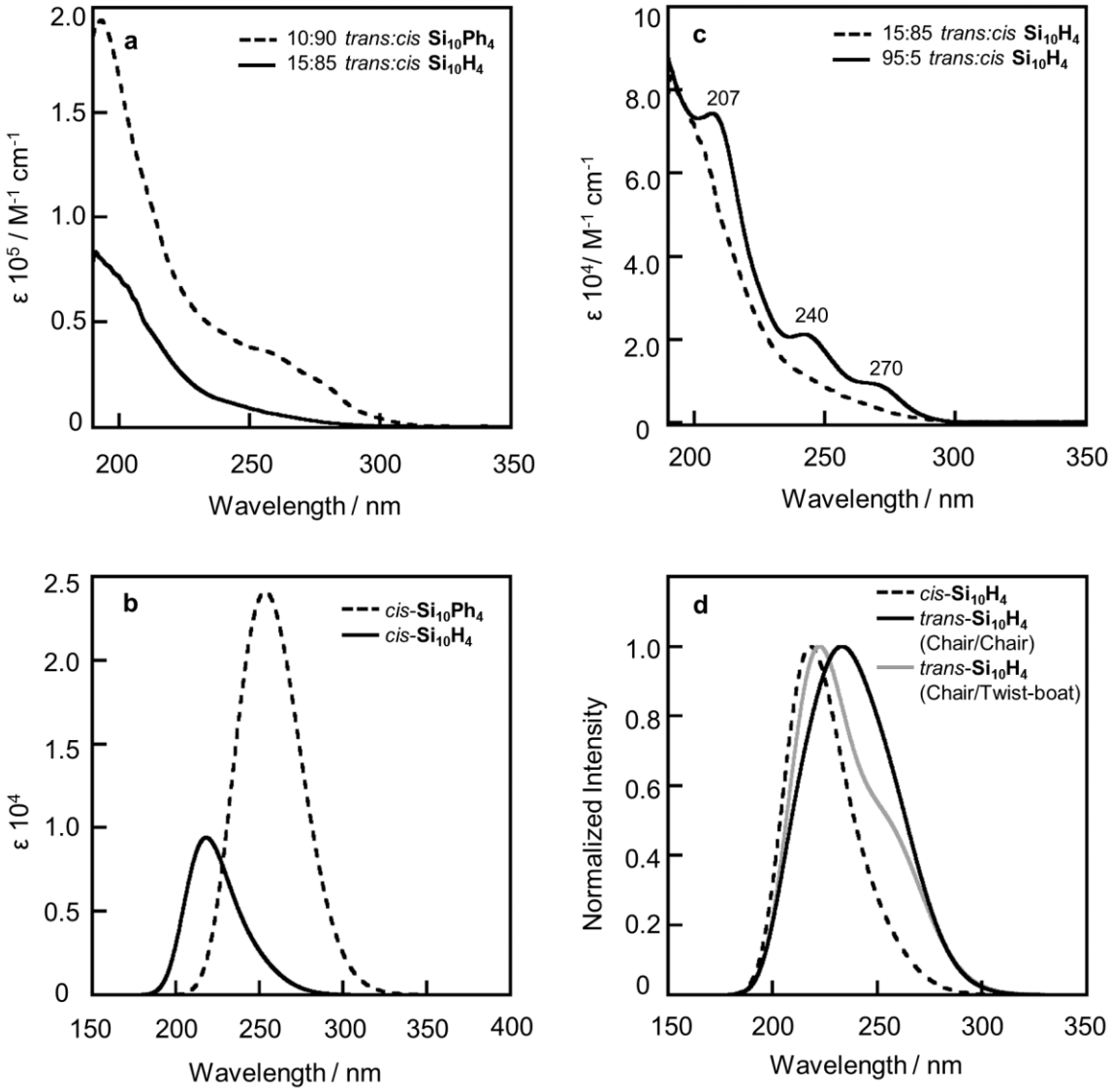

Figure 5.7. Experimental and simulated absorbance spectra. Comparison of Ph- and H-functionalized siladecalins. (a) Absorbance spectra of 15:85 *trans*:*cis* **$Si_{10}H_4$** (solid) and 10:90 *trans*:*cis* **$Si_{10}Ph_4$** (dashed) in *n*-pentane. [compound] = 5 x 10^{-6} M. (b) Calculated absorbance spectra of *cis*-**$Si_{10}Ph_4$** (dashed), *cis*-**$Si_{10}H_4$ (**solid). TD-PBE0/6-311G(d)//B3LYP/6-31G(d). Comparison of cis- and trans-$Si_{10}H_4$. (c) Absorbance spectra of 95:5 *trans*:*cis* **$Si_{10}H_4$** (solid) and 15:85 *trans*:*cis* **$Si_{10}H_4$** (dashed) in *n*-pentane. *n*-Pentane spectral cutoff is 190 nm. [compound] = 5 x 10^{-6} M. (d) Calculated absorbance spectra of *cis*-**$Si_{10}H_4$** (dashed), chair/chair *trans*-**$Si_{10}H_4$ (**solid black), and chair/twist-boat *trans*-**$Si_{10}H_4$** (solid gray). TD-PBE0/6-311G(d)//B3LYP/6-31G(d).

Table 5.4. Tabulated details of absorbance spectra from TD-DFT. TD-PBE0/6-311G(d)//B3LYP/6-31G(d).

Compound	λ (nm)	Transition	% Contribution	Oscillator Strength
***trans*-$Si_{10}Ph_4$** (Chair/Chair)	300.70	HOMO-3 → LUMO	85%	0.0768
	325.49	HOMO → LUMO+4	54%	0.0594
		HOMO-1 → LUMO+2	25%	
	327.89	HOMO-1 → LUMO	54%	0.0640
		HOMO → LUMO+3	34%	
***trans*-$Si_{10}Ph_4$** (Chair/Twist)	257.70	Eight transitions, none above 50%		0.1903
	258.95	Six transitions, none above 50%		0.1514
	275.25	HOMO → LUMO	87%	0.0753
***cis*-$Si_{10}Ph_4$**	241.10	Eight transitions, none above 50%		0.1061
	251.64	Eight transitions, none above 50%		0.0938
	261.07	HOMO → LUMO +2	54%	0.1340
		HOMO -1 → LUMO +1	18%	
	268.32	HOMO → LUMO +1	70%	0.1258
***trans*-$Si_{10}H_4$** (Chair/Chair)	233.19	HOMO-1 → LUMO+1	77%	0.1821
	257.00	HOMO → LUMO	96%	0.1496
***trans*-$Si_{10}H_4$** (Chair/Twist)	225.54	HOMO → LUMO+3	89%	0.0557
	228.32	HOMO-1 → LUMO+1	75%	0.0720
	260.21	HOMO → LUMO	96%	0.0813
***cis*-$Si_{10}H_4$**	210.61	Ten transitions, none above 50%		0.0413
	215.46	Six transitions, none above 50%		0.0497
	221.29	HOMO-4 → LUMO	66%	0.0432
	231.24	HOMO → LUMO+1	67%	0.0368

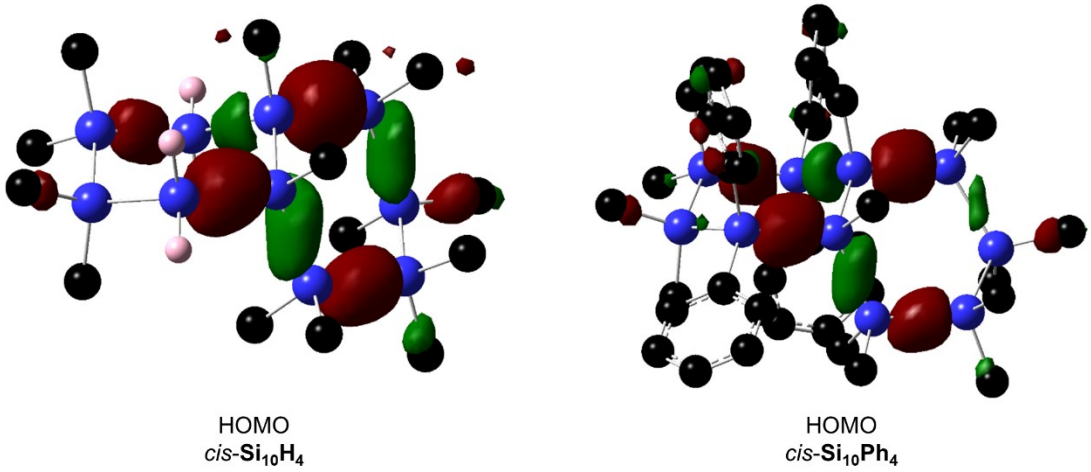

Figure 5.8. HOMOs of *cis*-$Si_{10}H_4$ and ***cis*-Si$_{10}$Ph$_4$** highlighting their similarity; orbital density is located on the silicon framework in both cases.

Simulated absorbance spectra were calculated (TD-PBE0/6-311G(d)//B3LYP/6-31G(d)). The onset of absorbance of pure ***cis*-Si$_{10}$H$_4$** was predicted to be 15 nm blue-shifted compared to ***trans*-Si$_{10}$H$_4$** (Figure 5.7d, dashed vs. solid black lines line). This may not be observed experimentally due to the minor component of ***trans*-Si$_{10}$H$_4$** present in the synthetic sample. Both a HOMO to LUMO transition and HOMO-1 to LUMO+1 transition contribute to the broad chair/chair ***trans*-Si$_{10}$H$_4$** simulated spectrum (Table 5.4). A simulated absorbance spectrum of ***trans*-Si$_{10}$H$_4$** in a chair-twist conformation (Figure 9d, gray) has a spectrum with a λ_{max} of 223 nm corresponding to the HOMO-1 to LUMO+1 transition and a shoulder at 260 nm corresponding to the HOMO to LUMO transition (Table 5.4).

The three features in 95:5 ***trans*-Si$_{10}$H$_4$** spectrum could correspond to the presence of both chair and twist ring conformers in the synthetic sample. Tekautz et al. found evidence of dodecamethylcyclohexasilane twist-boat conformers at room temperature by solid-state Raman spectroscopy.[46] Likewise, the broadness of the spectrum of majority ***cis*-Si$_{10}$H$_4$** could be a consequence of chair-flipping at room temperature. The time-

dependent DFT method used in this study was selected for its prior success in predicting optical properties of linear silanes[55], but a different method may be optimal for cyclosilanes.

5.7 NMR Spectroscopy

Polycyclic systems can exhibit unusual NMR spectra. *cis*-Decalin undergoes rapid ring-flipping, resulting in coalescence of the signals corresponding to axial and equatorial substituents. However, *trans*-decalin does not ring flip and its ^{1}H NMR spectrum shows closely overlapping peaks assigned to inequivalent axial and equatorial protons. [30,31]

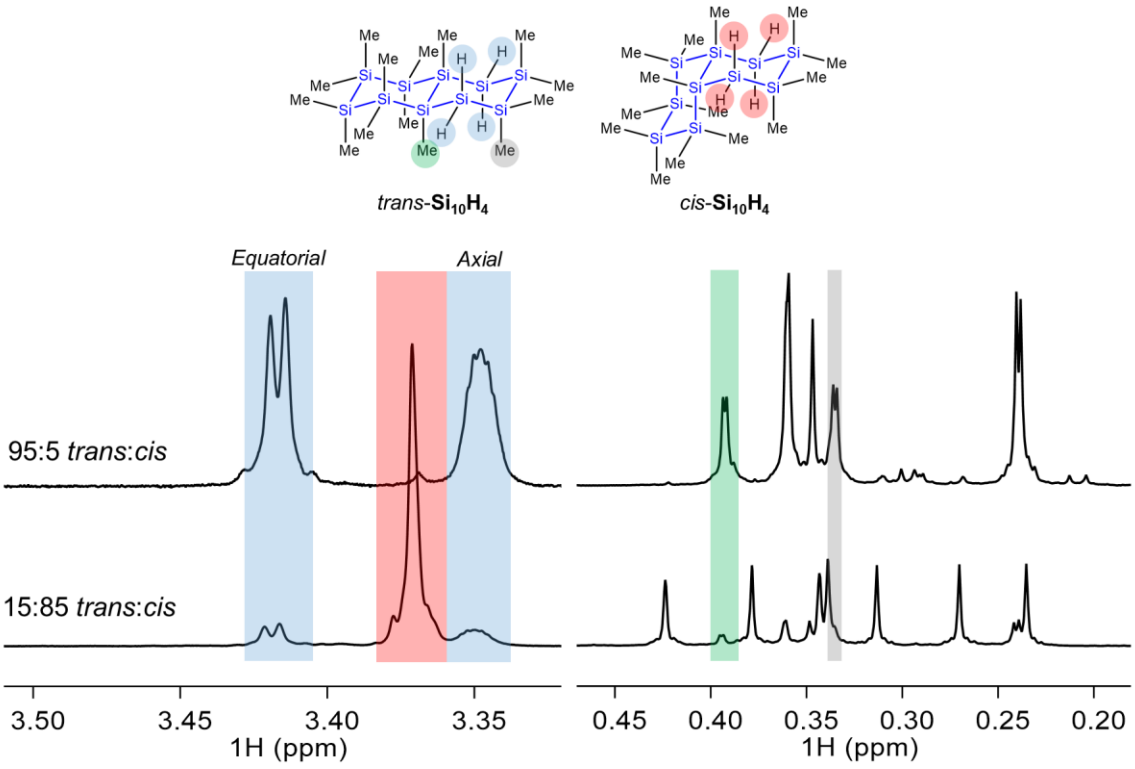

Figure 5.9. Cropped ^{1}H NMR spectra (400 MHz, C_6D_6) of 95:5 *trans:cis* **Si$_{10}$H$_4$** (top) and 15:85 *trans:cis* **Si$_{10}$H$_4$** (bottom). Only Si-H and Si-Me regions shown for clarity.

All *cis*- and *trans*-siladecalins isolated herein have sharp signals in their ^{1}H NMR spectra. Cropped ^{1}H NMR spectra of *cis*- and *trans*-**Si$_{10}$H$_4$** are shown in Figure 5.9, focusing on the SiH and SiMe regions of the spectra. Some remarkable differences are

observed. The *cis*-**$Si_{10}H_4$** has a single sharp peak (Figure 5.9, pink) due to rapid chair-flipping and coalescence of axial and equatorial SiH groups.

In contrast, the *trans*-**$Si_{10}H_4$** has two distinct resonances: a doublet (δ 3.42, J = 2.1 Hz) and a multiplet (δ 3.35) (Figure 5.9, blue). Both peaks integrate to 2H and are thought to correspond to axial and equatorial SiH's. NOESY spectroscopy was inconclusive in assigning each peak to the axial or the equatorial position.

The splitting patterns provided additional insight facilitating assignment. Long-range ($>^3$J) ^{1}H-^{1}H coupling in saturated systems is typically weak, with the exception of rigid cyclic systems that achieve particularly favorable geometric alignments.[56–58] W-coupling refers to a coplanar, *anti*-alignment of H-C-C-C-H bonds that results in detectable long-range coupling and has been identified in 1,3-functionalized cyclohexanes and in bicyclo[1.1.1]pentane scaffolds (Figure 5.10).[59,60] Spencer et al. reported W-coupling as a diagnostic tool in the identification of *cis*- and *trans*-decalins bearing angular methyl groups: the freely rotating methyl group in *trans*-10-methyldecalin has multiple W-coupled pathways with axial protons, while *cis*-10-methyldecalin does not.[61] This results in significant line broadening of the angular methyl resonance in the *trans* isomer compared to the *cis*.

In *trans*-**$Si_{10}H_4$**, only the axial proton is poised to undergo W-coupling with neighboring methyl groups (H-Si-Si-C-H, Figure 5.10b). The δ 3.35 multiplet was assigned to the axial Si-H. W-coupling can also be observed in the alkyl region, where two Si-Me resonances (Figure 5.9, green, grey) appear as doublets (J = 0.78–0.82 Hz). The δ 3.42 resonance was assigned to the equatorial proton with a splitting pattern dominated by geminal (^{2}J) coupling to the axial Si-H.

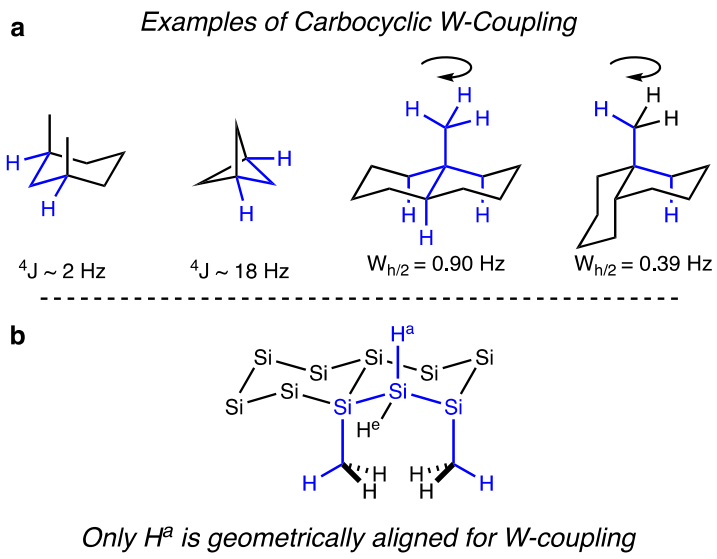

Figure 5.10. (a) Examples of W-coupling in carbocyclic systems. (b) Conformational analysis of W-coupling in *trans*-$\mathbf{Si_{10}H_4}$. Groups not implicated in W-coupling are omitted for clarity. ^4J = four-bond ^1H-^1H coupling constant; $W_{h/2}$ = line width at half-height of angular methyl groups. For comparison, TMS $W_{h/2}$ = 0.33 Hz. Values from references [59–61]

5.8 Conclusions

This chapter describes the stereocontrolled syntheses of several members of a family of *cis*- and *trans*-siladecalins. Phenyl and hydrogen functionalized siladecalins may serve as useful building blocks to higher order materials.[32,34,62,63] The identity of the countercation in the key salt metathesis step effects diastereoselectivity, favoring the *cis* isomer. Equilibration to the thermodynamically lower energy *trans* isomer was achieved with an anionic additive. Structural assignments are supported by X-ray crystallography.

Divergent conformational properties are expected for *cis* and *trans* siladecalin scaffolds, which are supported by NMR spectroscopy. Relative stereochemistry influences conformational properties, resulting in a strong effect on optical properties. The less dynamic *trans*-siladecalin frameworks have multiple sharp features, which are

proposed to reflect contributions from chair/chair, chair/twist, and twist/twist conformers. The highly flexible *cis*-siladecalins have broad, featureless absorption spectra.

Stereocontrolled synthesis is a powerful tool for the preparation of well-defined materials with novel properties. The synthetic approach outlined in this chapter may facilitate the synthesis of more examples of cyclosilanes bearing multiple chiral silicon centers.

5.9 Experimental Details

General Experimental Procedures: All experiments were performed under an atmosphere of dry nitrogen or argon with the rigid exclusion of air and moisture using standard Schlenk techniques or in a nitrogen glove box. All glassware was oven-dried overnight in a 175 °C oven.

Instrumentation: ^{1}H NMR, ^{13}C {^{1}H} NMR and ^{29}Si {^{1}H} NMR were recorded on either a Bruker Avance 300, 400 or III HD 400 MHz Spectrometer and chemical shifts are reported in parts per million (ppm). Spectra were recorded in benzene-d_6 or chloroform-d with tetramethylsilane or the residual solvent peak as the internal standard (^{1}H NMR: C_6H_6 $\delta = 7.16$; $CHCl_3$ $\delta = 7.26$). Multiplicities are as indicated: s (singlet), d (doublet), t (triplet), dd (doublet of doublets), tt (triplet of triplets), m (multiplet), and br (broad). Coupling constants, J, are reported in Hertz and integration is provided, along with assignments, as indicated. Mass Spectrometry (MS) and High Resolution Mass Spectrometry (HRMS) were either performed in the Department of Chemistry at Johns Hopkins University using a VG Instruments VG70S/E magnetic sector mass spectrometer with EI (70 eV) or in the Columbia University Department of Chemistry mass spectrometry facility using a Waters XEVO G2XS QToF mass spectrometer equipped with a UPC2 SFC inlet, electrospray

ionization (ESI) probe, atmospheric pressure chemical ionization (APCI) probe, and atmospheric solids analysis probe (ASAP). The UNIlab Plus Glove Box by MBRAUN was maintained under nitrogen atmosphere. All column chromatography was performed on a Teledyne ISCO Combiflash Rf+ using Redisep Rf silica columns. IR spectra were collected on either a Thermo Scientific Nicolet iS5 spectrometer equipped with iD5 ATR laminated diamond crystal attachment or a Thermo Scientific Nicolet Nexus 670 FT-IR. Elemental analysis was performed by Robertson Microlit Laboratories. Low carbon content in elemental analysis for silicon compounds may be due to incomplete combustion related to SiC formation. UV-Vis spectroscopy was performed on a Shimadzu UV-1800 UV-Vis spectrophotometer. The spectra were measured at room temperature in n-pentane in a quartz cuvette (10 mm).

Materials: Unless otherwise specified, all chemicals were used as purchased without further purification. Solvents used for extraction and column chromatography were reagent grade and used as received. Reaction solvents THF (Fisher, HPLC grade), diethyl ether (Fisher, anhydrous, butylated hydroxytoluene stabilized, certified ACS), dichloromethane (Fisher, cyclohexane stabilized, HPLC grade), pentane (Fisher, certified ACS), and toluene (Fisher, certified ACS) were dried on a J. C. Meyer Solvent Dispensing System (SDS) using stainless steel columns packed with neutral alumina (except for toluene which is dried with neutral alumina and Q5 reactant, a copper(II) oxide oxygen scavenger), following the manufacturer's recommendations for solvent preparation and dispensation unless otherwise noted.

Ethyl acetate (anhydrous), isopropyl magnesium chloride (2M in THF), lithium, lithium aluminum hydride (LAH), magnesium powder, magnesium bromide ethyl etherate ($MgBr_2$•OEt_2), were purchased from Sigma Aldrich.

Triethylamine hydrochloride, trifluoromethanesulfonic acid (triflic acid) were purchased from Acros Organics.

Copper(II) chloride, lithium bromide were purchased from Fisher Scientific.

Chloro(methyl)diphenylsilane was purchased from Alfa Aesar.

Compounds $[(18\text{-cr-}6)K]^+_2$**5.7, 5.10**, and $[(18\text{-cr-}6)K]^+$**5.15,** were synthesized according to literature procedures.[1,2]

Preparation of 5.11.

A 250 mL Schlenk flask equipped with a stir bar under argon was charged with Li (8.2 equiv., 270.16 mmol, 1.87 g). The Li was suspended in THF (67.5 mL) and then cooled to 0 °C in an ice/water bath. **5.9** (2.05 equiv., 67.54 mmol, 14.20 mL) was added dropwise via syringe over 10 minutes. During the addition, the solution went from colorless to yellow and eventually a dark brown. The reaction mixture was left to warm to room temperature and stir overnight (~15 hours).

The following morning, the reaction mixture was filtered through a fritted tube into a new 250 mL Schlenk flask with stir bar under argon. The reaction mixture was cooled to 0 °C in an ice/water bath. iPrMgCl (2.0 M in THF, 67.54 mmol, 33.8 mL) was added dropwise to the reaction mixture via syringe. After addition was complete, the reaction mixture was left to stir at 0 °C for 30 minutes. **5.10** (1.0 equiv., 32.95 mmol, 10.00 g) was

added dropwise via syringe to the cooled flask and the reaction mixture was left to warm to room temperature and stir overnight.

The following morning, the reaction was again cooled to 0 °C (ice/water bath). The septum was removed from the Schlenk flask and 34 mL of water was added slowly dropwise via pipette to quench the reaction (Caution! Vigorous quench). Then, 34 mL of saturated ammonium chloride was added and the mixture was transferred to a 500 mL separatory funnel. The aqueous and organic layers were separated. The aqueous layer was extracted with diethyl ether (3 x 70 mL). The combined organic layers were dried over anhydrous magnesium sulfate, filtered, and concentrated on a rotary evaporator to yield a white solid. The solid was subjected to automated column chromatography with 100% hexanes then with a gradient to 5% dichloromethane/95% hexanes to yield **5.11** as a colorless crystalline solid (Yield: 15.17 g, 73 %).

Tabulated Characterization Data for **5.11**

^{1}H NMR	(400 MHz, $CDCl_3$) δ = 7.49 – 7.45 (m, 9H), 7.35 – 7.30 (m, 13H), 0.63 (s, 6H), 0.20 (s, 12H), -0.05 (s, 12H).
^{13}C {^{1}H} NMR	(101 MHz, $CDCl_3$) δ 137.87, 134.99, 128.85, 127.94, -3.61, -4.27, -4.31.
^{29}Si {^{1}H} NMR	(79 MHz, $CDCl_3$) δ -19.00, -38.46, -42.92.
HRMS	Calcd. for $C_{34}H_{50}Si_6$: 626.2528. Found: 626.2521

Preparation of 5.12.

A 250 mL Schlenk flask equipped with a stir bar under argon was charged with **5.11** (1.0 equiv., 18.60 mmol, 11.67 g) and DCM (124.0 mL). In an inert atmosphere glove

box, trifluoromethanesulfonic acid (2.0 equiv., 37.21 mmol, 3.29 mL) was dispensed into a closed 5 mL addition funnel. The addition funnel was sealed and removed from the glove box. Under a heavy flow of argon, the addition funnel was attached to the Schlenk flask. The reaction mixture was cooled to 0 °C with an ice water bath and the trifluoromethanesulfonic acid was gradually added. 1 mL of DCM was added to the addition funnel to wash any residual trifluoromethanesulfonic acid into the reaction flask. After half an hour, the ice water bath was removed and the reaction mixture was stirred for 2 hours at room temperature.

After 2 hours volatile materials were removed under vacuum, and the resulting white solid was dissolved in diethyl ether (124.0 mL). LiBr (2.05 equiv., 38.14 mmol, 3.30 g) was weighed into a vial in a glove box, then capped. The vial was removed from the glove box, the septum was removed from the Schlenk flask and the LiBr was quickly poured into the reaction mixture. The reaction mixture was stirred for 1.5 hours. The LiBr is slow to dissolve, but a homogenous mixture was eventually observed.

After 1.5 hours of stirring, the reaction mixture was concentrated to a white solid under vacuum. The Schlenk flask was brought into the glove box, and the white residue suspended in pentane (30 mL). The suspension was filtered through a fritted funnel into a tared round bottom flask. The Schlenk flask was rinsed with pentane (3 x 10 mL) and passed through the fritted funnel. Pentane was removed under vacuum to provide **5.12** (11.62 g, 98%) as a white solid.

Tabulated Characterization Data for **5.12**

^{1}H NMR (400 MHz, $CDCl_3$) δ = 7.59 – 7.55 (m, 4H), 7.41 – 7.36 (m, 6H), 0.92 (s, 6H), 0.25 (d, *J*=3.54, 12H), 0.13 – 0.03 (m, 12H).

^{13}C {^{1}H} NMR (101 MHz, $CDCl_3$) δ 136.09, 133.83, 130.08, 128.25, 1.73, -4.45 (dd, *J*=10.5, 2.4), -5.02 (d, *J*=7.9).

^{29}Si {^{1}H} NMR (79 MHz, $CDCl_3$) δ 12.92, -39.29, -39.58.

Preparation of 5.13

In a glove box, powdered magnesium (4.0 equiv., 76.04 mmol, 1.85 g) was weighed into a 3-neck 250 mL round bottom flask. The round bottom flask was equipped with a stir bar, reflux condenser with a hose adapter with a stop cock on one neck, a glass stopper on another neck, and a rubber septum on the third neck. The round bottom flask was removed from the glove box and attached to a Schlenk line. I_2 (0.12 equiv., 2.21 mmol, 0.56 g) was added to the round bottom flask under heavy argon flow, and the flask resealed. The round bottom flask sat for about 15 minutes after the addition of I_2 before THF (60.0 mL) was added via syringe. The magnesium-THF suspension was then heated to reflux in a hot oil bath.

In a glove box, **5.12** (1.0 equiv., 19.01 mmol, 12.03 g) was weighed into a 250 mL Schlenk flask. The Schlenk flask was sealed with a septum, removed from the glove box and attached to a Schlenk line. **5.12** was dissolved in THF (25.0 mL). The solution of **12** was then added dropwise by syringe to the refluxing magnesium/THF suspension over 15 minutes. The flask containing **5.12** was rinsed twice (2x20 mL) with THF and each rinse added to the magnesium suspension. The reaction was left to reflux for 2 hours.

After 2 hours, consumption of starting material was checked by ^{1}H NMR. An aliquot of the reaction mixture (~0.05 mL) was taken by syringe, added to an oven dry 10 mL round bottom flask, and concentrated to a colorless oil. This round bottom flask was

taken into the glove box, and an air-free NMR sample was prepared from the colorless oil. If any starting material was left, the reaction mixture was cooled to room temperature, a spatula tip of I_2 was added, and the reaction was then refluxed for an additional 2 hours.

When the starting material was completely consumed, the reaction mixture was removed from the oil bath, cooled to room temperature then further cooled to 0 °C in an ice-water bath. The reaction was quenched by dropwise addition of deionized water by pipette. When the quench was no longer vigorous, additional deionized water (100 mL in total) was added to the reaction mixture. Residual magnesium was removed by gravity filtration, then re-suspended in deionized water and quenched with 1M HCl.

The filtrate was poured into a 500 mL separatory funnel and diluted with an additional 50 mL of deionized water. The organic and aqueous layers were separated. The aqueous layer was extracted with Et_2O (3 x 100 mL). The combined organics were dried with $MgSO_4$, filtered and concentrated on a rotary evaporator to a yellow oil. The oil was subjected to automated column chromatography (100% hexanes, then a gradient to 5% dichloromethane/95% hexanes) to yield **5.13** as a colorless oil which solidified upon storage (yield: 4.82 g, 54%). **5.13** was isolated in a 55:45 ratio of *trans:cis* isomers.

Samples of pure *cis*-**5.13** and pure *trans*-**5.13** were isolated from a smaller scale reaction (1.58 mmol of **5.12**) by automated column chromatography run with 100% hexanes, collecting the first 25 fractions and last 3 fractions respectively. Crystals of *cis*-**5.13** were grown by dissolving in hot methanol and slowly cooling to room temperature. Crystals of *trans*-**5.13** were grown by dissolving in hot methanol and slowly cooling to room temperature.

Tabulated Characterization Data for ***5.13***

^{1}H NMR	*trans*-**5.13** (400 MHz, $CDCl_3$) δ = 7.34 – 7.29 (m, 4H), 7.25 – 7.22 (m, 6H), 0.49 (s, 6H), 0.26 (s, 6H), 0.23 (s, 6H), 0.23 (s, 6H), 0.17 (s, 6H).
	cis-**5.13** (400 MHz, $CDCl_3$) δ = 7.26 – 7.16 (m, 10H), 0.46 (s, 6H), 0.21 (s, 6H), 0.20 (s, 6H), 0.17 (s, 6H), 0.13 (s, 6H).
^{13}C {^{1}H} NMR	*trans*-**5.13** (101 MHz, $CDCl_3$) δ 137.45, 134.78, 127.88, 127.61, -4.38, -5.12, -5.56, -6.56, -6.78.
	cis-**5.13** (101 MHz, $CDCl_3$) δ 137.37, 135.37, 128.14, 127.63, -5.10, -5.43, -5.63, -5.80, -6.69.
^{29}Si {^{1}H} NMR	*trans*-**5.13** ^{29}Si NMR (79 MHz, $CDCl_3$) δ -40.92, -41.26, -41.73.
	cis-**5.13** (79 MHz, $CDCl_3$) δ -40.07, -41.86, -42.07.
HRMS	Calcd. for $C_{22}H_{40}Si_6$: 472.1746. Found: 472.1753

Preparation of 5.8

A 250 mL Schlenk flask equipped with a stir bar under argon was charged with **5.13** (1.00 equiv., 10.2 mmol, 4.82 g) and pentane (100 mL). In an inert atmosphere glove box, trifluoromethanesulfonic acid (2.20 equiv., 22.4 mmol, 1.98 mL) was dispensed into a closed addition funnel. The addition funnel was sealed and removed from the glove box. Under a heavy flow of argon, the addition funnel was attached to the Schlenk flask. The reaction mixture was cooled to 0 °C with an ice water bath and the trifluoromethanesulfonic acid was added. 2.00 mL of pentane was added to the addition funnel to wash any residual trifluoromethanesulfonic acid into the reaction flask. After half an hour, the ice water bath was removed and the reaction mixture was stirred for 2 hours at room temperature.

After 2 hours volatile materials were removed under vacuum, and the resulting yellow oil dissolved in diethyl ether (100 mL). Triethylamine hydrochloride (2.00 equiv., 20.4 mmol, 2.80 g) was then added to the reaction mixture as a solid under a heavy flow of argon. The solid trimethylamine hydrochloride was slow to dissolve. The reaction mixture was left to stir overnight.

After stirring overnight, the reaction mixture was biphasic. The reaction mixture was cooled to -78 °C in a dry ice/acetone bath and the bottom layer of ionic liquid solidified. The top layer was cannula transferred to an oven dried 100 mL Schlenk flask and concentrated to a white solid. The solid was purified by sublimation under vacuum at 90 °C to yield **5.8** as a crystalline white solid (Yield: 3.56 g, 90%). **5.8** is isolated as a 24:76 *trans*:*cis* mixture of isomers.

Tabulated Characterization Data for **5.8**

^{1}H NMR (400 MHz, $CDCl_3$) δ = 0.69 (s, 6H), 0.64 (s, 2H), 0.34 (s, 2H), 0.28 (s, 6H), 0.27 (s, 6H), 0.24 (s, 2H), 0.22 (s, 7H)*, 0.22 (s, 2H), 0.19 (s, 6H), 0.16 (s, 2H). *Integral off due to overlap with minor isomer

^{13}C {^{1}H} NMR (101 MHz, C_6D_6) δ -0.84, -1.49, -5.81, -6.07, -6.11, -6.15, -6.38, -6.53, -6.72, -6.92.

^{29}Si {^{1}H} NMR (79 MHz, $CDCl_3$) δ 12.26, 10.56, -38.79, -39.22, -42.05, -42.18.

Preparation of 23:77 *trans*:*cis* $Si_{10}Ph_4$

In a glove box, an oven dried 500 mL Schlenk flask with stir bar was charged with $[(18\text{-cr-}6)K]^{+}_2$**5.7** (1.0 equiv., 5.43 mmol, 5.92 g) and sealed with a septum. A separate 250 mL Schlenk flask was charged with **5.8** (1.00 equiv., 5.43 mmol, 2.12 g). Both Schlenk flasks were removed from the glove box and attached to a Schlenk line under nitrogen.

Toluene (175 mL) was added to the 500 mL Schlenk flask by syringe, then the septum was replaced with an oven dry 150 mL addition funnel. Toluene (120 mL) was added to the 250 mL Schlenk flask to dissolve **5.8**, and it was transferred to the closed addition funnel. The solution of **5.8** was added over 1 hour. After the addition was complete, the reaction mixture was stirred for an hour.

The reaction mixture was quenched with deionized water (100 mL). The mixture was transferred to a 500 mL separatory funnel. The aqueous and organic layers were separated. The aqueous layer was extracted with diethyl ether (3 x 100 mL). The combined organics were dried over anhydrous magnesium sulfate, filtered and concentrated to a yellow oil. The solid was subjected to automated column chromatography with 100% hexanes then with a gradient to 5% dichloromethane/95% hexanes to yield **$Si_{10}Ph_4$** as a white solid (2.18 g, 50%). **$Si_{10}Ph_4$** is isolated as a 23:77 *trans*:*cis* mixture of isomers.

Tabulated Characterization Data for 23:77 trans:cis **$Si_{10}Ph_4$**

^{1}H NMR (400 MHz, $CDCl_3$) δ = 7.64 – 7.57 (m, 1H), 7.48 – 7.43 (m, 4H), 7.43 – 7.36 (m, 5H), 7.33 – 7.21 (m, 11H), 7.20 – 7.08 (m, 4H), 0.43 (s, 2H), 0.41 (s, 6H), 0.26 (s, 6H), 0.16 (s, 1H), 0.11 (s, 6H), 0.11 (s, 1H), 0.09 (s, 1H), 0.09 (s, 1H), 0.08 (s, 6H), 0.08 (s, 6H), 0.04 (s, 1H), -0.01 (s, 6H), -0.21 (s, 1H), -0.28 (s, 6H). *Due to peak overlap, integrations are not accurate.

^{13}C {^{1}H} NMR (101 MHz, $CDCl_3$) δ 137.62, 137.43, 137.09, 136.88, 136.38, 136.17, 136.08, 135.95, 128.73, 128.53, 128.16*, 127.60, 127.57, 127.55, 127.52, -2.04, -2.92, -3.55, -3.80, -4.53, -4.58, -4.79, -4.91, -5.01, -5.12,

	-5.78, -5.99, -6.46, -6.98 *At 128.16, a signal from the *cis* and *trans* isomer overlap
^{29}Si {^{1}H} NMR	(79 MHz, $CDCl_3$) δ -29.91, -31.10, -34.11, -36.62, -39.93, -41.00, -42.54, -75.66, -79.12.
HRMS	Calcd. for $C_{38}H_{62}Si_{10}$: 798.2544. Found: $[M+H]^+$ 799.2582

Preparation of 10:90 *trans*:*cis* $Si_{10}Ph_4$

In a glove box, an oven dried 50 mL round bottom flask with stir bar was charged with $[(18\text{-cr-}6)K]^+_2$**7** (1.0 equiv., 0.257 mmol, 0.279 g) and THF (10.0 mL). $MgBr_2$•Et_2O (1.1 equiv, 0.282 mmol, 0.073 g) was added as a solid. The red suspension changed to a yellow color within a minute. The round bottom flask was sealed with a rubber septum and stirred for 30 minutes.

A separate 25 mL round bottom flask was charged with **5.8** (1.00 equiv., 0.257 mmol, 0.100 g) and THF (10.0 mL). The solution of **5.8** was added dropwise via pipette over 5 minutes. Residual **5.8** was rinsed out of the round bottom flask with THF (2 x 2.5 mL) and added to the reaction mixture. The reaction mixture stirred at room temperature for 2 hours.

After 1 hour, the reaction mixture was removed from the glove box, the septum removed, and deionized water (20 mL) was added to quench the reaction. The reaction mixture was transferred to a 60 mL separatory funnel and the organics were separated. The aqueous layer was extracted with Et_2O (3 x 20 mL). The combined organics were dried over anhydrous magnesium sulfate, filtered and concentrated to a colorless oil. The oil was subjected to automated column chromatography with 100% hexanes, then with a gradient to 5% dichloromethane/95% hexanes to yield **$Si_{10}Ph_4$** as a white solid.

^{1}H NMR spectrum of the isolated compound matches the previously reported *trans*:*cis* 23:77 **$Si_{10}Ph_4$**.

Epimerization of $Si_{10}Ph_4$

In a glove box, a 500 mL Schlenk flask was charged with $[(18\text{-cr-}6)K]^+_2$**5.7** (0.25 equiv., 2.62 mmol, 2.10 g) and **$Si_{10}Ph_4$** (1.0 equiv., 0.657 mmol, 0.714 g) and sealed with a septum. The Schlenk flask was removed from the glove box and attached to a Schlenk line under nitrogen. Toluene (205 mL) was added to the Schlenk flask and the reaction mixture was heated to 60 °C for 3 hours.

After 3 hours, the reaction was quenched with deionized water (100 mL). The reaction mixture was transferred to a separatory funnel and the organics were separated. The aqueous layer was extracted with Et_2O (3 x 100 mL). The combined organics were dried over anhydrous magnesium sulfate, filtered and concentrated to a colorless oil. The oil was subjected to automated column chromatography with 100% hexanes then with a gradient to 5% dichloromethane/95% hexanes to yield **$Si_{10}Ph_4$** as a white solid (1.39 g, 66%). **$Si_{10}Ph_4$** is isolated as a 97:3 *trans*:*cis* mixture of isomers. X-ray quality crystals were grown by liquid-liquid diffusion using dichloromethane as the solvent and methanol as the antisolvent.

Tabulated Characterization Data for **$Si_{10}Ph_4$**

^{1}H NMR (400 MHz, $CDCl_3$) δ = 7.45 – 7.23 (m, 20H), 7.63 – 7.58 (m, 4H), 0.43 (s, 6H), 0.16 (s, 6H), 0.11 (s, 6H), 0.09 (s, 6H), 0.09 (s, 6H), 0.04 (s, 6H), -0.20 (s, 6H).

^{13}C {^{1}H} NMR (101 MHz, $CDCl_3$) δ 137.79, 137.59, 136.24, 136.12, 128.90, 128.31, 127.76, 127.68, -1.88, -3.39, -4.42, -4.75, -4.85, -5.83, -6.30.

^{29}Si {^{1}H} NMR (79 MHz, $CDCl_3$) δ -29.92, -34.12, -38.76, -39.94, -75.66.

HRMS Calcd. for $C_{38}H_{62}Si_{10}$: 798.2544. Found: $[M+H]^+$ 799.2582

Preparation of 15:85 *trans:cis* $Si_{10}H_4$

A 50 mL Schlenk flask equipped with a stir bar under argon was charged with 15:85 *trans*:*cis* **$Si_{10}Ph_4$** (1.0 equiv., 0.150 mmol, 0.120 g) and dichloromethane (2.25 mL). In an inert atmosphere glove box, trifluoromethanesulfonic acid (5.00 equiv., 0.750 mmol, 0.07 mL) was placed in an addition funnel. The addition funnel was sealed with two septa and removed from the glove box. Under a heavy flow of argon, the addition funnel was attached to the Schlenk flask. The reaction mixture was cooled to 0 °C with an ice water bath and the trifluoromethanesulfonic acid was added. 1.0 mL of DCM was added to the addition funnel to wash any residual trifluoromethanesulfonic acid into the reaction flask. After half an hour, the ice water bath was removed and the reaction mixture was stirred for 2 hours at room temperature.

After 2 hours volatile materials were removed under vacuum. The resulting yellow oil was dissolved in diethyl ether (1.5 mL). The silyl triflate solution was cooled to 0 °C with an ice water bath and a LAH suspension (2.40 equiv., 0.360 mmol, 0.014 g in 1.5 mL diethyl ether) was added dropwise via syringe. After half an hour, the ice water bath was removed and the reaction mixture was stirred for an additional 1.5 hours at room temperature.

The reaction mixture was cooled to 0 °C with an ice water bath and quenched with anhydrous ethyl acetate (0.15 mL) by dropwise addition via syringe. The quenched reaction

mixture was concentrated to a while solid and brought into a glove box. The white solid was rinsed with pentane and insoluble salts were removed by filtration through silica. The filtrate was concentrated to a colorless oil. The oil was subjected to automated column chromatography with 100% hexanes and fractions were quickly concentrated to a colorless oil and brought into the glove box for storage. (0.048 g, 65%).

Tabulated Characterization Data for **15:85 $Si_{10}H_4$**

^{1}H NMR	(400 MHz, C_6D_6) δ = 3.40 – 3.34 (m, 4H), 0.42 (s, 6H), 0.38 (s, 6H), 0.34 (s, 6H), 0.34 (s, 8H*), 0.31 (s, 6H), 0.27 (s, 6H), 0.23 (s, 6H). *Integral high due to overlap with *trans* isomer in sample
^{13}C {^{1}H} NMR	(101 MHz, C_6D_6) δ -3.28, -3.35, -3.75, -4.82, -5.58, -7.92.
^{29}Si {^{1}H} NMR	(79 MHz, C_6D_6) δ -38.30, -40.09, -41.53, -78.41, -101.36.
HRMS	Calcd. for $C_{14}H_{46}Si_{10}$: 494.1292. Found: 494.1287

Preparation of 95:5 $Si_{10}H_4$

A 100 mL Schlenk flask equipped with a stir bar under argon was charged with 97:3 *trans*:*cis* **$Si_{10}Ph_4$** (1.0 equiv., 1.24 mmol, 0.99 g) and DCM (27.0 mL). In an inert atmosphere glove box, trifluoromethanesulfonic acid (5.0 equiv., 6.19 mmol, 0.55 mL) was placed in an addition funnel. The addition funnel was sealed with two septa and removed from the glove box. Under a heavy flow of argon, the addition funnel was attached to the Schlenk flask. The reaction mixture was cooled to 0 °C with an ice water bath and the trifluormethanesulfonic acid was added dropwise. 2.0 mL of DCM was added to the addition funnel to wash any residual trifluoromethanesulfonic acid into the reaction flask.

After half an hour, the ice water bath was removed and the reaction mixture was stirred for 2 hours at room temperature.

After 2 hours volatile materials were removed under vacuum. The resulting yellow solid was dissolved in diethyl ether (15.0 mL). The silyl triflate solution was cooled to 0 °C with an ice water bath and a LAH suspension (2.40 equiv., 2.97 mmol, 0.113 g in 14.0 mL diethyl ether) was added dropwise via syringe. After half an hour, the ice water bath was removed and the reaction mixture was stirred for an additional 1.5 hours at room temperature.

The reaction mixture was cooled to 0 °C with an ice water bath and quenched with anhydrous ethyl acetate (1.24 mL) by dropwise addition via syringe. The quenched reaction mixture was concentrated to a while solid and brought into a glove box. The white solid was rinsed with pentane and insoluble salts were removed by filtration through silica. The filtrate was concentrated to a colorless oil. The oil was subjected to automated column chromatography with 100% hexanes and fractions were quickly concentrated to a colorless oil and brought into the glove box for storage. (0.41 g, 68%) The colorless oil solidified to a white solid overnight.

X-ray quality crystals of *trans*-**$Si_{10}H_4$** were grown by dissolving in hot acetonitrile and slow cooling to room temperature.

Tabulated Characterization Data for **95:5 $Si_{10}H_4$**

^{1}H NMR (400 MHz, C_6D_6) δ = 3.42 (d, *J*=2.1, 2H), 3.36 – 3.33 (m, 2H), 0.39 (d, *J*=0.8, 6H), 0.36 (s, 6H), 0.36 (s, 6H), 0.35 (s, 6H), 0.34 (d, *J*=0.8, 6H), 0.24 (s, 6H), 0.24 (s, 6H).

^{13}C {^{1}H} NMR (101 MHz, C_6D_6) δ -2.89, -3.41, -4.38, -5.48, -6.30, -8.03.

^{29}Si {^{1}H} NMR (79 MHz, C_6D_6) δ -36.79, -37.24, -39.55, -76.61, -108.69.

HRMS Calcd. for $C_{14}H_{46}Si_{10}$: 494.1292. Found: 494.1291

General Screening Procedures

Salt Metathesis

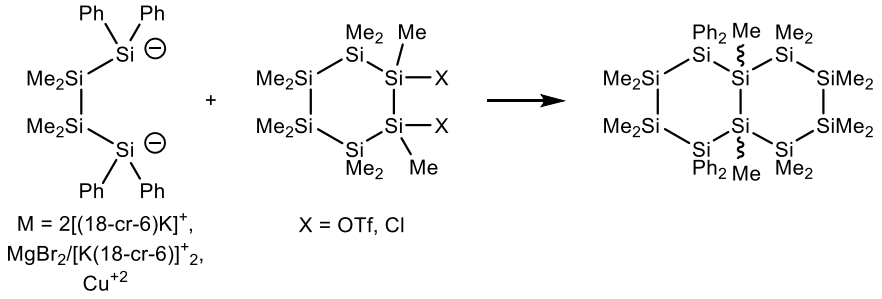

In a glove box, a suspension of $[(18\text{-cr-6})K]^{+}_{2}$**5.7** (1.00 equiv., 0.257 mmol, 0.279 g) in reaction solvent (10.0 mL) was prepared in a 50 mL oven dry round bottom flask. If a different cation is used, a stir bar and the respective salt (1.10 equiv., 0.282 mmol) was added to the suspension as a solid (1.10 equiv.) and the solution was stirred for 30 minutes at room temperature. A color change is usually observed.

A solution of **5.8** (1.00 equiv., 0.257 mmol, 0.100 g) or **5.14**(details below) in solvent (10.0 mL) is prepared in a separate 50 mL oven dry flask with stir bar. The solution of (**5.8** or **5.14**) was added dropwise to the silanide solution/suspension via pipette over 5 minutes. After complete addition, residual (**5.8** or **5.14**) solution was rinsed out of the round bottom flask with the reaction solvent (2 x 2.5 mL) and added to the reaction mixture, and the flask sealed with a rubber septum. The reaction was stirred at room temperature for 1 hour at room temperature.

After 1 hour, consumption of starting materials was confirmed by an airfree ^{1}H NMR spectroscopy of a reaction aliquot. The reaction mixture was removed from the glove box, and deionized water (20 mL) was added to quench the reaction. The reaction mixture was transferred to a 60 mL separatory funnel and the organics were separated. The aqueous layer was extracted with Et_2O (3 x 20 mL). The combined organics were dried over anhydrous magnesium sulfate, filtered and concentrated to a colorless oil. The oil was subjected to automated column chromatography with 100% hexanes then with a gradient to 5% dichloromethane/95% hexanes to yield **$Si_{10}Ph_4$** as a white solid.

Reactions using M=Mg: $MgBr_2$•OEt_2 (0.073 g) was added. The silanide suspension changed from red to yellow.

Reactions using M=Cu: $CuCl_2$ (0.035 g) was added. The silanide suspension changed from red to dark brown.

Reactions using X=OTf: Triflate was prepared from **5.13** (1.0 equiv., 0.258 mmol, 0.122 g) and TfOH (2.2 equiv., 0.567 mmol, 0.05 mL) in pentane (2.50 mL), as per the first half of the preparation of **5.8**. The yellow oil was used without further purification.

Epimerization

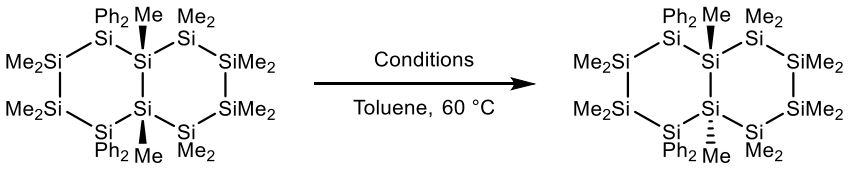

In a glove box, a 20 mL vial with stir bar was charged with **$Si_{10}Ph_4$** (1.0 equiv., 0.0375 mmol, 0.030 g) and the respective additives in the indicated amounts. Toluene (3.0 mL) was added, and the reaction was heated to 60 °C for the indicated time. Time points

were taken by removing a small aliquot (< 0.1 mL) from the vial and concentrating it under vacuum. The residue was then dissolved in C_6D_6 and the *trans*:*cis* was determined by ^1H NMR spectroscopy.

After the last time point was taken, the reaction was removed from the glove box. Deionized water (5 mL) was added to quench the reaction. The reaction mixture was transferred to a 30 mL separatory funnel and the organics were separated. The aqueous layer was extracted with Et_2O (3 x 5 mL). The combined organics were dried over anhydrous magnesium sulfate, filtered, and concentrated to a colorless oil. The oil was subjected to automated column chromatography with 100% hexanes then with a gradient to 5% dichloromethane/95% hexanes to yield **$Si_{10}Ph_4$** as a white solid.

Single Crystal X-Ray Crystallography

$Si_{10}Ph_4$

All reflection intensities were measured at 110(2) K using a SuperNova diffractometer (equipped with Atlas detector) with Mo *K*α radiation (λ = 0.71073 Å) under the program CrysAlisPro (Version CrysAlisPro 1.171.39.29c, Rigaku OD, 2017). The same program was used to refine the cell dimensions and for data reduction. The structure was solved with the program SHELXS-2014/7 (Sheldrick, 2015) and was refined on F^2 with SHELXL-2014/7 (Sheldrick, 2015). Numerical absorption correction based on gaussian integration over a multifaceted crystal model was applied using CrysAlisPro. The temperature of the data collection was controlled using the system Cryojet (manufactured by Oxford Instruments). The H atoms were placed at calculated positions using the instructions AFIX

43 or AFIX 137 with isotropic displacement parameters having values 1.2 or 1.5 *U*eq of the attached C atoms. The structure is partly disordered.

The fragment "–Si8(Me)$_2$–Si9(Me)$_2$–Si10Me–" of the Si backbone and two phenyl groups are disordered over two orientations. The occupancy factors of the major components can be retrieved from the .cif file.

Table 5.5. Experimental details for x-ray crystal structure of **Si$_{10}$Ph$_4$**.

	Si$_{10}$Ph$_4$
Crystal data	
Chemical formula	$C_{38}H_{62}Si_{10}$
M_r	799.77
Crystal system, space group	Triclinic, *P*-1
Temperature (K)	110
a, *b*, *c* (Å)	12.1961 (3), 12.2373 (2), 18.3114 (4)
α, β, γ (°)	93.9832 (17), 103.109 (2), 117.474 (2)
V (Å^3)	2313.09 (9)
Z	2
Radiation type	Mo *K*α
μ (mm^{-1})	0.31
Crystal size (mm)	0.42 × 0.23 × 0.10
Data collection	
Diffractometer	SuperNova, Dual, Cu at zero, Atlas
Absorption correction	Gaussian *CrysAlis PRO* 1.171.39.29c (Rigaku Oxford Diffraction, 2017) Numerical absorption correction based on gaussian integration over a multifaceted crystal model Empirical absorption correction using spherical harmonics, implemented in SCALE3 ABSPACK scaling algorithm.
T_{min}, T_{max}	0.390, 1.000
No. of measured, independent and observed [$I > 2\sigma$	35710, 10630, 9286

(I)] reflections	
R_{int}	0.022
$(\sin \theta/\lambda)_{max}$ (Å^{-1})	0.650
Refinement	
$R[F^2 > 2\sigma(F^2)]$, $wR(F^2)$, S	0.034, 0.085, 1.07
No. of reflections	10630
No. of parameters	612
No. of restraints	540
H-atom treatment	H-atom parameters constrained
$\Delta\rho_{max}$, $\Delta\rho_{min}$ (e Å^{-3})	0.59, -0.33

Computer programs: *CrysAlis PRO* 1.171.39.29c (Rigaku OD, 2017), *SHELXS2014*/7 (Sheldrick, 2015), *SHELXL2014*/7 (Sheldrick, 2015), *SHELXTL* v6.10 (Sheldrick, 2008).

trans-**$Si_{10}H_4$**

All reflection intensities were measured at 110(2) K using a SuperNova diffractometer (equipped with Atlas detector) with Mo *K*α radiation (λ = 0.71073 Å) under the program CrysAlisPro (Version CrysAlisPro 1.171.39.29c, Rigaku OD, 2017). The same program was used to refine the cell dimensions and for data reduction. The structure was solved with the program SHELXS-2018/3 (Sheldrick, 2018) and was refined on F^2 with SHELXL-2018/3 (Sheldrick, 2018). Numerical absorption correction based on gaussian integration over a multifaceted crystal model was applied using CrysAlisPro. The temperature of the data collection was controlled using the system Cryojet (manufactured by Oxford Instruments). The H atoms were placed at calculated positions (unless otherwise specified) using the instruction AFIX 137 with isotropic displacement parameters having values 1.5 U_{eq} of the attached C atoms. The H atoms attached to Si4A/Si4B were found from

difference Fourier maps, and their coordinates were refined pseudofreely using the DFIX instruction in order to keep the Si–H bond distances within an acceptable range. The H atoms attached to Si4' (minor component of the disorder) were initially placed at calculated positions using the instruction AFIX 23, then the Si–H bond distances were restrained within an acceptable range similarly to the H atoms attached to Si4A/Si4B. The structure is mostly ordered.

The asymmetric unit contains two molecules (molecules A and B) that are both found at two sites of twofold axial symmetry, and only their halves are crystallographically independent. Molecule B is found to be slightly disordered over two orientations, and the occupancy factor of the major component of the disorder refines to 0.9241(8).

Table 5.6. Experimental details for x-ray crystal structure of *trans*-**$Si_{10}H_4$**.

	trans-**$Si_{10}H_4$**
Crystal data	
Chemical formula	$C_{14}H_{46}Si_{10}$
M_r	495.41
Crystal system, space group	Monoclinic, *P*2/*c*
Temperature (K)	110
a, *b*, *c* (Å)	13.7763 (6), 15.0391 (4), 16.5372 (7)
β (°)	109.983 (5)
V (Å^3)	3219.9 (2)
Z	4
Radiation type	Mo *K*α
μ (mm^{-1})	0.41
Crystal size (mm)	0.45 × 0.44 × 0.07
Data collection	
Diffractometer	SuperNova, Dual, Cu at zero, Atlas
Absorption	Gaussian

correction	*CrysAlis PRO* 1.171.39.29c (Rigaku Oxford Diffraction, 2017) Numerical absorption correction based on gaussian integration over a multifaceted crystal model Empirical absorption correction using spherical harmonics, implemented in SCALE3 ABSPACK scaling algorithm.
T_{min}, T_{max}	0.484, 1.000
No. of measured, independent and observed [$I > 2\sigma(I)$] reflections	37846, 7393, 5512
R_{int}	0.042
$(\sin \theta/\lambda)_{max}$ ($Å^{-1}$)	0.650
Refinement	
$R[F^2 > 2\sigma(F^2)]$, $wR(F^2)$, S	0.036, 0.097, 1.04
No. of reflections	7393
No. of parameters	286
No. of restraints	200
H-atom treatment	H atoms treated by a mixture of independent and constrained refinement
$\Delta\rho_{max}$, $\Delta\rho_{min}$ (e $Å^{-3}$)	0.45, -0.21

Computer programs: *CrysAlis PRO* 1.171.39.29c (Rigaku OD, 2017), *SHELXS2018*/3 (Sheldrick, 2018), *SHELXL2018*/3 (Sheldrick, 2018), *SHELXTL* v6.10 (Sheldrick, 2008).

Computational Methods

All DFT calculations were performed using the Gaussian 09 package. Geometries were optimized using the B3LYP functional with the 6-31G(d) basis. No symmetry restrictions were applied to geometry optimizations. All optimized structures possess 0 imaginary frequencies. Relative energies were calculated employing corrections to thermal and zero-point energies. [4]

Chair/Chair *trans*-**1,4Si$_{10}$Ph$_4$** optimized in vacuum (charge = 0, multiplicity = 1)

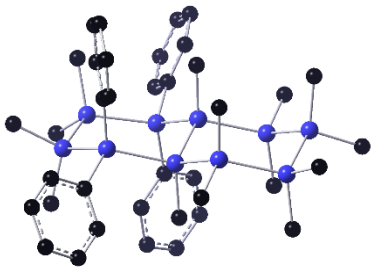

(Hydrogens omitted for clarity)

E(RB3LYP) = -4380.57747962 E_h

Center Number	Atomic Number	Forces (Hartrees/Bohr) X	Y	Z
1	14	-0.000012193	0.000017661	0.000011445
2	14	-0.000000128	-0.000001335	-0.000000531
3	14	-0.000003390	-0.000003954	-0.000012875
4	14	-0.000010437	0.000015582	-0.000007107
5	14	0.000006169	0.000000268	0.000009480
6	14	0.000005051	0.000003434	0.000004399
7	6	0.000000198	-0.000000238	-0.000004703
8	1	-0.000002546	-0.000002330	-0.000001797
9	1	-0.000002611	-0.000002178	-0.000001068
10	1	-0.000001428	-0.000002766	-0.000002127
11	6	0.000004998	-0.000003013	-0.000004216
12	1	-0.000002710	0.000000299	-0.000004032
13	1	-0.000005211	0.000002592	-0.000006024
14	1	-0.000003563	0.000000263	-0.000003263
15	6	0.000001291	0.000002045	0.000001177
16	1	0.000002365	0.000003133	0.000001255
17	1	-0.000000512	-0.000000010	0.000002607
18	1	0.000000556	0.000000122	-0.000001476
19	6	0.000000530	0.000002056	0.000000131
20	1	-0.000000563	0.000002424	-0.000001471
21	1	-0.000000357	0.000003174	-0.000003065
22	1	0.000001860	0.000003448	-0.000000892
23	6	-0.000005306	-0.000006373	0.000001902
24	1	0.000004155	0.000000280	0.000002328
25	1	0.000002526	-0.000000054	0.000001357
26	1	0.000001626	0.000001929	0.000003175
27	6	0.000000133	-0.000002647	-0.000003000
28	1	0.000005305	0.000005798	0.000000780
29	1	0.000004050	0.000003150	0.000006194
30	1	0.000001758	0.000004528	0.000004015
31	6	0.000000263	0.000001990	0.000005393
32	1	0.000000770	0.000005741	-0.000000675
33	1	0.000000570	0.000002846	-0.000004200
34	1	0.000000662	0.000002349	0.000001012
35	14	0.000000003	0.000002455	0.000002850

36	14	0.000005160	-0.000005535	-0.000004590
37	6	0.000001789	-0.000006394	-0.000002310
38	1	0.000000493	-0.000004405	0.000001481
39	1	-0.000001695	-0.000002127	0.000004082
40	1	0.000001181	-0.000005515	0.000005465
41	6	-0.000004168	-0.000005517	-0.000000669
42	1	-0.000002024	-0.000004394	0.000000382
43	1	-0.000001135	-0.000002436	-0.000000799
44	1	-0.000001616	-0.000004169	-0.000000361
45	6	-0.000002312	0.000001881	-0.000004611
46	1	0.000001795	-0.000002241	-0.000000159
47	1	-0.000005555	-0.000001890	-0.000001623
48	1	0.000000762	0.000001857	-0.000002409
49	14	-0.000000214	-0.000004218	0.000000703
50	14	-0.000000530	0.000000153	-0.000001724
51	6	-0.000000454	-0.000000907	-0.000001753
52	1	0.000000196	-0.000000330	-0.000000653
53	1	-0.000000520	0.000000099	0.000001131
54	1	-0.000001190	-0.000000656	0.000000169
55	6	-0.000001782	-0.000002284	0.000002261
56	1	0.000001240	-0.000001074	0.000003109
57	1	-0.000001366	-0.000004162	0.000000891
58	1	0.000001044	-0.000003780	0.000003065
59	6	0.000003493	-0.000000725	0.000002458
60	1	0.000001848	-0.000001916	0.000006134
61	1	0.000001990	0.000001026	0.000005746
62	1	0.000001043	0.000000155	0.000003368
63	6	0.000002758	0.000001855	0.000003287
64	1	0.000002348	-0.000000156	0.000004334
65	1	0.000002174	0.000002836	0.000004097
66	1	0.000001856	0.000001452	0.000001436
67	6	0.000006663	-0.000004711	0.000000528
68	6	0.000002751	0.000008645	0.000001897
69	6	0.000002367	0.000003644	0.000002318
70	6	0.000002126	0.000004535	-0.000000399
71	1	0.000001887	0.000004458	-0.000002219
72	6	0.000004807	0.000005627	0.000002426
73	1	0.000003451	0.000001302	0.000001792
74	6	0.000004517	0.000007052	-0.000000194
75	1	0.000003320	0.000006444	0.000001715
76	1	0.000002814	0.000002380	0.000004119
77	1	0.000003764	0.000004706	0.000003612
78	6	0.000010166	-0.000002321	0.000001454
79	6	0.000002748	0.000011097	-0.000003330
80	6	-0.000005707	0.000001596	-0.000004610
81	6	-0.000001454	0.000002420	-0.000003646
82	1	0.000001132	0.000001403	0.000000914
83	6	0.000000347	0.000003199	-0.000001679
84	1	0.000001327	0.000002563	-0.000001543
85	6	-0.000001805	0.000005923	-0.000006489
86	1	0.000001855	0.000005883	-0.000001641
87	1	-0.000001330	0.000004731	-0.000006447
88	1	0.000001072	0.000005894	-0.000003480
89	6	0.000002334	-0.000003261	-0.000007844
90	6	-0.000004004	-0.000003224	0.000000418
91	6	-0.000006201	-0.000002945	-0.000000419
92	6	-0.000003610	-0.000006570	-0.000002475

93	1	-0.000004243	-0.000006169	-0.000000343
94	6	-0.000007251	-0.000001667	-0.000005516
95	1	0.000000542	-0.000004288	-0.000000296
96	6	-0.000002009	-0.000007024	-0.000002118
97	1	-0.000005227	-0.000004660	-0.000003221
98	1	-0.000002739	-0.000003731	-0.000004352
99	1	-0.000005415	-0.000004295	-0.000005442
100	6	-0.000002419	-0.000007874	-0.000006029
101	6	0.000005502	-0.000000641	0.000003903
102	6	-0.000004199	-0.000006264	0.000003619
103	6	-0.000002019	-0.000004453	-0.000001990
104	1	0.000000237	-0.000001544	-0.000003030
105	6	0.000000455	-0.000004213	0.000003530
106	1	-0.000002825	-0.000002916	0.000002963
107	6	-0.000000325	-0.000002915	0.000006522
108	1	-0.000000343	-0.000003766	0.000004489
109	1	-0.000002817	-0.000006623	0.000000981
110	1	-0.000000733	-0.000006580	0.000002631

Chair/Twist *trans*-**1,4Si$_{10}$Ph$_4$** optimized in vacuum (charge = 0, multiplicity = 1)

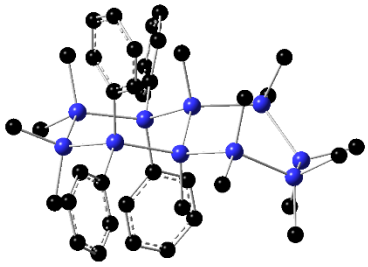

(Hydrogens omitted for clarity)

E(RB3LYP) = -4380.57558895

Center Number	Atomic Number	Forces (Hartrees/Bohr) X	Y	Z
1	14	0.000002098	0.000014066	0.000007635
2	14	-0.000000963	-0.000004047	0.000006527
3	14	-0.000001233	0.000006240	0.000004671
4	14	-0.000008168	-0.000005686	0.000002068
5	14	-0.000004956	0.000007659	-0.000000890
6	14	0.000004210	-0.000005821	-0.000006649
7	14	0.000003584	0.000007320	-0.000008767
8	6	0.000000133	-0.000005513	0.000001614
9	6	0.000004667	0.000001896	0.000005367
10	1	0.000004601	-0.000003708	-0.000000083
11	6	0.000004978	-0.000003456	-0.000000086
12	1	0.000006931	0.000001241	0.000001762
13	6	0.000005567	0.000003171	-0.000000487
14	1	0.000006137	-0.000000348	0.000001423

15	6	0.000002343	0.000001035	0.000003726
16	1	0.000002654	0.000000139	0.000001675
17	6	0.000002374	-0.000000465	-0.000005733
18	1	0.000000665	0.000000105	-0.000000005
19	6	-0.000002128	-0.000005746	-0.000006765
20	6	-0.000004141	-0.000001578	-0.000000809
21	1	0.000000314	0.000001124	-0.000000760
22	6	-0.000002099	0.000003002	-0.000002814
23	1	-0.000002772	-0.000000130	-0.000004679
24	6	-0.000004500	0.000000147	-0.000002088
25	1	-0.000006987	0.000000152	-0.000002654
26	6	-0.000004101	-0.000000282	-0.000001105
27	1	-0.000007258	0.000000103	0.000000084
28	6	-0.000007853	0.000002175	0.000001186
29	1	-0.000001739	-0.000002122	0.000001309
30	6	-0.000006911	-0.000006379	0.000010450
31	1	0.000001390	0.000001321	0.000007166
32	1	-0.000001399	-0.000000740	0.000000475
33	1	0.000002315	-0.000000698	0.000005895
34	6	0.000000962	-0.000003080	-0.000005708
35	1	-0.000000037	-0.000000312	0.000008645
36	1	0.000005872	-0.000001283	0.000005771
37	1	0.000002042	-0.000003920	0.000005404
38	6	-0.000000038	-0.000016030	-0.000000715
39	1	-0.000005263	-0.000000189	0.000006684
40	1	-0.000005405	0.000000462	0.000004594
41	1	-0.000008374	0.000000928	0.000004102
42	6	-0.000001180	0.000003223	0.000009632
43	1	-0.000003560	-0.000002953	0.000008402
44	1	-0.000000346	-0.000003197	0.000009113
45	1	-0.000003814	-0.000003529	0.000004637
46	6	0.000007506	-0.000001308	0.000000369
47	6	0.000004220	-0.000002270	0.000000348
48	1	-0.000003165	0.000000300	0.000003101
49	6	0.000003069	-0.000000884	0.000002499
50	1	0.000003127	-0.000000453	0.000002648
51	6	0.000004004	-0.000001037	0.000004722
52	1	0.000005485	-0.000000616	0.000004749
53	6	0.000003319	-0.000000959	0.000005523
54	1	0.000004579	-0.000001655	0.000006039
55	6	-0.000000882	-0.000001876	0.000004099
56	1	0.000000311	-0.000000898	0.000004458
57	6	-0.000014531	-0.000005568	0.000006986
58	6	0.000002113	0.000003741	-0.000000135
59	1	-0.000009715	-0.000002228	-0.000000088
60	6	-0.000006019	-0.000000210	0.000002066
61	1	-0.000007835	-0.000000985	0.000001412
62	6	-0.000007581	-0.000002852	0.000003019
63	1	-0.000006759	-0.000002165	0.000004300
64	6	-0.000005986	-0.000003592	0.000001867
65	1	-0.000004689	-0.000001132	0.000006031
66	6	0.000005388	0.000003836	0.000001027
67	1	-0.000005861	-0.000003571	0.000010514
68	6	0.000000257	0.000001740	0.000002647
69	1	-0.000006791	0.000000262	-0.000001889
70	1	-0.000003189	-0.000003358	-0.000002322
71	1	-0.000003783	0.000000635	-0.000001695

72	6	-0.000008982	-0.000000470	-0.000003250
73	1	-0.000000127	0.000000555	-0.000006136
74	1	-0.000001120	0.000002173	-0.000004766
75	1	-0.000002816	0.000000941	-0.000004506
76	6	-0.000002166	0.000008737	-0.000001244
77	1	-0.000003787	-0.000000407	-0.000000703
78	1	0.000000442	-0.000001312	0.000000734
79	1	0.000000208	-0.000001435	-0.000004638
80	6	-0.000000135	0.000004923	-0.000001894
81	1	0.000002925	0.000003114	-0.000006943
82	1	0.000003285	0.000001631	-0.000009244
83	1	-0.000001592	-0.000000809	-0.000008042
84	6	0.000000343	0.000002058	-0.000002256
85	1	0.000002372	0.000000451	-0.000002319
86	1	0.000004474	0.000001634	0.000001019
87	1	0.000009753	0.000001111	-0.000002399
88	14	0.000003213	-0.000002815	-0.000000301
89	14	0.000010979	-0.000004378	-0.000009346
90	14	-0.000006482	-0.000003686	0.000002949
91	6	0.000000681	0.000002286	-0.000011748
92	1	0.000000751	0.000005384	-0.000005504
93	1	0.000002081	0.000002438	-0.000007028
94	1	0.000006392	0.000003138	-0.000006769
95	6	0.000007425	0.000006316	-0.000004522
96	1	0.000007275	0.000000549	-0.000005953
97	1	0.000005825	0.000000275	-0.000003443
98	1	0.000006214	0.000000946	-0.000006708
99	6	-0.000001148	-0.000002827	-0.000004989
100	1	-0.000002133	0.000002729	-0.000007532
101	1	0.000001171	0.000003736	-0.000004400
102	1	-0.000001942	0.000003100	-0.000004121
103	6	0.000008421	-0.000001170	-0.000006996
104	1	0.000001823	0.000003947	-0.000002580
105	1	0.000002151	0.000000810	-0.000002698
106	1	0.000001463	0.000003895	-0.000004865
107	6	0.000002924	0.000010369	0.000001866
108	1	0.000007436	-0.000003180	-0.000001715
109	1	0.000005554	0.000000717	0.000000253
110	1	0.000001646	-0.000002668	0.000001219

cis-**$Si_{10}Ph_4$** optimized in vacuum (charge = 0, multiplicity = 1)

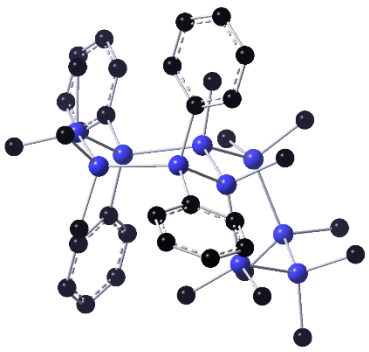

(Hydrogens omitted for clarity)

E(RB3LYP) = -4380.57010856 E_h

Center Number	Atomic Number	Forces (Hartrees/Bohr) X	Y	Z
1	14	-0.000010105	0.000003298	-0.000001622
2	14	0.000013241	0.000009337	0.000007097
3	14	-0.000006549	-0.000000484	0.000003992
4	14	0.000003269	0.000002105	0.000002917
5	14	0.000004646	0.000004832	0.000004394
6	14	-0.000013256	0.000003124	-0.000005720
7	14	0.000005400	0.000001597	-0.000004276
8	6	-0.000012744	-0.000003724	-0.000013037
9	6	0.000003249	0.000003097	-0.000001982
10	1	-0.000002635	0.000000396	0.000001155
11	6	-0.000003672	-0.000004474	0.000003722
12	1	-0.000005251	0.000001221	-0.000002900
13	6	-0.000008196	-0.000000914	-0.000002991
14	1	-0.000005879	0.000000930	-0.000002733
15	6	-0.000005252	-0.000000090	0.000001033
16	1	-0.000007162	-0.000001377	0.000000576
17	6	-0.000000241	0.000001423	0.000000647
18	1	-0.000005869	-0.000000655	-0.000000012
19	6	-0.000010731	0.000004061	0.000005222
20	1	0.000001774	-0.000002420	0.000007636
21	1	-0.000002697	-0.000005330	0.000004827
22	1	-0.000000939	-0.000001851	-0.000000985
23	6	-0.000003118	-0.000008522	0.000011204
24	1	0.000003480	-0.000004499	0.000003069
25	1	0.000001194	-0.000000676	0.000004492
26	1	0.000003614	0.000001743	0.000003204
27	6	-0.000007080	-0.000002170	-0.000006226
28	1	-0.000002525	0.000000355	0.000007327
29	1	-0.000004164	-0.000000335	0.000002002
30	1	-0.000002480	-0.000005443	0.000006158
31	6	-0.000012012	-0.000003581	0.000005974
32	1	0.000000442	-0.000006628	0.000007705
33	1	0.000000965	-0.000001160	0.000000185
34	1	-0.000002253	-0.000001042	0.000007320
35	6	0.000001869	-0.000001851	0.000004106
36	6	0.000000326	-0.000000710	0.000002266
37	1	0.000000426	-0.000001333	0.000002490
38	6	0.000003221	0.000000947	0.000001928
39	1	0.000004163	-0.000001118	0.000000969
40	6	0.000004061	-0.000000338	0.000003077
41	1	0.000005475	-0.000001481	0.000004304
42	6	0.000003832	-0.000002444	0.000003155
43	1	0.000003998	-0.000001216	0.000005277
44	6	0.000000552	0.000000358	0.000003377
45	1	0.000005179	-0.000008204	0.000004573
46	6	-0.000000291	0.000019355	0.000003469
47	1	-0.000000268	-0.000007974	0.000000595
48	1	-0.000003505	-0.000000134	-0.000006969

49	1	-0.000010931	-0.000004658	-0.000005955
50	6	0.000010933	0.000000448	-0.000003761
51	1	-0.000006823	0.000006934	-0.000004937
52	1	-0.000001124	0.000001960	-0.000008103
53	1	-0.000006471	0.000000364	-0.000002524
54	6	0.000004955	-0.000010636	-0.000009036
55	1	-0.000001041	0.000000616	0.000000880
56	1	0.000000050	0.000004895	-0.000002738
57	1	-0.000006960	0.000002983	0.000000397
58	6	0.000008953	-0.000004550	-0.000010122
59	1	0.000000827	0.000002618	-0.000007344
60	1	-0.000000830	0.000003149	-0.000002962
61	1	0.000001990	0.000008272	-0.000002561
62	6	-0.000008101	-0.000003554	0.000011026
63	1	0.000002860	0.000000226	-0.000005016
64	1	0.000008584	-0.000003917	-0.000001553
65	1	0.000006002	0.000004959	-0.000010287
66	6	-0.000000651	0.000000856	-0.000000506
67	6	0.000002132	0.000001936	0.000001660
68	1	0.000002605	-0.000000479	0.000005521
69	6	0.000000130	-0.000003851	-0.000002964
70	1	0.000001026	-0.000000311	0.000002874
71	6	0.000006802	-0.000000385	-0.000000129
72	1	0.000003501	0.000001207	0.000002308
73	6	0.000000418	0.000000605	-0.000003268
74	1	0.000002217	0.000001418	-0.000002438
75	6	0.000000346	0.000000843	0.000000822
76	1	-0.000001685	0.000002002	-0.000001667
77	6	-0.000004666	-0.000009685	0.000002480
78	6	-0.000003835	-0.000005007	0.000006324
79	1	-0.000005083	0.000004420	-0.000000431
80	6	-0.000005516	-0.000002625	0.000001356
81	1	-0.000006067	-0.000000395	0.000000446
82	6	-0.000004081	0.000000686	0.000004161
83	1	-0.000005355	-0.000002375	0.000002887
84	6	-0.000002600	0.000000184	0.000004874
85	1	-0.000003351	-0.000003633	0.000003259
86	6	-0.000001063	0.000000674	-0.000003212
87	1	-0.000001386	-0.000000955	0.000003779
88	14	-0.000002888	0.000006339	-0.000008796
89	14	0.000011741	0.000009060	-0.000006730
90	14	0.000002443	-0.000022771	0.000003778
91	6	0.000019389	-0.000000455	-0.000016175
92	1	0.000001253	0.000001024	0.000001183
93	1	0.000002393	0.000005578	-0.000002615
94	1	-0.000002721	0.000007701	-0.000004726
95	6	0.000002989	0.000007891	0.000011596
96	1	0.000007948	0.000000556	-0.000003703
97	1	0.000006113	0.000001094	-0.000004930
98	1	0.000007717	-0.000002404	-0.000008109
99	6	0.000001264	-0.000011683	0.000009196
100	1	0.000002224	0.000001116	0.000001869
101	1	0.000004168	0.000004858	-0.000005126
102	1	0.000005329	0.000001350	-0.000001922
103	6	0.000003785	0.000008259	0.000009864
104	1	0.000000088	-0.000000901	-0.000002711
105	1	0.000006675	-0.000007348	-0.000004662

106	1	0.000006484	0.000002743	-0.000003283
107	6	0.000009392	0.000005199	-0.000009914
108	1	-0.000000271	0.000006798	-0.000006392
109	1	-0.000005724	0.000003644	-0.000001629
110	1	-0.000002002	0.000001113	-0.000001593

Chair/Chair *trans*-**1,4Si$_{10}$H$_4$** optimized in vacuum (charge = 0, multiplicity = 1)

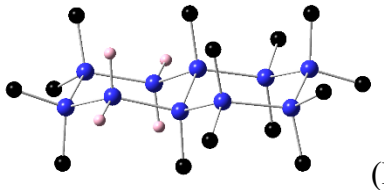

(Most hydrogens omitted for clarity)

E(RB3LYP) = -3456.35912240 E_h

Center Number	Atomic Number	Forces (Hartrees/Bohr) X	Y	Z
1	14	0.000002128	-0.000000371	-0.000001682
2	14	0.000000712	-0.000000844	0.000002068
3	14	-0.000001098	-0.000003463	0.000000515
4	14	-0.000001152	-0.000006111	-0.000001655
5	14	-0.000001008	-0.000002943	0.000003623
6	14	-0.000004181	-0.000001085	0.000000672
7	6	-0.000000815	0.000000287	0.000002216
8	1	0.000000375	-0.000001765	0.000002457
9	1	-0.000000411	0.000000425	-0.000001296
10	1	0.000000645	0.000001461	0.000001961
11	6	-0.000001019	-0.000000146	0.000004393
12	1	0.000000067	-0.000000014	0.000006219
13	1	-0.000000146	-0.000000439	0.000006145
14	1	-0.000002143	-0.000002686	0.000006906
15	6	-0.000006581	-0.000001826	-0.000005568
16	1	-0.000004719	-0.000004484	-0.000003850
17	1	-0.000002735	-0.000002331	-0.000004334
18	1	-0.000003586	-0.000003287	-0.000003817
19	6	-0.000004937	-0.000006965	0.000003724
20	1	-0.000005815	-0.000005345	0.000001107
21	1	-0.000005543	-0.000005502	0.000003909
22	1	-0.000007318	-0.000006805	0.000000626
23	6	-0.000004050	-0.000000451	-0.000004914
24	1	-0.000000437	-0.000000366	-0.000004603
25	1	-0.000002947	-0.000002066	-0.000005758
26	1	0.000000691	0.000000542	-0.000005981
27	6	-0.000004414	-0.000004885	-0.000002976
28	1	-0.000004531	-0.000003916	-0.000003590
29	1	-0.000004088	-0.000004136	-0.000003765
30	1	-0.000005564	-0.000003919	-0.000002910
31	6	-0.000001044	-0.000004825	0.000003315
32	1	-0.000004013	-0.000004208	0.000003807
33	1	-0.000002339	-0.000001709	0.000003820
34	1	-0.000003288	-0.000003249	0.000002604
35	14	0.000004264	0.000006673	-0.000003110
36	14	0.000000017	0.000000612	-0.000000538
37	6	0.000004986	0.000003924	-0.000004517

38	1	0.000004288	0.000004889	-0.000003973
39	1	0.000003271	0.000003554	-0.000004242
40	1	0.000005653	0.000005675	-0.000004063
41	6	0.000006602	0.000004814	0.000001506
42	1	0.000007368	0.000007157	0.000002042
43	1	0.000006136	0.000005684	0.000003889
44	1	0.000005622	0.000005748	0.000003061
45	6	0.000000932	0.000002227	0.000005645
46	1	0.000001130	-0.000001071	0.000004999
47	1	-0.000000078	-0.000000759	0.000005231
48	1	0.000002590	0.000001678	0.000006026
49	1	0.000003181	0.000003941	0.000002572
50	1	0.000001728	0.000002107	-0.000001692
51	1	-0.000007960	-0.000005502	-0.000000824
52	1	-0.000005011	-0.000003301	0.000003316
53	14	0.000001109	0.000000644	0.000001686
54	14	0.000003078	0.000003021	-0.000003178
55	6	0.000003914	0.000002583	0.000003912
56	1	0.000002874	0.000001894	0.000003930
57	1	0.000002513	0.000002018	0.000005130
58	1	0.000004921	0.000004320	0.000004752
59	6	0.000005655	0.000004182	-0.000001714
60	1	0.000004428	0.000005349	-0.000001193
61	1	0.000006505	0.000007685	-0.000000029
62	1	0.000005208	0.000005479	-0.000003864
63	6	0.000000236	0.000000360	-0.000005509
64	1	0.000002074	0.000002197	-0.000006499
65	1	-0.000000895	-0.000000328	-0.000006322
66	1	0.000000442	0.000001275	-0.000006308
67	6	0.000000370	-0.000000844	-0.000001087
68	1	0.000000686	0.000001426	-0.000001607
69	1	-0.000002733	-0.000000675	-0.000001854
70	1	0.000000197	-0.000001209	0.000001035

Chair/Twist *trans*-**1,4Si$_{10}$H$_4$** optimized in vacuum (charge = 0, multiplicity = 1)

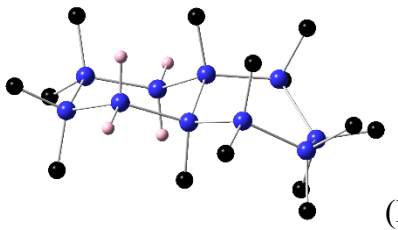

(Most hydrogens omitted for clarity)

E(RB3LYP) = -3456.35427195 E_h

Center Number	Atomic Number	Forces (Hartrees/Bohr) X	Y	Z
1	14	0.000005642	0.000006436	-0.000003870
2	14	0.000001451	0.000007896	-0.000002320
3	14	-0.000001959	0.000008166	-0.000002639
4	14	-0.000003516	-0.000000058	0.000003584
5	14	-0.000003442	-0.000001206	0.000000997
6	14	0.000000011	0.000001935	-0.000001701
7	14	-0.000009285	-0.000007144	0.000001277
8	6	0.000006351	0.000007003	-0.000002072
9	1	0.000006923	0.000012720	-0.000004001
10	1	0.000009658	0.000007287	-0.000005619
11	1	0.000009079	0.000011497	-0.000005192
12	6	0.000006829	0.000011260	0.000000704
13	1	0.000003689	0.000011322	-0.000001928
14	1	-0.000000289	0.000011163	-0.000001137
15	1	0.000000937	0.000013414	-0.000000786
16	6	0.000006701	-0.000000939	-0.000001193
17	1	0.000001455	0.000003103	-0.000001264
18	1	0.000003712	0.000000139	-0.000002233
19	1	0.000004637	0.000006094	-0.000002842
20	6	0.000000711	0.000011729	-0.000001335
21	1	0.000000568	0.000008570	0.000000249
22	1	-0.000000799	0.000009370	0.000003044
23	1	-0.000002078	0.000007060	0.000001828
24	6	-0.000000085	-0.000003580	-0.000001533
25	1	0.000005591	-0.000002624	-0.000003655
26	1	0.000001927	-0.000005018	-0.000001152
27	1	0.000004126	-0.000006016	-0.000001218
28	6	-0.000002593	-0.000012886	0.000002439
29	1	-0.000004006	-0.000010732	0.000002309
30	1	-0.000000243	-0.000008788	0.000000706
31	1	-0.000000998	-0.000009476	0.000000534
32	6	-0.000009684	-0.000002767	0.000003357
33	1	-0.000006121	-0.000007574	0.000004133
34	1	-0.000007219	-0.000002078	0.000005435
35	1	-0.000006916	-0.000008625	0.000004876
36	6	-0.000008369	-0.000006957	0.000003581
37	1	-0.000007578	-0.000007921	0.000005352
38	1	-0.000004875	-0.000011017	0.000002546
39	1	-0.000008857	-0.000009496	0.000005013
40	6	-0.000006194	-0.000000700	0.000004775
41	1	-0.000010623	-0.000000819	0.000005542
42	1	-0.000006022	0.000000634	0.000006045
43	1	-0.000006050	-0.000000904	0.000003402
44	14	0.000000955	-0.000006089	0.000002560
45	14	0.000004294	-0.000001563	-0.000003279
46	14	-0.000000964	0.000000246	-0.000000878
47	6	-0.000000794	-0.000009565	-0.000000956
48	1	0.000001159	-0.000006472	-0.000001316
49	1	-0.000000163	-0.000010565	-0.000000919
50	1	-0.000002403	-0.000008128	0.000001557
51	6	-0.000002107	0.000000363	-0.000000400
52	1	-0.000003184	-0.000000688	0.000003556
53	1	-0.000002410	0.000001507	0.000001708

54	1	-0.000002253	0.000000371	0.000001176
55	6	0.000001841	-0.000004737	-0.000002392
56	1	0.000007569	-0.000005053	-0.000004463
57	1	0.000004772	-0.000007055	-0.000003361
58	1	0.000006282	-0.000006679	-0.000003126
59	6	0.000005129	0.000000739	-0.000005144
60	1	0.000005559	0.000000079	-0.000002612
61	1	0.000003465	0.000001223	-0.000001627
62	1	0.000006406	0.000000794	-0.000003385
63	6	0.000000895	0.000005902	-0.000000314
64	1	-0.000002195	0.000003104	0.000002054
65	1	-0.000001999	0.000004649	0.000001094
66	1	-0.000000706	0.000006707	0.000000400
67	1	0.000006216	0.000005704	-0.000004362
68	1	0.000008849	0.000001740	-0.000003573
69	1	-0.000003634	0.000000497	0.000002165
70	1	-0.000002779	0.000003494	0.000001799

cis-**1,4Si$_{10}$H$_4$** optimized in vacuum (charge = 0, multiplicity = 1)

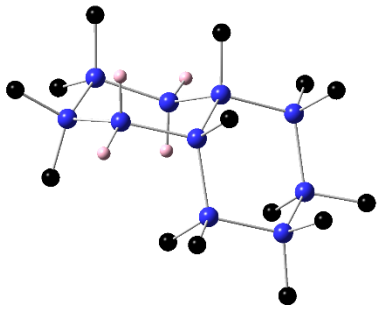

(Most hydrogens omitted for clarity)

E(RB3LYP) = -3456.35724770 E_h

Center Number	Atomic Number	Forces (Hartrees/Bohr) X	Y	Z
1	14	-0.000001756	-0.000001649	0.000000759
2	14	-0.000002232	-0.000001202	0.000000975
3	14	-0.000003136	-0.000005229	0.000003569
4	14	-0.000001741	-0.000002166	0.000001408
5	14	-0.000003146	-0.000001222	-0.000002431
6	14	-0.000000726	0.000000755	0.000000852
7	14	0.000000902	0.000000173	-0.000000963
8	6	-0.000002903	-0.000004821	0.000001509
9	1	-0.000002911	-0.000005124	0.000003021
10	1	-0.000004684	-0.000004526	0.000001274
11	1	-0.000002846	-0.000003648	0.000001194
12	6	0.000000957	-0.000002917	0.000002407
13	1	0.000000886	-0.000001913	0.000002912
14	1	0.000001517	-0.000001838	0.000003289

15	1	0.000000704	-0.000003191	0.000004522
16	6	-0.000004261	-0.000006683	0.000001759
17	1	-0.000004892	-0.000005928	0.000002333
18	1	-0.000004996	-0.000004899	0.000000654
19	1	-0.000005085	-0.000005985	0.000002238
20	6	-0.000001277	-0.000005379	0.000005974
21	1	-0.000001705	-0.000006592	0.000004942
22	1	-0.000000367	-0.000004784	0.000005532
23	1	-0.000001658	-0.000006983	0.000005566
24	6	-0.000002206	-0.000002489	-0.000001169
25	1	-0.000005345	-0.000002208	-0.000001380
26	1	-0.000004333	-0.000002064	-0.000000803
27	1	-0.000005016	-0.000000971	-0.000002792
28	6	-0.000002515	0.000001334	-0.000002978
29	1	-0.000000727	0.000002300	-0.000003716
30	1	-0.000001263	0.000002196	-0.000003410
31	1	-0.000002551	0.000001239	-0.000003156
32	6	-0.000001040	0.000000224	-0.000000088
33	1	-0.000002103	-0.000002749	0.000000393
34	1	0.000000085	-0.000001773	0.000001896
35	1	0.000000504	-0.000000909	0.000000202
36	6	0.000002118	0.000003499	-0.000000709
37	1	0.000005114	0.000004428	-0.000000984
38	1	0.000002547	0.000005007	-0.000002378
39	1	0.000003635	0.000002362	-0.000000468
40	6	0.000004495	0.000001280	0.000000847
41	1	0.000002875	0.000001080	0.000003616
42	1	0.000003502	0.000000989	0.000002615
43	1	0.000004658	0.000001577	0.000002862
44	14	0.000004194	0.000003302	0.000000136
45	14	0.000000796	0.000003072	-0.000001226
46	14	0.000002428	-0.000001332	-0.000003551
47	6	0.000000606	0.000006429	-0.000003227
48	1	0.000000870	0.000004513	-0.000003798
49	1	0.000002561	0.000005233	-0.000004705
50	1	0.000002973	0.000005560	-0.000004241
51	6	0.000006443	0.000004231	-0.000001987
52	1	0.000005877	0.000004139	0.000000299
53	1	0.000005155	0.000006665	-0.000000488
54	1	0.000005032	0.000005751	-0.000000452
55	6	0.000002310	0.000003858	0.000000065
56	1	0.000002859	0.000000052	0.000002043
57	1	0.000004382	0.000001881	0.000002001
58	1	0.000002615	0.000000778	0.000001419
59	6	0.000002192	0.000004003	-0.000002862
60	1	0.000000985	0.000004640	-0.000003881
61	1	0.000001543	0.000002592	-0.000001009
62	1	0.000004393	0.000004575	-0.000002155
63	6	-0.000003721	0.000002068	-0.000005271
64	1	-0.000001838	0.000002098	-0.000003920
65	1	-0.000000990	0.000002708	-0.000005093
66	1	-0.000003763	0.000001135	-0.000003404
67	1	-0.000003975	-0.000000883	-0.000001282
68	1	-0.000002136	-0.000000167	-0.000001109
69	1	-0.000000561	-0.000003531	0.000002787
70	1	0.000001695	-0.000001969	0.000003217

Calculated Excitations for *cis*-$Si_{10}Ph_4$

```
Excitation energies and oscillator strengths:
Excited State 1: Singlet-?Sym 4.5289 eV 273.76 nm f=0.0382 <S**2>=0.000
     215 -> 216        0.64424
     215 -> 218       -0.18123
Excited State 2: Singlet-?Sym 4.6208 eV 268.32 nm f=0.1258 <S**2>=0.000
     214 -> 216       -0.23065
     214 -> 217       -0.20440
     215 -> 217        0.59280
Excited State 3: Singlet-?Sym 4.6691 eV 265.54 nm f=0.0065 <S**2>=0.000
     214 -> 216        0.47768
     214 -> 217        0.14271
     214 -> 218       -0.25864
     215 -> 217        0.23610
     215 -> 218       -0.17832
     215 -> 220       -0.14606
Excited State 4: Singlet-?Sym 4.7492 eV 261.07 nm f=0.1340 <S**2>=0.000
     214 -> 216        0.24549
     214 -> 217       -0.30337
     214 -> 220        0.10373
     215 -> 216        0.13013
     215 -> 218        0.52031
Excited State 5: Singlet-?Sym 4.8533 eV 255.46 nm f=0.0334 <S**2>=0.000
     213 -> 216        0.12974
     214 -> 216       -0.12271
     214 -> 217        0.44223
     214 -> 219        0.13411
     215 -> 216        0.13954
     215 -> 217        0.14339
     215 -> 218        0.31223
     215 -> 219       -0.28028
Excited State 6: Singlet-?Sym 4.8796 eV 254.09 nm f=0.0273 <S**2>=0.000
     212 -> 216        0.19568
     213 -> 216        0.34013
     214 -> 216        0.17211
     214 -> 218        0.20144
     215 -> 217        0.10217
     215 -> 219        0.34553
     215 -> 220        0.20949
     215 -> 221       -0.10786
Excited State 7: Singlet-?Sym 4.9014 eV 252.95 nm f=0.0257 <S**2>=0.000
     212 -> 216        0.28306
     213 -> 216        0.34579
     213 -> 218       -0.16949
     214 -> 216       -0.14918
     214 -> 217       -0.20955
     214 -> 218       -0.19121
     215 -> 217       -0.11784
     215 -> 219       -0.15571
     215 -> 220       -0.24330
Excited State 8: Singlet-?Sym 4.9270 eV 251.64 nm f=0.0938 <S**2>=0.000
     212 -> 216        0.15674
     214 -> 217       -0.15742
     214 -> 218       -0.11481
     214 -> 219        0.20823
```

```
     214 -> 221       -0.11116
     215 -> 216       -0.11237
     215 -> 219       -0.31951
     215 -> 220        0.44694
     215 -> 221       -0.13961
Excited State 9: Singlet-?Sym 4.9742 eV 249.26 nm f=0.0168 <S**2>=0.000
     214 -> 216        0.18741
     214 -> 217       -0.13968
     214 -> 218        0.43389
     214 -> 220       -0.23426
     215 -> 217        0.10083
     215 -> 219       -0.22414
     215 -> 221        0.25542
Excited State 10: Singlet-?Sym 5.0227 eV 246.85 nm f=0.0263 <S**2>=0.000
     211 -> 216        0.12679
     212 -> 216        0.44531
     212 -> 218       -0.11914
     213 -> 216       -0.16506
     213 -> 217        0.18168
     213 -> 218        0.10612
     213 -> 220       -0.10034
     214 -> 217        0.11082
     214 -> 219        0.14309
     214 -> 223       -0.12822
     215 -> 219        0.19126
     215 -> 221        0.14923
Excited State 11: Singlet-?Sym 5.0264 eV 246.67 nm f=0.0124 <S**2>=0.000
     207 -> 216        0.10944
     212 -> 216       -0.14359
     214 -> 218       -0.19552
     214 -> 220       -0.18961
     214 -> 222       -0.17181
     215 -> 220        0.26004
     215 -> 221        0.37745
     215 -> 222       -0.15850
Excited State 12: Singlet-?Sym 5.0622 eV 244.92 nm f=0.0271 <S**2>=0.000
     212 -> 216       -0.12543
     212 -> 217        0.32747
     213 -> 216        0.11164
     213 -> 217        0.23668
     214 -> 218        0.14550
     214 -> 219        0.22932
     214 -> 220        0.17426
     214 -> 221        0.15621
     215 -> 221       -0.11569
     215 -> 222       -0.23542
Excited State 13: Singlet-?Sym 5.0666 eV 244.71 nm f=0.0023 <S**2>=0.000
     208 -> 219        0.10885
     212 -> 217        0.28059
     213 -> 217        0.39358
     214 -> 218       -0.12182
     214 -> 219       -0.18365
     214 -> 220       -0.17197
     215 -> 222        0.23082
     215 -> 223        0.13599
Excited State 14: Singlet-?Sym 5.1254 eV 241.90 nm f=0.0057 <S**2>=0.000
     208 -> 219       -0.15316
```

```
     211 -> 216        0.10413
     212 -> 216        0.15890
     212 -> 217        0.32879
     212 -> 218        0.18087
     213 -> 219       -0.10684
     214 -> 219       -0.18892
     214 -> 223        0.14738
     214 -> 224       -0.14981
     215 -> 219       -0.10438
     215 -> 223       -0.14914
     215 -> 224        0.18806
Excited State 15: Singlet-?Sym 5.1360 eV 241.40 nm f=0.1061 <S**2>=0.000
     212 -> 217        0.27004
     212 -> 218       -0.21427
     213 -> 216       -0.17172
     213 -> 217       -0.23304
     213 -> 218       -0.22990
     214 -> 219        0.24768
     214 -> 220       -0.22644
     215 -> 222        0.21793
Excited State 16: Singlet-?Sym 5.1584 eV 240.35 nm f=0.0140 <S**2>=0.000
     212 -> 218        0.34259
     213 -> 218        0.19567
     214 -> 216        0.11356
     214 -> 219        0.10607
     214 -> 220       -0.24772
     214 -> 221        0.21919
     215 -> 221       -0.25748
     215 -> 224       -0.12247
Excited State 17: Singlet-?Sym 5.1630 eV 240.14 nm f=0.0071 <S**2>=0.000
     212 -> 218        0.18316
     213 -> 216        0.20265
     213 -> 217        0.15855
     213 -> 218        0.16529
     214 -> 219        0.36066
     214 -> 222        0.12994
     215 -> 219        0.12347
     215 -> 221        0.16591
     215 -> 222        0.14887
     215 -> 223       -0.11720
Excited State 18: Singlet-?Sym 5.1793 eV 239.39 nm f=0.0024 <S**2>=0.000
     208 -> 219       -0.10206
     211 -> 217       -0.14966
     212 -> 217       -0.22635
     213 -> 217        0.30812
     213 -> 218       -0.14430
     214 -> 220       -0.25892
     214 -> 223        0.12667
     214 -> 224       -0.12068
     215 -> 221       -0.12770
     215 -> 223       -0.24168
Excited State 19: Singlet-?Sym 5.2120 eV 237.88 nm f=0.0219 <S**2>=0.000
     206 -> 217        0.10181
     206 -> 218       -0.15962
     206 -> 220       -0.10131
     211 -> 216        0.36137
     211 -> 217       -0.17088
```

```
     212 -> 220       -0.15955
     212 -> 221        0.14388
     213 -> 218       -0.15282
     214 -> 220        0.15370
     215 -> 222        0.13178
Excited State 20: Singlet-?Sym 5.2385 eV 236.68 nm f=0.0375  <S**2>=0.000
     205 -> 217        0.14343
     211 -> 216       -0.17968
     213 -> 218        0.11233
     214 -> 219       -0.14244
     214 -> 221        0.31154
     214 -> 222        0.13547
     215 -> 220        0.13639
     215 -> 221        0.21259
     215 -> 222        0.18247
     215 -> 223       -0.18750
```

Calculated Excitations for *cis*-$Si_{10}H_4$

```
Excitation energies and oscillator strengths:
Excited State 1: Singlet-?Sym 4.9071 eV 252.66 nm f=0.0121 <S**2>=0.000
     135 ->136         0.69088
Excited State 2: Singlet-?Sym 4.9898 eV 248.48 nm f=0.0194 <S**2>=0.000
     133 ->136         0.11702
     134 ->136         0.65250
     134 ->138         0.10748
Excited State 3: Singlet-?Sym 5.2276 eV 237.17 nm f=0.0134 <S**2>=0.000
     132 ->136         0.34643
     133 ->136         0.57995
     134 ->136        -0.13651
Excited State 4: Singlet-?Sym 5.3131 eV 233.35 nm f=0.0065 <S**2>=0.000
     132 ->136         0.48365
     132 ->137        -0.11719
     133 ->136        -0.30464
     134 ->137         0.11188
     134 ->138         0.12114
     135 ->137        -0.26391
Excited State 5: Singlet-?Sym 5.3617 eV 231.24 nm f=0.0368 <S**2>=0.000
     132 ->136         0.18941
     133 ->136        -0.11165
     134 ->137         0.16315
     135 ->137         0.57781
     135 ->138         0.19096
Excited State 6: Singlet-?Sym 5.4713 eV 226.61 nm f=0.0082 <S**2>=0.000
     134 ->137         0.20135
     135 ->137        -0.21639
     135 ->138         0.58895
Excited State 7: Singlet-?Sym 5.5189 eV 224.65 nm f=0.0124 <S**2>=0.000
     134 ->137         0.58245
     134 ->138        -0.14689
     135 ->138        -0.26426
Excited State 8: Singlet-?Sym 5.5683 eV 222.66 nm f=0.0004 <S**2>=0.000
     131 ->136         0.13218
     132 ->137         0.12208
     133 ->137         0.18107
```

```
     135 ->137        -0.10115
     135 ->139         0.60019
Excited State 9: Singlet-?Sym 5.6029 eV 221.29 nm f=0.0432 <S**2>=0.000
     131 ->136         0.57614
     133 ->137        -0.14173
     133 ->138        -0.19317
     134 ->138        -0.14341
     134 ->139         0.11837
     135 ->140         0.12305
Excited State 10: Singlet-?Sym 5.6568 eV 219.18 nm f=0.0295 <S**2>=0.000
     131 ->136         0.11161
     132 ->136        -0.17548
     132 ->137        -0.11264
     134 ->136        -0.10409
     134 ->137         0.14775
     134 ->138         0.58647
     134 ->139         0.10536
Excited State 11: Singlet-?Sym 5.6819 eV 218.21 nm f=0.0036 <S**2>=0.000
     132 ->137         0.11694
     132 ->139        -0.10083
     133 ->137         0.49159
     133 ->138        -0.13841
     134 ->139         0.28151
     135 ->139        -0.22828
     135 ->141         0.16311
Excited State 12: Singlet-?Sym 5.7544 eV 215.46 nm f=0.0497 <S**2>=0.000
     132 ->139        -0.11863
     133 ->137         0.14705
     133 ->139        -0.31889
     134 ->139        -0.29877
     135 ->140         0.42703
     135 ->141        -0.10407
Excited State 13: Singlet-?Sym 5.7734 eV 214.75 nm f=0.0036 <S**2>=0.000
     131 ->136        -0.19841
     132 ->136        -0.12000
     132 ->137        -0.15497
     133 ->139         0.33210
     134 ->139         0.27306
     135 ->139         0.10084
     135 ->140         0.42184
Excited State 14: Singlet-?Sym 5.8257 eV 212.82 nm f=0.0018 <S**2>=0.000
     130 ->136        -0.14605
     131 ->136         0.18071
     132 ->137        -0.18177
     132 ->139         0.10375
     133 ->137         0.29102
     133 ->138         0.38425
     133 ->139         0.22787
     134 ->140        -0.10925
     135 ->139        -0.10188
     135 ->141        -0.18776
Excited State 15: Singlet-?Sym 5.8609 eV 211.54 nm f=0.0027 <S**2>=0.000
     130 ->136        -0.19378
     133 ->137        -0.21214
     133 ->138         0.28371
     133 ->139        -0.30919
     134 ->139         0.35565
```

```
     134 ->140        -0.20544
Excited State 16: Singlet-?Sym 5.8636 eV 211.45 nm f=0.0080 <S**2>=0.000
     130 ->136         0.21910
     132 ->137        -0.20174
     132 ->138         0.20777
     133 ->138         0.29480
     134 ->137        -0.10953
     134 ->140         0.26585
     135 ->141         0.38470
Excited State 17: Singlet-?Sym 5.8870 eV 210.61 nm f=0.0413 <S**2>=0.000
     132 ->137         0.29905
     132 ->139         0.24760
     133 ->139         0.14492
     133 ->140        -0.10711
     134 ->138         0.13980
     134 ->139        -0.15693
     134 ->140        -0.19540
     135 ->140         0.21390
     135 ->141         0.21013
     135 ->142         0.25699
Excited State 18: Singlet-?Sym 5.9110 eV 209.75 nm f=0.0198 <S**2>=0.000
     130 ->136        -0.14131
     132 ->137         0.27736
     132 ->139         0.19817
     133 ->138         0.12444
     134 ->140         0.43615
     134 ->141        -0.21555
     135 ->141        -0.19467
Excited State 19: Singlet-?Sym 5.9539 eV 208.24 nm f=0.0052 <S**2>=0.000
     130 ->136         0.45523
     132 ->138        -0.29689
     132 ->139         0.15998
     133 ->138         0.12996
     133 ->139        -0.11741
     133 ->140        -0.14007
     134 ->139         0.11300
     134 ->141        -0.10242
     135 ->141        -0.11987
Excited State 20: Singlet-?Sym 5.9698 eV 207.69 nm f=0.0035 <S**2>=0.000
     131 ->136         0.11779
     131 ->137         0.44220
     132 ->138        -0.31328
     132 ->139        -0.17559
     133 ->138         0.14857
     133 ->140         0.11819
     134 ->141        -0.12131
     135 ->141         0.14392
```

Calculated Excitations for *trans*-$Si_{10}Ph_4$ (Chair/Chair)

```
Excitation energies and oscillator strengths:
Excited State 1: Singlet-?Sym 3.6092 eV 343.53 nm f=0.0008 <S**2>=0.000
     214 -> 219        0.12637
     215 -> 216        0.68416
```

```
Excited State 2: Singlet-?Sym 3.6179 eV 342.70 nm f=0.0198 <S**2>=0.000
     214 -> 218        0.11605
     215 -> 217        0.68400
Excited State 3: Singlet-?Sym 3.6546 eV 339.25 nm f=0.0011 <S**2>=0.000
     214 -> 217        0.21789
     215 -> 218        0.66271
Excited State 4: Singlet-?Sym 3.7000 eV 335.09 nm f=0.0007 <S**2>=0.000
     214 -> 216        0.42408
     215 -> 219        0.55864
Excited State 5: Singlet-?Sym 3.7513 eV 330.51 nm f=0.0019 <S**2>=0.000
     214 -> 217        0.53783
     215 -> 218       -0.18649
     215 -> 220       -0.39910
Excited State 6: Singlet-?Sym 3.7813 eV 327.89 nm f=0.0640 <S**2>=0.000
     214 -> 216        0.52167
     214 -> 218        0.14636
     215 -> 219       -0.41099
Excited State 7: Singlet-?Sym 3.7990 eV 326.36 nm f=0.0291 <S**2>=0.000
     214 -> 216       -0.13265
     214 -> 217       -0.14124
     214 -> 218        0.60815
     215 -> 217       -0.11329
     215 -> 220       -0.20199
     215 -> 221       -0.11892
Excited State 8: Singlet-?Sym 3.8091 eV 325.49 nm f=0.0594 <S**2>=0.000
     214 -> 217        0.35262
     214 -> 218        0.26271
     215 -> 220        0.51907
Excited State 9: Singlet-?Sym 3.8338 eV 323.40 nm f=0.0168 <S**2>=0.000
     214 -> 218        0.12340
     215 -> 221        0.67151
Excited State 10: Singlet-?Sym 3.8813 eV 319.44 nm f=0.0009 <S**2>=0.000
     214 -> 219       -0.13495
     214 -> 221       -0.18711
     215 -> 222        0.65777
Excited State 11: Singlet-?Sym 3.8888 eV 318.83 nm f=0.0086 <S**2>=0.000
     214 -> 219       -0.23199
     214 -> 220        0.64792
Excited State 12: Singlet-?Sym 3.9046 eV 317.54 nm f=0.0113 <S**2>=0.000
     213 -> 219        0.11043
     214 -> 219        0.60901
     214 -> 220        0.22253
     215 -> 216       -0.10178
     215 -> 222        0.16458
Excited State 13: Singlet-?Sym 3.9922 eV 310.57 nm f=0.0188 <S**2>=0.000
     214 -> 221        0.66477
     215 -> 222        0.17066
Excited State 14: Singlet-?Sym 4.0291 eV 307.72 nm f=0.0043 <S**2>=0.000
     213 -> 216        0.40036
     214 -> 222        0.57341
Excited State 15: Singlet-?Sym 4.0480 eV 306.29 nm f=0.0014 <S**2>=0.000
     213 -> 216        0.12256
     213 -> 217        0.68468
Excited State 16: Singlet-?Sym 4.0573 eV 305.58 nm f=0.0333 <S**2>=0.000
     212 -> 216       -0.22727
     213 -> 216        0.51401
     213 -> 217       -0.14425
```

```
     214 -> 222       -0.36806
Excited State 17: Singlet-?Sym 4.0923 eV 302.97 nm f=0.0008 <S**2>=0.000
     213 -> 218        0.66616
     215 -> 223        0.22146
Excited State 18: Singlet-?Sym 4.1064 eV 301.93 nm f=0.0001 <S**2>=0.000
     212 -> 218       -0.11017
     213 -> 218       -0.21645
     215 -> 223        0.65384
Excited State 19: Singlet-?Sym 4.1232 eV 300.70 nm f=0.0768 <S**2>=0.000
     212 -> 216        0.65164
     213 -> 216        0.18509
Excited State 20: Singlet-?Sym 4.1437 eV 299.21 nm f=0.0046 <S**2>=0.000
     212 -> 217        0.13504
     215 -> 224        0.68379
```

Calculated Excitations for *trans*-$Si_{10}H_4$ (Chair/Chair)

```
Excitation energies and oscillator strengths:
Excited State 1: Singlet-?Sym 4.8242 eV 257.00 nm f=0.1496 <S**2>=0.000
     135 ->136         0.69229
Excited State 2: Singlet-?Sym 4.9059 eV 252.73 nm f=0.0017 <S**2>=0.000
     134 ->136         0.61598
     135 ->137         0.27232
Excited State 3: Singlet-?Sym 5.0930 eV 243.44 nm f=0.0094 <S**2>=0.000
     132 ->136         0.15658
     133 ->136        -0.33900
     134 ->136        -0.19014
     135 ->137         0.55111
Excited State 4: Singlet-?Sym 5.1126 eV 242.51 nm f=0.0376 <S**2>=0.000
     132 ->136        -0.16499
     133 ->136         0.55305
     134 ->136        -0.22569
     135 ->137         0.31091
Excited State 5: Singlet-?Sym 5.2578 eV 235.81 nm f=0.0012 <S**2>=0.000
     132 ->136         0.24028
     134 ->139         0.17025
     135 ->138         0.61660
Excited State 6: Singlet-?Sym 5.3170 eV 233.19 nm f=0.1821 <S**2>=0.000
     133 ->137         0.27386
     134 ->137         0.62066
Excited State 7: Singlet-?Sym 5.3258 eV 232.80 nm f=0.0167 <S**2>=0.000
     133 ->137         0.62501
     134 ->137        -0.26323
     134 ->138        -0.12950
Excited State 8: Singlet-?Sym 5.3848 eV 230.25 nm f=0.0134 <S**2>=0.000
     132 ->136         0.50816
     133 ->136         0.22637
     133 ->140        -0.10380
     134 ->139         0.24314
     135 ->138        -0.29510
Excited State 9: Singlet-?Sym 5.4645 eV 226.89 nm f=0.0051 <S**2>=0.000
     134 ->138         0.22979
     135 ->139         0.64032
Excited State 10: Singlet-?Sym 5.5640 eV 222.83 nm f=0.0029 <S**2>=0.000
     133 ->138        -0.11983
```

```
     134 ->137         0.13596
     134 ->138        -0.34768
     135 ->140         0.54264
Excited State 11: Singlet-?Sym 5.6074 eV 221.11 nm f=0.0439 <S**2>=0.000
     132 ->138         0.13213
     133 ->138        -0.12774
     134 ->138         0.53107
     135 ->139        -0.20773
     135 ->140         0.31633
Excited State 12: Singlet-?Sym 5.6692 eV 218.70 nm f=0.0105 <S**2>=0.000
     131 ->137         0.12097
     132 ->137         0.38699
     133 ->138         0.46505
     135 ->139        -0.11528
     135 ->140         0.20359
     135 ->143         0.11245
Excited State 13: Singlet-?Sym 5.7136 eV 217.00 nm f=0.0019 <S**2>=0.000
     131 ->136        -0.26843
     133 ->139         0.24950
     134 ->139         0.12950
     134 ->140        -0.14007
     135 ->141         0.53526
Excited State 14: Singlet-?Sym 5.7256 eV 216.54 nm f=0.0434 <S**2>=0.000
     131 ->137        -0.11465
     132 ->137         0.53017
     133 ->138        -0.38306
     135 ->143        -0.10652
Excited State 15: Singlet-?Sym 5.7493 eV 215.65 nm f=0.0018 <S**2>=0.000
     131 ->136         0.12271
     132 ->136        -0.13570
     134 ->139         0.18611
     134 ->140         0.56507
     135 ->141         0.21021
Excited State 16: Singlet-?Sym 5.7653 eV 215.05 nm f=0.0118 <S**2>=0.000
     132 ->136        -0.28841
     133 ->139         0.20321
     133 ->140        -0.15051
     134 ->139         0.47982
     135 ->141        -0.28065
Excited State 17: Singlet-?Sym 5.8456 eV 212.10 nm f=0.0014 <S**2>=0.000
     131 ->136        -0.20343
     132 ->139        -0.14856
     133 ->139         0.49452
     133 ->140         0.17099
     134 ->139        -0.18005
     134 ->140         0.26322
     135 ->141        -0.18993
Excited State 18: Singlet-?Sym 5.9149 eV 209.61 nm f=0.0027 <S**2>=0.000
     131 ->136         0.56273
     132 ->139        -0.17033
     133 ->139         0.30666
     134 ->140        -0.14854
     135 ->141         0.12108
Excited State 19: Singlet-?Sym 5.9243 eV 209.28 nm f=0.0470 <S**2>=0.000
     131 ->137         0.16562
     132 ->138        -0.29495
     133 ->138        -0.18659
```

```
     133 ->141         0.18209
     134 ->141         0.46965
     135 ->140         0.11101
     135 ->143         0.11355
Excited State 20: Singlet-?Sym 5.9448 eV 208.56 nm f=0.0240 <S**2>=0.000
     133 ->140         0.57110
     134 ->139         0.16852
     135 ->142        -0.27874
```

Calculated Excitations for *trans*-$Si_{10}H_4$ (Chair/Twist)

```
Excitation energies and oscillator strengths:
Excited State 1: Singlet-?Sym 4.7648 eV 260.21 nm f=0.0813 <S**2>=0.000
     135 ->136         0.69264
Excited State 2: Singlet-?Sym 4.9928 eV 248.33 nm f=0.0215 <S**2>=0.000
     134 ->136         0.66301
     135 ->137         0.12092
Excited State 3: Singlet-?Sym 5.0138 eV 247.28 nm f=0.0236 <S**2>=0.000
     132 ->136         0.15270
     133 ->136         0.65929
     135 ->137         0.11645
Excited State 4: Singlet-?Sym 5.1250 eV 241.92 nm f=0.0047 <S**2>=0.000
     132 ->136        -0.16833
     134 ->136        -0.10071
     135 ->137         0.63490
     135 ->138        -0.11144
Excited State 5: Singlet-?Sym 5.2574 eV 235.83 nm f=0.0052 <S**2>=0.000
     132 ->136         0.10667
     135 ->137         0.14686
     135 ->138         0.65492
Excited State 6: Singlet-?Sym 5.3317 eV 232.54 nm f=0.0029 <S**2>=0.000
     132 ->136         0.55416
     133 ->136        -0.17846
     134 ->138        -0.17358
     134 ->139        -0.17876
     135 ->137         0.14853
     135 ->138        -0.14338
Excited State 7: Singlet-?Sym 5.3776 eV 230.56 nm f=0.0105 <S**2>=0.000
     132 ->137         0.10520
     133 ->137         0.66918
Excited State 8: Singlet-?Sym 5.4303 eV 228.32 nm f=0.0720 <S**2>=0.000
     132 ->138        -0.11793
     133 ->138        -0.20440
     134 ->137         0.61342
     135 ->141         0.13663
Excited State 9: Singlet-?Sym 5.4972 eV 225.54 nm f=0.0557 <S**2>=0.000
     131 ->136         0.10868
     135 ->139         0.66584
Excited State 10: Singlet-?Sym 5.5934 eV 221.66 nm f=0.0135 <S**2>=0.000
     132 ->138         0.13336
     133 ->138         0.48564
     134 ->137         0.27242
     134 ->138        -0.17272
     135 ->140         0.16566
     135 ->141        -0.22594
Excited State 11: Singlet-?Sym 5.6481 eV 219.52 nm f=0.0288 <S**2>=0.000
```

```
     132 ->136         0.20139
     133 ->138         0.19726
     133 ->139         0.12352
     134 ->138         0.57790
Excited State 12: Singlet-?Sym 5.6666 eV 218.80 nm f=0.0301 <S**2>=0.000
     131 ->136         0.19730
     133 ->138        -0.26035
     133 ->139        -0.11557
     135 ->140         0.51022
     135 ->141        -0.21529
Excited State 13: Singlet-?Sym 5.7378 eV 216.08 nm f=0.0058 <S**2>=0.000
     130 ->136         0.34933
     132 ->137        -0.24159
     132 ->138        -0.14078
     133 ->139         0.38545
     134 ->138        -0.15997
     134 ->139         0.15148
     134 ->140        -0.10856
     135 ->140         0.11083
     135 ->141        -0.13258
Excited State 14: Singlet-?Sym 5.7569 eV 215.37 nm f=0.0226 <S**2>=0.000
     130 ->136        -0.10866
     131 ->136         0.26135
     132 ->137        -0.30296
     132 ->139         0.11648
     133 ->138         0.22565
     135 ->140         0.14228
     135 ->141         0.43166
Excited State 15: Singlet-?Sym 5.7842 eV 214.35 nm f=0.0201 <S**2>=0.000
     132 ->136         0.15012
     132 ->137         0.37736
     134 ->139         0.36865
     135 ->140         0.23578
     135 ->141         0.26911
Excited State 16: Singlet-?Sym 5.7956 eV 213.93 nm f=0.0082 <S**2>=0.000
     131 ->136         0.21051
     132 ->136         0.16158
     132 ->137        -0.23929
     133 ->139        -0.20058
     134 ->139         0.42815
     134 ->141        -0.11364
     135 ->140        -0.21078
     135 ->141        -0.15694
Excited State 17: Singlet-?Sym 5.8202 eV 213.03 nm f=0.0063 <S**2>=0.000
     130 ->136         0.31248
     131 ->136         0.49426
     132 ->137         0.22045
     134 ->139        -0.13709
     135 ->140        -0.16783
Excited State 18: Singlet-?Sym 5.8558 eV 211.73 nm f=0.0022 <S**2>=0.000
     130 ->136        -0.30384
     131 ->136         0.10878
     132 ->138         0.29246
     132 ->139         0.14361
     133 ->139         0.46507
     134 ->140         0.12334
Excited State 19: Singlet-?Sym 5.9174 eV 209.52 nm f=0.0251 <S**2>=0.000
```

```
     130 ->136         0.31330
     131 ->136        -0.15888
     132 ->138         0.30799
     133 ->140         0.20163
     133 ->141        -0.16903
     134 ->140         0.24183
     134 ->141        -0.19574
     134 ->143        -0.10105
     135 ->141         0.14671
Excited State 20: Singlet-?Sym 5.9582 eV 208.09 nm f=0.0126 <S**2>=0.000
     130 ->136         0.13732
     132 ->138         0.30212
     133 ->140        -0.23490
     133 ->141         0.19811
     134 ->141         0.20763
     135 ->142         0.40230
     135 ->143         0.10745
```

5.10 References

(1) Hengge, E.; Janoschek, R. *Chem. Rev.* **1995**, *95* (5), 1495–1526.
(2) He, G.; Shynkaruk, O.; Lui, M. W.; Rivard, E. *Chem. Rev.* **2014**, *114* (16), 7815–7880.
(3) Heider, Y.; Scheschkewitz, D. *Dalt. Trans.* **2018**, *47* (21), 7104–7112.
(4) Sekiguchi, A.; Yatabe, T.; Kabuto, C.; Sakurai, H. *J. Am. Chem. Soc.* **1993**, *115* (13), 5853–5854.
(5) Abersfelder, K.; Russell, A.; Rzepa, H. S.; White, A. J. P.; Haycock, P. R.; Scheschkewitz, D. *J. Am. Chem. Soc.* **2012**, *134* (38), 16008–16016.
(6) Sekiguchi, A.; Yatabe, T.; Kamatani, H.; Kabuto, C.; Sakurai, H. *J. Am. Chem. Soc.* **1992**, *114* (15), 6260–6262.
(7) Matsumoto, H.; Higuchi, K.; Kyushin, S.; Goto, M. *Angew. Chemie Int. Ed. English* **1992**, *31* (10), 1354–1356.
(8) Unno, M. In *Functional Molecular Silicon Compounds II*; Scheschkewitz, D., Ed.; Springer, Cham, 2013; pp 49–84.
(9) Schepers, T.; Michl, J. *J. Phys. Org. Chem.* **2002**, *15* (8), 490–498.
(10) Tsuji, H.; Michl, J.; Tamao, K. *J. Organomet. Chem.* **2003**, *685* (1–2), 9–14.
(11) Tsurusaki, A.; Koyama, Y.; Kyushin, S. *J. Am. Chem. Soc.* **2017**, *139* (11), 3982–3985.
(12) Fischer, R.; Konopa, T.; Ully, S.; Baumgartner, J.; Marschner, C. *J. Organomet. Chem.* **2003**, *685* (1–2), 79–92.
(13) Fischer, R.; Frank, D.; Gaderbauer, W.; Kayser, C.; Mechtler, C.; Baumgartner, J.; Marschner, C. *Organometallics* **2003**, *22* (18), 3723–3731.
(14) Kayser, C.; Kickelbick, G.; Marschner, C. *Angew. Chemie Int. Ed.* **2002**, *41* (6), 989–992.
(15) Fischer, J.; Baumgartner, J.; Marschner, C. *Science (80-.).* **2005**, *310* (5749), 825.
(16) Präsang, C.; Scheschkewitz, D. In *Structure and Bonding*; Scheschkewitz, D., Ed.; Springer, 2013; Vol. 156, pp 1–47.
(17) Garner, M. H.; Li, H.; Chen, Y.; Su, T. A.; Shangguan, Z.; Paley, D. W.; Liu, T.; Ng, F.; Li, H.; Xiao, S.; Nuckolls, C.; Venkataraman, L.; Solomon, G. C. *Nature*

2018, *558* (7710), 415–419.
(18) Li, H.; Garner, M. H.; Shangguan, Z.; Chen, Y.; Zheng, Q.; Su, T. A.; Neupane, M.; Liu, T.; Steigerwald, M. L.; Ng, F.; Nuckolls, C.; Xiao, S.; Solomon, G. C.; Venkataraman, L. *J. Am. Chem. Soc.* **2018**, *140* (44), 15080–15088.
(19) West, R.; Indriksons, A. *J. Am. Chem. Soc.* **1972**, *94* (17), 6110–6115.
(20) Jenkner, P. K.; Hengge, E.; Czaputa, R.; Kratky, C. *J. Organomet. Chem.* **1993**, *446* (1–2), 83–90.
(21) Xu, L.-W.; Li, L.; Lai, G.-Q.; Jiang, J.-X. *Chem. Soc. Rev.* **2011**, *40* (3), 1777–1790.
(22) Bauer, J. O.; Strohmann, C. *Eur. J. Inorg. Chem.* **2016**, *2016* (18), 2868–2881.
(23) Oestreich, M. *Synlett* **2007**, *2007* (11), 1629–1643.
(24) Schmidt, D. R.; O'Malley, S. J.; Leighton, J. L. *J. Am. Chem. Soc.* **2003**, *125* (5), 1190–1191.
(25) Oestreich, M.; Rendler, S. *Angew. Chemie Int. Ed.* **2005**, *44* (11), 1661–1664.
(26) Rendler, S.; Oestreich, M.; Butts, C. P.; Lloyd-Jones, G. C. *J. Am. Chem. Soc.* **2007**, *129* (3), 502–503.
(27) Fischer, R.; Konopa, T.; Ully, S.; Baumgartner, J.; Marschner, C. *J. Organomet. Chem.* **2003**, *685* (1–2), 79–92.
(28) Li, H.; Garner, M. H.; Shangguan, Z.; Zheng, Q.; Su, T. A.; Neupane, M.; Li, P.; Velian, A.; Steigerwald, M. L.; Xiao, S.; Nuckolls, C.; Solomon, G. C.; Venkataraman, L. *Chem. Sci.* **2016**, *7* (9), 5657–5662.
(29) Eliel, E. L.; Allinger, N. L.; Angyal, S. J.; Morrison, G. A. *Conformational Analysis*; Interscience Publishers, Inc.: New York, NY, 1981.
(30) Moniz, W. B.; Dixon, J. A. *J. Am. Chem. Soc.* **1961**, *83* (7), 1671–1675.
(31) Musher, J.; Richards, R. E. *Proc. Chem. Soc.* **1958**, 230.
(32) Press, E. M.; Marro, E. A.; Surampudi, S. K.; Siegler, M. A.; Tang, J. A.; Klausen, R. S. *Angew. Chemie - Int. Ed.* **2017**, *56* (2), 568–572.
(33) Marro, E. A.; Press, E. M.; Purkait, T. K.; Jimenez, D.; Siegler, M. A.; Klausen, R. S. *Chem. - A Eur. J.* **2017**, *23* (62), 15633–15637.
(34) Marro, E. A.; Press, E. M.; Siegler, M. A.; Klausen, R. S. *J. Am. Chem. Soc.* **2018**, *140* (8), 5976–5986.
(35) Purkait, T. K.; Press, E. M.; Marro, E. A.; Siegler, M. A.; Klausen, R. S. *Organometallics* **2019**, *38*, 1688–1698.
(36) Uhlig, W. *Chem. Ber.* **1996**, *129* (7), 733–739.
(37) Corriu, R. J. P.; Guérin, C.; Moreau, J. J. E. John Wiley & Sons, Ltd, 2007; pp 43–198.
(38) Couzijn, E. P. A.; Slootweg, J. C.; Ehlers, A. W.; Lammertsma, K. *J. Am. Chem. Soc.* **2010**, *132* (51), 18127–18140.
(39) Bauer, J. O.; Strohmann, C. *J. Am. Chem. Soc.* **2015**, *137* (13), 4304–4307.
(40) Suzuki, K.; Kawakami, Y.; Velmurugan, D.; Yamane, T. *J. Org. Chem.* **2004**, *69* (16), 5383–5389.
(41) Purkait, T. K.; Press, E. M.; Marro, E. A.; Siegler, M. A.; Klausen, R. S. *Organometallics* **2019**, *38* (8).
(42) Tamao, K.; Kawachi, A. *Adv. Organomet. Chem.* **1995**, *38*, 1–58.
(43) Gaderbauer, W.; Zirngast, M.; Baumgartner, J.; Marschner, C.; Tilley, T. D. *Organometallics* **2006**, *25* (10), 2599–2606.
(44) Stevenson, W. H.; Martin, J. C. *J. Am. Chem. Soc.* **1985**, *107* (22), 6352–6358.

(45) Casarini, D.; Lunazzi, L.; Mazzanti, A. *J. Org. Chem.* **1998**, *63* (24), 9125–9127.
(46) Tekautz, G.; Binter, A.; Hassler, K.; Flock, M. *ChemPhysChem* **2006**, *7* (2), 421–429.
(47) Bande, A.; Michl, J. *Chem. - A Eur. J.* **2009**, *15* (34), 8504–8517.
(48) Gilman, H.; Atwell, W. H.; Schwebke, G. L. *J. Organomet. Chem.* **1964**, *2* (4), 369–371.
(49) Tsuji, H.; Terada, M.; Toshimitsu, A.; Tamao, K. *J. Am. Chem. Soc.* **2003**, *125* (25), 7486–7487.
(50) Albinsson, B.; Teramae, H.; Downing, J. W.; Michl, J. *Chem. - A Eur. J.* **1996**, *2* (5), 529–538.
(51) Miller, R. D.; Michl, J. *Chem. Rev.* **1989**, *89* (6), 1359–1410.
(52) Krempner, C.; Krempner; Clemens. *Polymers (Basel).* **2012**, *4* (1), 408–447.
(53) Su, T. A.; Li, H.; Klausen, R. S.; Widawsky, J. R.; Batra, A.; Steigerwald, M. L.; Venkataraman, L.; Nuckolls, C. *J. Am. Chem. Soc.* **2016**, *138* (24), 7791–7795.
(54) Surampudi, S.; Yeh, M.-L.; Siegler, M. A.; Hardigree, J. F. M.; Kasl, T. A.; Katz, H. E.; Klausen, R. S. *Chem. Sci.* **2015**, *6* (3), 1905–1909.
(55) Kanazawa, Y.; Tsuji, H.; Ehara, M.; Fukuda, R.; Casher, D. L.; Tamao, K.; Nakatsuji, H.; Michl, J. *ChemPhysChem* **2016**, *17* (19), 3010–3022.
(56) Barfield, M.; Chakrabarti, B. *Chem. Rev.* **1969**, *69* (6), 757–778.
(57) Contreras, R. H.; Peralta, J. E. *Prog. Nucl. Magn. Reson. Spectrosc.* **2000**, *37* (4), 321–425.
(58) Thomas, W. A. *Prog. Nucl. Magn. Reson. Spectrosc.* **1997**, *30* (3–4), 183–207.
(59) Wiberg, K. B.; Connor, D. S. *J. Am. Chem. Soc.* **1966**, *88* (19), 4437–4441.
(60) Padwa, A.; Shefter, E.; Alexander, E. *J. Am. Chem. Soc.* **1968**, *90* (14), 3717–3721.
(61) Williamson, K. L.; Howell, T.; Spencer, T. A. *J. Am. Chem. Soc.* **1966**, *88* (2), 325–334.
(62) Folster, C. P.; Klausen, R. S. *Polym. Chem.* **2018**, *9*, 1938–1941.
(63) Lu, X.; Anderson, K. J.; Boudjouk, P.; Korgel, B. A. *Chem. Mater.* **2015**, *27* (17), 6053–6058.

Chapter 6: Low-Energy Electronic Transition in SiB Rings

The work presented in this chapter has been published as: Purkait, T. K.; Press, E. M.; Marro, E. A.; Siegler, M. A.; Klausen, R. *Organometallics* **2019**, *38*, 1688-1698.

All synthetic and experimental results described in this chapter were performed by Dr. Tapas Purkait and Mr. Eric Marro.

All computational results described in this chapter were performed by Dr. Eric Press.

Dr. Maxime Siegler obtained single crystal x-ray data and solved crystal structures.

6.1 Introduction

The incorporation of main group elements such as B, P, and Se into conjugated materials promises the ability to modulate electronic transitions while retaining atomic-level structural precision.[1] A fundamental understanding of the influence of the main group substituent on molecular properties is essential for the design and synthesis of tailored structures. In the case of boron-containing π-conjugated materials, p-π conjugation is invoked in which conjugation is extended through the vacant p-orbital of boron.[2–4] Boron-functionalized π-conjugated materials have found wide application[5] based on the unique properties conferred by boron that can be exploited for sensing,[6–9] non-linear optics,[10–12] and n-type charge transport.[13–15]

Far less is understood about the electronic properties of boron-functionalized σ-conjugated silicon materials.[16–18] Sodium-mediated Wurtz coupling of boron and silicon halides yielded a SiB copolymer used as a ceramic precursor.[19] Matsumi et al. reported the dehydrocoupling copolymerization of phenylsilane ($PhSiH_3$) with mesitylborane ($MesBH_2$), yielding colorless low-molecular polymers.[20] DFT calculations suggested p-σ

type conjugation, in which orbital density delocalized uniformly across a linear Si–B–Si chain. Theoretical studies of *B*-substituted polysilanes suggested a lowering of the band gap upon heteroatom substitution.[21] The synthesis of molecular monosilylboranes[22,23] is better precedented than polysilylboranes and these compounds have found wide utility as reagents in organic synthesis.[24] With respect to optoelectronic properties, Rayez et al. reported the synthesis of compounds with the general formula $Ph_2RSi–BMes_2$ that exhibit solvatochromic emission attributed to charge transfer character.[25] Hybrid σ-π organosilanes also exhibit photoinduced charge transfer.[26–28]

This chapter describes the synthesis and optical characterization of two new SiB rings (**Si4B** and **Si5B**), as well as all silicon analogs. **Si5B** is the first example of a six-membered SiB ring. The possibility of two mechanisms for electron delocalization – σ-p conjugation and charge transfer – motivates the detailed characterization of optoelectronic properties.

6.2 Synthesis of Cyclosilanes Containing Boron

Cyclosilanes containing boron atoms rings were synthesized by coupling nucleophilic disilanides **6.1a-b** with tetramethylpiperidinyldichloroborane **6.2**. In chapters three and four, disilanides **6.1a-b** were coupled to chlorosilanes in the synthesis of site-specifically functionalized cyclohexasilanes, precursors to poly(cyclosilane)s. [29–32] The addition of magnesium salts to the coupling reaction resulted in suppressed undesired fragmentation by modulating silanide nucleophilicity.[31,33]

This trend was also observed in the synthesis of boron containing cyclosilanes. Five-membered ring **Si4B** was isolated in 74% yield and six-membered ring **Si5B** in 34% yield (Scheme 6.1a-b). In the case of **Si5B**, a change in solvent from THF to toluene

suppressed the formation of 1,1,2,2-tetraphenylhexamethylcyclopentasilane, an undesired intramolecular coupling product. Hengge reported the first synthesis of a five-membered SiB ring via coupling of a dianion to a chloroboranes, a strategy later employed by Marschner.[34,35] Neither Hengge nor Marschner reported the synthesis of six-membered SiB cycles and a CSD search suggests such as structure has not been crystallographically characterized.

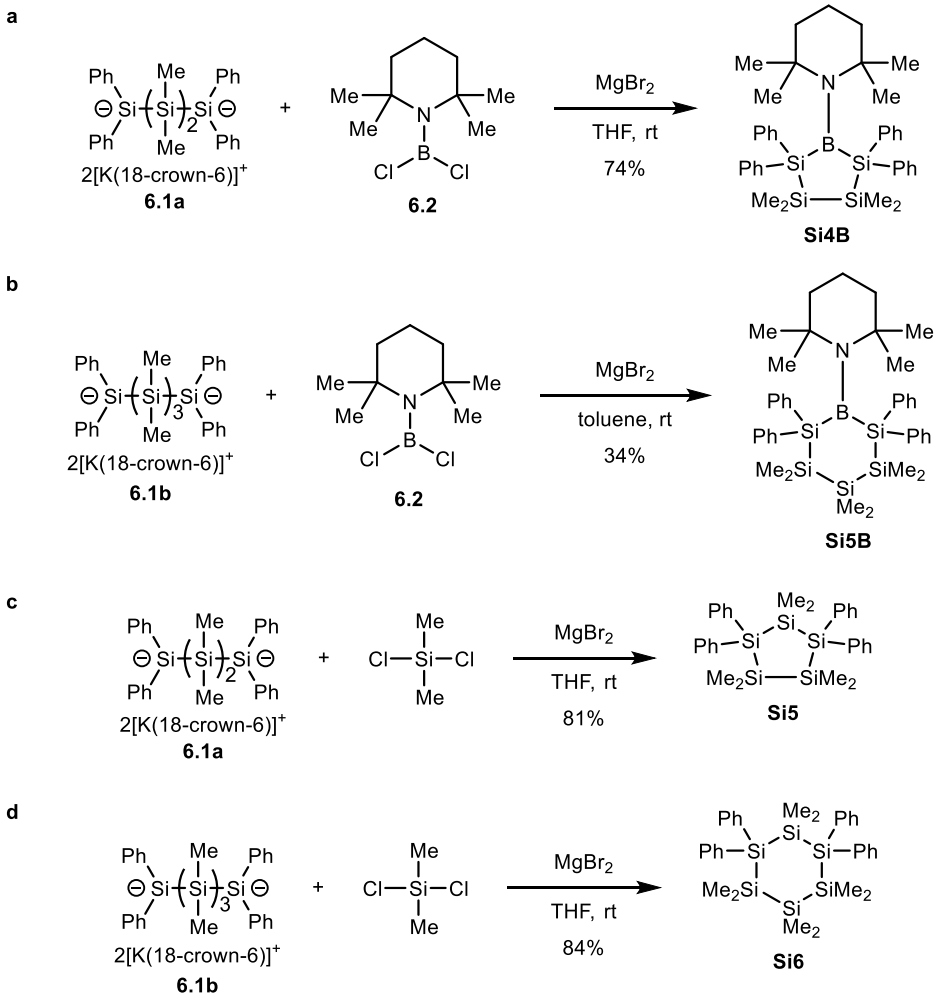

Scheme 6.1. Synthesis of (a) **Si4B**, (b) **Si5B**, (c) **Si5**, and (d) **Si6**.

SiB compounds are stable when stored neat on the benchtop or exposed to water for a short period of time, but prolonged exposure to atmospheric conditions or moisture

causes degradation of these compounds. Silicon analogs **Si5** and **Si6** were synthesized by treating **6.1a-b** with magnesium bromide, followed by dichlorodimethylsilane (Scheme 6.1c-d).

6.3 Single-Crystal X-Ray Crystallography

Single crystals of **Si4B** and **Si5B** suitable for X-ray structure determination were grown from solution at –30 °C in heptane. Crystal structures are shown in Figure 6.1. Table 6.1 summarizes selected structural parameters.

The BN bond in **Si4B** has double bond character. Bond angles between 120–128° are observed around the BN bond, with the exception of the smaller endocyclic Si–B–Si angles. A trigonal planar geometry is observed at boron (sum of all bond angles around B is 360°). The BN bond length of ca. 1.408(2) Å is significantly shorter than the 1.58(2) Å BN bond distance of ammonia borane (H_3N-BH_3).[36] The short BN bond distance is consistent with other aminoboranes with π-bond character.[37] The tetrasubstituted BN bond is modestly twisted from planarity, with a ca. 30° torsion angle observed between substituents on boron and nitrogen. The twisting is attributed to relieving unfavourable steric interactions between the TMP methyl substituents and the phenyl substituents on silicon. The five-membered ring of **Si4B** adopts an envelope-like conformation (Figure 6.1a). Overall, the structure of **Si4B** is similar to the related five-membered SiB cycle reported by Marschner et al., which also features an envelope-like conformation.[35]

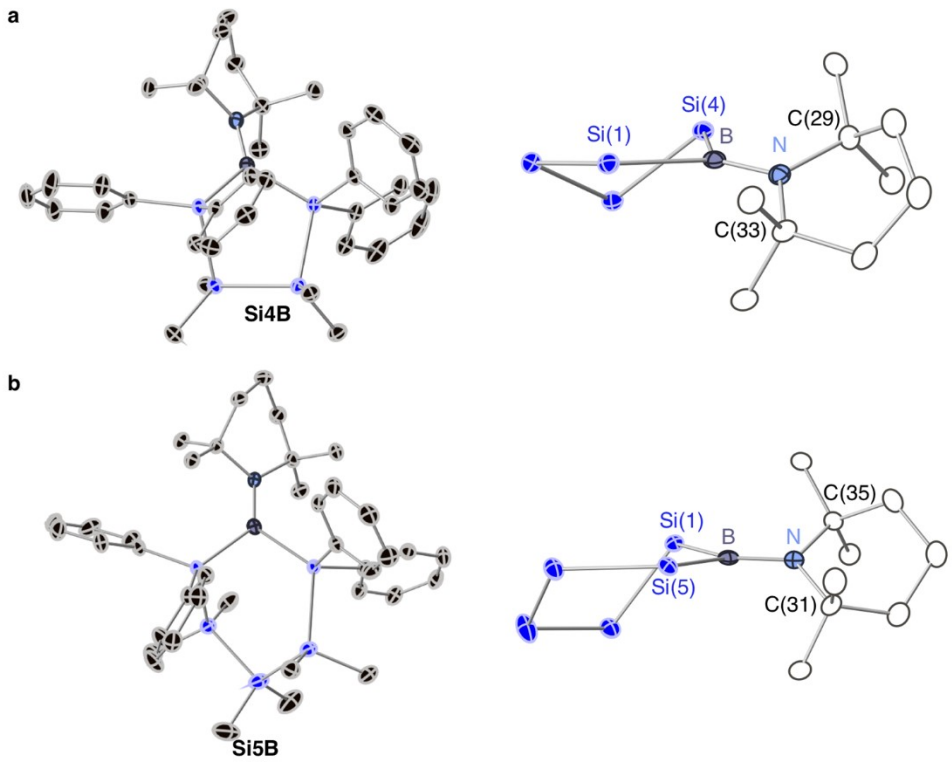

Figure 6.1. X-ray crystal structures of (a) **Si4B** and (b) **Si5B**. Hydrogens omitted for clarity. Side-on views of ring conformations in **Si4B** and **Si5B** are shown. For clarity, in side-on views, methyl and phenyl groups and hydrogens are omitted. Blue = silicon; black = carbon; purple = boron; light blue = nitrogen. Displacement ellipsoids shown at 50% probability level. Carbon atoms of tetramethylpiperdine ring are shown as hollow ellipsoids. Selected elements are labelled for reference to Tables 6.1-6.2.

Si5B adopts a boat-like conformation (Figure 6.1b). The structural parameters of the BN bond are also consistent with a double bond. Bond angles around the B atom range between 108.5-126.0°, with the endocyclic Si–B–Si angle falling at the lower end of the range. The sum of all bond angles is 360°, indicating a trigonal planar boron center. The BN bond is short (1.409(3) Å) and a ca. 30 torsion angle indicates a twisted double bond.

The cyclosilanes **Si5** and **Si6** exhibit typical SiSi bond lengths and endocyclic bond angles (Table 6.2). No evidence of ring strain is apparent. **Si5** crystallizes in an

envelope conformation, while **Si6** adopts a chair conformation in the solid state (Figure 6.2a-b).

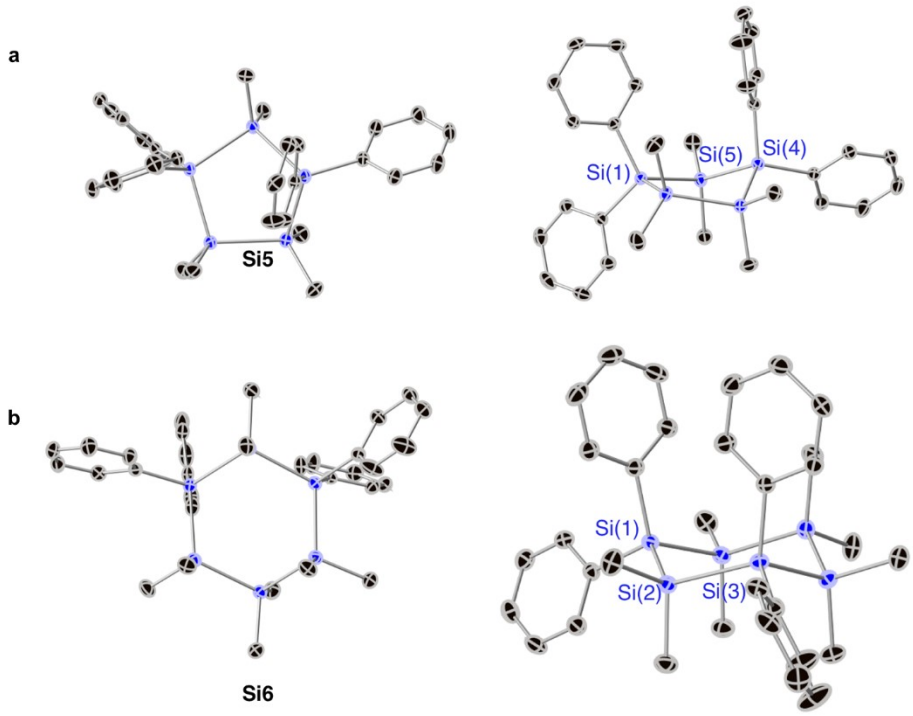

Figure 6.2. X-ray crystal structures of (a) **Si5** and (b) **Si6**. Hydrogens omitted for clarity. Side-on views of ring conformations in **Si5** and **Si6** are shown. Blue = silicon; black = carbon; light blue = nitrogen. Displacement ellipsoids shown at 50% probability level.

6.4 DFT – Geometry and Electronic Structure

Geometry optimized structures of **Si4B** and **Si5B** were calculated. (CAM B3LYP/6-31G(d)). The calculated structures of both compounds converged to structures similar to the crystal structures. The BN bond possesses double bond character as assessed by bond lengths and the sum of the bond angles (Table 6.3). Predicted ring conformations are also similar to the x-ray crystal structures with **Si4B** adopting an envelope-like conformation and **Si5B** adopting a boat-like conformation (Figure 6.3).

Table 6.1. Selected Geometric Parameters for the Experimental Crystal Structures of **Si4B** and **Si5B**

	Si4B		**Si5B**	
Bond Lengths (Å)	B–N	1.408(2)	B–N	1.409(3)
	Si(1)–B	2.0717(17)	Si(1)–B	2.065(2)
	Si(4)–B	2.1174(17)	Si(5)–B	2.131(3)
Bond Angles (deg)	Si(1)-B-Si(4)	105.44(7)	Si(1)-B-Si(5)	108.50(11)
	Si(1)-B-N	126.15(11)	Si(1)-B-N	126.04(18)
	Si(4)-B-N	128.41(11)	Si(5)-B-N	125.43(16)
	C(33)-N-B	123.78(12)	C(31)-N-B	121.38(18)
	C(29)-N-B	120.97(12)	C(35)-N-B	123.83(18)
Torsion Angles (deg)	Si(1)-B-N-C(33)	-32.90(19)	Si(1)-B-N-C(35)	34.4(3)
	Si(4)-B-N-C(29)	-30.42(19)	Si(5)-B-N-C(31)	37.7(3)

Table 6.2. Selected Geometric Parameters for the Experimental Crystal Structures of **Si5** and **Si6**

	Si5		**Si6**	
Bond Lengths (Å)	Si(1)–Si(5)	2.3582(4)	Si(1)–Si(2)	2.3677(5)
	Si(4)–Si(5)	2.3656(5)	Si(2)–Si(3)	2.3605(5)
Bond Angles (deg)	Si(1)-Si(5)-Si(4)	101.704(16)	Si(1)-Si(2)-Si(3)	111.186(19)
	mean Si-Si-Si	103.9	mean Si-Si-Si	111.38

Table 6.3. Selected Geometrical Parameters for Geometry Optimized Structures of **Si4B** and **Si5B**

	Si4B		**Si5B**	
Bond Lengths (Å)	B–N	1.419	B–N	1.425
	Si(1)–B	2.098	Si(1)–B	2.089
	Si(4)–B	2.128	Si(5)–B	2.151
Bond Angles (deg)	Si(1)-B-Si(4)	106.70	Si(1)-B-Si(5)	108.83
	Si(1)-B-N	126.04	Si(1)-B-N	126.38
	Si(4)-B-N	127.25	Si(5)-B-N	124.74
	C(33)-N-B	123.84	C(31)-N-B	123.31
	C(29)-N-B	120.89	C(35)-N-B	121.50
Torsion Angles (deg)	Si(1)-B-N-C(33)	-32.84	Si(1)-B-N-C(31)	-36.68
	Si(4)-B-N-C(29)	-32.37	Si(5)-B-N-C(35)	-38.46

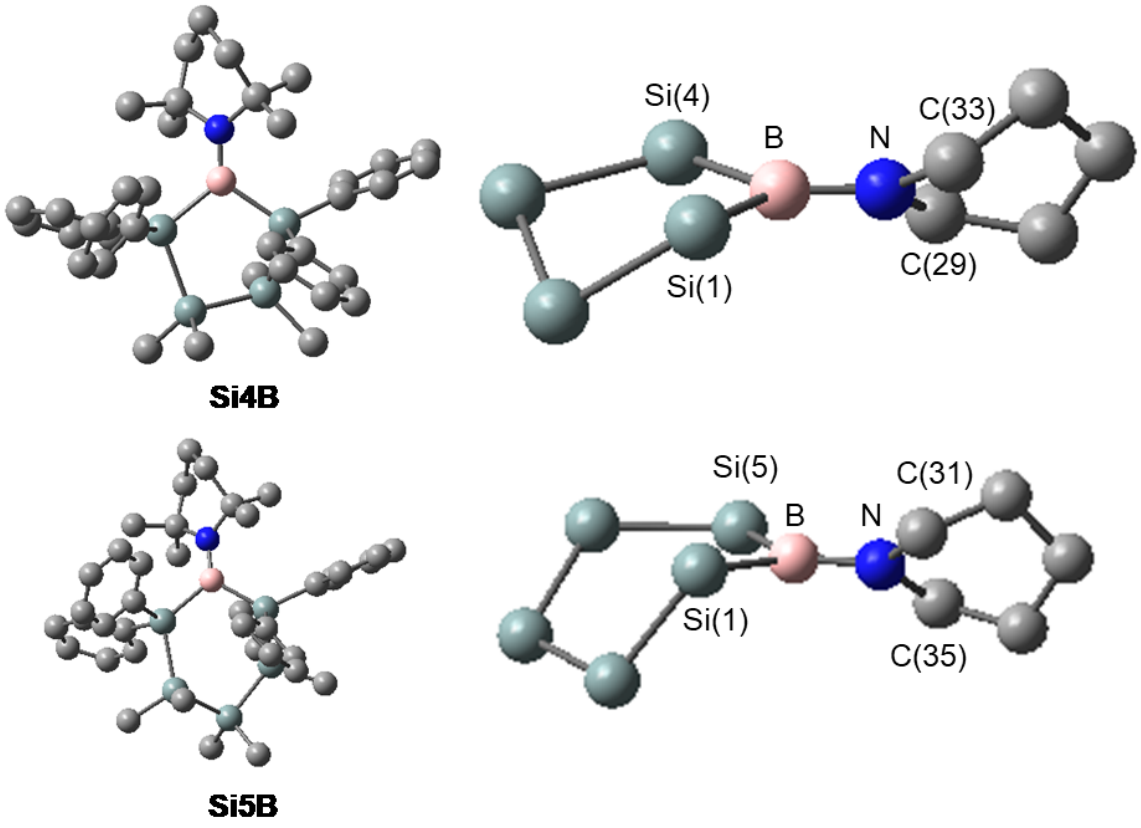

Figure 6.3. Geometry optimized structures of **Si4B** and **Si5B**. DFT-CAM-B3LYP/6-31G(d). Hydrogens omitted for clarity. Side-on views of ring conformations in **Si4B** and **Si5B** are also included. For clarity, in side-on views, methyl and phenyl groups and hydrogens are omitted. The geometries of the optimized **Si4B** and **Si5B** are similar to the geometries **Si4B** and **Si5B** adopt in the solid state (Figure 6.1).

Isodensity plots of the HOMO-1, HOMO, and LUMO of all four compounds and associated orbital energies are shown in Figure 6.4. In all cases, the HOMO and HOMO-1 are close in energy and concentrated on the cyclic framework. However, when comparing SiB rings and cyclosilanes, significant differences are observed in the LUMO energies and isodensity plots.

The LUMOs of the SiB rings are on the BN bond and have π* symmetry. In both cases, the LUMO energy is 0.5 eV lower in energy than the cyclosilane of comparable ring size. An isodensity plot shows that the LUMO of **Si5** is significantly delocalized

across both the σ framework and the exocyclic phenyl rings. The LUMO of **Si5** has π symmetry: above and below the ring, fused, delocalized orbitals reminiscent of benzene are observed. This π symmetry may aid in mixing with the exocyclic phenyl rings. The LUMO of cyclohexasilane **Si6** is also found on both the Si and Ph groups. The LUMO+1 of $TMPBH_2$ is on the BN bond and has π* symmetry. The energy of this orbital is 0.12 eV which is much larger than the energy of the LUMOs of **Si4B** and **Si5B** suggesting extended conjugation in the **Si4B** and **Si5B** LUMOs.

Isodensity plots of the highest occupied orbitals in the SiB rings shows that in the HOMO-1 and HOMO orbital density is localized on the ring system. In **Si4B**, orbital densities in the HOMO-1 are delocalized along the $Ph_2Si–(SiMe_2)_2–SiPh_2$ backbone. Minimal orbital density is seen on exocyclic methyl or phenyl substituents. In the HOMO, orbital density is on the $Ph_2Si–B–SiPh_2$ fragment, suggesting σ-p delocalization. **Si5B** shows the same alternation between the Si and Si–B–Si fragments in the HOMO-1 and HOMO.

The HOMO and HOMO-1 of the **Si5** cyclosilane also alternate between halves of the ring system, an effect that is likely due to the enforced bent conformation (vide infra). The **Si6** HOMO and HOMO-1 are more evenly distributed around the Si framework. In both materials, the HOMO and HOMO-1 are σ(SiSi) in nature.

Calculations predict that SiB rings should have significantly smaller HOMO-LUMO gaps and red-shifted electronic transitions compared to all silicon rings due to a combination of the HOMO-raising effect of σ-p delocalization and the LUMO-lowering effect of the low-lying BN π*.[38–40] In the following sections, experimental and theoretical evidence for the unique Si–B low-energy electronic transition is presented.

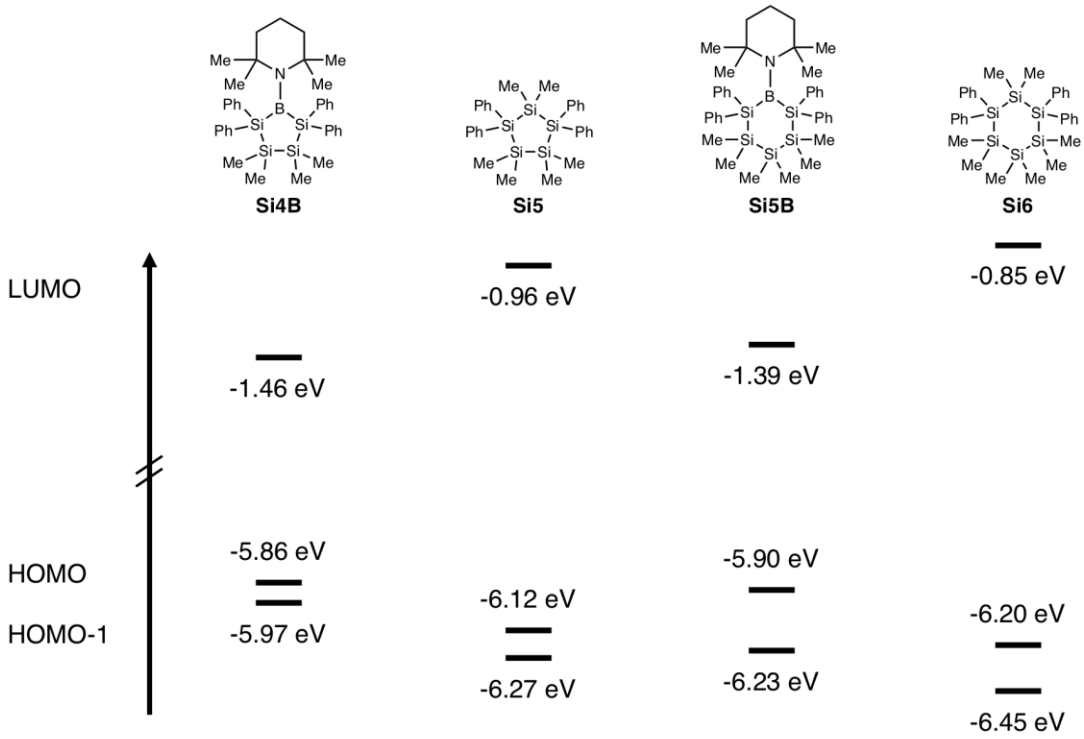

	Si4B	Si5	Si5B	Si6
LUMO				
HOMO				
HOMO-1				

Figure 6.4. Frontier molecular orbitals of Si4B, Si5, Si5B, and Si6 calculated at the PBE0/6-311+G(2d,p)//CAM-B3LYP/6-31G(d) level. Hydrogens omitted for clarity. MOs visualized with an isodensity value of 0.04.

6.5 Absorbance Spectroscopy

UV–Vis absorption spectra of SiB compounds were recorded in *n*-pentane at room temperature to obtain the widest possible spectral window (Figure 6.5a-b). UV-vis spectra of cyclosilane control compounds were recorded under similar conditions (Figure 6.5c-d).

All four compounds have absorption bands at ca. 195 and 250 nm, but only the SiB rings have an additional weak feature at ca. 350 nm (Figure 6.5e-f and Table 6.4). The broad low-energy transition unique to **Si4B** and **Si5B** must involve the low-lying orbitals associated with the BN π*. The ca. 195 nm transition is assigned to energy states associated with the oligosilane backbone, while the ca. 250 nm transition is associated with the phenyl rings.

These assignments are consistent with DFT calculations, which show that SiB rings have significantly lower energy LUMOs than all Si rings (Figure 6.4) in which orbital density is centered on the BN π* orbital. The weakness of the ca. 350 nm transition ($\varepsilon \sim 1000$ L mol^{-1} cm^{-1}) is consistent with a formally disallowed electronic transition, such as $\sigma \rightarrow \pi^*$.

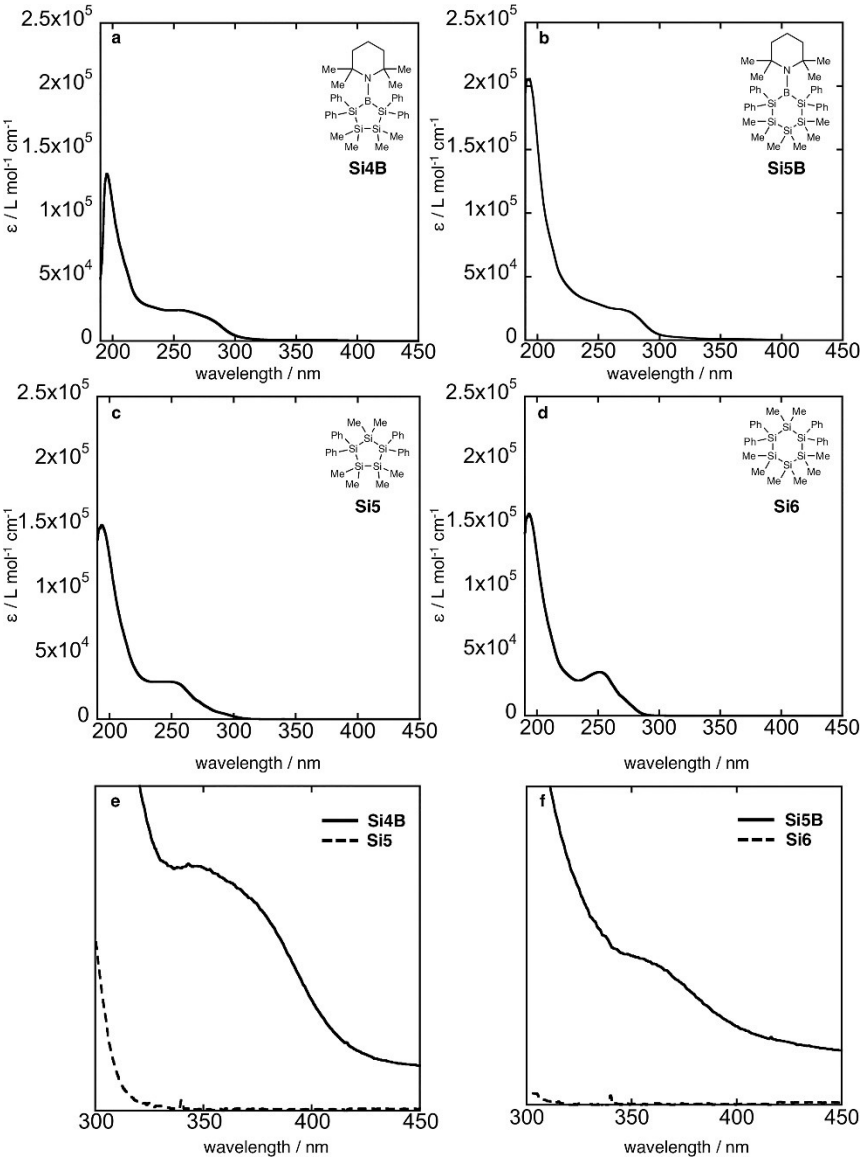

Figure 6.5. UV-visible absorbance spectra of a) **Si4B**, b) **Si5B**, c) **Si5**, and d) **Si6**. Spectra recorded in *n*-pentane at room temperature ([compound] = 1.0 x 10^{-5} M). Offset and cropped UV-visible spectra of e) five-membered and f) six-membered rings highlighting a broad transition at ca. 350 nm in Si–B interelement cycles. Spectra recorded in *n*-pentane at room temperature ([compound] = 5.0 x 10^{-5} M).

Cisoid Oligosilane. Oligosilane conformation strongly influences σ-electron delocalization, with corresponding effects on molecular orbital structure and energies, electronic transitions, and photophysical properties.[41] Oligosilanes populate more conformations than alkanes and Michl and West have proposed an expanded

nomenclature for oligosilane conformations based on the torsion angle ω summarized in figure 6.6.[42] The preferred conformations are substituent dependent. In permethyloligosilanes, *anti* and *gauche*/*ortho* conformations are both energy minima.[42,43] σ-Conjugation, or the stabilization afforded by the interaction of σ-orbitals, is strongest in the fully extended *anti* conformation, while *cisoid* kinks disrupt σ-conjugation.[44] The Ladder C model provides an explanation for the observed conformation dependence.[45,46] The photophysics of cyclic oligosilanes are less well-studied than linear oligosilanes, although hybrid C–Si and medium-sized rings have been used to probe conformational effects.[47,48]

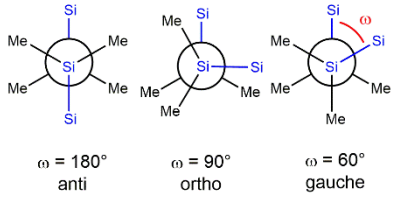

Entry	ω	Name
1	180	*anti*
2	165	*transoid*
3	150	*deviant*
4	90	*ortho*
5	60	*gauche*
6	40	*cisoid*

Figure 6.6. Dihedral angles in oligosilanes and Michl−West nomenclature. [42]

The photophysical properties of short chain linear oligosilanes with the general formula Si_nMe_{2n+2} (n = 4, 6) are well studied as model systems for higher polysilanes. At room temperature in solution, the *anti*[42] conformation is typically dominant. In the *anti* conformation, the highest occupied molecular orbital (HOMO) has σ symmetry and is delocalized across the silicon framework and the lowest unoccupied molecular orbital (LUMO) has similar symmetry and delocalization.[48-51] Changes in conformation disrupt σ-orbital conjugation, shifting the HOMO to higher energy. In addition, the symmetry of the LUMO changes from σ to π so that the lowest energy electronic transition is σπ*

instead of σσ*. The combination of these effects results in significantly hypsochromically shifted absorption in *cisoid* linear oligosilanes.

The enforced *cisoid* conformation of the 5-membered cyclosilanes (Figure 5) suggests that their photophysical properties should be more comparable to shorter chain systems than linear silanes with the same number of silicon atoms. Indeed, the 195 nm transition in **Si4B** and **Si5** is comparable to hexamethyldisilane (Si_2Me_6) and blue-shifted relative to decamethyltetrasilane (n-Si_4Me_{10}). DFT calculations on disilanes indicate that short chain systems are unique relative to longer oligosilanes.[52] While the HOMO in all cases is σ(SiSi), in disilanes the LUMO includes contributions from SiC antibonding orbitals. Isodensity plots of the LUMOs in **Si5** and **Si6** show contributions from both Si and Ph rings.

The ca. 195 nm transition in six-membered rings **Si5B** and **Si6** is assigned to the oligosilane backbone by analogy.

Phenyl-Terminated Oligosilanes. The broad ca. 250 nm transition observed in all four rings is attributed to the exocyclic phenyl rings. As first reported by Gilman in the 1960s, phenyl-substituted oligosilanes have a bathochromically shifted onset of absorbance compared to methyl-functionalized systems.[53,54] The contribution of σ,π-conjugation to these phenomena has been previously described.[55,56] Mixing of Ph and Si orbitals is apparent in the frontier molecular orbital calculations (Figure 6.4).

Calculated Spectra. The nature of the excitations observed for all compounds were further probed with TD-DFT calculations. The PBE0/6-311+G(2d,p) level of theory was selected for its prior success in calculating the excited states of oligosilanes.[48,50,58] Theory reproduces the experimental observation of a low energy excitation unique to the

SiB rings (Figure 6.7). As observed experimentally, the intensity of this feature is somewhat more pronounced in the Si_4B than the Si_5B ring.

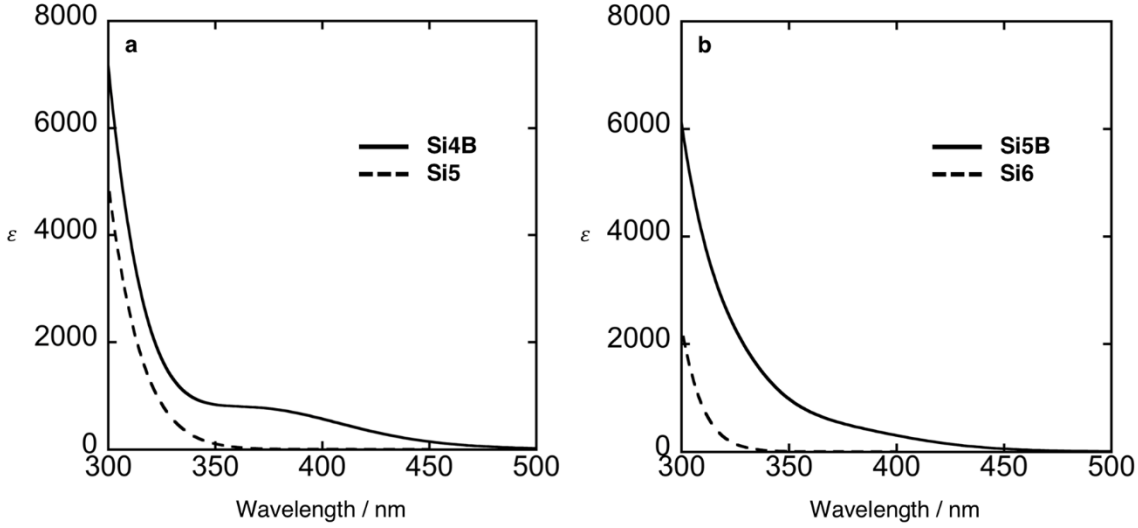

Figure 6.7. Cropped simulated UV-Vis spectra of a) five-membered rings **Si4B** and **Si5** and b) six-membered rings **Si5B** and **Si6.** TD-DFT PBE0/6-311+G(2d,p)//CAM-B3LYP/6-31G(d). Only SiB compounds show a feature in the 350-400 nm region.

TD-DFT assigns the lowest energy feature in **Si4B** to a combination of HOMO to LUMO (47%) and HOMO-1 to LUMO (48%) excitations, both of which are σ→π*. The HOMO and HOMO-1 of **Si4B** differ in whether the σ framework is localized on exclusively SiSi bonds or a mixture of SiSi and SiB bonds. The lowest energy transition in the Si_5B ring is also HOMO to LUMO (σ→π*).

Table 6.4. Comparison of Predicted and Experimental σ(SiSi)-π*(BN) Transitions.

	Si4B		**Si5B**	
Entry	**Experiment**	**Theory**	**Experiment**	**Theory**
λ_{max}	340	362	363	371
λ_{onset}	416	460	406	438
E_g	2.98	2.70	3.05	2.83

Theory slightly underestimates the energy of these transitions (Table 6.4). The experimental onset of absorbance in **Si4B** is 416 nm, while theory predicts an onset of absorbance at 460 nm. Similarly, **Si5B** is predicted to have an onset of absorbance at 438 nm compared to the experimental onset at 406 nm.

6.6 Conclusions

Five and six membered SiB rings were synthesized from nucleophilic disilanides and electrophilic chloroboranes, including the first six-membered SiB ring. A change in solvent suppressed an undesired intramolecular coupling reaction, enabling clean isolation of the target compounds. Materials are characterized both spectroscopically (^{1}H, ^{11}B, ^{13}C, ^{29}Si NMR) and crystallographically.

This study provides new understanding to the diversity of ways in which boron substitution influences conjugation. The pale-yellow SiB rings are characterized by steady state UV-vis absorbance spectroscopy, revealing a low energy feature unique to the mixed heterocycles. Calculations support assignment of the low-energy feature to $\sigma \rightarrow \pi^*$ transitions from the silicon backbone of the ring to the BN π^* and σ-p delocalization in the highest occupied molecular orbitals.

6.7 Experimental Section

All experimental details can be found in *Organometallics* **2019**, *38*, 1688-1698.

6.8 References

(1) He, X.; Baumgartner, T. *RSC Adv.* **2013**, *3* (29), 11334.
(2) Matsumi, N.; Naka, K.; Chujo, Y. *J. Am. Chem. Soc.* **1998**, *120* (20), 5112–5113.
(3) Corriu, R. J.-P.; Deforth, T.; Douglas, W. E.; Guerrero, G.; Deforth, T.; Siebert, W. S. *Chem. Commun.* **1998**, *0* (9), 963–964.
(4) Matsumi, N.; Chujo, Y. *Polym. J.* **2008**, *40* (2), 77–89.
(5) Jäkle, F. *Chem. Rev.* **2010**, *110* (7), 3985–4022.
(6) Yamaguchi, S.; Akiyama, S.; Tamao, K. *J. Am. Chem. Soc.* **2001**, *123* (46), 11372–11375.

(7) Zhao, H.; Gabbaï, F. P. *Organometallics* **2012**, *31* (6), 2327–2335.
(8) Song, K. C.; Lee, K. M.; Nghia, N. Van; Sung, W. Y.; Do, Y.; Lee, M. H. *Organometallics* **2013**, *32* (3), 817–823.
(9) Wade, C. R.; Broomsgrove, A. E. J.; Aldridge, S.; Gabbaï, F. P. *Chem. Rev.* **2010**, *110* (7), 3958–3984.
(10) Yuan, Z.; Collings, J. C.; Taylor, N. J.; Marder, T. B.; Jardin, C.; Halet, J.-F. *J. Solid State Chem.* **2000**, *154* (1), 5–12.
(11) Entwistle, C. D.; Marder, T. B. *Chemistry of Materials*. American Chemical Society 2004, pp 4574–4585.
(12) Entwistle, C. D.; Marder, T. B. *Angewandte Chemie International Edition*. WILEY-VCH Verlag August 2002, pp 2927–2931.
(13) Kobayashi, H.; Sato, N.; Ichikawa, Y.; Miyata, M.; Chujo, Y.; Matsuyama, T. *Synth. Met.* **2003**, *135–136*, 393–394.
(14) Cataldo, S.; Fabiano, S.; Ferrante, F.; Previti, F.; Patanè, S.; Pignataro, B. *Macromol. Rapid Commun.* **2010**, *31* (14), 1281–1286.
(15) Meng, B.; Ren, Y.; Liu, J.; Jäkle, F.; Wang, L. *Angew. Chemie Int. Ed.* **2018**, *57* (8), 2183–2187.
(16) Miller, R. D.; Michl, J. *Chem. Rev.* **1989**, *89* (6), 1359–1410.
(17) Klausen, R. S.; Widawsky, J. R.; Steigerwald, M. L.; Venkataraman, L.; Nuckolls, C. *J. Am. Chem. Soc.* **2012**, *134* (10), 4541–4544.
(18) Su, T. A.; Li, H.; Klausen, R. S.; Kim, N. T.; Neupane, M.; Leighton, J. L.; Steigerwald, M. L.; Venkataraman, L.; Nuckolls, C. *Acc. Chem. Res.* **2017**, *50* (4), 1088–1095.
(19) Hsu, M.-T. S.; Chen, T. S.; Riccitiello, S. R. *J. Appl. Polym. Sci.* **1991**, *42* (3), 851–861.
(20) Puneet, P.; Vedarajan, R.; Matsumi, N. *Polym. Chem.* **2016**, *7* (25), 4182–4187.
(21) Zhang, G.; Ma, J.; Jiang, Y. *J. Phys. Chem. B* **2005**, *109* (28), 13499–13509.
(22) Nöth, H.; Höllerer, G. *Angew. Chemie Int. Ed. English* **1962**, *1* (10), 551–552.
(23) Tsurusaki, A.; Yoshida, K.; Kyushin, S. *Dalt. Trans.* **2017**, *46* (27), 8705–8708.
(24) Oestreich, M.; Hartmann, E.; Mewald, M. *Chem. Rev.* **2013**, *113* (1), 402–441.
(25) Araujo da Silva, J. C.; Pillot, J.-P.; Birot, M.; Desvergne, J.-P.; Liotard, D.; Rayez, J.-C.; Rayez, M.-T. *J. Organomet. Chem.* **2008**, *693* (15), 2592–2596.
(26) Surampudi, S.; Yeh, M.-L.; Siegler, M. A.; Hardigree, J. F. M.; Kasl, T. A.; Katz, H. E.; Klausen, R. S. *Chem. Sci.* **2015**, *6* (3), 1905–1909.
(27) Zhou, J.; Surampudi, S. K.; Bragg, A. E.; Klausen, R. S. *Chem. - A Eur. J.* **2016**, *22* (18), 6204–6207.
(28) Zhou, J.; Folster, C. P.; Surampudi, S. K.; Jimenez, D.; Klausen, R. S.; Bragg, A. E. *Dalt. Trans.* **2017**, *46*, 8716–8726.
(29) Press, E. M.; Marro, E. A.; Surampudi, S. K.; Siegler, M. A.; Tang, J. A.; Klausen, R. S. *Angew. Chemie - Int. Ed.* **2017**, *56* (2), 568–572.
(30) Marro, E. A.; Press, E. M.; Purkait, T. K.; Jimenez, D.; Siegler, M. A.; Klausen, R. S. *Chem. - A Eur. J.* **2017**, *23* (62), 15633–15637.
(31) Marro, E. A.; Press, E. M.; Siegler, M. A.; Klausen, R. S. *J. Am. Chem. Soc.* **2018**, *140* (18), 5976–5986.
(32) Folster, C. P.; Klausen, R. S. *Polym. Chem.* **2018**, *9*, 1938–1941.
(33) Gaderbauer, W.; Zirngast, M.; Baumgartner, J.; Marschner, C.; Tilley, T. D.

Organometallics **2006**, *25* (10), 2599–2606.
(34) Hengge, E.; Wolfer, D. *Angew. Chemie Int. Ed. English* **1973**, *12* (4), 315–316.
(35) Markov, J.; Fischer, R.; Wagner, H.; Noormofidi, N.; Baumgartner, J.; Marschner, C. *Dalt. Trans.* **2004**, *51* (14), 2166.
(36) Klooster, W. T.; Koetzle, T. F.; Siegbahn, P. E. M.; Richardson, T. B.; Crabtree, R. H. *J. Am. Chem. Soc.* **1999**, *121* (27), 6337–6343.
(37) Alcaraz, G.; Vendier, L.; Clot, E.; Sabo-Etienne, S. *Angew. Chemie - Int. Ed.* **2010**, *49* (5), 918–920.
(38) Jaska, C. A.; Emslie, D. J. H.; Bosdet, M. J. D.; Piers, W. E.; Sorensen, T. S.; Parvez, M. *J. Am. Chem. Soc.* **2006**, *128* (33), 10885–10896.
(39) Bosdet, M. J. D.; Piers, W. E.; Sorensen, T. S.; Parvez, M. *Angew. Chemie Int. Ed.* **2007**, *46* (26), 4940–4943.
(40) van de Wouw, H. L.; Lee, J. Y.; Siegler, M. A.; Klausen, R. S. *Org. Biomol. Chem.* **2016**, *14* (12), 3256–3263.
(41) Jovanovic, M.; Michl, J. *J. Am. Chem. Soc.* **2018**, *140* (36), 11158–11160.
(42) Michl, J.; West, R. *Acc. Chem. Res.* **2000**, *33* (12), 821–823.
(43) Albinsson, B.; Antic, D.; Neumann, F.; Michl, J. *J. Phys. Chem. A* **1999**, *103* (14), 2184–2196.
(44) Tsuji, H.; Terada, M.; Toshimitsu, A.; Tamao, K. *J. Am. Chem. Soc.* **2003**, *125* (25), 7486–7487.
(45) Bande, A.; Michl, J. *Chem. - A Eur. J.* **2009**, *15* (34), 8504–8517.
(46) Jovanovic, M.; Antic, D.; Rooklin, D.; Bande, A.; Michl, J. *Chem. - An Asian J.* **2017**, *12* (11), 1250–1263.
(47) Tamao, K.; Tsuji, H.; Terada, M.; Asahara, M.; Yamaguchi, S.; Toshimitsu, A. *Angew. Chemie* **2000**, *39* (18), 3287–3290.
(48) Kanazawa, Y.; Tsuji, H.; Ehara, M.; Fukuda, R.; Casher, D. L.; Tamao, K.; Nakatsuji, H.; Michl, J. *ChemPhysChem* **2016**, *17* (19), 3010–3022.
(49) Albinsson, B.; Teramae, H.; Downing, J. W.; Michl, J. *Chem. - A Eur. J.* **1996**, *2* (5), 529–538.
(50) Tsuji, H.; Fogarty, H. A.; Ehara, M.; Fukuda, R.; Casher, D. L.; Tamao, K.; Nakatsuji, H.; Michl, J. *Chem. - A Eur. J.* **2014**, *20* (30), 9431–9441.
(51) Plitt, H. S.; Michl, J. *Chem. Phys. Lett.* **1992**, *198* (3–4), 400–405.
(52) Piqueras, M. C.; Crespo, R.; Michl, J. *J. Phys. Chem. A* **2008**, *112* (50), 13095–13101.
(53) Gilman, H.; Atwell, W. H.; Schwebke, G. L. *J. Organomet. Chem.* **1964**, *2* (4), 369–371.
(54) Gilman, H; Atwell, W, H; Schwebke, G. *Chem. Ind.* **1964**, No. 25, 1063.
(55) Sakurai, H. *J. Organomet. Chem.* **1980**, *200*, 261–286.
(56) Pitt, C. G.; Carey, R. N.; Toren, E. C. *J. Am. Chem. Soc.* **1972**, *94* (11), 3806–3811.
(57) MacLeod, M. K.; Kobr, L.; Michl, J. *J. Phys. Chem. A* **2012**, *116* (43), 10507–10517.
(58) Fogarty, H. A.; Tsuji, H.; David, D. E.; Ottosson, C. H.; Ehara, M.; Nakatsuji, H.; Tamao, K.; Michl, J. *J. Phys. Chem. A* **2002**, *106* (10), 2369–2373.
(59) Dreuw, A.; Head-Gordon, M. *Chem. Rev.* **2005**, *105* (11), 4009–4037.
(60) Steinmann, S. N.; Piemontesi, C.; Delachat, A.; Corminboeuf, C. *J. Chem. Theory Comput.* **2012**, *8* (5), 1629–1640.
(61) Sini, G.; Sears, J. S.; Brédas, J.-L. *J. Chem. Theory Comput.* **2011**, *7* (3), 602–609.

(62) Vydrov, O. A.; Scuseria, G. E. *J. Chem. Phys.* **2006**, *125* (23), 234109.
(63) Chai, J.-D.; Head-Gordon, M. *Phys. Chem. Chem. Phys.* **2008**, *10* (44), 6615.

Chapter 7: Curriculum Vitae

Eric A. Marro
Johns Hopkins University
3400 North Charles Street - Remsen 207
Baltimore, MD 21218
emarro1@jhu.edu

Education

2014 - 2019	Johns Hopkins University, Baltimore, MD Ph.D. – Department of Chemistry Advisor: Prof. Rebekka S. Klausen Thesis Title: Strategic Synthesis of Complex Functionalized Silane Frameworks
2007 – 2011	Boston College, Chestnut Hill, MA B.S., Chemistry, *cum laude* Advisor: Prof. Kian L. Tan

Professional Experience

2017 – 2019	Johns Hopkins Technology Ventures, Baltimore, MD *Commercialization Academy Intern*
2011 – 2014	Cabot Corporation, Billerica, MA *Sr. Research Associate* (May 2012 – August 2014) *Research Associate* (July 2011 – May 2012) Research: Surface modification of carbon black towards low rolling resistance tire

Publications

7 publications from doctoral research (* = front cover article)

7. R. W. Dorn, **E. A. Marro**, M. P. Hanrahan, R. S. Klausen, A. J. Rossini, "Investigating the Microstructure of Poly(Cyclosilane) by ^{29}Si Solid-State NMR Spectroscopy and DFT Calculations", *Chemistry of Materials*, ASAPs. (DOI: 10.1021/acs.chemmater.9b03606)

6. **E. A. Marro**, C. P. Folster, E. M. Press, H. Im, J. T. Ferguson, M. A. Siegler, R. S. Klausen, "Stereocontrolled Syntheses of Functionalized *cis*- and *trans*-Siladecalins", *Journal of the American Chemical Society*, ASAPs. (DOI: 10.1021/jacs.9b09902)

5. **E. A. Marro**, R. S. Klausen, "Conjugated Polymers Inspired by Crystalline Silicon", *Chemistry of Materials*, 2019, *31,* 2202 – 2211. (DOI: 10.1021/acs.chemmater.9b00131)

4. * T. K. Purkait, E. M. Press, **E. A. Marro**, M. A. Siegler, R. S. Klausen, "Low-Energy Electronic Transition in SiB Rings", *Organometallics*, 2019, *38*, 1688 – 1698. (DOI: 10.1021/acs.organomet.8b00804)

3. **E. A. Marro**, E. M. Press, M. A. Siegler, R. S. Klausen, "Directional Building Blocks Determine Linear and Cyclic Silicon Architectures", *Journal of the American Chemical Society*, 2018, *140*, 5976 – 5986. (DOI: 10.1021/jacs.8b02541)

2. **E. A. Marro**, E. M. Press, T. K. Purkait, D. Jimenez, M. A. Siegler, R. S. Klausen, "Cooperative Noncovalent Interactions Induce Ion Pair Separation in Diphenylsilanides", *Chemistry: A European Journal*, 2017, *23*, 15633 – 15637. (DOI: 10.1002/chem.201704217)

1. E. M. Press, **E. A. Marro**, S. K. Surampudi, M. A. Siegler, J. A. Tang, R. S. Klausen, "Synthesis of a Fragment of Crystalline Silicon: Poly(Cyclosilane)", *Angewandte Chemie - International Edition,* 2017, *56*, 568 – 572. (DOI: 10.1002/anie.201610208)

Presentations

Oral:

3. **E. A. Marro**, R. S. Klausen, "Introducing Complexity to Polysilanes Using Fused Ring Bilding Blocks: Poly(siladecalin)", Presented at the 258th American Chemical Society National Meeting, San Diego, CA, August 2019.

2. **E. A. Marro**, E. M. Press, R. S. Klausen, "Directional Building Blocks Provide Curvature in Poly(cyclohexasilane)", Presented at the 256th American Chemical Society National Meeting, Boston, MA, August 2018.

1. **E. A. Marro**, E. M. Press, T. K. Purkait, M. A. Siegler, R. S. Klausen, "Synthesis and Characterization of Diphenylsilyl Nucleophiles", Presented at the 254th American Chemical Society National Meeting, Washington D.C., August 2017.

Poster:

1. **E. A. Marro**, E. M. Press, M. A. Siegler, R. S. Klausen, "Directional building blocks determine linear and cyclic structures", Presented at the U.S.-Japan Meeting on Advances in Organic/Inorganic Hybrid Materials, Newark, NJ, June 2018

Awards

- 2019 Shepherd Memorial Travel Award – Awarded to a graduate student to defray cost of attending a conference
- 2018 Rudolph Sonneborn Fellowship - Awarded to an outstanding advanced-year graduate student

Teaching Assistant

Spring 2018	AS.030.228 Intermediate Organic Chemistry Laboratory
Spring 2016	AS.030.228 Intermediate Organic Chemistry Laboratory
Fall 2015	AS.030.205 Organic Chemistry I
Spring 2015	AS.030.102 Introductory Chemistry II
Fall 2014	AS.030.101 Introductory Chemistry I